Molecular characterization of water balance disturbances

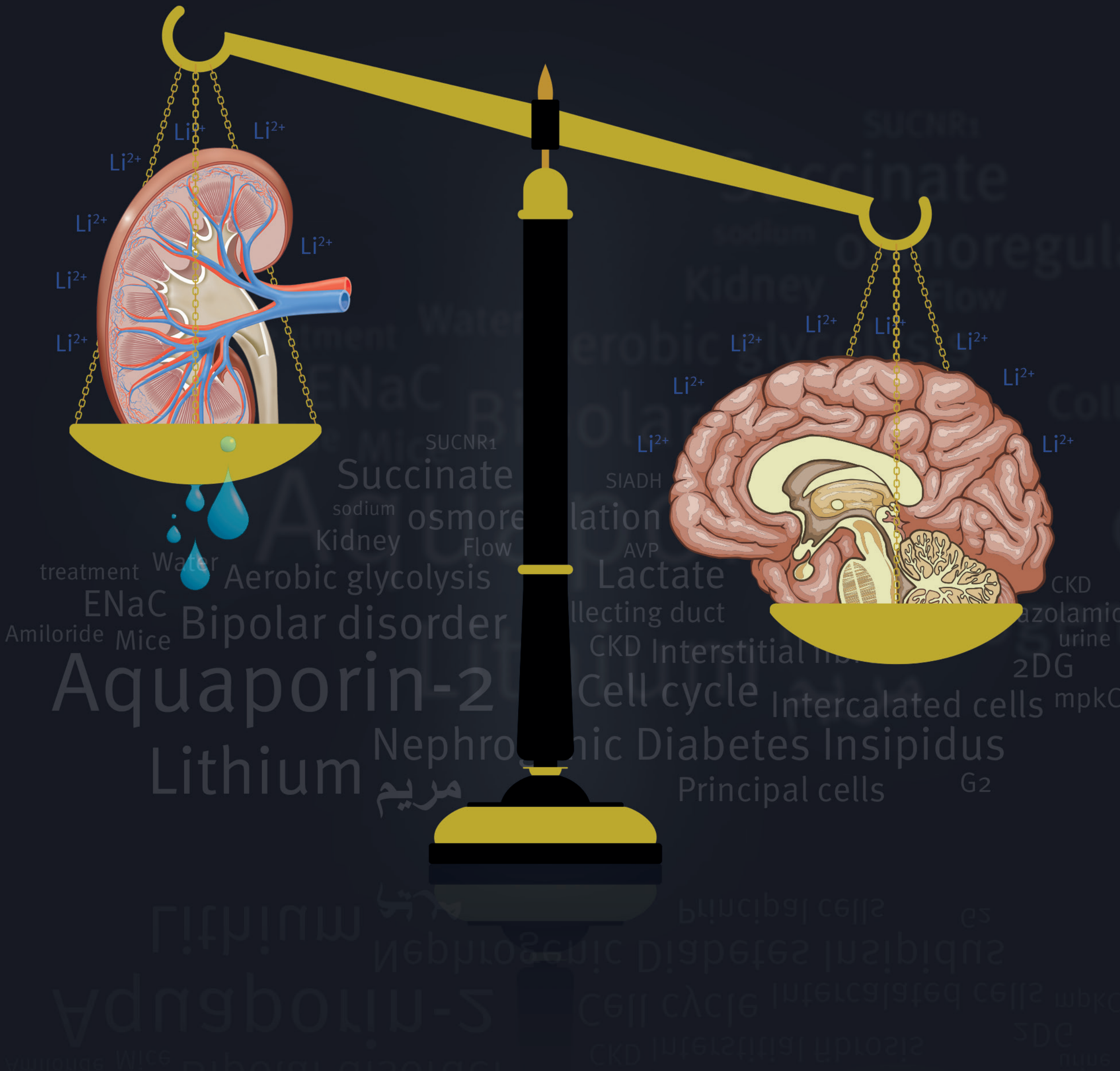

Mohammad Alsady

Molecular characterization of water balance disturbances

Mohammad Alsady

The research presented in this thesis was performed at the department of Physiology, Radboud Institute for Molecular Life Sciences, Radboud university medical center, The Netherlands. The project was financially supported by a grant from the Society of Experimental Laboratory Medicine and the publication of this thesis was financially supported by the Dutch Kidney Foundation.

ISBN
978-94-92896-32-2

Design/lay-out
Promotie In Zicht, Arnhem

Print
Ipskamp Printing, Enschede

Thesis number
RIMLS 2018-12

Molecular characterization of water balance disturbances

Proefschrift

ter verkrijging van de graad van doctor
aan de Radboud Universiteit Nijmegen
op het gezag van de rector magnificus prof. dr. J.H.J.M. van Krieken,
volgens besluit van het college van decanen
in het openbaar te verdedigen op donderdag 21 juni 2018
om 10:30 uur precies

door

Mohammad Alsady
geboren op 7 April 1987
te Arbil, Irak

Promotor
Prof. dr. P.M.T. Deen

Copromotor
Dr. T. de Groot (Canisius Wilhelmina Ziekenhuis, Nijmegen)

Manuscriptcommissie
Prof. dr. F.G.M. Russel, voorzitter
Prof. dr. L.B. Hilbrands
Prof. dr. E.J. Hoorn (Erasmus MC)

Molecular characterization of water balance disturbances

Doctoral Thesis

to obtain the degree of doctor
from Radboud University Nijmegen
on the authority of the Rector Magnificus prof. dr. J.H.J.M. van Krieken,
according to the decision of the Council of Deans
to be defended in public on Thursday, June 21, 2018
at 10.30 hours

by

Mohammad Alsady
Born on April 7, 1987
in Arbil, Irak

Supervisor
Prof. dr. P.M.T. Deen

Co-supervisor
Dr. T. de Groot, Canisius Wilhelmina Ziekenhuis, Nijmegen

Doctoral Thesis Committee
Prof. dr. F.G.M. Russel (chairman)
Prof. dr. L.B. Hilbrands
Prof. dr. E.J. Hoorn (Erasmus MC)

Table of contents

Chapter 1	General introduction	9
Chapter 2	Lithium causes G2 arrest of renal principal cells	25
Chapter 3	Acetazolamide attenuates Lithium-Induced Nephrogenic Diabetes Insipidus	47
Chapter 4	Lithium induces aerobic glycolysis and glutaminolysis in collecting duct principal cells	71
Chapter 5	The succinate receptor 1 has no role in the development of lithium-induced nephrogenic diabetes insipidus	93
Chapter 6	Amiloride prevents lithium-induced metabolic acidosis and proliferation of collecting duct cells	105
Chapter 7	Long-term lithium treatment causes renal interstitial fibrosis in mice	119
Chapter 8	Single-Tubule RNA-Seq Reveals Signaling Mechanisms That Defend Against Hyponatremia in SIADH	141
Chapter 9	Flow, cell proliferation and microcyst formation in relation to Aquaporin-2	175
Chapter 10	General discussion and summary	189
Chapter 11	Nederlandse samenvatting	207
Chapter 12	List of abbreviations	219
	List of publications	221
	Curriculum vitae	223
	Research data management	225
	RIMLS portfolio	227
Chapter 13	Dankwoord – Acknowledgments	231
Chapter 14	Arabic summary – ملخص عربي	237

Chapter 1

General introduction

Adapted from Alsady et al. 2016; Lithium in the kidney: Friend or Foe?
J Am Soc Nephrol. 2016 Jun;27(6):1587-95

General introduction

The kidneys are paired organs and the renal parenchyma comprises a cortex and an outer and inner medulla (1, 2). Each kidney contains approximately one million nephrons, which are the functional unit of the kidney. Each nephron is made up of a glomerulus, proximal tubule, loop of Henle, distal tubule and collecting duct. The renal tubules are lined by epithelial cells, which are cuboidal except in the thin limb of the loop of Henle where they are flat. Proximal tubular cells differ from other cells of the system as they have a luminal brush border. The collecting ducts contain two cell types with different functions, namely principal cells and intercalated cells. An essential feature of renal function is that a large volume of blood passes through the two million glomeruli. A hydrostatic pressure provides the driving force for ultrafiltration of virtually protein-free and fat-free fluid across the glomerular capillary wall into Bowman's space and so into the renal tubule.

Each day, ultra-filtration of 170–180 L of water and unbound small- molecular-weight constituents of blood occurs. If these large volumes of ultra-filtrate were excreted unchanged as urine, it would be necessary to ingest huge amounts of water and electrolytes to stay in balance. This is avoided by the selective reabsorption of water, essential electrolytes and other blood constituents, such as glucose and amino acids, from the filtrate in transit along the nephron. Accordingly, 60–80% of filtered water, sodium and potassium is reabsorbed in the proximal tubule along with almost all the bicarbonate, glucose and amino acids. Additional water and sodium chloride is reabsorbed more distally, and fine-tuning of salt and water balance is achieved in the distal tubules and collecting ducts resulting in final urine volume of 1–2 L per day. Water is the main component of the human body and is essential to facilitate many enzymatic processes, but also to maintain blood volume and osmolality homeostasis. The regulation of volume homeostasis is important for proper control of blood pressure, which is essential for providing tissues a proper supply of energy and oxygen via perfusion. Volume balance is mainly regulated by the modulation of urinary reabsorption of sodium as sodium is the major determinant of plasma osmolality and water crosses cell membranes freely from areas of low solute concentration to areas of high solute concentration. Thus, with increased sodium reabsorption and water that follows the generated osmotic gradient, our blood volume is increased. Besides volume balance, our body uses water to regulate the osmobalance. Osmobalance disturbances, named hypo- and hypertonicity or hypo- and hypernatremia, respectively, need to be corrected to prevent changes in cell volume, which would compromise cell function. This is mainly regulated by the modulation of drinking and steering the reabsorption of water from pro-urine through renal action of vasopressin.

Blood volume is sensed by low- and high-pressure baroreceptors that trigger increased action potential generation rates when blood vessel pressure is increased and provide this information to the central nervous system. The brain translates this signal into several responses that can affect blood volume over either the short or the long term. The short-term effects occur as the autonomic nervous system and humoral mechanisms modulate the heart and blood vessels to control blood pressure while long-term effects occur as nervous, humoral, and hemodynamic mechanisms modulate the kidney to control sodium excretion by using four parallel effector pathways. The first effector pathway is the renin-angiotensin-aldosterone system (RAAS) that promotes sodium retention in the kidney via the actions of both angiotensin II (ANG II) and aldosterone. A reduced blood volume is sensed by the juxtaglomerular cells in the kidneys that convert intracellular prorenin into renin and then secrete this directly into the circulation. Plasma renin then converts angiotensinogen into angiotensin I that is subsequently converted into angiotensin II by the enzyme angiotensin-converting enzyme (ACE) found in the endothelial cells of the capillaries throughout the body, within the lungs and the epithelial cells of the kidneys. Angiotensin II causes blood vessels to constrict, resulting in increased blood pressure, and stimulates the secretion of aldosterone from the adrenal cortex. Both stimulate the renal reabsorption of sodium. The second and third effector pathways are neural. Baroreceptors detect decreases in blood volume and communicate this via afferent neurons to the medulla of the brain stem. From the medulla, two types of efferent signals emerge that ultimately act on the kidney. In one, increased activity of the sympathetic division of the autonomic nervous system reduces renal blood flow, and thus reduces sodium excretion. In the other effector pathway, the posterior pituitary increases its secretion of arginine vasopressin (AVP; also known as antidiuretic hormone; ADH). The latter mechanism becomes active only after large declines in effective circulating volume. The final pathway is also hormonal. Reduced blood volume decreases the release of atrial natriuretic peptide (ANP), therewith reducing sodium excretion. All four parallel effector pathways modulate renal sodium excretion, correcting the primary change in blood volume. These pathways are also interlinked. For example, by binding their receptors in AVP-producing supraoptic nucleus (SON), Angiotensin II also stimulates AVP secretion, while ANP inhibits AVP secretion (3).

Blood osmolality is tightly regulated to maintain a blood osmolality around 290 mOsm/kg (4). Extracellular osmolality is sensed by osmoreceptors that are located in the vascular organ of lamina terminalis (OVLT) and subfornical organ (SFO) (5). When blood osmolality is elevated by only 2%-3%, the osmoreceptors induce a thirst sensation to increase water intake, but this signaling also results in the release of AVP from the posterior pituitary to increase renal water reabsorption and increase in urine osmolality (6). After secretion into the circulation from the posterior pituitary gland,

AVP is delivered to the kidney, where it binds the V2 receptor (V2R) (Figure 1). The V2R is a G protein-coupled receptor that is expressed in the basolateral membrane of the renal connecting tubuli and collecting ducts (7). The binding of AVP to the V2R increases intracellular level of cyclic AMP (cAMP) (8). This rise in intracellular cAMP increases aquaporin-2 water channel (AQP2) transcription through phosphorylated activation of the cAMP response element-binding protein (CREB) transcription factor and induces translocation of AQP2 from intracellular vesicles to the apical membrane by dephosphorylating AQP2 at Ser261 and by phosphorylating AQP2 at Ser256, Ser264 and Thr269 thereby increasing water permeability and allowing urine concentration (Figure 1) (8).

Disorders of excessive water reabsorption

As may become apparent from its function above, inappropriate secretion of ADH leads to increased retention of water and thus hyponatremia. The presentation is usually vague, with confusion, nausea, irritability and, later, fits or in acute cases even coma (1). There is no oedema nor hypervolemia/hypertension. Mild symptoms usually occur with plasma sodium levels below 125 mmol/L and serious manifestations are likely below 115 mmol/L. The elderly may show symptoms with milder abnormalities. In individuals with the syndrome of inappropriate antidiuretic hormone secretion (SIADH), high levels of circulating vasopressin persist even when serum osmolality falls to levels that totally suppress neurohypophyseal vasopressin secretion (9). Consequently, the kidney continues to reabsorb free water, leading to a progressive fall in serum sodium concentration, and thus osmolality (Figure 2). SIADH is the most common cause of hyponatremia in hospitalized patients with causes ranging from neurological diseases, small-cell carcinoma of the lung, pulmonary lesions, congestive heart failure, hepatic cirrhosis or through the use of a wide variety of medications such as chlorpropamide and carbamazepine (10). There are four distinct categories of SIADH, which can be classified according to the pattern of AVP secretion (11). Type A is the most common pattern of abnormal AVP secretion (40%). This type has been reported particularly with small cell lung tumors, which can synthesize and secrete bioactive AVP. Plasma AVP secretion is completely unregulated in Type A SIADH and plasma AVP secretion is not suppressed as plasma osmolality falls and significant hyponatremia may occur, if drinking continues (12). In type B SIADH, the pattern of AVP secretion is characterized by a lower osmotic threshold for AVP secretion. The threshold is reset to a lower level than would be physiologically normal. Type C and D SIADH forms are rare where type C is characterized by plasma osmolalities above the usual osmotic threshold of 284 mOsm/kg but the linear relationship between plasma AVP and plasma osmolality is preserved. However, lowered plasma osmolalities do not

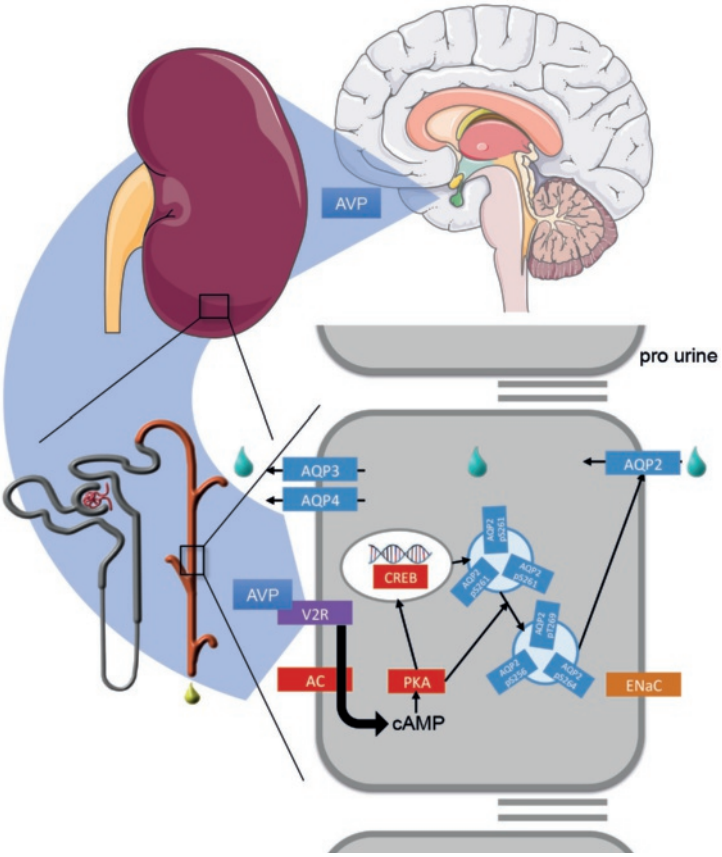

Figure 1. The regulation of AQP2-mediated water reabsorption. With water loss or increase in plasma osmolality, osmoreceptors in the brain sense this and trigger a thirst response and stimulate the release of vasopressin (AVP) form the pituitary. Upon binding of AVP to its V2R in the principal cell of the collecting duct in the kidney, it initiates a cAMP signaling cascade resulting in increased *AQP2* gene and protein expression, de-phosphorylation of AQP2 at Ser261, and phosphorylation of AQP2 at Ser256, Ser264, and Thr269. This leads to the redistribution of AQP2 from intracellular vesicles into the apical membrane thereby increasing water permeability. Water enters the principal cell through AQP2 and subsequently exit the cells through AQP3 and AQP4 thereby allowing urine concentration.

suppress AVP secretion, probably due to dysfunction of inhibitory neurons in the hypothalamus, so that low plasma concentrations of AVP are always detectable in the plasma (12). In type D SIADH, also called nephrogenic syndrome of inappropriate antidiuresis (NSIAD), the clinical presentation consist of hyponatremia and the lack of

urinary dilution with very low or undetectable plasma AVP levels (13). NSIAD is rare and caused by an activating mutation in the V2R, resulting in constitutive AVP-independent renal reabsorption of water (13).

Inappropriately increased plasma AVP levels in SIADH increase the expression of AQP2 in the renal tubule and water retention causing hyponatremia. Fortunately, the degree of the hyponatremia is limited by a process that is called 'vasopressin escape' that counters the water-retaining action of vasopressin and allows the kidneys to excrete more free water despite sustained high levels of circulating vasopressin (14). There is still little known about the molecular mechanisms underlying this escape. However, Ecelbarger et al. developed an animal model for vasopressin escape in which rats were infused with dDAVP, a V2R-selective agonist of vasopressin, while being fed a liquid diet (15). In this study, they demonstrated that the onset of vasopressin escape coincided temporally with a marked decrease in renal AQP2 protein and mRNA expression in renal collecting ducts. It is worth to mention that the phenomenon of vasopressin escape has never been shown in humans.

Disorders of excessive aquaresis

Disorders of excessive aquaresis, named diabetes insipidus (DI), are characterized by impaired renal water reabsorption caused by the downregulation of AQP2, resulting in polyuria and polydipsia. DI patients can present with hypernatremia, but this is often corrected by an adapted extent of drinking induced by the thirst mechanism. There are four forms of DI (central, gestational, dispogenic and nephrogenic), each with a different set of causes. In central DI, normal AVP production is impaired and this can be caused by mutations in the *AVP* gene, but might also occur due to head trauma or diseases in the hypothalamus or pituitary gland (16). Gestational DI might occur during pregnancy, due to an unusual increase in AVP-degrading enzyme, vasopressinase, that is produced by the placenta (17). Dipsogenic DI is rare and is due to abnormal thirst stimulation in the hypothalamus. The fourth form of DI is nephrogenic DI (NDI) that is caused by the failure of the kidney to respond to AVP stimulation.

There are two forms of NDI, congenital or acquired. The congenital form can be further divided into X-linked, autosomal recessive and autosomal dominant NDI. More than 90% of all congenital NDI patients suffer from X- linked NDI that is caused by loss-of-function mutations in the *V2R* gene (18). This results in principal cells that are insensitive to AVP and a severe urine concentration defect. About 10% of the patients diagnosed with NDI have mutations in the *AQP2* gene of which 90% is of autosomal recessive inheritance. Nearly all mutations in autosomal recessive NDI cause misfolding of the protein that is subsequently trapped in the ER and further degraded by the

proteasomes (19). Autosomal dominant NDI is caused by mutations in the C-terminal tail of AQP2. In this form, AQP2 mutants form heterotetramers with wild-type AQP2 and are missorted to other subcellular destinations (19). This leads to severely decreased amounts of AQP2 in the apical membrane of principal cells. This explains the dominant mode of inheritance of NDI in these patients. The acquired form of NDI is caused by drug therapy (e.g. lithium), hypokalemia, hypercalcemia, malnutrition of protein, and recovery from ureteral obstruction (20, 21). Lithium-induced nephrogenic diabetes insipidus (Li-NDI) is the most common form of NDI and will be further discussed below.

Lithium-induced nephrogenic diabetes insipidus (Li-NDI)

Lithium is the main treatment of bipolar disorder that is a severe mental illness that affects about 2% of the world's population (22, 23). Patients suffer from a disturbance of mood with periods of depression or elation. This has a severe impact on the lives of most patients, demonstrated by the fact that more than 30% of bipolar patients attempt suicide during their lifetime (24, 25). Moreover, the annual direct and indirect economic burden of bipolar disorder was estimated to be 151 billion American dollars in the USA only (26). Lithium is the best-established long-term treatment for bipolar disorder and it has been shown to reduce the risk of manic relapses by 38%, depressive relapse by 28% and the risk of suicide by more than 50% (27, 28). Prior to the introduction of lithium, individuals with manic-depressive illness often required months or years of hospitalization, experienced both a severe disruption in their social lives and a loss of productivity, and frequently committed suicide (29, 30). Those who are treated with lithium often respond well and live a remarkably improved life. At least 1 per 1000 people in western countries uses lithium and, as such, lithium usage saves our society huge amounts of health costs. An important drawback of lithium medication is the development of severe renal side effects (21). On the short term (months-years), lithium causes NDI in ~20% of patients. This inability to concentrate urine causes polyuria, dehydration, thirst, and compensatory polydipsia. Furthermore, dependent on dose and duration of treatment, long term (decades) lithium therapy causes a 6-8-fold increase in the chance to develop chronic kidney disease (CKD) (31-33). Li-NDI and Li-CKD are explained in more detail below.

As explained earlier, urine concentration is mediated by the principal cells of the collecting duct that express AQP2 in their apical membrane and thereby allow transcellular water reabsorption. Lithium treatment causes down regulation of AQP2 on the short-term and loss of principal cells on the long-term (Figure 2) (34, 35). Lithium-induced AQP2 downregulation is a consequence of ENaC-mediated influx of lithium into principal cells, as shown by studies on cultured mpkCCD cells (36). In agreement, ENaC inhibition or ablation prevented the development of lithium-induced NDI (37-39).

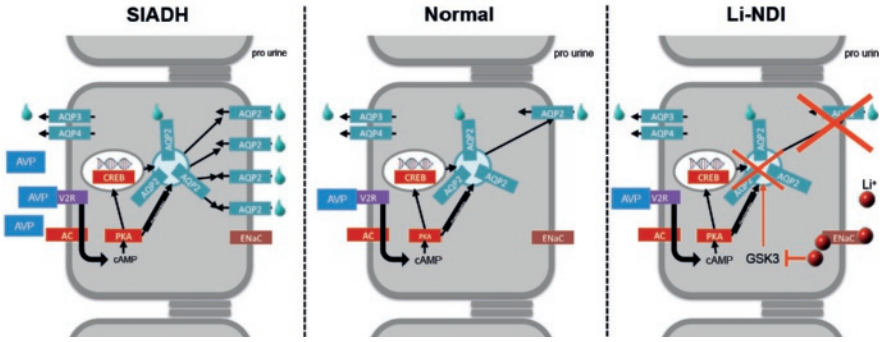

Figure 2. The pathophysiology of AQP2 in SAIDH and Li-NDI. Under physiological conditions, binding of AVP to its V2R results in expression and translocation of AQP2 to the apical membrane thereby allowing water reabsorption from pro-urine (middle). However, in SIADH (left), plasma AVP levels are high resulting in increased apical abundance of AQP2 and subsequent increased water reabsorption. With Li-NDI, however, lithium enters the principal cells through ENaC and downregulates AQP2 by a mechanism that is most likely GSK3 related (right). Due to the decrease in the abundance of AQP2 in the apical membrane, water reabsorption in the principal cells is reduced.

Lithium inhibits glycogen synthase kinase type 3 (GSK3), a serine/threonine protein kinase regulating many signaling pathways including cell cycle progression, cell differentiation and normal epithelial function and survival (40-44). GSK3 consists of two isoforms (α and β), which are directly inhibited by lithium, but also indirectly, via the increased phosphorylation of serine 9 and 21 on GSK3β and –α, respectively (45). Different studies demonstrated that GSK3 plays an important role in urine concentration and lithium-induced NDI, as the use of other GSK3 inhibitors, structurally different from lithium, also reduced AQP2 abundance in collecting duct cell cultures (36). Furthermore, ablation of GSK3α or -β in mice caused polyuria and a reduced AQP2 abundance, while subsequent lithium treatment in the GSK3α knockout mice only slightly reduced their urine concentrating ability (46, 47). How inhibition of GSK3 by lithium ultimately leads to NDI has not been identified.

Li-induced chronic kidney disease

The most relevant clinical side effect of lithium is the development of CKD, which is marked by development of renal interstitial fibrosis. CKD implies long-standing, and usually progressive, impairment in renal function that is characterized by decrease in glomerular filtration rate. The prevalence of CKD in lithium-using patients is ~1.5%, which is 6-8 times higher than in the general population (33, 48). The duration of lithium treatment is an important factor as the vast majority of CKD patients was

treated for more than 15 years with lithium. Although a report in 2014 suggested that the less-controlled treatment regime for lithium in the 1960s and 1970s likely contributed to the development of CKD, a later report demonstrated that 5% of patients who started lithium treatment after 1980 and continued for 10-29 years also displayed evidence of CKD (32, 49). Whether the current treatment regime reduces the occurrence of lithium-induced CKD as compared to the practices in the 1960s and 1970s remains to be addressed.

Kidney damage in humans and rodents chronically treated with lithium is virtually always characterized by proximal tubular atrophy and chronic interstitial fibrosis (50-53). Some lithium-treated patients also display glomerulosclerosis, but animal studies revealed that this pathology only occurs long after the onset of interstitial fibrosis and tubular atrophy (33, 50, 53-56). Besides these pathological features, a number of lithium treated patients display renal microcysts as shown by histology on biopsies or MRI scans (56, 57). The development of these cysts is likely a direct consequence of lithium uptake by principal cells, as these cysts mainly originate from the distal tubule and collecting duct (56). Renal cyst formation often results from disturbances in the function of the primary cilium (58). As cilium function is dependent on GSK3 activity (58), the high levels of inactive GSK3, as observed in renal tubules and cysts from lithium-treated animals (59), might be the primary cause for renal cyst formation.

Aim of the thesis

The maintenance of water homeostasis is critical for body and cell function. However, this tightly-regulated mechanism is disturbed in diseases such as Li-NDI and SIADH. Therefore, the aim of this thesis was to gain insight into the pathophysiology of water balance disturbances with the focus on renal side effects of lithium and SIADH. Chapters 2-7 focus on the renal effects of lithium, whereas chapters 8 and 9 focus on the role of AQP2 in other renal pathologies

The first chapters focus on the renal side effects of lithium. Beside the downregulation of AQP2 water channel in the collecting duct, lithium treatment decreases the percentage of these cells in the long-term resulting in a phenomenon called collecting duct remodeling, which is paradoxical as lithium induces proliferation in these cells specifically. In **chapter 2**, we investigate the cause of lithium-induced collecting duct remodeling. Moreover, Li-NDI patients are currently treated with amiloride and hydrochlorothiazide. Amiloride blocks the entrance of lithium into the principal cells through ENaC, but hydrochlorothiazide was shown to have anti carbonic anhydrase activity beside the inhibition of the sodium chloride cotransporter (NCC) (60, 61). Accordingly,

in **Chapter 3** we explored whether acetazolamide, that is specific carbonic anhydrase inhibitor, is a better treatment for Li-NDI than co-treatment of amiloride and hydrochlorothiazide. Furthermore, proliferating cells often generate their energy by a process called "aerobic glycolysis", which takes place regardless of tissue oxygen levels. In **Chapter 4**, we investigated whether lithium induces aerobic glycolysis in principal cells of the collecting duct and if the inhibition of glycolysis could serve as an alternative treatment for Li-NDI in mpkCCD cells and mice. One of the metabolites that is extensively produced during aerobic glycolysis and glutaminolysis is succinate. Secreted succinate binds to the succinate receptor 1 (SUCNR1), which is also expressed at the plasma membrane of tubular cells. In **chapter 5**, therefore, we studied the role of SUCNR1 in the development of Li-NDI. Additionally, as mentioned earlier, amiloride blocks the entrance of lithium into the principal cells and prevents Li-NDI. However, it still not known whether amiloride attenuates proliferation and collecting duct remodeling that are induced by lithium. Therefore, in **chapter 6**, we explored the other renal ameliorating effects of amiloride. Furthermore, as long-term lithium treatment is associated with development of renal interstitial fibrosis, in **Chapter 7** we present mice as a model to investigate lithium induced interstitial fibrosis.

In the remaining chapters, we focused on the role of AQP2 water channel in other renal pathologies. In **Chapter 8**, we employed RNA-seq technique to determine pathways involved in the development of syndrome of inappropriate antidiuretic hormone secretion (SAIDH). In **chapter 9**, we employed mpkCCD cells and with the help of an NDI patient lacking AQP2, we tested the potential role of AQP2 in cell migration, proliferation and microcyst formation. Finally, the thesis concludes with a summary and general discussion presented in **chapter 10.**

References

1. Kumar P, Clark M. Clinical Medicine. seventh ed2009.
2. Boron WF, Boulpaep EL. Medical Physiology. second ed: ELSEVIER; 2009.
3. Matsukawa T, Miyamoto T. Angiotensin II-stimulated secretion of arginine vasopressin is inhibited by atrial natriuretic peptide in humans. Am J Physiol Regul Integr Comp Physiol. 2011;300(3):R624-9.
4. Bourque CW. Central mechanisms of osmosensation and systemic osmoregulation. Nat Rev Neurosci. 2008;9(7):519-31.
5. McKinley MJ, Johnson AK. The physiological regulation of thirst and fluid intake. News Physiol Sci. 2004;19:1-6.
6. Bankir L. Antidiuretic action of vasopressin: quantitative aspects and interaction between V1a and V2 receptor-mediated effects. Cardiovasc Res. 2001;51(3):372-90.
7. Mutig K, Paliege A, Kahl T, Jons T, Muller-Esterl W, Bachmann S. Vasopressin V2 receptor expression along rat, mouse, and human renal epithelia with focus on TAL. Am J Physiol Renal Physiol. 2007;293(4):F1166-77.
8. Pearce D, Soundararajan R, Trimpert C, Kashlan OB, Deen PM, Kohan DE. Collecting duct principal cell transport processes and their regulation. Clin J Am Soc Nephrol. 2015;10(1):135-46.
9. Knepper MA, Kwon TH, Nielsen S. Molecular Physiology of Water Balance. N Engl J Med. 2015;373(2):196.
10. Hannon MJ, Thompson CJ. The syndrome of inappropriate antidiuretic hormone: prevalence, causes and consequences. Eur J Endocrinol. 2010;162 Suppl 1:S5-12.
11. Cuesta M, Thompson CJ. The syndrome of inappropriate antidiuresis (SIAD). Best Pract Res Clin Endocrinol Metab. 2016;30(2):175-87.
12. Smith D, Moore K, Tormey W, Baylis PH, Thompson CJ. Downward resetting of the osmotic threshold for thirst in patients with SIADH. Am J Physiol Endocrinol Metab. 2004;287(5):E1019-23.
13. Levtchenko EN, Monnens LA. Nephrogenic syndrome of inappropriate antidiuresis. Nephrol Dial Transplant. 2010;25(9):2839-43.
14. Ecelbarger CA, Murase T, Tian Y, Nielsen S, Knepper MA, Verbalis JG. Regulation of renal salt and water transporters during vasopressin escape. Prog Brain Res. 2002;139:75-84.
15. Ecelbarger CA, Nielsen S, Olson BR, Murase T, Baker EA, Knepper MA, et al. Role of renal aquaporins in escape from vasopressin-induced antidiuresis in rat. J Clin Invest. 1997;99(8):1852-63.
16. Fujiwara TM, Morgan K, Bichet DG. Molecular biology of diabetes insipidus. Annu Rev Med. 1995;46:331-43.
17. Ananthakrishnan S. Diabetes insipidus in pregnancy: etiology, evaluation, and management. Endocr Pract. 2009;15(4):377-82.
18. Wesche D, Deen PM, Knoers NV. Congenital nephrogenic diabetes insipidus: the current state of affairs. Pediatr Nephrol. 2012;27(12):2183-204.
19. Robben JH, Knoers NV, Deen PM. Cell biological aspects of the vasopressin type-2 receptor and aquaporin 2 water channel in nephrogenic diabetes insipidus. Am J Physiol Renal Physiol. 2006;291(2):F257-70.
20. Sands JM, Bichet DG, American College of P, American Physiological S. Nephrogenic diabetes insipidus. Ann Intern Med. 2006;144(3):186-94.
21. Alsady M, Baumgarten R, Deen PM, de Groot T. Lithium in the Kidney: Friend and Foe? J Am Soc Nephrol. 2016;27(6):1587-95.
22. Merikangas KR, Jin R, He JP, Kessler RC, Lee S, Sampson NA, et al. Prevalence and correlates of bipolar spectrum disorder in the world mental health survey initiative. Arch Gen Psychiatry. 2011;68(3):241-51.
23. Merikangas KR, Akiskal HS, Angst J, Greenberg PE, Hirschfeld RM, Petukhova M, et al. Lifetime and 12-month prevalence of bipolar spectrum disorder in the National Comorbidity Survey replication. Arch Gen Psychiatry. 2007;64(5):543-52.
24. Novick DM, Swartz HA, Frank E. Suicide attempts in bipolar I and bipolar II disorder: a review and meta-analysis of the evidence. Bipolar Disord. 2010;12(1):1-9.
25. Anderson IM, Haddad PM, Scott J. Bipolar disorder. BMJ. 2012;345:e8508.
26. Dilsaver SC. An estimate of the minimum economic burden of bipolar I and II disorders in the United States: 2009. J Affect Disord. 2011;129(1-3):79-83.

27. Cipriani A, Pretty H, Hawton K, Geddes JR. Lithium in the prevention of suicidal behavior and all-cause mortality in patients with mood disorders: a systematic review of randomized trials. Am J Psychiatry. 2005;162(10):1805-19.
28. Geddes JR, Miklowitz DJ. Treatment of bipolar disorder. Lancet. 2013;381(9878):1672-82.
29. Bramness JG, Weitoft GR, Hallas J. Use of lithium in the adult populations of Denmark, Norway and Sweden. J Affect Disord. 2009;118(1-3):224-8.
30. Wyatt RJ, Henter ID, Jamison JC. Lithium revisited: savings brought about by the use of lithium, 1970-1991. Psychiatr Q. 2001;72(2):149-66.
31. Dols A, Sienaert P, van Gerven H, Schouws S, Stevens A, Kupka R, et al. The prevalence and management of side effects of lithium and anticonvulsants as mood stabilizers in bipolar disorder from a clinical perspective: a review. Int Clin Psychopharmacol. 2013;28(6):287-96.
32. Aiff H, Attman PO, Aurell M, Bendz H, Ramsauer B, Schon S, et al. Effects of 10 to 30 years of lithium treatment on kidney function. J Psychopharmacol. 2015;29(5):608-14.
33. Bendz H, Schon S, Attman PO, Aurell M. Renal failure occurs in chronic lithium treatment but is uncommon. Kidney Int. 2010;77(3):219-24.
34. Christensen BM, Marples D, Kim YH, Wang W, Frokiaer J, Nielsen S. Changes in cellular composition of kidney collecting duct cells in rats with lithium-induced NDI. Am J Physiol Cell Physiol. 2004;286(4):C952-64.
35. de Groot T, Alsady M, Jaklofsky M, Otte-Holler I, Baumgarten R, Giles RH, et al. Lithium causes G2 arrest of renal principal cells. J Am Soc Nephrol. 2014;25(3):501-10.
36. Kortenoeven ML, Li Y, Shaw S, Gaeggeler HP, Rossier BC, Wetzels JF, et al. Amiloride blocks lithium entry through the sodium channel thereby attenuating the resultant nephrogenic diabetes insipidus. Kidney Int. 2009;76(1):44-53.
37. Christensen BM, Zuber AM, Loffing J, Stehle JC, Deen PM, Rossier BC, et al. alphaENaC-mediated lithium absorption promotes nephrogenic diabetes insipidus. JAmSocNephrol. 2011;22(2):253-61.
38. Batlle DC, von Riotte AB, Gaviria M, Grupp M. Amelioration of polyuria by amiloride in patients receiving long- term lithium therapy. The New England journal of medicine. 1985;312:408-14.
39. Kortenoeven ML, Li Y, Shaw S, Gaeggeler HP, Rossier BC, Wetzels JF, et al. Amiloride blocks lithium entry through the sodium channel thereby attenuating the resultant nephrogenic diabetes insipidus. Kidney Int. 2009;76(1):44-53.
40. Rao R. Glycogen synthase kinase-3 regulation of urinary concentrating ability. Current opinion in nephrology and hypertension. 2012;21(5):541-6.
41. Doble BW, Woodgett JR. GSK-3: tricks of the trade for a multi-tasking kinase. Journal of cell science. 2003;116(Pt 7):1175-86.
42. Force T, Woodgett JR. Unique and overlapping functions of GSK-3 isoforms in cell differentiation and proliferation and cardiovascular development. The Journal of biological chemistry. 2009;284(15):9643-7.
43. Rao R, Zhang MZ, Zhao M, Cai H, Harris RC, Breyer MD, et al. Lithium treatment inhibits renal GSK-3 activity and promotes cyclooxygenase 2-dependent polyuria. AmJPhysiol Renal Physiol. 2005;288(4):F642-F9.
44. Nielsen J, Hoffert JD, Knepper MA, Agre P, Nielsen S, Fenton RA. Proteomic analysis of lithium-induced nephrogenic diabetes insipidus: mechanisms for aquaporin 2 down-regulation and cellular proliferation. ProcNatlAcadSciUSA. 2008;105(9):3634-9.
45. Quiroz JA, Gould TD, Manji HK. Molecular effects of lithium. Molecular interventions. 2004;4(5):259-72.
46. Norregaard R, Tao S, Nilsson L, Woodgett JR, Kakade V, Yu AS, et al. Glycogen synthase kinase 3alpha regulates urine concentrating mechanism in mice. American journal of physiology Renal physiology. 2015;308(6):F650-60.
47. Rao R, Patel S, Hao C, Woodgett J, Harris R. GSK3beta mediates renal response to vasopressin by modulating adenylate cyclase activity. Journal of the American Society of Nephrology: JASN. 2010;21(3):428-37.
48. Aiff H, Attman PO, Aurell M, Bendz H, Schon S, Svedlund J. End-stage renal disease associated with prophylactic lithium treatment. Eur Neuropsychopharmacol. 2014;24(4):540-4.
49. Aiff H, Attman PO, Aurell M, Bendz H, Schon S, Svedlund J. The impact of modern treatment principles may have eliminated lithium-induced renal failure. Journal of psychopharmacology. 2014;28(2):151-4.
50. Walker RJ, Leader JP, Bedford JJ, Gobe G, Davis G, Vos FE, et al. Chronic interstitial fibrosis in the rat kidney induced by long-term (6-mo) exposure to lithium. Am J Physiol Renal Physiol. 2013;304(3):F300-7.

51. Hansen HE, Hestbech J, Sorensen JL, Norgaard K, Heilskov J, Amdisen A. Chronic interstitial nephropathy in patients on long-term lithium treatment. Q J Med. 1979;48(192):577-91.
52. Presne C, Fakhouri F, Noel LH, Stengel B, Even C, Kreis H, et al. Lithium-induced nephropathy: Rate of progression and prognostic factors. Kidney international. 2003;64(2):585-92.
53. Ottosen PD, Sigh B, Kristensen J, Olsen S, Christensen S. Lithium induced interstitial nephropathy associated with chronic renal failure. Reversibility and correlation between functional and structural changes. Acta Pathol Microbiol Immunol Scand A. 1984;92(6):447-54.
54. Walker RG, Escott M, Birchall I, Dowling JP, Kincaid-Smith P. Chronic progressive renal lesions induced by lithium. Kidney Int. 1986;29(4):875-81.
55. Ottosen PD, Nyengard JR, Olsen TS, Christensen S. Interstitial focal fibrosis and reduction in proximal tubular length in adult rats after lithium treatment. Acta Pathol Microbiol Immunol Scand A. 1986;94(6):401-3.
56. Markowitz GS, Radhakrishnan J, Kambham N, Valeri AM, Hines WH, D'Agati VD. Lithium nephrotoxicity: a progressive combined glomerular and tubulointerstitial nephropathy. J Am Soc Nephrol. 2000;11(8):1439-48.
57. Farres MT, Ronco P, Saadoun D, Remy P, Vincent F, Khalil A, et al. Chronic lithium nephropathy: MR imaging for diagnosis. Radiology. 2003;229(2):570-4.
58. Thoma CR, Frew IJ, Hoerner CR, Montani M, Moch H, Krek W. pVHL and GSK3beta are components of a primary cilium-maintenance signalling network. Nat Cell Biol. 2007;9(5):588-95.
59. Kjaersgaard G, Madsen K, Marcussen N, Christensen S, Walter S, Jensen BL. Tissue injury after lithium treatment in human and rat postnatal kidney involves glycogen synthase kinase-3beta-positive epithelium. Am J Physiol Renal Physiol. 2012;302(4):F455-65.
60. Sinke AP, Kortenoeven ML, de Groot T, Baumgarten R, Devuyst O, Wetzels JF, et al. Hydrochlorothiazide attenuates lithium-induced nephrogenic diabetes insipidus independently of the sodium-chloride cotransporter. Am J Physiol Renal Physiol. 2014;306(5):F525-33.
61. Pickkers P, Garcha RS, Schachter M, Smits P, Hughes AD. Inhibition of carbonic anhydrase accounts for the direct vascular effects of hydrochlorothiazide. Hypertension. 1999;33(4):1043-8.

Chapter 2

Lithium causes a G2 arrest of renal principal cells

de Groot T [1], Alsady M [1], Jaklofsky M [1], Otte-Höller I [2], Baumgarten R [3], Giles RH [4] and Deen PMT [1*]

[1] Department of Physiology, Nijmegen Centre for Molecular Life Sciences, and [2] Department of Pathology, Radboud University Nijmegen Medical Centre, Nijmegen, The Netherlands; [3] Society of Experimental Laboratory Medicine, Amersfoort, The Netherlands; [4] Department of Nephrology, University Medical Center Utrecht, The Netherlands.

J Am Soc Nephrol. 2014 Mar; 25(3): 501–510.

Abstract

Vasopressin-regulated expression and insertion of Aquaporin-2 (AQP2) water channels in the luminal membrane of renal principal cells is essential for urine concentration. Lithium, the mainstay treatment of bipolar disorder, affects urine concentrating ability, resulting in ~20% of patients with nephrogenic diabetes insipidus (NDI), a disorder characterized by polyuria and polydipsia. Lithium-induced NDI is caused by AQP2 downregulation and a reduced ratio of principal/intercalated cells. Surprisingly, lithium induces principal cell proliferation, as shown by increased principal cell staining for the proliferation marker PCNA. Here, we studied how lithium-induced principal cell proliferation can lead to a reduced ratio of principal/intercalated cells. 2D and 3D polarized cultures of mouse renal collecting duct (mpkCCD) cells and mice were treated with clinically-relevant lithium concentrations. DNA image cytometry and immunoblotting for proteins of different cell cycle stages revealed that lithium initiated proliferation of mpkCCD cells, but also increased the G2/S ratio, indicating a G2/M phase arrest. Mice treated with lithium for 4, 7, 10 or 13 days developed NDI (polyuria, reduced urine osmolality/AQP2) and demonstrated many PCNA-positive principal cells in the papilla. Remarkably, 30-40% of the PCNA-positive principal cells also stained for pHistone-H3, a late G2/M phase marker, which is around 20% in undisturbed cell proliferation. Our data thus reveal that lithium treatment initiates proliferation of renal principal cells, but that a significant percentage is arrested in the late G2 cycle phase, providing an explanation for the reduced principal/intercalated cell ratio and possibly the molecular pathway for long-term development of lithium-induced renal fibrosis.

Introduction

Lithium is widely used as treatment for bipolar disorders, a common chronic psychiatric illness typically requiring treatment for the rest of the patient's life. An important side effect of lithium treatment, however, is Nephrogenic Diabetes Insipidus (NDI), a disorder in which urine concentration is impaired, resulting in polyuria and polydipsia (1). While lithium treatment for a period of weeks already reduces urine concentrating ability in humans (2), approximately 20% of patients receiving long-term lithium therapy will develop clinically extreme concentration defects resulting in NDI (3). Nevertheless, cessation of lithium therapy is usually not an option because bipolar disorder has a larger impact on the patient's quality of life than NDI. Moreover, due to its efficacy, toxicity profile, and low cost, lithium remains the preferred therapy for bipolar disorders (4).

Urine concentration is regulated by arginine vasopressin (AVP), which is released from the pituitary in response to hypovolemia or hypernatremia. In the kidney, AVP binds its type-2 receptor at the basolateral membrane of principal cells of the collecting duct, leading to the redistribution of aquaporin-2 (AQP2) water channels from intracellular vesicles to the apical membrane. Driven by the transcellular osmotic gradient, water then enters the cell via AQP2 and exits through aquaporin-3 (AQP3) and -4 (AQP4) in the basolateral membrane, resulting in correction of the water deficit and in concentrated urine (5).

Based on studies in rodents, the development of lithium-induced NDI is thought to occur in two phases. In the first short-term phase, lithium causes a decrease in AQP2 expression (6). Lithium mainly enters principal cells through the epithelial sodium channel (ENaC) at the apical surface (6, 7) and consequently accumulates in principal cells due to the low affinity of the basolateral Na^+ efflux pump Na^+/K^+-ATPase for lithium (6, 8). How lithium downregulates AQP2 remains unclear, but likely involves glycogen synthase kinase type 3β (GSK-3β) which is of importance in AVP-regulated antidiuresis and which is inhibited by lithium (9-11). Lithium also affects AQP2-mediated water reabsorption by the elevated tubular release of prostaglandin E2 (PGE_2) (11-13).

In a second phase, lithium reduces the percentage of principal cells in the collecting duct, which are "exchanged" for intercalated cells, involved in acid-base homeostasis. (14) Paradoxically, but in line with increased WNT/βcatenin induced activity,(15, 16) lithium is known to induce proliferation of principal cells (17, 18). Apoptosis or principal-to-intercalated cell conversion could be explanations, but Christensen *et al.* concluded that the number of detected apoptotic events or cells co-staining for principal and intercalating cell marker proteins in lithium-NDI rats was too low to support these explanations (17). In this study, we provide an explanation for this paradox.

Materials and Methods

Animal experiments

Mice (C57bl6/j), 15-20 g, were obtained from Harlan Laboratories and maintained at the animal facility of the Radboud UMC. Mice were divided in 5 groups of 3 male and 3 female mice. Group 1 (control): mice received normal rodent diet (ssniff® R/M-H V1534, ssniff Spezialdiaten GmbH, Germany) for 7 days. Groups 2-5; mice received lithium chloride in a concentration of 40 mmol/kg of chow and were sacrificed after 4 (group 2), 7 (group 3), 10 (group 4) or 13 (group 5) days of lithium exposure. All mice had free access to water, food, and a sodium chloride block. For the last 48 hours of the experiment, mice were housed in metabolic cages in order to measure water intake and urine output during the last 24 hours. Mice were anaesthetized with isofluorothane and, after removal of blood by eye extraction, killed by cervical dislocation, after which the kidneys were removed.

One kidney was fixed for immunohistochemistry by overnight immersion in 4% (wt/vol) paraformaldehyde in PBS, while the other kidney was stored at -20°C for immunoblotting. These experiments were approved by the Animal Experiments Committee of the Radboud University Nijmegen Medical Centre.

Urine was centrifuged at 4000g for 5 min to remove sediment. Urine samples were then analysed for osmolality with use of Micro-Osmometer Model 3320 (Advanced® instruments Inc., Massachusetts, USA).

Cell culture and lithium treatment assay

2D filter model: Murine principal collecting duct (mpkCCD) cells were cultured as described (19). In short, the cells were cultured in a modified defined medium containing DMEM:Ham's F12 1:1 vol/vol; 60 nM sodium selenate, 5 µg/ml transferrin, 2 mM glutamine, 50 nM dexamethasone, 1 nM triiodothyronine, 10 ng/ml epidermal growth factor, 5 µg/ml insulin, 20 mM D-glucose, 2% fetal calf serum, and 20 mM HEPES (pH 7.4). Cells were seeded at a density of $1.5x10^5$ cells/cm^2 on semi-permeable filters (Transwell, 0.4 µm pore size, Corning Costar, Cambridge, MA). After 72 hours, the cells were treated with 1 nM 1-deamino-8-Darginine vasopressin (dDAVP) at the basolateral side to induce AQP2 expression. Simultaneously, cells were incubated with 1 mM lithium chloride at the basolateral side and 10 mM lithium chloride at the apical side. After 4, 7 or 11 days of lithium exposure, the cells were either trypsinized, collected in medium and then used for the DNA image cytometry or peletted and prepared for immunoblotting.

3D spheroid model: MpkCCD cells were prepared at a concentration of $12x10^5$ cells/ml in medium containing 2 nM dDAVP with or without 20 mM lithium chloride, and mixed 1:1 (vol/vol) with Matrigel (Becton Dickinson, Bedford, United Kingdom). Then, 0.36 ml aliquots were plated into 48 well plates (Corning Costar, New York, USA).

The cell/Matrigel mix was incubated at 37°C for 2 hours to allow gelling. Afterwards, the wells were filled with dDAVP-containing medium with/without lithium. After three days, the cells were collected in Recovery medium (Becton Dickinson, Bedford, United Kingdom) and used for DNA Image cytometry or peletted and prepared for immunoblotting.

DNA image cytometry

DNA image cytometry was performed as described (20). In short, the cells were collected in medium and centrifuged at 150g for 10 minutes, after which the pelleted cells were fixed in 4% formalin for 30 minutes. After centrifugation at 150g for 10 minutes, the pellets were collected in PBS. Samples from the spheroid 3D model were then treated with 5 mg/mL pepsin (Sigma Aldrich, Zwijndrecht, The Netherlands) in PBS (pH 1.5 with HCl) for 10 minutes at 37°C. Next, the pellets of nuclei were collected by centrifugation (150g) and counted using a Coulter counter (Beckman Coulter, Woerden, The Netherlands). Subsequently, the suspensions were centrifuged (150g) and the pellets were re-suspended in PBS to a dilution of $4x10^5$ nuclei per ml. A cytospin of $4x10^4$ nuclei /100 µL was prepared (100 µL, 10 min, 100g), followed by fixation in Böhm fixative at room temperature for 60 minutes. Next, the slides were rinsed with methanol, dried to air, incubated in 1 M HCl solution for 60 min at 25°C, washed in distilled water and stained for 60 min in Schiff's reagent. After incubation, the slides were washed for 20 min in running tap water followed by increasing concentrations of alcohol and after washing in xylol mounted with permount (Fisher Scientific, Fair Lawn, USA).

Thereafter, DNA Image cytometry was performed with Q-path DNA software to determine DNA ploidy of the nuclei (Leica Imaging Systems Ltd, Cambridge, UK). The analysis was performed as described (20). Briefly, DNA content of 5000 nuclei was calculated automatically for each sample. Images of overlapping nuclei were manually excluded from the analysis. The data were then further analyzed using the MultCycle™ AV software (Phoenix Flow Systems, Washington, USA). Cell cycle phase was determined according to the consensus criteria of the European Society for Analytical Cellular Pathology (21). In short, the measured Internal Optical density (IOD) of each segmented nucleus is plotted in a histogram and the G1 phase is recognized by a Gaussian peak. G2 and mitotic cells, having twice the normal G1 DNA content produce a Gaussian peak with a mean position of approximately twice of that of the G1 peak. S phase cells are observed just above the position occupied by all the G1 cells and extends to just below the position of the G2 cells. MultiCycle AV (Phoenix flow systems, San Diego, CA, USA) was used to determine the amount of cells in each phase via a deconvolution method and curve fitting.

Immunoblotting

Cells were lysed in Laemmli buffer, incubated at 37°C for 30 minutes, sonicated with a Branson Sonifier (Branson Ultrasonics Corporation, Danbury, USA) and analyzed by SDS-PAGE and immunoblotting as described.(22) As primary antibodies, affinity-purified rabbit R7 AQP2 (1:1500) (23), mouse cyclin B1 (1:1000, Abcam, Cambridge, UK), rabbit Histone-H3 (1:5000, Abcam, Cambridge, UK), rabbit phosphoSer10-Histone-H3 (pHistone-H3; 1:4000, Cell Signaling, Massachusetts, USA), mouse PCNA (1:1000, Abcam, Cambridge, UK), mouse Cdc2 (CDK1; 1:1000, Santa Cruz Biotechnology, Santa Cruz, USA), rabbit phosphoTyr15-cdc2 (p-CDK1; 1:1000, Cell Signaling, Massachusetts, USA), mouse β-actin (1:10000, Sigma, St. Louis, USA), and rabbit cyclin D1 Sp4 (1:800, ImmunoLogic, Duiven, Netherlands) were used. As secondary antibodies 1:10000-diluted goat anti-rabbit or sheep anti-mouse peroxidase-conjugated antibodies were used. Proteins were visualized using enhanced chemiluminescence (ECL; Thermo scientific, Rockford, USA). Pictures of the blots were taken using BioRad Universal Hood II and Quantity I software package (Bio-rad Laboratories Inc., Hercules, USA). Later, blots were stained with coomassie blue G250 (Serva, Heidelberg, Germany) to confirm loading of protein equivalents.

Immunocytochemistry

Culture medium was removed from matrigel-cultured mpkCCD cells and cells were subsequently washed 3 times with ice-cold PBS/0.5 mM $CaCl_2$/1.0 mM $MgCl_2$ and fixed for 30 min at room temperature with 4% w/v paraformaldehyde in PBS. After washing twice with PBS, cells were treated with permeabilization buffer (0.5% v/v Triton X-100 and in PBS with 0.7% w/v gelatin) for 30 min. Then, cells were incubated at 4°C overnight with primary antibodies (1:50 Rb5 AQP2 and 1:500 α-tubulin (Invitrogen, Camarillo, USA) in permeabilization buffer and after washing for 3 times with secondary antibodies conjugated to Alexa dyes (Invitrogen, Paisly, UK) (1:500) for 2-3 hours at 37°C. Finally, cells were mounted in Vectashield containing DAPI (Vector Laboratories, Burlingame, USA) and imaged by confocal microscopy (Olympus FV1000, Center Valley, PA, USA).

Immunohistochemistry

Immunohistochemistry was performed as described (24). In short, the kidneys were removed and incubated O/N in paraformaldehyde (4%) in PBS at 4°C. After fixation, kidneys were dehydrated and embedded in paraffin. Five-micrometer sections were cut, stretched in 37°C water, and dried on gelatin-coated object glass (Menzel Gläser, Braunschweig, Germany) for at least 1 hour at 37°C. After the sections were deparaffinized with xylol and rehydrated with ethanol and water, sections were boiled in 10 mM sodium citrate (pH 6.0) for 30 min. After cooling down in TN buffer (0.15 M NaCl, 0.1 M Tris/HCl, pH 7.5) for 3 hours, sections were incubated for 30 min in 20mM

Glycine in TN buffer and subsequently, after washing, incubated for 30 min with 0.3% H_2O_2 in TN buffer. Next, sections were incubated for 30 min in TNB buffer (TN buffer containing 0.5% (w/v) blocking reagent from NEN Life Science Products, Zaventem, Belgium) and incubated O/N at 4°C with 1:1000 rabbit anti-pHistone-H3 in TNB buffer. Sections were then washed three times with TNT buffer (TN buffer containing 0.05% (v/v) Tween 20) and incubated for 60 min at room temperature with biotin-labeled secondary anti-rabbit antibody (1:1000). After washing with TNT, sections were incubated for 30 min with 1:100 Streptavidin-HRP (TSA Fluorescein System, PerkinElmer, Waltham, USA) in TNB, washed again and incubated O/N at 4°C with 1:100 mouse PCNA and 1:400 rabbit H^+-ATPase (gift from Dr. S. Nielsen, Denmark) in TNB. After washing, sections were incubated with secondary antibodies conjugated to Alexa dyes (1:1000) for 1 hour at 37 °C, washed again and incubated O/N at 4°C with 1:100 guinea pig AQP4. Next day, sections were washed, incubated with an Alexa-conjugated secondary antibody against guinea pig for 1 hour at 37°C, washed again, and incubated for 7 min with 1:50 Fluorescein Tyramide in Amplification Diluent (TSA Fluorescein System, PerkinElmer, Waltham, USA). After washing and incubation with DAPI (1:10.000 in TN) for 30 min, sections were embedded in Fluoromount G (Southern Biotech, Birmingham, USA).

Statistical analysis

The difference between groups was tested by student t-test and one-way ANOVA corrected by the Newmans-Keuls multiple-comparisons procedure. A p-value ‹ 0.05 was considered statistically significant.

Results

Lithium initiates proliferation of mpkCCD cells

To study lithium-induced NDI *in vitro*, mpkCCD cells were cultured on 2D Transwell filters as described (6, 12) and treated with 1 and 10 mM lithium at the basolateral and apical side, respectively, for 4, 7 and 11 days. Immunoblotting showed significant downregulation of the dDAVP-induced expression of endogenous AQP2 at all time-points (Figure 1A). The effect of lithium on mpkCCD cells was also studied when grown as spheroids, as this condition mimics the physiological 3D structure of the collecting duct (25). Immunoblotting and immunocytochemistry revealed that treatment of spheroid-grown mpkCCD cells with 10 mM lithium for 3 days significantly reduced endogenous AQP2 abundance (Figure 1B and C).

To assess the effect of lithium on proliferation, mpkCCD cell cycle profiles were obtained using DNA image cytometry (Figure 2A) and immunoblotting. In line with lithium-induced proliferation, the 2D model demonstrated a significant decrease in

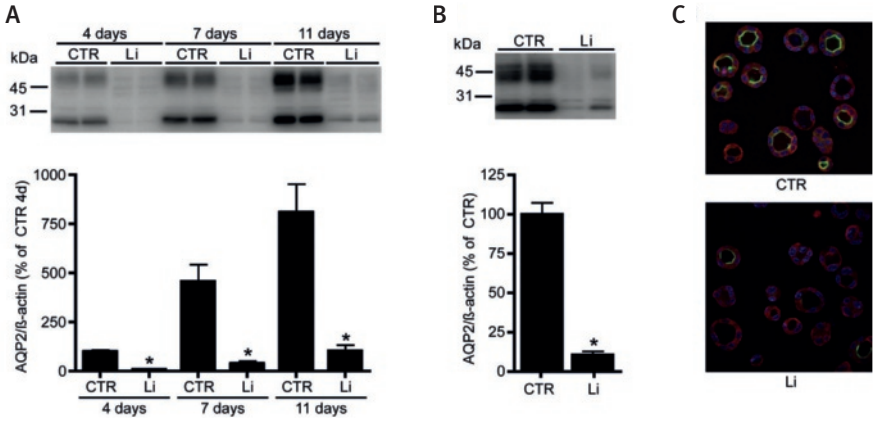

Figure 1. Lithium-induced AQP2 downregulation in two mpkCCD cell models. (A) MpkCCD cells were cultured on Transwell filters to study the long-term effect of lithium (Li) treatment. Following growth to confluency for 96 hours, cells were treated at the basolateral side with 1 mM lithium chloride and at the apical side with 10 mM lithium chloride. After 4, 7 and 11 days of lithium exposure, cells were collected, lysed and immunoblotted for AQP2 (upper panel). Quantification is depicted in the lower panel (n=4 for each condition and time point). (B, C) MpkCCD cells were cultured in Matrigel and treated with (Li) or without (CTR) 10 mM lithium chloride. After three days, cells were lysed and immunoblotted for AQP2 and signals quantified, corrected for β-actin (n=4 for each condition). Figure C demonstrates immunocytochemistry of 3D-grown mpkCCD cells. AQP2 expression is visualized in green, while α-tubulin and the nuclear DAPI-staining are depicted in red and blue, respectively. The asterisk denotes a significant difference ($P<0.05$) from CTR.

cells in the G0/1 phase, which was accompanied by a significant increase of cells in the S and G2 phase at all days tested (Figure 2B). With 3D grown cells, similar data were obtained (Figure 2C). Immunoblotting revealed that in our transwell model lithium significantly increased the abundance of the S/G2 and G2/M phase marker proteins PCNA and phospho-Histone-H3 (pHistone-H3), respectively, but the effect gradually decreased in time (Figure 3A,B). The abundance of cyclin-D1, a protein essential for the transition from the G0/1- to the S-phase and whose proteolysis is mediated by GSK3β activity (26), was strongly elevated upon lithium treatment, while β-actin levels remained constant. With 3D spheroids, the effects of lithium on PCNA, pHistone-H3 and cyclin-D1 levels was similar as in 2D-grown mpkCCD cells, but β-actin abundance was significantly reduced (Figure 3C,D). The reduction in β-actin levels in lithium-treated spheroids is due to a reduced cell number as the total Histone-H3 abundance and area-equivalents of proteins (not shown) were also reduced.

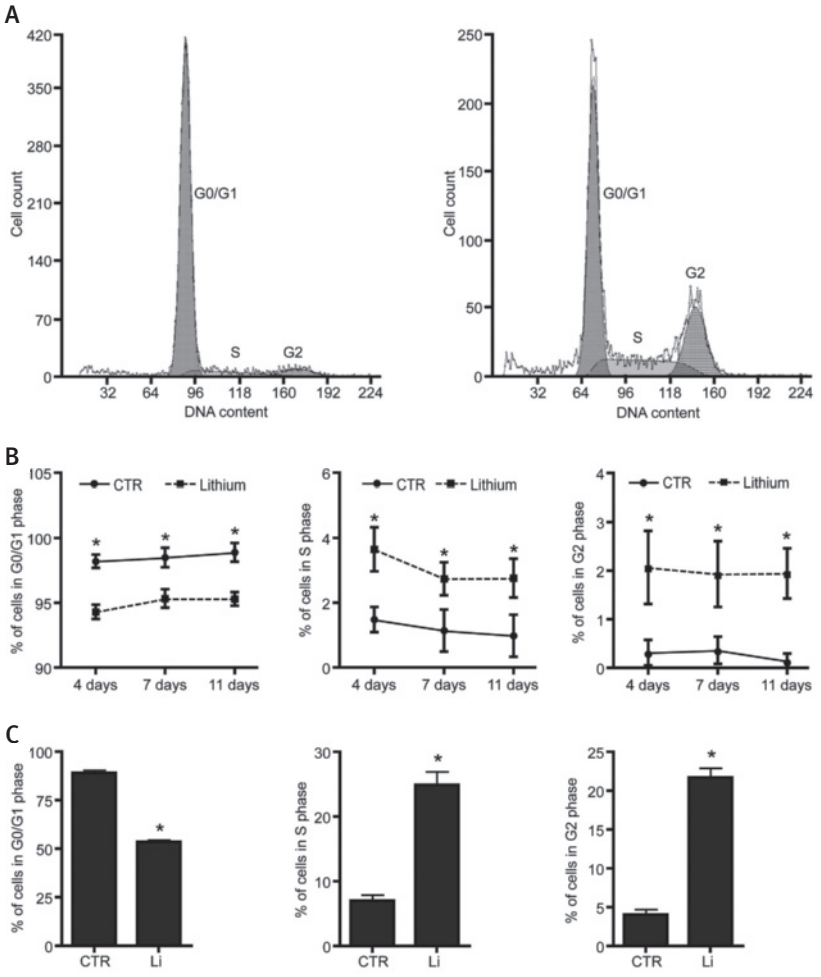

Figure 2. Lithium treatment induces proliferation. (A) Representative cell cycle profiles of Matrigel-cultured mpkCCD cells treated with 10 mM lithium chloride for three days (right panel) or without lithium (control; left panel). The x-axis represents the DNA content of the nuclei population, whereas the y-axis identifies the number of nuclei. The DNA content per cell cycle phase is indicated. (B) Distribution of the cell cycle phases of mpkCCD cells cultured on Transwell filters for 4, 7 or 11 days treated with (Li) or without (CTR) lithium chloride (n=6 for each conditions and time point). (C) Averaged data of the distribution of the cell cycle phases of Matrigel-cultured mpkCCD cells treated without (CTR) or with (Li) lithium chloride (n=4 for each condition). Asterisks indicate to a significant difference ($P<0.05$) as compared to CTR.

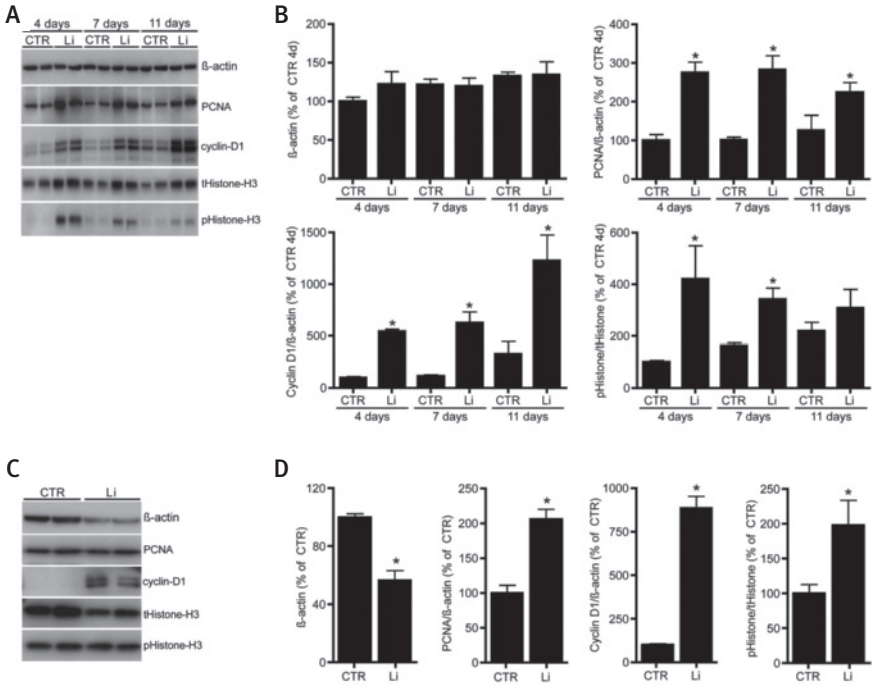

Figure 3. The effect of lithium on different cell cycle markers. MpkCCD cells were cultured and treated with lithium on Transwell filters (A) or in matrigel (C) as described in the legend of Figure 1. lysed and immunoblotted for PCNA, cyclin D1, Histone H3, phospho-Histone H3 (pHistone-H3) and β-actin (B, D) Quantification of protein abundances of filter (B) or matrigel (C) grown cells, corrected for β-actin and related to the abundances of control cells of day 4 (n=4 for each conditions and time point). Asterisks indicate to a significant difference ($P<0.05$) as compared to CTR.

Lithium induces a Chk1-dependent accumulation in the G2 phase

To ensure that cell division occurs flawlessly, the transition from one phase to the next phase of the cell cycle is controlled at the G1/S and G2/M checkpoints.(27) As lithium increased the number of cells present in S and G2 phase, we investigated whether lithium affects the G2/M transition step; we therefore assessed the percentage of cells in the G2 phase relative to all cells in the S and G2 phase. Interestingly, in both cell models, we observed a significant accumulation of cells in the G2 phase after lithium treatment as compared to the control situation (Figures 4A, D). Importantly, this percentage remained significantly elevated at all time-points tested (Figure 4A), demonstrating that the G2 cell cycle arrest was sustained for these cells. Subsequent

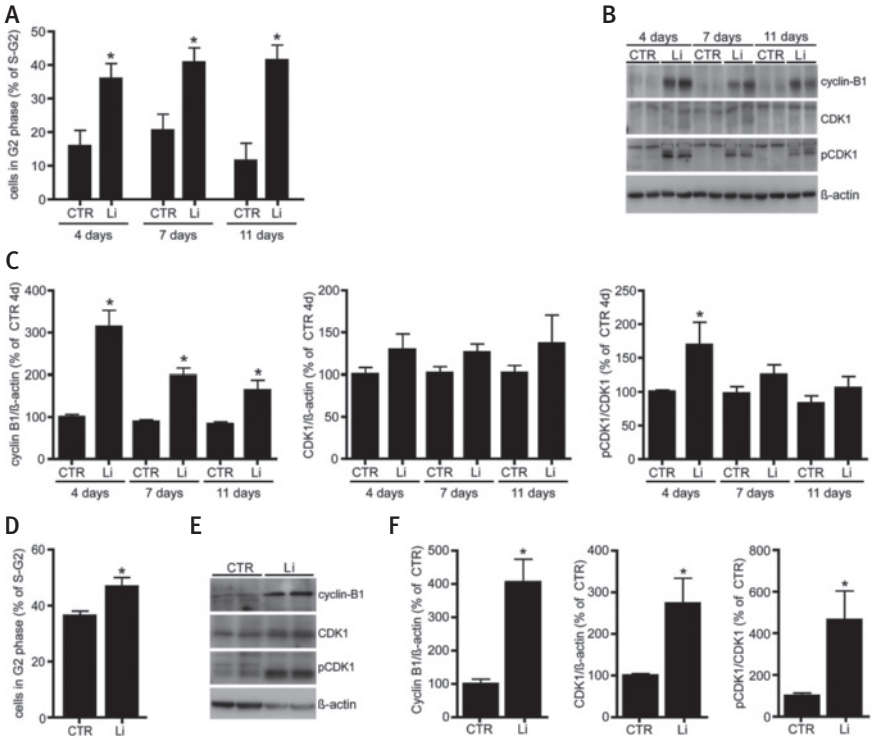

Figure 4. Lithium treatment of mpkCCD cells causes accumulation in G2 phase. MpkCCD cells were cultured and treated with lithium on Transwell filters (A-C) or in matrigel (D-F) as described in the legend of Figure 1 and the percentage of cells in the G2 phase was determined (A,D; transwell: n=6 for each conditions and time point; matrigel: n=4 for each condition). Cell lysates of Transwell filter-cultured (B) or matrigel-cultured (D) cells were lysed and immunoblotted for cyclin B1, CDK1, pCDK1 and β-actin. (C,F) Quantification of protein abundances of filter (B) or matrigel (E) grown cells, corrected for β-actin and related to the abundances of control cells of day 4 (n=4 for each conditions and time point). Asterisks indicate to a significant difference ($P<0.05$) as compared to CTR.

assessment of several proteins essential for G2/M transition revealed that in both models cyclin-B1 and phospho-CDK1 protein levels were significantly increased (Figures 4B, C, E, F). Comparison between the two model systems demonstrated that the abundance of cyclin-B1 and phospho-CDK1 gradually declined over time in the 2D model and that the abundance of CDK1 was only elevated in the spheroid culture system.

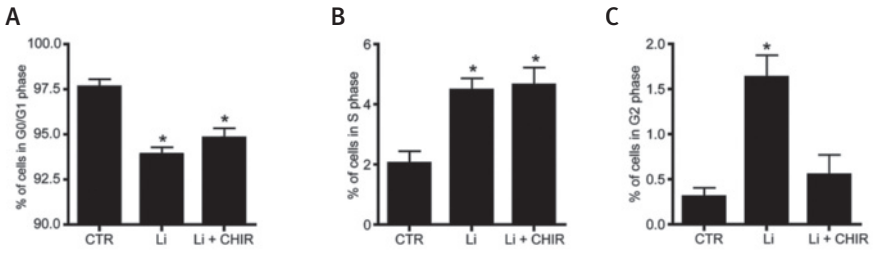

Figure 5. Chk1 kinase blockage prevents lithium-induced cell cycle arrest. MpkCCD cells were grown and treated with or without lithium (Li) on transwells for 4 days as described in the legend of Figure 1 Cells treated with lithium were cultured in the presence or absence of 500 nM of the Chk blocker CHIR-124. Then, cells were trypsinized, stained and analyzed by DNA image cytometry (n=5). The asterisk denotes a significant difference ($P<0.05$) from CTR.

Because a G2 cell cycle arrest is often coupled with activation of checkpoint kinase 1 (Chk1) (28), the involvement of Chk1 was studied by use of the selective Chk1 inhibitor CHIR-124. Treatment of mpkCCD cells with 500nM CHIR-124 for the last 4 days did not affect the lithium-induced reduction of cells in the G0/G1 phase or increase of cells present in S-phase. However, the lithium-induced increase in cells present in the G2 was abolished in cells treated with CHIR-124, demonstrating an essential role for Chk1 in lithium-induced G2 accumulation (Figure 5).

In vivo lithium treatment induces a G2 cell cycle arrest of principal cells

Our *in vitro* data revealed that, besides proliferation, lithium induced a G2/M phase cell cycle arrest. To investigate whether lithium also caused a G2 cell cycle arrest *in vivo*, mice were treated with or without 40 mmol lithium/kg food for 4-13 days. As anticipated, lithium treatment caused a time-dependent increase in urine volume (Figure 6A) and decrease in urine osmolality (Figure 6B). Of note and for unexplained reasons, at 13 days of lithium treatment, the urine volume decreased as compared to 10 days, but was still significantly increased as compared to controls. Immunoblotting confirmed a parallel reduction in AQP2 abundance (Figure 6C). Subsequently, kidney sections were co-stained with antibodies against AQP4, H^+-ATPase, PCNA and pHistone-H3 to mark principal cells, intercalated cells, proliferation, and the late G2 phase of the cell cycle, respectively. As reported earlier (17), lithium strongly increased the number of cells positive for PCNA, being most pronounced at the inner stripe of the outer medulla (ISOM). A representative staining of the ISOM of mice treated for 7 days with lithium is given in Figure 7A. Counting collecting duct cells (~500 cells/mouse) in the ISOM demonstrated that the principal/intercalated cell ratio had the tendency to decrease with longer lithium exposure (3.1 (± 0.1) at day 0 to 2.6 (± 0.5) at day 13), but

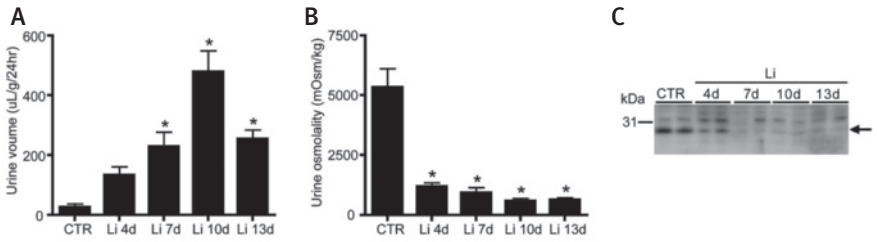

Figure 6. Lithium-treated mice develop nephrogenic diabetes insipidus. Mice were exposed to food without (CTR) or with 40 mM lithium chloride/kg food for 4, 7, 10 and 13 days. Mice were placed in metabolic cages for 48 hours and urine output (A) and urine osmolality (B) was determined during the last 24 hours (n=6 per time points for CTR and Li 4-10 days, n=5 for Li 13 days). (C) AQP2 immunoblotting data of whole kidneys of (CTR) and lithium chloride treated (Li) mice. The asterisk denotes a significant difference ($P<0.05$) from CTR.

did not reach significance (Figure 7B). The percentage of PCNA-positive principal cells changed from 0% at day 0 to 25%, 58%, 26% and 27% at days 4, 7, 10 and 13, respectively (Figure 7B). This was higher than of intercalated cells, as the percentage of PCNA-positive intercalated cells changed from 0 at day 0 to 4%, 12%, 23% and 20% on days 4-13.

To assess whether the PCNA-positive principal and/or intercalated cells were accumulating in the late G2 phase, cells with pHistone-H3-positive nuclear foci (Figure 7A) were counted. The percentage of PCNA-positive principal cells in the late G2 phase changed from 17% at day 4 to 36%, 27% and 38% at days 7, 10 and 13, respectively (Figure 7C). For the intercalated cells, these numbers ranged from 51% to 34% and 30% at days 7, 10 and 13 (Figure 7C). The percentages for PCs and ICs at day 7 and for PCs at day 13 were significantly elevated compared to the percentage of pHistone-H3-positive PCNA-positive cells found in a renal cell population of non-treated mice (22%; reference value obtained from Yang et al(29)). Note that percentages for pHiston-H3-PCNA-positive PC and IC cells for t=0 and for t=4 days for IC cells could not be given, because of the too low number of PCNA-positive cells. Of note, at 10 days a small subset of cells (2.5%) expressed marker proteins of intercalated and principal cells (Figure 7D).

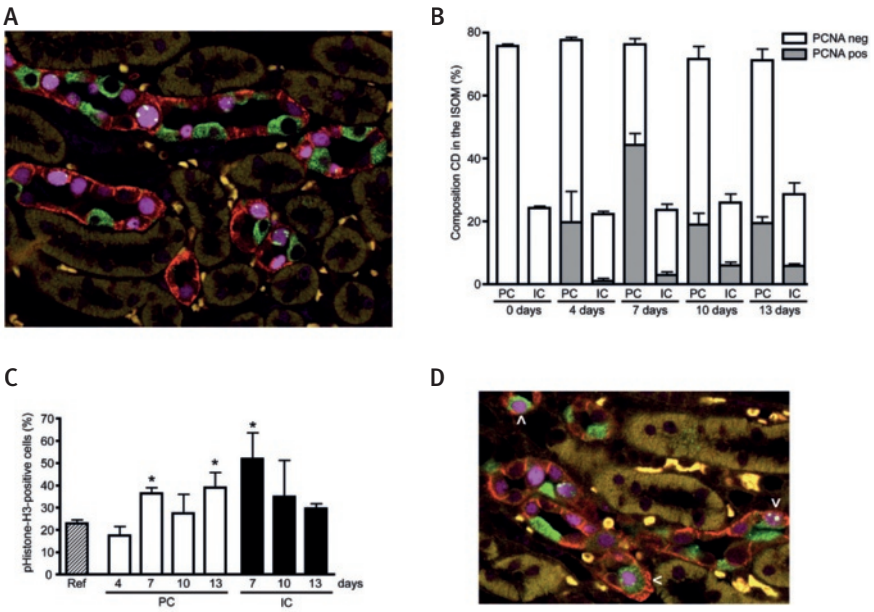

Figure 7. Lithium causes a G2 cell cycle arrest of principal cells *in vivo*. Kidneys of mice treated or not with lithium chloride as described in the legend of Figure 6 were isolated, fixed, paraffin-embedded, sectioned, and subjected to immunohistochemistry. Simultaneous staining was done for AQP4 (principal cell [PC]; red), H^+-ATPase (intercalated cell [IC]; green), PCNA (nucleus; purple), and pHistone-H3 (G2 cell cycle phase; green). (A) representative immunohistochemical staining of ISOM area of a mouse treated for 7 days with lithium. (B) The principal-intercalated cell composition (in % of the total number of cells) of the collecting duct of the inner stripe of the outer medulla (ISOM) of mice treated for 0-13 days (indicated) with lithium and the % of PCNA-positive cells in PC and IC cells. For each time point ~500 collecting duct cells per mouse for in total 3 mice were counted. (C) Percentage of positive pHistone-H3 cells from the PCNA positive population at day 4-13. The asterisk denotes a significant difference ($P<0.05$) from the reference value, obtained from a renal cell population of non-treated mice. (D) Immunohistochemical staining of a kidney after 10 days of lithium treatment. The arrow indicates cells that stain for markers of both intercalated and principal cells.

Discussion

Lithium enhances G1/S cell cycle progression

In this study the 3D spheroid cell model was used for the first time to study the effect of lithium on AQP2 regulation. It is stated that cells grown in 3-dimensions (i.e. spheroids) are more like renal tubules and can thereby reach a higher level of epithelial

polarity compared to 2D cell culture (30). However, in our study the percentage of 2D cells in the S-G2 phase (2%) was more similar to *in vivo* as compared to spheroids (~12%). Therefore, we rather see the spheroid-grown cells as an alternative model for 2D-grown cells instead of a better model. Lithium treatment of mpkCCD cells grown as polarized monolayer or as spheroids increased the number of cells in S and G2 phase. This was accompanied by an enhanced expression of the proliferation markers PCNA and cyclin D1, which was also found at the later time points of 7 or 11 days. The sustained effect of lithium on cell cycle progression is in line with the progressive decline of collecting duct function and morphology in rodents treated with lithium (31). In addition to our mpkCCD model, we observed a stimulatory effect of lithium on the initiation of cell division in mice, as demonstrated by the high number of cells positive for PCNA. At day 4 and day 7 of lithium treatment a large number of principal cells was positive for PCNA (25% and 58% respectively), while these percentages were much smaller for intercalated cells (4% and 12%) or for both cell types in control mice, in which a negligible number of PCNA positive cell was found. This is in agreement with earlier findings (9, 17). The percentages of PCNA positive cells are similar between both cell types at 10 and 13 days. The observation that lithium first initiates proliferation of principal cells and only later of intercalated cells indicates that there might be two different mechanisms by how lithium induces proliferation of both cell types.

Lithium induces a Chk1-dependent G2 cell cycle arrest

At clinically relevant concentrations (1 mM basolateral and 10 mM apical) we show here for the first time that lithium causes a G2 phase arrest of polarized collecting duct cells. This cell cycle arrest is likely the cause of the reduced β-actin abundance in the lithium-treated spheroids, as it prevents the continuation of cell division, leading to a reduced number of cells. Protein levels of cyclin B1 and CDK1 in the lithium-treated mpkCCD cells were elevated, suggesting that CDK1-cyclin complex formation, essential for cell cycle progression through the G2 phase, was not affected by lithium. Next, we observed that lithium caused an accumulation of the Tyr15-phosphorylated form of CDK1. CDK1 phosphorylation should indeed take place after complex formation, however this complex will remain inactive until the phosphate is removed. This final and essential step of the removal of the inhibitory phosphate is performed by cdc25 phosphatase, which in turn is negatively regulated by Chk1 (32). The accumulation of pCDK1 upon lithium treatment suggests that removal of the phosphate did not take place, supporting a role for the cdc25-Chk1 signaling pathway in lithium-induced G2 phase arrest. Indeed, treatment with 500 nM CHIR-124, a selective Chk1 inhibitor (33), prevented the G2 phase arrest induced by lithium, indicating to the involvement of Chk1 kinase in the lithium-induced G2 phase arrest. These findings are in line with data of Wang et al. (2008), who showed that lithium enhanced the activity of Chk1 kinase in 7721 cells (34). How lithium increases Chk1 activity is unknown.

Besides mpkCCD cells, our data indicate that lithium also induced a G2 cell cycle arrest *in vivo*. Using the pHistone-H3 positive foci as a marker for late G2 phase, we found that 30-40% of principal cells were in the late G2 phase during the 7-13 days of lithium treatment, which is markedly higher than found in renal tubular cells (~20%) in non-treated 8-10 weeks old male BALB/c mice (29). Thus, lithium also induced a G2 phase arrest *in vivo*. The question whether chronic lithium treatment for months or years would lead to a sustained cell cycle arrest was not answered by our study, as the mice received lithium for a maximum of 13 days. However, we did not see any decrease in the percentage of arrested principal cells during the time course 7-13 days in mice or in cells treated for 4-11 days with lithium. Interesting in this aspect are the findings of Kling *et al*. who demonstrated an increased presence of nuclear variation (irregular size and shape) of collecting duct cells in rats treated with lithium for 3, 9 and 18 weeks (31). These data are consistent with cells arrested in the G2 phase because an altered nuclear morphology in G2-arrested cells has been previously documented (35-37). The consequences of such a prolonged G2 cell cycle arrest are not fully understood, although recent investigations of different acute kidney injury models indicate that activation of c-jun NH_2-terminal (JNK) signaling in G2-arrested cells can lead to renal fibrosis due to the upregulation of profibrotic cytokines, including transforming growth factor-β1 (TGF-β1) (29). As fibrosis and chronic kidney disease are also observed after long-term lithium treatment (38), and lithium has been shown to activate JNK signaling (16) and stimulate TGF-β1 production in the collecting duct (38), the role of G2-arrested cells in lithium-induced fibrosis should be further investigated.

Various studies demonstrated that lithium increased the number of principal cells incorporated with ^{3}H-thymidine or positive for PCNA and concluded that lithium enhances proliferation of principal cells (17, 31, 39). Our study reveals that PCNA positive cells are not necessarily proliferating and that additional proof is required to assess whether cells are actually dividing or whether their cell cycle is arrested. We also noted that the small number of PCNA positive intercalated cells also exhibited a higher percentage of pHistone-H3 positivity than cells with unaffected cell division. Considering the generally-accepted view that lithium cannot enter intercalated cells, we do not have an explanation for cell cycle arrest of the intercalated cells. Possibly, the altered cell polarization/proliferation status of its neighboring principal cells might also affect the intercalated cells. Another explanation may be that these intercalated cells are derived from principal cells, as principal cells can transit to intercalated cells (40). Perhaps the pHistone-H3 positive intercalated cells were originally principal cells, but transformed into intercalated cells upon lithium entry. In line with this hypothesis, a small subset of ISOM CD cells (2.5%) at day 10 of lithium treatment expressed marker proteins of intercalated and principal cells.

The G2 arrest of principal cells may contribute to collecting duct remodeling in lithium-induced NDI

Besides the loss of AQP2 expression, lithium treatment induces collecting duct remodeling, in which the ratio of principal-to-intercalated cells decreases (14, 41). We found a tendency of collecting duct remodeling after 13 days of lithium treatment. The paradoxical finding that lithium induces cell proliferation of principal cells, but nevertheless ends up in a reduced principal/intercalated cell ratio is not understood. Christensen et al., being aware of this paradox, checked different options, but only sparsely observed apoptosis of principal cells or conversion into intercalated cells during lithium treatment and therefore excluded these as potential causes for the reduced percentage of principal cells (17). Our study provides an explanation for this paradox as a large proportion of PCNA-positive principal cells is arrested in the late G2 phase, indicating that they do not divide further.

We, however, believe that the G2-phase arrest of principal cells is not the sole factor leading to collecting duct cell remodeling. Different earlier studies demonstrated that lithium treatment of rats induced an increased number of cells in the collecting duct (31, 39, 42). The increased number of cells likely constitutes mostly intercalated cells. The question remains why intercalated cells proliferate. Interestingly, as lithium treatment is known to cause a metabolic acidosis (43-45), this might be the trigger for intercalated cells to divide to get rid of the excess of acid. Accordingly, an acetazolamide-induced metabolic acidosis did indeed stimulate the proliferation of intercalated cells, resulting in a similar collecting duct remodeling as observed during lithium-NDI (46). Thus, the lithium-induced collecting duct remodeling could be explained by a rather stable population of principal cells, which are partly in a cell cycle arrest, and a proliferating population of intercalated cells.

In conclusion, in the present study we demonstrated that lithium not only induces principal cell division *in vitro* and *in vivo*, but also and for the first time, that lithium induces an cell cycle arrest in the late G2 phase, likely involving inhibited Chk1 activity. The lithium-induced cell cycle arrest is likely to contribute to the reduced percentage of principal cells and collecting duct remodeling in developed lithium-induced NDI.

Acknowledgements

We would like to thank Dr. Karolina Andralojc for the analysis of the microscopical images. PMTD is a recipient of VICI grant 865.07.002 of the Netherlands Organization for Scientific research (NWO). This project received support from the VICI grant 865.07.002, a RUNMC grant (2004.55), a grant from the Society of Experimental Laboratory Medicine to PMTD, the Niels Stensen Fellowship to TG, and the EU FP7/2009 Consortium “SYSCILIA” (241955) to RHG.

Statement of competing financial interests

The authors declare that the research was conducted in the absence of any commercial or financial relationships that could be construed as a potential conflict of interest.

References

1. Timmer RT, Sands JM. Lithium intoxication. J Am Soc Nephrol. 1999;10(3):666-74.
2. Walker RJ, Weggery S, Bedford JJ, McDonald FJ, Ellis G, Leader JP. Lithium-induced reduction in urinary concentrating ability and urinary aquaporin 2 (AQP2) excretion in healthy volunteers. Kidney Int. 2005;67(1):291-4.
3. Bendz H, Aurell M. Drug-induced diabetes insipidus: incidence, prevention and management. Drug Saf. 1999;21(6):449-56.
4. Geddes JR, Miklowitz DJ. Treatment of bipolar disorder. Lancet. 2013;381(9878):1672-82.
5. Boone M, Deen PM. Physiology and pathophysiology of the vasopressin-regulated renal water reabsorption. Pflugers Arch. 2008;456(6):1005-24.
6. Kortenoeven ML, Li Y, Shaw S, Gaeggeler HP, Rossier BC, Wetzels JF, et al. Amiloride blocks lithium entry through the sodium channel thereby attenuating the resultant nephrogenic diabetes insipidus. Kidney Int. 2009;76(1):44-53.
7. Christensen BM, Zuber AM, Loffing J, Stehle JC, Deen PM, Rossier BC, et al. alphaENaC-mediated lithium absorption promotes nephrogenic diabetes insipidus. J Am Soc Nephrol. 2011;22(2):253-61.
8. Dunham PB, Senyk O. Lithium efflux through the Na/K pump in human erythrocytes. Proc Natl Acad Sci U S A. 1977;74(7):3099-103.
9. Kjaersgaard G, Madsen K, Marcussen N, Christensen S, Walter S, Jensen BL. Tissue injury after lithium treatment in human and rat postnatal kidney involves glycogen synthase kinase-3beta-positive epithelium. Am J Physiol Renal Physiol. 2012;302(4):F455-65.
10. Rao R, Patel S, Hao C, Woodgett J, Harris R. GSK3beta mediates renal response to vasopressin by modulating adenylate cyclase activity. J Am Soc Nephrol. 2010;21(3):428-37.
11. Rao R, Zhang MZ, Zhao M, Cai H, Harris RC, Breyer MD, et al. Lithium treatment inhibits renal GSK-3 activity and promotes cyclooxygenase 2-dependent polyuria. Am J Physiol Renal Physiol. 2005;288(4): F642-9.
12. Kortenoeven ML, Schweer H, Cox R, Wetzels JF, Deen PM. Lithium reduces aquaporin-2 transcription independent of prostaglandins. Am J Physiol Cell Physiol. 2012;302(1):C131-40.
13. Kwon. Dysregulation of Renal Cyclooxygenase-2 in Rats with Lithium-induced Nephrogenic Diabetes Insipidus. Electrolyte & Blood Pressure. 2007;5:68-74.
14. Christensen BM, Marples D, Kim YH, Wang W, Frokiaer J, Nielsen S. Changes in cellular composition of kidney collecting duct cells in rats with lithium-induced NDI. Am J Physiol Cell Physiol. 2004;286(4):C952-64.
15. Rao AS, Kremenevskaja N, Resch J, Brabant G. Lithium stimulates proliferation in cultured thyrocytes by activating Wnt/beta-catenin signalling. Eur J Endocrinol. 2005;153(6):929-38.
16. Nielsen J, Hoffert JD, Knepper MA, Agre P, Nielsen S, Fenton RA. Proteomic analysis of lithium-induced nephrogenic diabetes insipidus: mechanisms for aquaporin 2 down-regulation and cellular proliferation. Proc Natl Acad Sci U S A. 2008;105(9):3634-9.
17. Christensen BM, Kim YH, Kwon TH, Nielsen S. Lithium treatment induces a marked proliferation of primarily principal cells in rat kidney inner medullary collecting duct. Am J Physiol Renal Physiol. 2006;291(1):F39-48.
18. Rojek A, Nielsen J, Brooks HL, Gong H, Kim YH, Kwon TH, et al. Altered expression of selected genes in kidney of rats with lithium-induced NDI. Am J Physiol Renal Physiol. 2005;288(6):F1276-89.
19. Hasler U, Mordasini D, Bens M, Bianchi M, Cluzeaud F, Rousselot M, et al. Long term regulation of aquaporin-2 expression in vasopressin-responsive renal collecting duct principal cells. J Biol Chem. 2002;277(12):10379-86.
20. van der Avoort IA, van de Nieuwenhof HP, Otte-Holler I, Nirmala E, Bulten J, Massuger LF, et al. High levels of p53 expression correlate with DNA aneuploidy in (pre)malignancies of the vulva. Hum Pathol. 2010;41(10):1475-85.
21. Haroske G, Giroud F, Reith A, Bocking A. 1997 ESACP consensus report on diagnostic DNA image cytometry. Part I: basic considerations and recommendations for preparation, measurement and interpretation. European Society for Analytical Cellular Pathology. Anal Cell Pathol. 1998;17(4):189-200.

22. Kamsteeg EJ, Wormhoudt TA, Rijss JP, van Os CH, Deen PM. An impaired routing of wild-type aquaporin-2 after tetramerization with an aquaporin-2 mutant explains dominant nephrogenic diabetes insipidus. EMBO J. 1999;18(9):2394-400.
23. Deen PM, Croes H, van Aubel RA, Ginsel LA, van Os CH. Water channels encoded by mutant aquaporin-2 genes in nephrogenic diabetes insipidus are impaired in their cellular routing. J Clin Invest. 1995;95(5): 2291-6.
24. van Balkom BW, Boone M, Hendriks G, Kamsteeg EJ, Robben JH, Stronks HC, et al. LIP5 interacts with aquaporin 2 and facilitates its lysosomal degradation. J Am Soc Nephrol. 2009;20(5):990-1001.
25. Otto EA, Hurd TW, Airik R, Chaki M, Zhou W, Stoetzel C, et al. Candidate exome capture identifies mutation of SDCCAG8 as the cause of a retinal-renal ciliopathy. Nat Genet. 2010;42(10):840-50.
26. Diehl JA, Cheng M, Roussel MF, Sherr CJ. Glycogen synthase kinase-3beta regulates cyclin D1 proteolysis and subcellular localization. Genes Dev. 1998;12(22):3499-511.
27. Houtgraaf JH, Versmissen J, van der Giessen WJ. A concise review of DNA damage checkpoints and repair in mammalian cells. Cardiovasc Revasc Med. 2006;7(3):165-72.
28. Lossaint G, Besnard E, Fisher D, Piette J, Dulic V. Chk1 is dispensable for G2 arrest in response to sustained DNA damage when the ATM/p53/p21 pathway is functional. Oncogene. 2011;30(41):4261-74.
29. Yang L, Besschetnova TY, Brooks CR, Shah JV, Bonventre JV. Epithelial cell cycle arrest in G2/M mediates kidney fibrosis after injury. Nat Med. 2010;16(5):535-43, 1p following 143.
30. O'Brien LE, Jou TS, Pollack AL, Zhang Q, Hansen SH, Yurchenco P, et al. Rac1 orientates epithelial apical polarity through effects on basolateral laminin assembly. Nat Cell Biol. 2001;3(9):831-8.
31. Kling MA, Fox JG, Johnston SM, Tolkoff-Rubin NE, Rubin RH, Colvin RB. Effects of long-term lithium administration on renal structure and function in rats. A distinctive tubular lesion. Lab Invest. 1984;50(5): 526-35.
32. Lam MH, Rosen JM. Chk1 versus Cdc25: chking one's levels of cellular proliferation. Cell Cycle. 2004;3(11): 1355-7.
33. Tse AN, Rendahl KG, Sheikh T, Cheema H, Aardalen K, Embry M, et al. CHIR-124, a novel potent inhibitor of Chk1, potentiates the cytotoxicity of topoisomerase I poisons in vitro and in vivo. Clin Cancer Res. 2007;13(2 Pt 1):591-602.
34. Wang XM, Li J, Feng XC, Wang Q, Guan DY, Shen ZH. Involvement of the role of Chk1 in lithium-induced G2/M phase cell cycle arrest in hepatocellular carcinoma cells. J Cell Biochem. 2008;104(4):1181-91.
35. Yang L, Wu S, Zhang Q, Liu F, Wu P. 23,24-Dihydrocucurbitacin B induces G2/M cell-cycle arrest and mitochondria-dependent apoptosis in human breast cancer cells (Bcap37). Cancer Lett. 2007;256(2):267-78.
36. Solhaug A, Holme JA, Haglund K, Dendele B, Sergent O, Pestka J, et al. Alternariol induces abnormal nuclear morphology and cell cycle arrest in murine RAW 264.7 macrophages. Toxicol Lett. 2013;219(1):8-17.
37. Wang Y, Deng L, Zhong H, Wang Y, Jiang X, Chen J. Natural plant extract tubeimoside I promotes apoptosis-mediated cell death in cultured human hepatoma (HepG2) cells. Biol Pharm Bull. 2011;34(6):831-8.
38. Walker RJ, Leader JP, Bedford JJ, Gobe G, Davis G, Vos FE, et al. Chronic interstitial fibrosis in the rat kidney induced by long-term (6-mo) exposure to lithium. Am J Physiol Renal Physiol. 2013;304(3):F300-7.
39. Jacobsen NO, Olesen OV, Thomsen K, Ottosen PD, Olsen S. Early changes in renal distal convoluted tubules and collecting ducts of lithium-treated rats: light microscopy, enzyme histochemistry, and 3H-thymidine autoradiography. Lab Invest. 1982;46(3):298-305.
40. Wu H, Chen L, Zhou Q, Zhang X, Berger S, Bi J, et al. Aqp2-expressing cells give rise to renal intercalated cells. J Am Soc Nephrol. 2013;24(2):243-52.
41. Ecelbarger CA. Lithium treatment and remodeling of the collecting duct. Am J Physiol Renal Physiol. 2006;291(1):F37-8.
42. Ottosen PD, Nyengard JR, Jacobsen NO, Christensen S. A morphometric and ultrastructural study of lithium-induced changes in the medullary collecting ducts of the rat kidney. Cell Tissue Res. 1987;249(2):311-5.
43. Roscoe JM, Goldstein MB, Halperin ML, Wilson DR, Stinebaugh BJ. Lithium-induced impairment of urine acidification. Kidney Int. 1976;9(4):344-50.
44. Perez GO, Oster JR, Vaamonde CA. Incomplete syndrome of renal tubular acidosis induced by lithium carbonate. J Lab Clin Med. 1975;86(3):386-94.

45. Kim YH, Kwon TH, Christensen BM, Nielsen J, Wall SM, Madsen KM, et al. Altered expression of renal acid-base transporters in rats with lithium-induced NDI. Am J Physiol Renal Physiol. 2003;285(6):F1244-57.
46. Welsh-Bacic D, Nowik M, Kaissling B, Wagner CA. Proliferation of acid-secretory cells in the kidney during adaptive remodelling of the collecting duct. PLoS One. 2011;6(10):e25240.

Chapter 3

Acetazolamide attenuates Lithium-Induced Nephrogenic Diabetes Insipidus

de Groot T [1#], Sinke AP [1#], Kortenoeven ML [1&], Alsady M [1], Baumgarten R [2], Devuyst O [3], Loffing J [4], Wetzels JF [5], Deen PMT [1#]

[#]: These authors contributed equally to this work
[&]: present address: Department of Biomedicine, Aarhus University, Aarhus, Denmark

[1] Department of Physiology and [5] Nephrology, Radboud University Medical Center, The Netherlands; [2] Vivium Care Group, Huizen, The Netherlands; [3] Institute of Physiology, Zurich Centre for Integrative Human Physiology, and [4] Anatomy, University of Zurich, Zurich, Switzerland.

J Am Soc Nephrol. 2016 Jul;27(7):2082-91.

Abstract

To reduce lithium-induced nephrogenic diabetes insipidus (lithium-NDI), bipolar patients are treated with thiazide/amiloride, which are thought to induce antidiuresis by a compensatory increased pro-urine uptake in proximal tubules. However, as thiazides induced an antidiuresis in lithium-NDI mice lacking the sodium-chloride co-transporter and alkalinized their urine, this concept was challenged and suggested that inhibition of carbonic anhydrases (CA) conferred the beneficial thiazide effect. Therefore, we here tested the effect of the CA-specific blocker acetazolamide in lithium-NDI.

In collecting duct (mpkCCD) cells, acetazolamide reduced the cellular lithium content and attenuated lithium-induced downregulation of AQP2 through a mechanism different from amiloride. Treatment of lithium-NDI mice with acetazolamide or thiazide/amiloride revealed a similar antidiuresis, increased urine osmolality and AQP2 abundance. The reduced inulin clearance and cortical NHE3 expression demonstrated that the antidiuresis with acetazolamide was partially due to a tubular-glomerular feedback (TGF) response and reduced GFR. The TGF response and/or direct effect on collecting duct principal or intercalated cells may underlie the reduced urinary PGE2 levels with acetazolamide, thereby contributing to the attenuated lithium-NDI. Thiazide/amiloride-treated mice showed hyponatremia, hyperkalemia, hypercalcaemia, metabolic acidosis and increased serum lithium concentrations; side effects also observed in patients, but not seen in acetazolamide-treated mice.

In conclusion, we have shown that CAs activity contributes to lithium-NDI development, that acetazolamide attenuates lithium-induced NDI by inducing a TGF response and through a direct action on collecting duct cells, and that acetazolamide attenuates lithium-NDI development similar to thiazide/amiloride but with less side effects.

Introduction

Lithium is the drug of choice for the treatment of bipolar disorders and is also regularly used to treat schizoaffective disorders and depression. Lithium is a frequently prescribed drug as it is provided to 0.1% of the western population. Unfortunately, in 2-85% of patients, and depending on age, lithium usage leads to nephrogenic diabetes insipidus (Li-NDI), a disorder characterized by an impaired response of the kidney to vasopressin (AVP) leading to polyuria and polydipsia (1-3). Patients with Li-NDI are at risk for dehydration-induced lithium toxicity, and prolonged lithium treatment might lead to cyst formation and end stage renal disease (4). However, cessation of lithium therapy is not an option for most patients with NDI, because bipolar disorder symptoms have a larger impact on the patient's quality of life.

From studies in rats, it became clear that Li-NDI develops in two stages. At short term (10 days), Li-NDI coincides with downregulation of aquaporin-2 (AQP2) water channels, which is due to a reduced AQP2 transcription (5-7). Despite an increased proliferation of the AQP2-expressing principal cells of the collecting duct, long-term lithium treatment (4 weeks) also results in a severe loss of AQP2-expressing principal cells, which might be attributed to a lithium-induced G2/M phase cell cycle arrest (8, 9). This principal cell loss is 'compensated' by an increased number of α-intercalated cells, which are involved in acid secretion (8).

To reduce polyuria in patients receiving lithium, a low-sodium diet together with thiazide and amiloride diuretics is prescribed (10). Amiloride acts on the principal cell epithelial sodium channel (ENaC) and we and others found that amiloride blocks principal cell lithium entry through ENaC, thereby attenuating polyuria in rodents and humans (11-13). Thiazides are known to block sodium and chloride reabsorption via the NaCl co-transporter (NCC) in the renal distal convoluted tubule and the antidiuretic effect has been ascribed to a hypovolemia-induced activation of the renin-angiotensin-aldosterone system (RAAS) and a compensatory increased uptake of sodium and water in proximal tubules. Recently, however, we discovered that thiazide also has an NCC-independent effect, as NCC knockout mice with Li-NDI showed a clear antidiuretic response upon treatment with thiazide (14).

As urine of our thiazide-treated mice was alkalinized and thiazides are derived from carbonic anhydrase (CA) inhibitors (15), our data indicated that the antidiuretic effect of thiazide in Li-NDI may involve CA inhibition. CAs catalyse the hydration of carbon dioxide to form carbonic acid, which then rapidly dissociates to form protons and bicarbonate, and play major roles in pH balance regulation. Here, we show that CAs are indeed involved in lithium-induced AQP2 downregulation and that, by inducing a tubular glomerular feedback response and through direct action on collecting duct cells, the CA-selective drug acetazolamide not only attenuates Li-NDI, but yields superior *in vivo* effects as compared to the presently-used treatment for Li-NDI.

Materials and Methods

Cell culture

MpkCCD cells were cultured as described (16). Cells were seeded at a density of $1.5x10^5$ cells/cm^2 on semi-permeable filters (Transwell, 0.4 µm pore size, Corning Costar, Cambridge, MA) and cultured for 8 days. Unless stated otherwise, the cells were exposed to 1 nM of dDAVP at the basolateral side for the last 96 hr, to induce AQP2 expression. Lithium and compounds were administered as indicated. At the end of the experiment, transcellular electrical resistance and voltage were measured using a Millicell-ERS meter (Millipore corp., Bedford, MA, USA). On day 8, cells were harvested and lysed in Laemmli buffer for western blotting or stored in Trizol reagent (Invitrogen, Carlsbad, CA) at -80°C for RNA-isolation.

Lithium assays

Determination of intracellular lithium concentrations was done as described (11). Shortly, $mpkCCD_{cl4}$ cells were grown on 4.7 cm^2 filters. To determine the extent of lithium contamination from the extracellular side, fluorescein isothiocyanate (FITC) dextran was added to the lithium-containing medium to a final concentration of 10 µM just before harvesting, after which the medium was mixed. Then, the filters were washed three times with iso-osmotic sucrose (pH 7.3) at 4°C and cells were lysed by sonication in 1 ml milli-Q water. Of 800 µl sample, the amount of lithium was determined by flame photometry, from which the total amount of lithium in the sample was calculated.

Of 100 µl sample, the amount of FITC-dextran was measured using spectrofluorophotometry (Shimadzu RF-5301, Japan) at 492 nM (excitation) and 518 nm (emission) wavelengths. By comparing the obtained values with a two-fold FITC-dextran dilution series, the FITC-dextran concentration in each sample was determined, from which the extent of extracellular lithium contamination was calculated. This was subtracted from the total amount to obtain the intracellular lithium amount. With the used FITC-dextran concentration, a contamination above 1:5000 would be detected. To correct for differences in cellular yield, the intracellular lithium amounts were normalized for the protein amount in each sample, which was determined using the Biorad Protein Assay (München, Germany).

Experimental animals

8-10 weeks old female C57Bl6/JOlaHsd mice (Harlan Laboratories, The Netherlands) were maintained in a temperature-controlled room with lights on 8.00 AM and PM. They received normal diet (ssniff R/M-H V1534, ssniff Spezialdiaten GmbH, Soest, Germany) with additions (see below) and water ad libitum for 10 days. For the

experiments, mice were divided into four groups (n = 8), which were treated as follows: Group *1:* Control mice given a normal diet; Group *2:* Normal diet with 40 mmol LiCl /kg of dry food (17). Group *3:* diet of group 2 with 200 mg amiloride (11) and 350 mg hydrochlorothiazide per kg dry food(18). Group 4: diet of group 2 with 180 mg acetazolamide /kg dry food.(19) LiCl, amiloride, hydrochlorothiazide and acetazolamide were solubilized in water and mixed with the chow after which it was dried. All mice had free access to water, food, and a sodium-chloride block.

For the last 48 hr of the experiment, mice were housed in metabolic cages to measure water intake and urine output during the last 24 hr. Mice were anesthetized with isofluorothane after which their blood was removed by orbita extraction. Then, mice were killed by cervical dislocation and the kidneys rapidly removed. One kidney was processed for immunohistochemistry, whereas the other kidney was used for immunoblotting, both as described below. For immunoblotting, the tissue was homogenized using a Polytron homogenizer (VWR international, Amsterdam, The Netherlands) in 1 ml of ice-cold homogenization buffer A (20 mM Tris, 5 mM $MgCl_2$, 5 mM Na_2HPO_4, 1 mM EDTA, 80 mM sucrose and protease inhibitors (1 mM PMSF, 5 µg/ml pepstatin A, 5 µg/ml leupeptin, and 5 µg/ml a-protinin) and cleared from nuclei and unbroken cells by centrifugation at 4000 x g for 15 min and diluted in Laemmli buffer to a final protein concentration of 1 µg/µl.

Determination of glomerular filtration rate using FITC-inulin.

To determine the glomerular filtration rate via the FITC-inulin clearance method (20, 21) we used mice as described above and these mice were also treated as before (n=8/group). Four days after the start of the diet, minipumps (Model 2001, Alzet) containing 3% FITC inulin were subcutaneously implanted in the isofluorane-anesthetized mice. At treatment days 9 and 10, mice were housed in metabolic cages and 24 hr urine was collected in amber tubes at day 10. During this 24 hr, metabolic cages and urine collection tubes were covered with aluminium foil to prevent exposure to light. Traces of left FITC-inulin urine in metabolic cages were added to the collected urine by washing the cage with 5 mL of 500 mmol HEPES buffer. On day 10, mice were anesthetized with isofluorane, blood was collected by retro-orbital bleeding and mice were killed by cervical dislocation. Urine fluorescence was determined using a Cytofluor II fluorescence multi-well plate reader (PerSeptive Biosystems, Framingham, MA, USA) with 485 nm excitation and 538 nm emission. The excretion rate of inulin (24 hr urinary fluorescence counts/plasma fluorescence counts per ml) was taken as the GFR.

Blood and urine analysis

Whole blood was analyzed immediately for sodium, potassium, hematocrit, and pH using the EG7+ cartridge and the I-Stat Clinical Analyzer (Abbott BV, Hoofddorp, The Netherlands). The remaining blood was collected in a BD microtainer SST tube (REF

#365968, Becton Dickinson BV, Breda, The Netherlands) for serum and centrifuged at 10.000 x g for 3 min to sediment the red blood cells. Serum and urine samples were analyzed for osmolality using an osmometer (Fiske, Needham Heights, MA), and electrolyte concentrations were measured on a Synchron CX5 analyzer (Beckman Coulter, Brea, CA), following the manufacturer's protocols. Urine PGE2 levels were determined by measuring stable PGE2 metabolite (PGEM) after chemical derivation of PGE2 and its primary metabolites, 13,14-dihydro-15-keto PGE2 and 13,14-dihydro-15-keto PGA2, to the single PGEM compound. PGEM concentrations were determined with the prostaglandin E metabolite EIA kit (Cayman Chemical Company, Ann Arbor, MI, USA) according to the manufacturer's instructions.

Immunoblotting

MpkCCD cells from 1.13 cm^2 filters were lysed in 200 µl Laemmli buffer and sonicated. MpkCCD lysate and 5-10 µg kidney material in Laemmli were denatured for 30 min at 37°C. Protein concentration was determined using the BioRad protein assay (Bio-Rad Laboratories GmbH, München, Germany), according to manufacturer's instructions. SDS-PAGE, blotting and blocking of the PVDF membranes were done as described (22). Membranes were incubated for 16 hr at 4°C with 1:2000 affinity-purified rabbit pre-c-tail AQP2 antibody recognizing aa 236-255,(23) in Tris-Buffered Saline Tween-20 (TBS-T) supplemented with 1% non-fat dried milk. In an identical way, other blots were incubated with a rabbit CA12 antibody (kind gift from Prof. William S. Sly, Saint Louis University School of Medicine, St. Louis, MO, USA) and a rabbit CA2 antibody (Abcam, Cambridge, UK). After washing in TBS-T, all blots were incubated for 1 hr with 1:5000-diluted goat anti-rabbit IgG's (Sigma, St. Louis, MO) as secondary antibody coupled to horseradish peroxidase. Proteins were visualized using enhanced chemiluminescence (ECL, Pierce, Rockford, IL). Densitrometric analyses were performed using Biorad quantification equipment (Bio-Rad 690c densitometer, Chemidoc XRS) and software (QuantityOne, Bio-Rad Laboratories GmbH, München, Germany). Equal loading of the samples was confirmed by staining of the blots with Coomassie blue.

Immunohistochemistry

Kidneys were fixed by immersion for 24h in 4% paraformaldehyde in 0.1M phosphate buffer at 4°C, embedded in paraffin and cut into 3-4 µm-thick sections. After de-paraffinization, sections were placed into a microwave oven and heated for 10 minutes at 98°C in 0.01 M sodium-citrate buffer (pH 6.0) for antigen retrieval. Subsequently, sections were incubated overnight at 4°C with 1:80000-diluted rabbit polyclonal AQP2 antibodies or 1:2000-diluted rabbit polyclonal H^+-ATPase antibodies as described (24, 25). The bound primary antibodies were revealed with Cy3-coupled goat-anti rabbit IgG (Jackson ImmunoResearch Laboratories, PA, USA). To check for unspecific binding of primary or secondary antibodies, incubations with non immune sera or

without any primary antibodies were performed. All control experiments were negative. Cryosections were studied by epifluorescence using a Leica microscope (Wetzlar, Germany). Connecting tubules and cortical collecting ducts were distinguished based on their specific localization in the cortical labyrinth and the medullary rays, respectively. Images were acquired with a charge-coupled device camera. For overviews, single images were taken with the automated scanning mode of the microscope and afterwards stitched using the Leica Application Suite. Digital images were processed electronically with Adobe Photoshop and Microsoft Powerpoint software. Adjustments for brightness and contrast were kept constant for each kidney section.

Statistics

One-way ANOVA with Bonferroni correction was applied. A p value of less than 0.05 was considered significant. Data are presented as mean and standard error of the mean (SEM).

Study approval

All animal studies (DEC nr 2011-010) were approved by the Animal Ethical Committee of the Radboud University Medical Center.

Results

The clinically used drug acetazolamide attenuates lithium-induced downregulation of AQP2 in mpkCCD cells

MpkCCD cells are mouse collecting duct cells showing dDAVP-dependent expression of endogenous AQP2 and we have shown that thiazide reduces lithium-induced downregulation of AQP2 in these cells, while they lack NCC expression (7, 11, 14). As our previous animal studies suggested that thiazides reduced polyuria in our NCC knockout mice by inhibiting CAs, we wanted to test whether acetazolamide, a stable CA inhibitor and commonly used in patients, could also rescue lithium-induced AQP2 downregulation in mpkCCD cells. Indeed, whereas lithium again reduced the AQP2 abundance in mpkCCD cells, acetazolamide significantly attenuated this down-regulation (Fig. 1A, B). As our data suggest that both thiazide and acetazolamide influence lithium-reduced AQP2 abundances through CAs, we assessed whether the action mechanism of acetazolamide differs from that of amiloride. If so, we anticipated that acetazolamide and amiloride together should attenuate the lithium-induced AQP2 downregulation better than cells treated with amiloride only. Indeed, immunoblotting revealed a significantly higher AQP2 abundance in cells treated with amiloride and acetazolamide as compared to amiloride only (Fig. 1C, D). Others and we discovered

that ENaC is the main cellular entry site for lithium and that amiloride strongly reduced the intracellular lithium levels in mpkCCD cells (11, 14). Determination of the intracellular lithium concentrations revealed that amiloride indeed reduced the intracellular lithium concentration with 87%, while this was only 30% with acetazolamide (Fig. 1E). The mean intracellular lithium concentration was nominally lower with amiloride/acetazolamide; however, there was no significant difference (p=0.23). Transcellular transport of sodium and potassium via ENaC, ROMK and the Na/K-ATPase is electrogenic and therefore generates a transcellular voltage (Tv) over mpkCCD cell monolayers. Lithium slightly reduced the Tv, which was not further decreased with acetazolamide (Fig. 1F). In contrast, amiloride completely blocked the Tv in lithium-treated mpkCCD cells. Together, these data reveal that the CA-specific inhibitor acetazolamide attenuates lithium-induced downregulation of AQP2 *in vitro* and that its mechanism of action is different from that of amiloride.

Acetazolamide attenuates development of lithium-induced NDI in mice

To investigate whether acetazolamide attenuates development of Li-NDI, mice were maintained on lithium chow only or on lithium combined with acetazolamide or thiazide/amiloride for 10 days. As reported (11, 26), mice treated with lithium developed severe polyuria and polydipsia, combined with a significantly-reduced urine osmolality (Fig. 2A-C). Interestingly, acetazolamide treatment induced a significant antidiuresis and increase in urine osmolality, which was slightly, but not significantly, better than in mice treated with thiazide/amiloride. Consistent with the induced antidiuresis, water intake was significantly reduced with the acetazolamide treatment as compared to lithium only.

As long-term lithium treatment coincides with reduced AQP2 and increased H^+-ATPase abundance in the kidney (6), we also analyzed their abundances. Immunoblot analysis revealed that lithium reduced AQP2 abundance (Fig. 3A, B), which was significantly attenuated by both acetazolamide and thiazide/amiloride (Figs. 3A-D). With acetazolamide or thiazide/amiloride, however, AQP2 levels did not return to control levels. H^+-ATPase levels were similar for all groups (Supplementary Figs. 1A-D), which is in line with the notion that lithium-induced collecting duct remodeling is not present after 10 days of lithium treatment in rodents (9, 26).

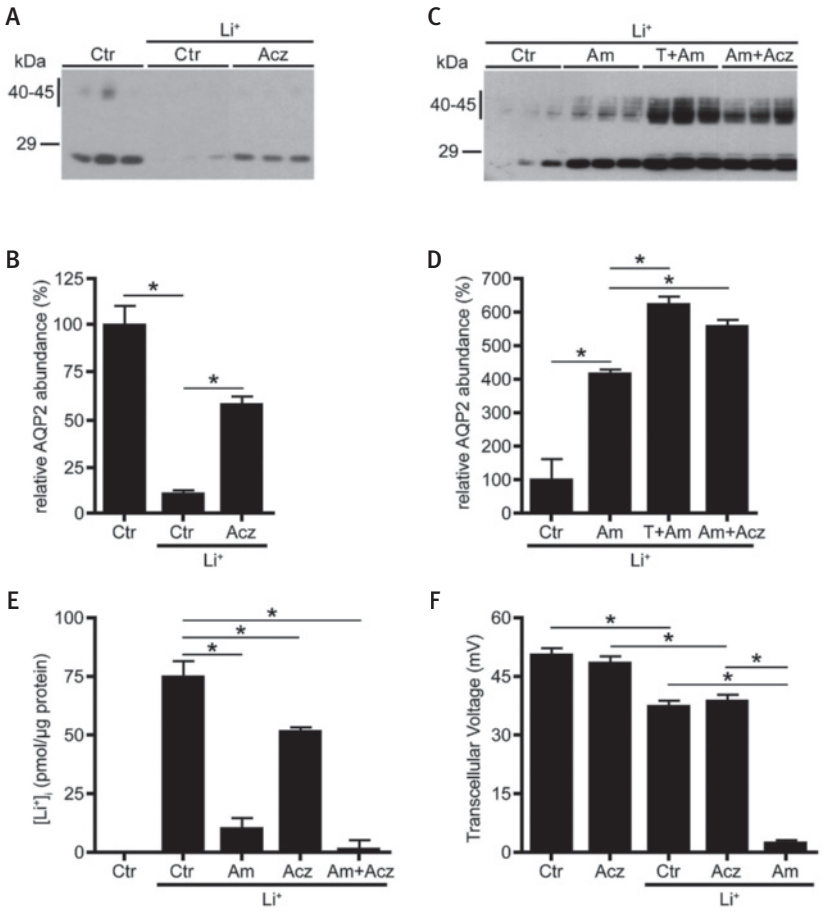

Figure 1. Acetazolamide reduces lithium-induced downregulation of AQP2 abundance in mpkCCD cells. Native mpkCCD cells were grown to confluence for 4 days and subsequently exposed to 1 nM dDAVP for another 4 days. During the last 2 days, cells were incubated in the absence (Ctr) or presence of lithium only (Li+) or with lithium and 100 µM acetazolamide (Acz), 10 µM amiloride (Am), 100 µM hydrochlorothiazide and amiloride (T+Am) or amiloride and acetazolamide (Am+Acz). At the basolateral and apical side, final concentrations of 1 and 10 mM lithium were used, respectively. Following measurements of transcellular voltage (**F**), cells were lysed and subjected to AQP2 immunoblotting (**A**, **C**). Molecular masses (in kDa) are indicated. The signals for non-glycosylated (29 kDa) and complex-glycosylated (40-45 kDa) AQP2 were densitometrically quantified (**B**, **D**). Mean values +/- SEM of normalized AQP2 abundance are given relative to control. (**E**) Intracellular lithium concentrations were determined, which were corrected for contamination with extracellular lithium and normalized for the amount of protein ([Li+] +/- SEM in pmol/µg protein). Data from 3 independent experiments, one way ANOVA, Bonferroni's Multiple Comparison Test, *p<0.05.

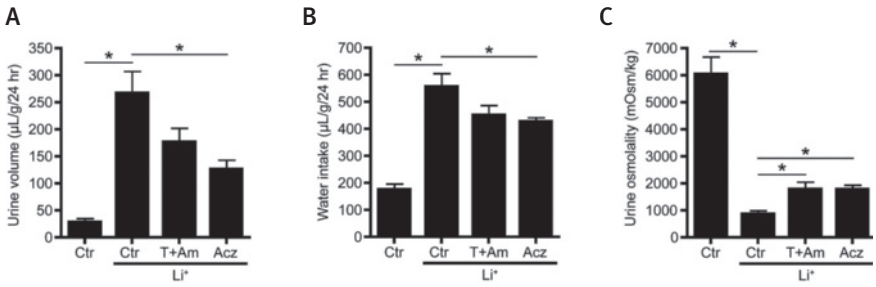

Figure 2. The antidiuretic effect of thiazide/amiloride and acetazolamide treatment on lithium-treated mice. Urine volume (**A**), water intake (**B**) and urine osmolality (**C**) of untreated mice (CTR) or of mice treated for 10 days with lithium (Li+) or in combination with thiazide/amiloride (T+Am) or acetazolamide (Acz). During the last 48 hr mice were housed in metabolic cages and during the last 24 hr water intake was measured and urine was collected to determine urine volume and osmolality. n=8 mice/group, one way ANOVA, Bonferroni's Multiple Comparison Test, *p<0.05.

To examine segment-specific effects of the different therapies on AQP2 abundance, immunohistochemistry was performed. Consistent with our immunoblot data, lithium treatment strongly reduced AQP2 staining, which was clearly attenuated in kidneys of mice treated with lithium and acetazolamide or thiazide/amiloride (Fig. 3E). Interestingly, while lithium abolished AQP2 expression in the entire kidney, the increased AQP2 abundance in the thiazide/amiloride treated group mainly localized to the inner medulla of the kidney, whereas in the acetazolamide treated mice, AQP2 abundance was increased along the connecting tubule and entire collecting duct. Consistent with our immunoblot data, immunohistochemistry revealed no clear changes in H^+-ATPase labeling between the different groups (Supplementary Fig. 2).

Acetazolamide shows an improved overall electrolyte balance over thiazide/amiloride.

Some patients on thiazide/amiloride therapy have been reported to develop hyponatremia, hyperkalemia, metabolic acidosis and/or hypercalcemia (27-30). Moreover, initiating thiazide/amiloride treatment in Li-NDI patients often leads to elevated blood lithium levels, necessitating adjustment of the lithium dose (31). Therefore, to assess and compare the effect of acetazolamide and thiazide/amiloride on these parameters, we analyzed blood and urine for lithium and electrolyte levels (Table 1). Indeed, while mice treated with thiazide/amiloride had a reduced bodyweight and developed hyponatremia, hyperkalemia, and a metabolic acidosis, these parameters were not affected in acetazolamide-treated mice. Also, thiazide/amiloride treatment induced

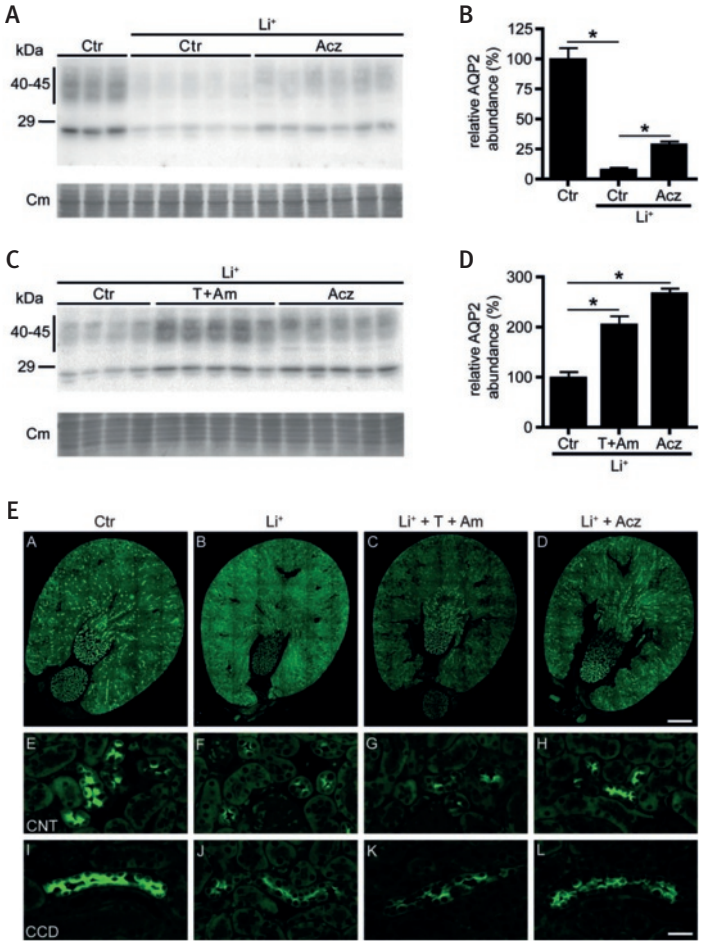

Figure 3. Thiazide/amiloride and acetazolamide reduce lithium-induced downregulation of AQP2 in lithium-NDI mice. (**A-D**) Immunoblot and corresponding densitometric analysis of AQP2 of mouse kidneys that are untreated (Ctr), treated with lithium only (Li+) or with lithium together with acetazolamide (Acz) or thiazide/amiloride (T+Am). The signals for AQP2 densitometrically quantified (**B** and **D**). Mean values +/- SEM of normalized AQP2 abundance is given relative to control. Asterisks indicate significant differences ($p<0.05$) from controls. Equal loading of the samples was confirmed by staining of the blots with coomassie blue (Cm). One way ANOVA, Bonferroni's Multiple Comparison Test, *$p<0.05$. (**E**) Paraffin sections of immersion-fixed kidneys from control (Ctr; A, E, I), lithium-treated (Li+; B, F, J), lithium/amiloride/thiazide-treated (Li+ + T + Am; C, G, K), and lithium/acetazolamide-treated mice (Li+ + Acz; D, H, L) were incubated with a rabbit polyclonal AQP2 antibody followed by a Cy3-coupled goat-anti rabbit IgG. Overviews (A-D) and high magnifications of representative connecting tubules (CNT; E-H), and cortical collecting ducts (CCD; I-L).

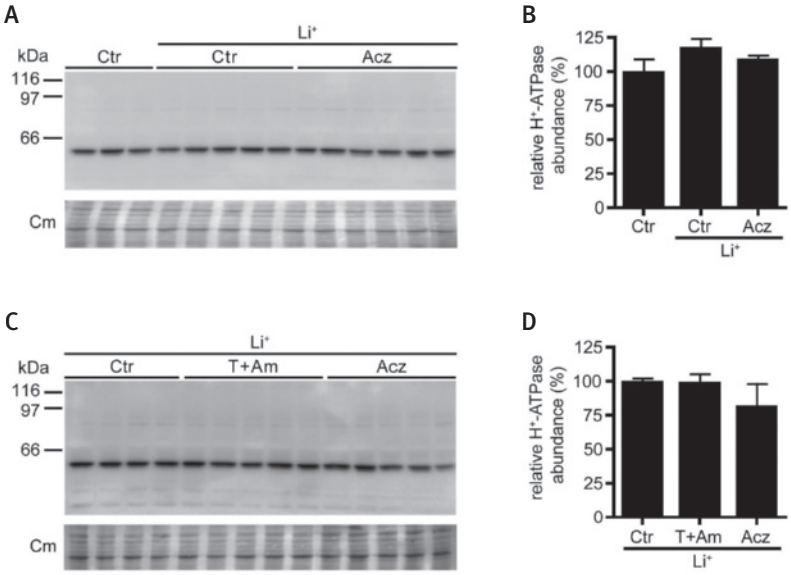

Supplementary figure 1. Effect thiazide/amiloride and H+-ATPase abundance in lithium-NDI mice. (**A-D**) Immunoblot and corresponding densitometric analysis of H+-ATPase abundance of mice that are untreated (Ctr), treated with lithium only (Li+) or with lithium together with acetazolamide (Acz) or thiazide/amiloride (T+Am). The signals for H+-ATPase were densitometrically quantified (**B** and **D**). Mean values +/- SEM of normalized H+-ATPase abundance is given relative to control. Asterisks indicate significant differences ($p<0.05$) from controls. Equal loading of the samples was confirmed by staining of the blots with coomassie blue (Cm).

hypercalcemia, which was significantly reduced with acetazolamide, although not to control levels. Moreover, and consistent with patients, serum lithium concentrations were significantly increased in our thiazide/amiloride mice, but were unchanged in our acetazolamide mice as compared to lithium controls.

The antidiuretic effect of acetazolamide coincides with a lowered GFR and a reduced prostaglandin E2 release

Paradoxically, the clear antidiuresis found in our acetazolamide group (Figs. 2A-C) coincided with a significantly-increased creatinine clearance (Fig. 4A). However, as the creatinine clearance in especially mice highly depends on both creatinine secretion and reabsorption in the proximal tubule, the segment mainly influenced by acetazolamide (32, 33), we hypothesized that acetazolamide may affect proximal tubular creatinine reabsorption/secretion in our mice and thus that the creatinine

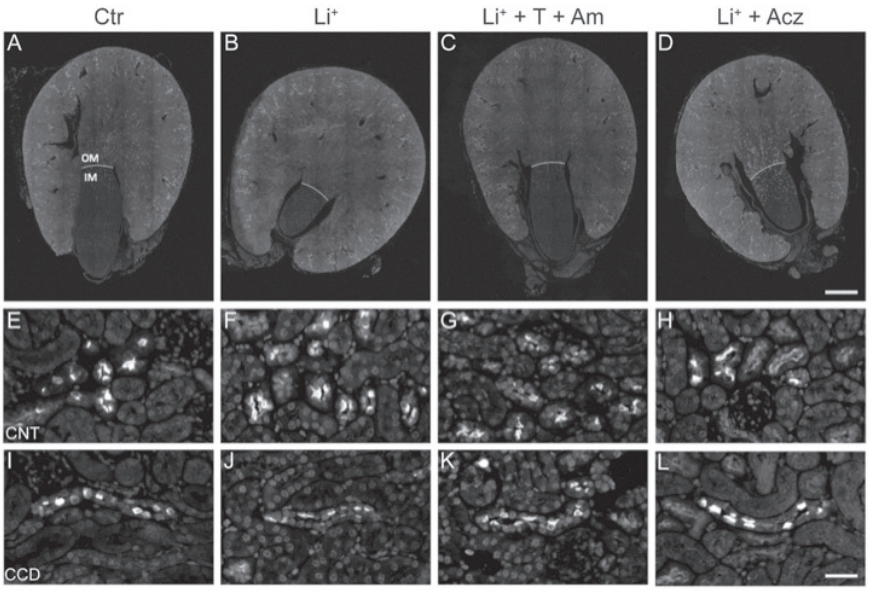

Supplementary figure 2. Expression and distribution of H+-ATPase in kidneys of lithium-NDI mice treated with thiazide/amiloride or ACZ. Paraffin sections of immersion-fixed kidneys from control (Ctr; **A**, **E**, **I**), lithium-treated (Li+; **B**, **F**, **J**), lithium/amiloride/thiazide-treated (Li+ + T + Am; **C**, **G**, **K**), and lithium/ACZ-treated mice (Li+ + Acz; **D**, **H**, **L**) were incubated with a rabbit polyclonal H+-ATPase antibody followed by a Cy3-coupled goat-anti rabbit IgG. Overviews (**A-D**) and high magnifications of representative connecting tubules (CNT; **E-H**), and cortical collecting ducts (CCD; **I-L**).

clearance did not properly reflect the GFR. Therefore we used FITC-inulin to determine the GFR in an identically-performed animal experiment. While acetazolamide again significantly attenuated Li-NDI (not shown), the clearance of FITC-inulin was significantly reduced with acetazolamide (Fig. 4B), indicating that acetazolamide reduced the GFR. Urinary prostaglandin E2 (PGE2), which extensively contributes to AQP2 downregulation in Li-NDI(34), was significantly increased in our Li-NDI mice, but was fully attenuated in our mice treated with lithium/acetazolamide (Fig. 4C). Moreover and consistent with its CA inhibitory action in proximal tubules, acetazolamide further increased urinary pH (Fig. 4D) and strongly reduced the abundance of NHE3 in the renal cortex as compared the cortex of mice treated with lithium only (Fig. 4E, F).

Table 1. Metabolic parameters of mice treated for 10 days with standard chow only (Ctr) or together with lithium (Li^+), lithium + thiazide + amiloride (Li^+ + T + Am), or lithium + acetazolamide (Li^+ + Acz).

	Ctr	Li^+	Li^+ + Am + T	Li^+ + Acz
Serum Osmolality (mOsm/kg)	320 ± 1	319 ± 1	311 ± 0.5**	321 ± 3 †
Serum Sodium (mmol/l)	150 ± 0.3	149 ± 0.4	139 ± 0.8**	150 ± 0.5†
Serum Potassium (mmol/l)	5.3 ± 0.1	5.6 ± 0.2	7.6 ± 0.5**	5.4 ± 0.2†
Serum Lithium (mmol/l)	/	0.63 ± 0.04*	2.11 ± 0.12**	0.69 ± 0.04†
Serum Creatinine (mg/dl)	0.08 ± 0.01	0.09 ± 0.00	0.06 ± 0.01**	0.04 ± 0.01**/†
Blood Ionized Calcium (mmol/l)	1.24 ± 0.00	1.32 ± 0.01*	1.34 ± 0.01	1.27 ± 0.01**/†
Blood pH	7.34 ± 0.01	7.32 ± 0.01	7.24 ± 0.02**	7.35 ± 0.02†
Urine sodium (mmol/l)	352 ± 40	46 ± 6*	484 ± 68 **	112 ± 12†
Urine potassium (mmol/l)	870 ± 83	131 ± 15*	154 ± 19	271 ± 31**/†
Urine lithium (mmol/l)	/	20 ± 3*	24 ± 3	38 ± 8
Urine Creatinine (mg/dl)	70 ± 7	10 ± 1*	14 ± 2	18 ± 2**
Total sodium excretion (mmol/24 hr)	0.17 ± 0.02	0.16 ± 0.01	1.26 ± 0.12**	0.22 ± 0.02†
Total potassium excretion (mmol/24 hr)	0.42 ± 0.05	0.55 ± 0.02*	0.40 ± 0.03**	0.54 ± 0.05
Total lithium excretion (mmol/24 hr)	/	84 ± 3*	64 ± 6	72 ± 11
Bodyweight (g)	18.9 ± 0.4	18.0 ± 0.2*	16.0 ± 0.5**	17.4 ± 0.4†
Food Intake (mg/g/24 hr)	214 ± 8	198 ± 10	188 ± 5	228 ± 5**/†
Feces Production (mg/g/24 hr)	111 ± 7	98 ± 8	82 ± 2	123 ± 9†

Li^+, lithium; T, thiazide; Am, amiloride; Acz, acetazolamide.
Values are means ± s.e.m.
* $P<0.05$ compared to control treatment
** $P<0.05$ compared to lithium treatment
† $P<0.05$ compared to lithium/thiazide/amiloride treatment
/ Below detection limit

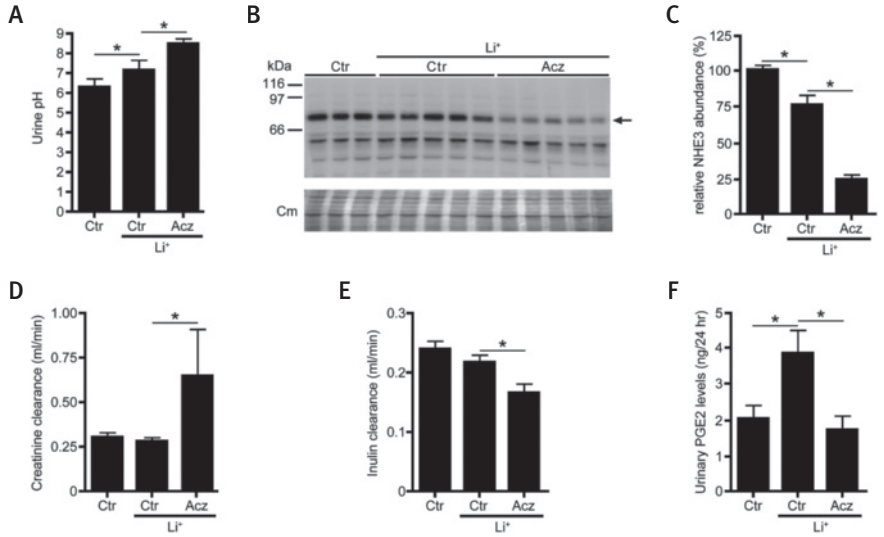

Figure 4. The effect of acetazolamide on urinary pH, NHE3 abundance, glomerular filtration rate and prostaglandin-E2 release. Mice were treated for 10 days with control diet (Ctr) or diet containing lithium (Li+) only or lithium in combination with acetazolamide (Acz). During the last 48 hr, mice were housed in metabolic cages and during the last 24 hr urine was collected to determine creatinine clearance (**A**), PGE2 levels (**C**) and urinary pH (**D**). At day 10, mice were sacrificed and blood and kidneys were isolated, enabling the analysis of renal NHE3 abundance (**E, F**). In (**E**) the arrow indicates the ~85kDa band of NHE3. To measure GFR, using FITC-inulin, the above-mentioned experiment was repeated, however at day 4 osmotic minipumps containing FITC-inulin, were implanted and at day 10 FITC-inulin levels were measured in 24 hr urine and serum (**B**). n=8 mice/group, one way ANOVA, Bonferroni's Multiple Comparison Test, *p<0.05.

Discussion

Acetazolamide is superior to thiazide/amiloride to attenuate lithium-NDI

Our mouse studies revealed that acetazolamide attenuates development of Li-NDI to the same extent as thiazide/amiloride, but, in contrast to acetazolamide, our thiazide/amiloride treated mice developed hyponatremia, hyperkalemia, and metabolic acidosis. In humans, hyponatremia is mostly a consequence of upregulated AQP2 expression by high circulating AVP levels. Although AVP levels are elevated in Li-NDI, this cannot explain hyponatremia in our thiazide/amiloride treated mice, because AQP2 is downregulated here. Instead, our data indicate that the hyponatremia is due to the induced natriuresis caused by thiazide and amiloride in a status of polyuria and

polydipsia, because our Li-NDI mice were normonatremic and our thiazide/amiloride mice were highly natriuretic as compared to the other groups. Note, however, that part of the increased natriuresis must be due to an increased consumption of salt from the provided salt block, because food intake was not increased. The mice apparently drank water to satiety, because the hematocrit was not different between the groups (not shown). Similarly, congenital NDI patients also sometimes develop hyponatremia when treated with thiazide combinations (35, 36).

The observed hyperkalemia is likely due to inhibition of ENaC by amiloride, as renal secretion of potassium occurs only in exchange of ENaC-mediated sodium reabsorption (37). Lithium itself can lead to metabolic acidosis (38), which would even be increased with inhibition of bicarbonate uptake by acetazolamide, but we only found metabolic acidosis in our thiazide/amiloride treated mice. Whereas metabolic acidosis in our acetazolamide group may have been compensated by increased ventilation, metabolic acidosis in the thiazide/amiloride group may be secondary to the observed hyperkalemia, as mammals attenuate hyperkalemia at the expense of development of metabolic acidosis (39).

Our Li-NDI mice developed hypercalcemia, which was sustained in our thiazide/amiloride treated mice, but not in our acetazolamide mice. Hyperparathyroidism is common with lithium-using patients and the occurrence of hypercalcemia in Li-NDI has been ascribed to inhibition of calcium-sensing receptor signaling by lithium in the parathyroid (40-42). The corrected blood calcium levels with acetazolamide, however, may be unrelated to the parathyroid effect of lithium, because plasma calcium is increased by bone resorption, a process that involves CA2 activity in osteoclast and that is strongly inhibited by acetazolamide (43, 44).

Another important advantage of the use of acetazolamide over thiazide/amiloride is that plasma lithium concentrations remained unchanged with acetazolamide. Blood lithium is mainly set by the amount reabsorbed in proximal tubules, a process in which the apical NHE3 is highly involved and which is stimulated by thiazide (18, 45). Considering this, the unaltered blood lithium levels with acetazolamide is best explained by combinatory effects of the reduced NHE3 abundance in proximal tubules and the reduced GFR.

Acetazolamide attenuates Li-NDI by a dual mode of action

Our data indicate that the observed antidiuresis and reduced GFR with acetazolamide is due to a tubular glomerular feedback (TGF) response caused by inhibition of CAs in the proximal tubule (46, 47). Ninety percent of renal HCO_3^- is reabsorbed in proximal tubules, which is strongly facilitated by CA4/14 (luminal/apical), CA2 (intracellular) and CA4/12 (basolateral) hydrating CO_2 and dehydrating H_2CO_3 (48). In this process, secretion of protons by NHE3 is important. By blocking these CA, acetazolamide prevents the intracellular generation of H^+, which is needed for NHE3 to reabsorb

filtered Na^+ (49-52). The consequently increased tubular salt and water load in the proximal tubule leads to an increased fluid delivery and tubular [Cl^-] at the macula densa, which induces a TGF response (i.e. a reduced GFR) (47). Indeed, acetazolamide in our Li-NDI mice led to an increased urinary pH, reduced NHE3 abundance and reduced GFR and are in agreement with reported data on NHE3 knockout mice (47, 50, 53).

Besides intercalated cells (see below), the increased fluid delivery to the macula densa with acetazolamide may also partially explain the observed lower urinary levels of PGE2, thereby attenuating Li-NDI. By acting on EP1/3 receptors, increased urinary PGE2 levels in Li-NDI reduce principal cell AQP2 expression and thus water reabsorption (54). In Li-NDI, a fraction of the elevated urinary PGE2 levels is thought to be derived from macula densa and surrounding cTAL cells, which produce PGE2 to increase renin synthesis and release in response to a reduced fluid delivery to the TAL/hypovolemia. As such, the increased fluid delivery to the TAL with acetazolamide will reduce the cortical release of PGE2 and therewith Li-NDI.

However, our *in vitro* data indicate that acetazolamide also directly protects collecting duct cells from lithium, but it is at present unclear whether *in vivo* acetazolamide acts directly on principal cells or indirectly via intercalated cells. Support for the first is that mpkCCD cells endogenously express and show proper regulation of the typical principal cell proteins, AQP2 and ENaC. Moreover, mpkCCD cells express high CA2 mRNA levels (http://esbl.nhlbi.nih.gov/mpkCCD-transcriptome/), which is also expressed in principal cells *in vivo* (48, 55-57). Also, the *in vivo* activity of ENaC, the lithium entry site of principal cells, has been reported to be functionally paired with CA activity, as, CA inhibition by acetazolamide reduced the intracellular pH and reduced ENaC activity in sweat duct cells and colon (58, 59).

However, mpkCCD cells may not fully represent principal cells and, as intercalated cells express abundant levels of CAs 2, 4, 12, and 15 (48), acetazolamide may increase principal cell AQP2 expression and water uptake indirectly by inhibiting ACs in intercalated cells. Indeed, long-term lithium treatment leads to metabolic acidosis, which underlies the increased number of α-intercalated cells (11, 60) and, as lithium inhibits intercalated cell H^+-ATPase and H^+/K^+-ATPase activity (61, 62), it has been suggested that acidosis-induced proliferation of α-intercalated cells may contribute to Li-NDI (26). It is unlikely, however, that attenuation of Li-NDI in our mice is due to direct action of acetazolamide on α-intercalated cells or collecting duct remodeling for several reasons: At first, acetazolamide increases the number of α-intercalated cells in rodents, as it causes acidosis itself (63, 64). Secondly and consistent with the unchanged H^+-ATPase expression in our mice, collecting duct remodeling is not observed with 10 days of lithium treatment, but only starts at about 4 weeks of treatment (9, 65).

An effect of acetazolamide on β-intercalated cells, however, may be more likely. While

lithium treatment did not reduce the number of these cells (66), exciting recent studies revealed the existence of extensive cross-talk between **β-intercalated and principal cells** in the regulating collecting duct function (67-70). While Eladari *et al* elegantly showed that in rodents, the sodium-dependent chloride bicarbonate exchanger (NDCBE/SLC4a8) and chloride bicarbonate exchanger protein pendrin allow for NaCl reabsorption through β-intercalated cells, chloride permeation through pendrin also appeared necessary for ENaC mediated sodium reabsorption and expression (71). Also, in mice lacking functional intercalated cell-specific H^+-ATPase, the observed natriuresis and aquaresis was due to dysfunctional and lower abundances of ENaC and pendrin/NDCBE, and reduced AQP2 levels, respectively (69). The authors further showed that the lack/inhibition of **β-intercalated cells** H^+-ATPase led, via flow-stimulated luminal ATP release, to autocrine and paracrine release of PGE2, which reduced the cortical and medullary ENaC activity and AQP2 abundance. Importantly, thiazides inhibited NCC-independent NaCl reabsorption through NDCBE/pendrin (68) and acetazolamide reduced pendrin abundance(72), drugs we showed to attenuate Li-induced downregulation of AQP2 and Li-NDI through a similar mechanism. As such, the attenuated Li-NDI with acetazolamide, which was given during the entire lithium treatment, may be due to an impaired functioning of pendrin, resulting in increased ATP/PGE2 release, reduced ENaC activity in principal cells, and thus reduced influx of lithium from pro-urine. The finding that acetazolamide is beneficial chiefly in the cortical segments that contain intercalated cells is consistent with the possibility that intercalated cell CAs could be involved. A prime candidate here is CA12, as it is highly sensitive to acetazolamide and patients with reduced CA12 activity have a preponderance to hyponatremic dehydration (73). Whether one of these mechanisms underlies the beneficial effect of acetazolamide in Li-NDI remains to be studied.

Taken together, we have shown that CAs activity contributes to Li-NDI development, that acetazolamide attenuates lithium-induced NDI by inducing a TGF response and through a direct action on the collecting duct, and that acetazolamide attenuates Li-NDI development similar to thiazide/amiloride but with less side effects.

Acknowledgments

We thank Marthe Minderman, Marcel Jaklofsky and Monique Carrel for their expert help. PMTD is a recipient of VICI grant 865.07.002 of the Netherlands Organization for Scientific research (NWO). The H^+-ATPase antibody was kind gift of Dr. Carsten Wagner. This project received support from the VICI grant 865.07.002, RUMC grant (2004.55) and a grant from the Society of Experimental Laboratory Medicine to PMTD, a Niels Stensen Fellowship and Marie Curie Fellowship PIOF-GA-2012-332395 to TG, a Swiss National Science Foundation grant (310030_143929/1) to JL, and grants from the European Community's Seventh Framework Programme (FP7/2007-2013; agreement

n° 305608 (EURenOmics)), the Swiss National Science Foundation (310030_146490) and the KFSP RADIZ (Rare Disease Initiative Zurich) from the University of Zurich to OD.

Statement of competing financial interests

The authors declare that the research was conducted in the absence of any commercial or financial relationships that could be construed as a potential conflict of interest.

References

1. Grunfeld JP, Rossier BC. Lithium nephrotoxicity revisited. NatRevNephrol. 2009;5(5):270-6.
2. Walker RJ, Weggery S, Bedford JJ, McDonald FJ, Ellis G, Leader JP. Lithium-induced reduction in urinary concentrating ability and urinary aquaporin 2 (AQP2) excretion in healthy volunteers. Kidney Int. 2005;67(1):291-4.
3. Rej S, Herrmann N, Shulman K. The effects of lithium on renal function in older adults--a systematic review. Journal of geriatric psychiatry and neurology. 2012;25(1):51-61.
4. Farres MT, Ronco P, Saadoun D, Remy P, Vincent F, Khalil A, et al. Chronic lithium nephropathy: MR imaging for diagnosis. Radiology. 2003;229(2):570-4.
5. Laursen UH, Pihakaski-Maunsbach K, Kwon TH, Ostergaard JE, Nielsen S, Maunsbach AB. Changes of rat kidney AQP2 and Na,K-ATPase mRNA expression in lithium-induced nephrogenic diabetes insipidus. Nephron ExpNephrol. 2004;97(1):e1-16.
6. Marples D, Christensen S, Christensen EI, Ottosen PD, Nielsen S. Lithium-induced downregulation of aquaporin-2 water channel expression in rat kidney medulla. The Journal of clinical investigation. 1995;95:1838-45.
7. Li Y, Shaw S, Kamsteeg EJ, Vandewalle A, Deen PM. Development of lithium-induced nephrogenic diabetes insipidus is dissociated from adenylyl cyclase activity. J Am Soc Nephrol. 2006;17(4):1063-72.
8. Christensen BM, Marples D, Kim YH, Wang W, Frokiaer J, Nielsen S. Changes in cellular composition of kidney collecting duct cells in rats with lithium-induced NDI. Am J Physiol Cell Physiol. 2004;286(4):C952-C64.
9. de Groot T, Alsady M, Jaklofsky M, Otte-Holler I, Baumgarten R, Giles RH, et al. Lithium causes g2 arrest of renal principal cells. J Am Soc Nephrol. 2014;25(3):501-10.
10. Batlle DC, von Riotte AB, Gaviria M, Grupp M. Amelioration of polyuria by amiloride in patients receiving long- term lithium therapy. N Engl J Med. 1985;312:408-14.
11. Kortenoeven ML, Li Y, Shaw S, Gaeggeler HP, Rossier BC, Wetzels JF, et al. Amiloride blocks lithium entry through the sodium channel thereby attenuating the resultant nephrogenic diabetes insipidus. Kidney Int. 2009;76(1):44-53.
12. Bedford JJ, Leader JP, Jing R, Walker LJ, Klein JD, Sands JM, et al. Amiloride restores renal medullary osmolytes in lithium-induced nephrogenic diabetes insipidus. AmJPhysiol Renal Physiol. 2008;294(4):F812-F20.
13. Bedford JJ, Weggery S, Ellis G, McDonald FJ, Joyce PR, Leader JP, et al. Lithium-induced nephrogenic diabetes insipidus: renal effects of amiloride. Clin J Am Soc Nephrol. 2008;3(5):1324-31.
14. Sinke AP, Kortenoeven ML, de Groot T, Baumgarten R, Devuyst O, Wetzels JF, et al. Hydrochorothiazide attenuates lithium-induced Nephrogenic Diabetes Insipidus independently of the sodium-chloride co-transporter. Am J Physiol Renal Physiol. 2013.
15. Pickkers P, Garcha RS, Schachter M, Smits P, Hughes AD. Inhibition of carbonic anhydrase accounts for the direct vascular effects of hydrochlorothiazide. Hypertension. 1999;33(4):1043-8.
16. Hasler U, Mordasini D, Bens M, Bianchi M, Cluzeaud F, Rousselot M, et al. Long term regulation of aquaporin-2 expression in vasopressin-responsive renal collecting duct principal cells. JBiolChem. 2002;277(12):10379-86.
17. Wood AJ, Goodwin GM, De SR, Green AR. The pharmacokinetic profile of lithium in rat and mouse; an important factor in psychopharmacological investigation of the drug. Neuropharmacology. 1986;25(11):1285-8.
18. Nijenhuis T, Vallon V, van der Kemp AW, Loffing J, Hoenderop JG, Bindels RJ. Enhanced passive Ca2+ reabsorption and reduced Mg2+ channel abundance explains thiazide-induced hypocalciuria and hypomagnesemia. JClinInvest. 2005;115(6):1651-8.
19. Nijenhuis T, Renkema KY, Hoenderop JG, Bindels RJ. Acid-base status determines the renal expression of Ca2+ and Mg2+ transport proteins. JAmSocNephrol. 2006;17(3):617-26.
20. Qi Z, Whitt I, Mehta A, Jin J, Zhao M, Harris RC, et al. Serial determination of glomerular filtration rate in conscious mice using FITC-inulin clearance. Am J Physiol Renal Physiol. 2004;286(3):F590-6.
21. Fenton RA, Flynn A, Shodeinde A, Smith CP, Schnermann J, Knepper MA. Renal phenotype of UT-A urea transporter knockout mice. J Am Soc Nephrol. 2005;16(6):1583-92.

22. Kamsteeg EJ, Wormhoudt TA, Rijss JPL, van Os CH, Deen PMT. An impaired routing of wild-type aquaporin-2 after tetramerization with an aquaporin-2 mutant explains dominant nephrogenic diabetes insipidus. EMBO J. 1999;18(9):2394-400.
23. Kamsteeg EJ, Bichet DG, Konings IB, Nivet H, Lonergan M, Arthus MF, et al. Reversed polarized delivery of an aquaporin-2 mutant causes dominant nephrogenic diabetes insipidus. JCell Biol. 2003;163(5):1099-109.
24. Wagner CA, Lukewille U, Valles P, Breton S, Brown D, Giebisch GH, et al. A rapid enzymatic method for the isolation of defined kidney tubule fragments from mouse. Pflugers Arch. 2003;446(5):623-32.
25. Wagner CA, Loffing-Cueni D, Yan Q, Schulz N, Fakitsas P, Carrel M, et al. Mouse model of type II Bartter's syndrome. II. Altered expression of renal sodium- and water-transporting proteins. AmJPhysiol Renal Physiol. 2008;294(6):F1373-F80.
26. Christensen BM, Kim YH, Kwon TH, Nielsen S. Lithium treatment induces a marked proliferation of primarily principal cells in rat kidney inner medullary collecting duct. Am J Physiol Renal Physiol. 2006;291(1):F39-F48.
27. Fidler HM, Goldman J, Bielawska CA, Rai GS, Hoffbrand BI. A study of plasma sodium levels in elderly people taking amiloride or triamterene in combination with hydrochlorothiazide. PostgradMedJ. 1993;69(816):797-9.
28. Mathew TH, Boyd IW, Rohan AP. Hyponatraemia due to the combination of hydrochlorothiazide and amiloride (Moduretic): Australian spontaneous reports 1977-1988. MedJAust. 1990;152(6):308-9.
29. Bayer AJ, Farag R, Browne S, Pathy MS. Plasma electrolytes in elderly patients taking fixed combination diuretics. PostgradMedJ. 1986;62(725):159-62.
30. Jaffey L, Martin A. Malignant hyperkalaemia after amiloride/hydrochlorothiazide treatment. Lancet. 1981;1(8232):1272.
31. Boton R, Gaviria M, Batlle DC. Prevalence, pathogenesis, and treatment of renal dysfunction associated with chronic lithium therapy. American Journal of Kidney Diseases. 1987;10:329-45.
32. Eisner C, Faulhaber-Walter R, Wang Y, Leelahavanichkul A, Yuen PS, Mizel D, et al. Major contribution of tubular secretion to creatinine clearance in mice. Kidney Int. 2010;77(6):519-26.
33. Musso CG, Michelangelo H, Vilas M, Reynaldi J, Martinez B, Algranati L, et al. Creatinine reabsorption by the aged kidney. Int Urol Nephrol. 2009;41(3):727-31.
34. Kwon T. Dysregulation of Renal Cyclooxygenase-2 in Rats with Lithium-induced Nephrogenic Diabetes Insipidus. Electrolyte & Blood Pressure. 2007;5:68-74.
35. Anton-Gamero M, Garcia-Martinez E, Fernandez-Ramos J, Rodriguez-Salas M, Gil-Campos M. Nephrogenic diabetes insipidus: the key element of paradoxical hyponatremia. Pediatr Nephrol. 2009;24(11):2277-8.
36. Boussemart T, Nsota J, Martin–Coignard D, Champion G. Nephrogenic diabetes insipidus: treat with caution. Pediatric Nephrology. 2009;24(9):1761-3.
37. Christensen BM, Perrier R, Wang Q, Zuber AM, Maillard M, Mordasini D, et al. Sodium and potassium balance depends on alphaENaC expression in connecting tubule. J Am Soc Nephrol. 2010;21(11):1942-51.
38. Nascimento L, Rademacher DR, Hamburger R, Arruda JA, Kurtzman A. On the mechanism of lithium-induced renal tubular acidosis. The Journal of laboratory and clinical medicine. 1977;89(3):455-62.
39. Palmer BF. Metabolic complications associated with use of diuretics. Semin Nephrol. 2011;31(6):542-52.
40. McHenry CR, Racke F, Meister M, Warnaka P, Sarasua M, Nemeth EF, et al. Lithium effects on dispersed bovine parathyroid cells grown in tissue culture. Surgery. 1991;110(6):1061-6.
41. Brown EM. Lithium induces abnormal calcium-regulated PTH release in dispersed bovine parathyroid cells. The Journal of clinical endocrinology and metabolism. 1981;52(5):1046-8.
42. McHenry CR, Stenger DB, Racke F. Investigation of calcium-induced hydrolysis of phosphoinositides in normal and lithium-treated parathyroid cells. American journal of surgery. 1995;170(5):484-7.
43. Brown GM, Morris CA, Mitnick MA, Insogna KL. Treatment of humoral hypercalcemia of malignancy in rats with inhibitors of carbonic anhydrase. Journal of bone and mineral research : the official journal of the American Society for Bone and Mineral Research. 1990;5(10):1037-41.
44. Lehenkari P, Hentunen TA, Laitala-Leinonen T, Tuukkanen J, Vaananen HK. Carbonic anhydrase II plays a major role in osteoclast differentiation and bone resorption by effecting the steady state intracellular pH and Ca2+. Exp Cell Res. 1998;242(1):128-37.

45. Timmer RT, Sands JM. Lithium intoxication. J Am Soc Nephrol. 1999;10(3):666-74.
46. Cogan MG, Maddox DA, Warnock DG, Lin ET, Rector FC, Jr. Effect of acetazolamide on bicarbonate reabsorption in the proximal tubule of the rat. Am J Physiol. 1979;237(6):F447-54.
47. Leyssac PP, Karlsen FM, Holstein-Rathlou NH, Skott O. On determinants of glomerular filtration rate after inhibition of proximal tubular reabsorption. AmJPhysiol. 1994;266(5 Pt 2):R1544-R50.
48. Purkerson JM, Schwartz GJ. The role of carbonic anhydrases in renal physiology. Kidney Int. 2007;71(2): 103-15.
49. Schnermann J. Sodium transport deficiency and sodium balance in gene-targeted mice. Acta Physiol Scand. 2001;173(1):59-66.
50. Amlal H, Ledoussal C, Sheriff S, Shull GE, Soleimani M. Downregulation of renal AQP2 water channel and NKCC2 in mice lacking the apical Na+-H+ exchanger NHE3. JPhysiol. 2003;553(Pt 2):511-22.
51. Maren TH. Carbonic anhydrase: chemistry, physiology, and inhibition. Physiol Rev. 1967;47(4):595-781.
52. Deng A, Miracle CM, Lortie M, Satriano J, Gabbai FB, Munger KA, et al. Kidney oxygen consumption, carbonic anhydrase, and proton secretion. Am J Physiol Renal Physiol. 2006;290(5):F1009-15.
53. Brooks HL, Sorensen AM, Terris J, Schultheis PJ, Lorenz JN, Shull GE, et al. Profiling of renal tubule Na+ transporter abundances in NHE3 and NCC null mice using targeted proteomics. The Journal of physiology. 2001;530(Pt 3):359-66.
54. Olesen ET, Fenton RA. Is there a role for PGE2 in urinary concentration? J Am Soc Nephrol. 2013;24(2):169-78.
55. Brown D, Kumpulainen T, Roth J, Orci L. Immunohistochemical localization of carbonic anhydrase in postnatal and adult rat kidney. Am J Physiol. 1983;245(1):F110-8.
56. Lonnerholm G, Wistrand PJ, Barany E. Carbonic anhydrase isoenzymes in the rat kidney. Effects of chronic acetazolamide treatment. Acta Physiol Scand. 1986;126(1):51-60.
57. Parkkila S, Parkkila AK, Saarnio J, Kivela J, Karttunen TJ, Kaunisto K, et al. Expression of the membrane-associated carbonic anhydrase isozyme XII in the human kidney and renal tumors. JHistochemCytochem. 2000;48(12):1601-8.
58. Spicer Z, Clarke LL, Gawenis LR, Shull GE. Colonic H(+)-K(+)-ATPase in K(+) conservation and electrogenic Na(+) absorption during Na(+) restriction. Am J Physiol Gastrointest Liver Physiol. 2001;281(6):G1369-77.
59. Reddy MM, Wang XF, Quinton PM. Effect of cytosolic pH on epithelial Na+ channel in normal and cystic fibrosis sweat ducts. J Membr Biol. 2008;225(1-3):1-11.
60. Trepiccione F, Capasso G, Nielsen S, Christensen BM. Evaluation of cellular plasticity in the collecting duct during recovery from lithium-induced nephrogenic diabetes insipidus. Am J Physiol Renal Physiol. 2013;305(6):F919-29.
61. Eiam-Ong S, Dafnis E, Spohn M, Kurtzman NA, Sabatini S. H-K-ATPase in distal renal tubular acidosis: urinary tract obstruction, lithium, and amiloride. Am J Physiol. 1993;265(6 Pt 2):F875-80.
62. Dafnis E, Kurtzman NA, Sabatini S. Effect of lithium and amiloride on collecting tubule transport enzymes. JPharmacolExpTher. 1992;261(2):701-6.
63. Bagnis C, Marshansky V, Breton S, Brown D. Remodeling the cellular profile of collecting ducts by chronic carbonic anhydrase inhibition. AmJPhysiol Renal Physiol. 2001;280(3):F437-F48.
64. Welsh-Bacic D, Nowik M, Kaissling B, Wagner CA. Proliferation of acid-secretory cells in the kidney during adaptive remodelling of the collecting duct. PLoSOne. 2011;6(10):e25240.
65. Christensen BM, Zuber AM, Loffing J, Stehle JC, Deen PM, Rossier BC, et al. alphaENaC-mediated lithium absorption promotes nephrogenic diabetes insipidus. JAmSocNephrol. 2011;22(2):253-61.
66. Kim YH, Kwon TH, Christensen BM, Nielsen J, Wall SM, Madsen KM, et al. Altered expression of renal acid-base transporters in rats with lithium-induced NDI. Am J Physiol Renal Physiol. 2003;285(6):F1244-F57.
67. Roy A, Al-bataineh MM, Pastor-Soler NM. Collecting duct intercalated cell function and regulation. Clinical journal of the American Society of Nephrology : CJASN. 2015;10(2):305-24.
68. Leviel F, Hubner CA, Houillier P, Morla L, El MS, Brideau G, et al. The Na+-dependent chloride-bicarbonate exchanger SLC4A8 mediates an electroneutral Na+ reabsorption process in the renal cortical collecting ducts of mice. J ClinInvest. 2010;120(5):1627-35.
69. Gueutin V, Vallet M, Jayat M, Peti-Peterdi J, Corniere N, Leviel F, et al. Renal beta-intercalated cells maintain body fluid and electrolyte balance. J Clin Invest. 2013;123(10):4219-31.

70. Eladari D, Chambrey R, Peti-Peterdi J. A new look at electrolyte transport in the distal tubule. Annu Rev Physiol. 2012;74:325-49.
71. Jacques T, Picard N, Miller RL, Riemondy KA, Houillier P, Sohet F, et al. Overexpression of pendrin in intercalated cells produces chloride-sensitive hypertension. J Am Soc Nephrol. 2013;24(7):1104-13.
72. Hafner P, Grimaldi R, Capuano P, Capasso G, Wagner CA. Pendrin in the mouse kidney is primarily regulated by Cl- excretion but also by systemic metabolic acidosis. AmJPhysiol Cell Physiol. 2008;295(6):C1658-C67.
73. Feldshtein M, Elkrinawi S, Yerushalmi B, Marcus B, Vullo D, Romi H, et al. Hyperchlorhidrosis caused by homozygous mutation in CA12, encoding carbonic anhydrase XII. Am J Hum Genet. 2010;87(5):713-20.

Chapter 4

Lithium induces aerobic glycolysis and glutaminolysis in collecting duct principal cells

Alsady M [1#], de Groot T [1,3#], Kortenoeven MLA [5], Carmone C [1], Neijman K [1], Bekkenkamp-Grovenstein M [1], Engelke U [2], Wevers RA [2], Baumgarten R [4], Korstanje R [3] and Deen PMT [1*]

[#]: shared first authorships

[1] Department of Physiology and [2] Laboratory Medicine, Radboud University Medical Center, Nijmegen, The Netherlands; [3] The Jackson Laboratory Nathan Shock Center of Excellence in the Basic Biology of Aging, The Jackson Laboratory, Bar Harbor, USA; [4] Society of Experimental Laboratory Medicine, Amersfoort, The Netherlands; [5] Department of Biomedicine, Aarhus University, Aarhus, Denmark.

Am J Physiol Renal Physiol 314: F230–F239, 2018.

Abstract

Lithium, given to bipolar disorder patients, causes nephrogenic diabetes insipidus (Li-NDI), a urinary concentrating defect. Li-NDI is due to downregulation of principal cell AQP2 expression, which coincides with principal cell proliferation. The metabolic effect of lithium on principal cells, however, is unknown and investigated here. Earlier, we have shown that the carbonic anhydrase (CA) inhibitor acetazolamide attenuated Li-induced downregulation in mouse collecting duct (mpkCCD) cells. Of the eight CAs present in mpkCCD cells, siRNA and drug treatments showed that downregulation of CA9 and to some extent CA12 attenuated Li-induced AQP2 downregulation. Moreover, lithium induced cell proliferation and increased the secretion of lactate. Lithium also increased urinary lactate levels in wildtype mice that developed Li-NDI, but not in lithium-treated mice lacking ENaC, the principal cell entry site for lithium. Inhibition of aerobic glycolysis with 2-deoxyglucose (2DG) attenuated lithium-induced AQP2 downregulation in mpkCCD cells, but did not attenuate Li-NDI in mice. Interestingly, NMR analysis demonstrated that lithium also increased the urinary succinate, fumarate, citrate, and NH_4^+ levels, which were, in contrast to lactate, not decreased by 2DG. Together, our data reveal that lithium induces aerobic glycolysis and glutaminolysis in principal cells and that inhibition of aerobic glycolysis, but not the glutaminolysis, does not attenuate Li-NDI.

Introduction

Lithium is the first-choice medication for treatment of bipolar disorder and is frequently given to patients with depression (1). This drug is taken by 0.1% of the western population and its use is expected to increase as it is also tested as a treatment for other neurological disorders, such as Alzheimer's, Parkinson's, and Huntington's (2). In approximately 50% of treated patients, however, lithium causes a urine concentrating defect, which develops in 20% of patients into symptomatic Nephrogenic Diabetes Insipidus (NDI), a disorder characterized by polyuria and polydipsia due to the downregulation of aquaporin-2 (AQP2) water channels in the principal cells of the collecting duct (3-5). Lithium also alters the cellular composition of the collecting duct, as it increases the fraction of type-A intercalated cells and lowers the fraction of principal cells (4, 6). Despite the fact that the fraction of principal cells in the collecting duct decreases compared to the fraction of intercalated cells, lithium treatment results in principal cells that are in the proliferative state, as they were positive for proliferating cell nuclear antigen (PCNA), a marker for cell proliferation (7). It is however questionable whether these PCNA-positive cells are actually dividing, as we found that lithium induces a G2/M cell cycle arrest, which partly explains the discrepancy between the reduced percentage of principal cells while being positive for PCNA (8).

Recently, we found that the carbonic anhydrase (CA) inhibitor acetazolamide attenuated AQP2 downregulation in mouse collecting duct (mpkCCD) cells and in mice treated with lithium, which coincided with a reduced Li-NDI (9). To understand its mechanism, we here analyzed the CA involved, which indicated that lithium induces aerobic glycolysis in principal cells. Differentiated cells, such as principal cells, generate their energy primarily via mitochondrial oxidative phosphorylation in which biomolecules and ATP are produced from glucose and in which oxygen is required (10)'. However, proliferating cells, including tumors, often generate their energy by a process called "aerobic glycolysis", also known as the Warburg effect, which takes place regardless of tissue oxygen levels. Although this process is an inefficient way to generate ATP, it allows the synthesis of biomolecules such as nucleotides, amino acids, and lipids that are required to build the new cells (10). Aerobic glycolysis is characterized by an increase in lactate production (10). As principal cells are in a proliferative state when treated with lithium, we here subsequently investigated whether lithium induces aerobic glycolysis in collecting duct principal cells and, if so, whether inhibition of aerobic glycolysis attenuates Li-NDI.

Materials and methods

Animal experiments

Animal experiments were performed as described (8). Female C57BL/6 mice were obtained from The Jackson Laboratory (Bar Harbor, USA). Collecting duct-specific epithelial sodium channel knockout (NMR16J ENaC-KO) mice (11) were kindly provided by Edith Hummler, Lausanne, Switzerland and crossed with C57BL/6 mice, obtained from Harlan Laboratories (Horst, the Netherlands). Male ENaC-KO mice and their wild-type (WT) littermates were used for the experiments. Mice were housed in a climate-controlled facility with a 12-hour:12-hour light-dark cycle. All mice had free access to rodent diet (7013, NIH-31 Modified, Harlan Laboratories, Inc., Madison, WI, USA), acidified water and a sodium chloride block throughout the experiment. At 10 weeks of age, one group of mice received normal rodent diet, while the other mice received the same diet supplemented with 40 mmol lithium chloride (LiCl)/kg food or LiCl diet with twice daily IP injection with 250 mg/kg BW 2-Deoxy-D-glucose in saline for 10 days (8). During the last 48 hours of an experiment, mice were housed in metabolic cages in order to measure water intake and urine output during the last 24 hours. Next, mice were anesthetized with isoflurane and euthanized by cervical dislocation, after which the kidneys were removed. All animal studies were approved by the Animal Ethical Committee of the Radboud University Medical Center and by The Jackson Laboratory's Animal Care and Use Committee.

1H NMR Spectroscopy

One-dimensional 1H NMR spectroscopy was performed as described (12). 24h Urine was centrifuged 10 minutes at 3000xg before analysis. A small volume of 20 µL of 20.2 mM trimethylsilyl-2,2,3,3-tetradeuteropropionic acid (TSP, sodium salt; Aldrich) in D2O was added to 700 µL of the urine to serve as an internal quantity reference for subsequent handlings. The pH of each sample was adjusted to 2.50 ± 0.05 with concentrated HCl. Finally, 650 µL of the sample was placed in a 5 mm NMR tube (Wilmad Royal Imperial; Wilmad LabGlass, USA). 1H NMR spectra were obtained using a Bruker 500 MHz spectrometer (pulse angle, 90°; delay time, 4 s; number of scans, 256). Water resonance was suppressed by gated irradiation centered on the water frequency. The spectral width in the F1 and F2 domains was 5500 Hz. A total of 2K data points were collected in t2, 256 t1 increments with 32 transients per increment were used. The relaxation delay was set to 2 seconds. Before the Fourier transformation, a sine-bell function was applied in both time domains. During the relaxation delay, the water resonance was pre-saturated.

The free-induction decays measured for these samples were processed using Topspin software (Bruker BioSpin, Rheinstetten, Germany). Fourier transformation was applied on the free-induction decay of the samples and the resulting spectra were phase and baseline corrected. The chemical shifts in the spectra were referenced to the internal standard, TSP. Assignment of peak positions for compound identification was performed by comparing the peak positions in the spectra of the metabolites with the reference spectral database of model compounds at pH 2.5 using Amix version 3.9.14 (Bruker BioSpin, Rheinstetten, Germany). Quantification of identified compounds was performed by manual integration of chosen peak(s) for a specific metabolite.

Cell culture assays

MpkCCD cells were cultured as described (4). In short, cells were cultured in a modified defined medium containing DMEM:Ham's F12 1:1 vol/vol; 60 nM sodium selenate, 5 µg/ml transferrin, 2 mM glutamine, 50 nM dexamethasone, 1 nM triiodothyronine, 10 ng/ml epidermal growth factor (EGF), 5 µg/ml insulin, 28 mM D-glucose, 2% fetal calf serum (FCS), and 20 mM HEPES (pH 7.4). Cells were seeded at a density of $1.5x10^5$ cells/cm^2 on semi permeable filters (Transwell, 0.4 µm pore size, Corning Costar, Cambridge, MA). After 96 hours, cells were treated with 1 nM 1-deamino-8-D-arginine vasopressin (dDAVP) at the basolateral side to induce AQP2 expression. For the last 48 hours, cells were cultured in a FCS/EGF-free medium and treated with or without 1 mM LiCl at the basolateral side and 10 mM LiCl at the apical side in the presence or absence of 10 µM 6- and 7-hydroxycoumarin (6HC and 7HC) , 10 µM amiloride or 1 mM 2-deoxy-d-glucose (2DG). To determine the cell viability and extent of transcellular sodium transport, Trans Epithelial Electrical Resistance (TEER) and transcellular voltage (Tv) were measured on day 8. Next, cells were harvested and prepared for immunoblotting as described (4). The concentrations of 2DG, 6HC and 7HC were determined experimentally by testing concentrating series on mpkCCD cells that were cultured as described above. For siRNA knockdown in mpkCCD cells, siGENOME SMARTpool (Thermo Fisher Scientific, Lafayette, CO, USA) siRNAs were obtained against the indicated mouse carbonic anhydrases (CAs) and a scrambled non-targeting siRNA as a control. The SMARTpool siRNA consists of a mixture of 4 siRNA provided as a single reagent and have been shown in large scale siRNA screens to have high potency and specificity to silence the target gene (13, 14). The cells were seeded at $1.5*10^5$ cells/cm^2 on 24-well (0.33 cm^2) semi-permeable filters (Costar Corning Transwell®, 0.4 µm pore size) and transfected with 20 pmol siRNA, combined with 1 µl Metafectene Pro (Biontex, Martinsried, Germany) at day 1. For the last 72 hours, 1 nM dDAVP was added to the medium at the basolateral side, while cells were treated with lithium for the last 48 hours as describe above. After 4 days, cells were harvested and prepared for immunoblotting. Of note: we found that mpkCCD cells are best transfected before seeding and that the ability of siRNAs to knockdown mRNAs in mpkCCD cells

only last about 4 days. Therefore, to allow determination of the effect of siRNAs, mpkCCD cells had to be analysed for AQP2 at 4 days following seeding/transfection, at which they are less polarized and thus express less AQP2. Consequently, lithium induced downregulation of AQP2 is less prominent in siRNA experiments compared to our standard protocol in which we culture these cells for 8 days.

RT-PCR.

MpkCCD cells were grown as described (15). Total RNA was isolated using TriZol extraction reagent (Gibco BRL, Life Technologies, Rockville, USA), according to the manufacturer's instructions. To remove potentially contaminating DNA, total RNA was treated with DNase (Promega, Madison, USA) in DNase buffer, incubated for 1 hr. at 37 °C, extracted with phenol/chloroform and precipitated using sodium acetate (3M, pH 5.2) and100% ethanol. 1.5 µg RNA was reverse-transcribed into cDNA using MMLV Reverse Transcriptase (RT, Invitrogen, Carlsbad, USA) and random primers. A control reaction using H_2O instead of MMLV RT was conducted to exclude amplification of genomic DNA.

Intron-spanning primers were designed using primer3 primer design software on mouse cDNA sequences (table 1), see http://frodo.wi.mit.edu/primer3/ (16). Amplification of the proper fragments with the designed primers was verified by amplification of mouse cDNA from brain tissue (as indicated in table 1) as a positive control. Amplification was performed using the cDNA equivalent of 5 ng of RNA in a total volume of 50 µL for 40 cycles (95°C 45 sec, 50°C 1 min, 72°C 1.30 min). DNA was separated through agarose gel electrophoresis and visualized using ethidium bromide.

Biochemical analyses

To determine the lactate concentration of apical cell culture medium and urine samples, the Amplex® Red Glucose/Oxidase Assay Kit (Thermo Fisher scientific, Massachusetts, USA) was used according to the manufacturer's instructions, but adapted to measure lactate concentrations as described (17). Cell culture medium was refreshed an hour prior to the collection of the media. Urinary ammonium was determined using a Pointe Scientific kit (A7553; Canton, USA) modified for small volumes as described (18).

Cell surface biotinylation

Cell surface biotinylation was done as described (19). In short, mpkCCD cells were cultured in Transwells and treated with drugs as described above, incubated for 30 minutes at 4°C with 0.5 mg/ml sulfo-NHS-LC-LC-biotin (Pierce, Rockford, USA) diluted in PBS-CM (Phosphate buffered saline with 1 mM MgCl2 and 0,5 mM CaCl2) at the apical side of the cells, lysed (lysis buffer: 150 mM NaCl, 5 mM EDTA, 50 mM Tris (pH

7.5), 1% triton X-100), and incubated overnight with neutravidin-agarose beads (Pierce, Rockford, USA) to isolate cell surface biotinylated proteins. After washing of the beads with lysis buffer, proteins were eluted and denatured in Laemmli buffer, and immunoblotted.

Immunoblotting

Laemmli samples were denatured for 30 minutes at 37°C. SDS-PAGE, blotting, and blocking of the PVDF membranes was done as described (20). Membranes were incubated for 16 hours at 4°C with 1:1000 affinity–purified rabbit (Rb2) C tail AQP2 antibody in Tris-Buffered Saline Tween-20 (TBS-T) supplemented with 1% nonfat dried milk (21). In an identical way, other blots were incubated with 1:1000 rabbit CA12 antibody (kind gift from Prof. William S. Sly, Saint Louis University School of Medicine, St. Louis, MO, USA) and a rabbit CA2 antibody (Abcam, Cambridge, UK) and Cyclin D1 (Rabbit; cell signaling, Massachusetts, USA). After washing in TBS-T, all blots were incubated for 1 hour in TBS-T containing 1:10000-diluted goat anti–rabbit IgGs (Sigma-Aldrich, St. Louis, USA) coupled to horseradish peroxidase. Proteins were visualized using enhanced chemiluminescence (ECL; Pierce, Rockford, USA). Densitrometric analyses were performed using Bio-Rad quantification equipment (Bio-Rad 690c Densitometer; Chemidoc XRS) and Image studio software (LI-COR, Nebraska, USA). Equal loading of the samples was confirmed by staining of the blots with coomassie brilliant blue R-250 (BioRad, Hercules, USA).

Immunocytochemistry

Immunocytochemistry was done as described (22). In short, after removal of culture medium, mpkCCD cells were washed 3 times with ice-cold PBS-CM and fixed for 30 min at room temperature with 4% w/v paraformaldehyde in PBS. After washing twice with PBS, cells were treated with a permeabilization buffer (0.5% v/v Triton X-100 and in PBS with 0.7% w/v gelatin) for 30 min. Then, cells were incubated at 4°C overnight with AQP2 (Rb2 1:50; (21)) primary antibody in permeabilization buffer. After 3 washing steps, cells were incubated with anti-rabbit secondary antibody conjugated to an Alexa dye (Invitrogen, 1:500) for 2-3 hours at 37°C. Finally, cells were mounted in Vectashield containing DAPI (Vector Laboratories, Burlingame, USA) and imaged by confocal microscopy (Olympus FV1000, Center Valley, PA, USA).

Statistical analysis

Analysis of the difference between groups was performed with student t-test or one-way ANOVA corrected by the Bonferroni multiple-comparisons procedure. A p-value <0.05 was considered statistically significant.

Results

Inhibition of CA 9/12 attenuates lithium-induced AQP2 downregulation in mpkCCD cells

Recently, we have shown that acetazolamide, a specific carbonic anhydrase (CA) inhibitor, attenuated lithium-induced AQP2 downregulation in mpkCCD cells and mice (9). Next, we set out to identify, which CA was involved in the attenuation of lithium-induced downregulation of AQP2. Sixteen CA isoforms are known and most of them are expressed in the kidney (23). To examine which CAs are expressed in lithium-treated mpkCCD cells, we grew mpkCCD cells to polarization, induced AQP2 expression with dDAVP for 4 days and treated them with lithium for the last 2 days. Subsequent RNA isolation and RT-PCR analysis revealed DNA bands of the expected mass for CAs 1, 2, 5B, 6, 7, 9 and 11 to 15, which were absent in the RT- lanes (Fig.1A). The appearance of anticipated DNA fragments upon restriction enzyme digestion confirmed that the specific CA were amplified (Fig. 1B and Table 1).

If acetazolamide would act on one of these CAs, it was to be expected that down-regulation of the particular CA would attenuate lithium-induced downregulation of AQP2. Therefore, following transfection with CA-specific siRNAs against all CA-isoforms detected in this cell line, mpkCCD cells were grown to polarization and treated with dDAVP. Subsequent AQP2 immunoblotting revealed that only siRNAs silencing CA9 led to a significant increase in AQP2 abundance above the basal levels (Fig. 1C, D). Treatment with siRNAs downregulating CA12 showed a tendency to increase AQP2 abundance, but this effect was not significant. To validate the relevance of CA9/12 inhibition in this process differently, we employed 6- and 7- hydroxycoumarin (6HC and 7HC), which are drugs that inhibit CA9 and 12 far more efficient than other CA isoforms (24). Following treatment of mpkCCD cells with lithium as above and with or without 6HC or 7HC addition, subsequent immunoblotting for AQP2 revealed that both drugs indeed fully rescued the lithium-induced AQP2 downregulation (Fig. 1E, F).

Lithium increases lactate production in mpkCCD cells and mice through ENaC-mediated entry in the collecting duct

As an increased expression of especially CA9 and CA12 is observed in tumor cells (25, 26) and entry of lithium in principal cells leads to cell proliferation, which, in cancer cells often coincides with aerobic glycolysis, a metabolic state characterized by glycolysis and lactate production at physiological oxygen levels, we wanted to test whether lithium induces aerobic glycolysis in renal principal cells. For this, we grew mpkCCD cells, which are mouse collecting duct cells that endogenously express AQP2 in response to vasopressin (15), to confluence, stimulated them with dDAVP, and treated them for 2 days with lithium. To determine the cell viability and extent of

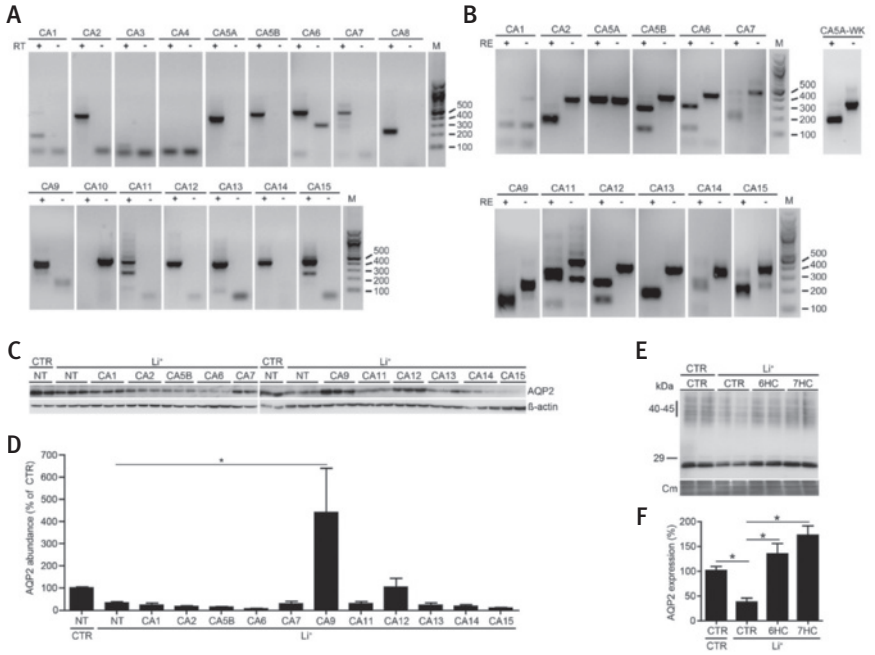

Figure 1. CA9 downregulation rescues lithium-induced AQP2 downregulation. Native mpkCCD were grown to confluence for 4 days and exposed to 1 nM dDAVP for another 4 days. During the last 24 hrs., the cells were incubated with lithium. On day 8, cells were harvested and RNA was isolated. After reverse transcriptase treatment and PCR amplification, the PCR products were visualized with ethidium bromide staining of agarose electrophoresis gels (**A**). Restriction enzyme digestion confirmed the specificity of the observed bands (**B**). For the siRNA experiment, mpkCCD cells were transfected with siRNAs targeting different CAs, seeded on Transwell filters and treated for the last 2 days without (CTR) or with lithium (Li+). AQP2 abundance as assessed by immunoblotting (**C**) and quantification of 4 independent experiments (**D**). Confluent mpkCCD cells were incubated during the last 2 days in the absence (CTR) or presence of lithium only (Li+) or lithium with 6-hydroxycoumarin (6HC) or 7-hydroxycoumarin (7HC). Unglycosylated AQP2 abundance as detected by immunoblotting (**E**) and quantification of 3 independent experiments (**F**). Equal loading of the samples was confirmed by staining of the blots with β-actin or Coomassie blue (Cm). Data presented are mean ± SEM. One way ANOVA, Bonferroni's Multiple Comparison Test, * $p<0.05$. NT. Abbreviations: NT, non-targeting; CA, carbonic anhydrase; RT, reverse transcriptase; M, marker; RE, restriction enzyme; WK, whole kidney.

transcellular sodium transport, the Trans Epithelial Electrical Resistance (TEER) and transcellular voltage (Tv) were measured. Lithium caused a slight reduction in TEER and Tv (Fig. 2), indicative of a reduced extent of cell polarization. Indeed, and as observed *in vivo (8)*, lithium increased the cyclin D1 abundance, besides decreased AQP2 levels (Fig. 2C). Analysis for lactate in medium indeed revealed that lithium treatment increased its release in mpkCCD cells (Fig. 2D). Earlier, we have shown that lithium enters principal cells via ENaC and that rodents lacking ENaC or in which ENaC was blocked with amiloride showed an absent/attenuated development of Li-NDI (4, 27). Interestingly, co-treatment of lithium with amiloride attenuated the reduction in TEER caused by lithium but further reduced the Tv. More importantly, amiloride attenuated lithium induced AQP2 downregulation and lithium induced increase in cyclin D1 abundance and lactate release (Figs 2A-D). Furthermore, we also analyzed lactate release after cotreatment with lithium and 6HC and 7HC. Consistent with their effect on lithium-induced downregulation of AQP2, we found that both inhibitors also attenuated the lithium-induced increase in lactate release (Fig 2E).
To test whether lithium also induces aerobic glycolysis *in vivo*, we treated normal and CD ENaC-KO mice with lithium and tested the urinary content for lactate. As shown before (27), lithium increased urine volume and decreased urine osmolality in WT mice, but not in ENaC-KO mice (Fig. 2F, G). Importantly and in line with the data above, the 24-hrs urinary lactate levels were strongly elevated in lithium treated WT mice, but not in lithium treated ENaC-KO mice (Fig. 2H). Together, these data indicated that ENaC-mediated entry of lithium causes principal cell aerobic glycolysis in vitro and in vivo.

2DG partly attenuates lithium-induced AQP2 downregulation in mpkCCD cells.

Recently, a switch to aerobic glycolysis has also been found to underlie autosomal dominant polycystic kidney disease (ADPKD) and treatment with 2DG, which reduces cellular glucose entry and usage in aerobic glycolysis, attenuated further ADPKD development (28). We therefore tested whether 2DG would also attenuate the *in vitro* effects of lithium. For this lithium and 2DG were added simultaneously to the apical and basolateral medium of mpkCCD cells during the last 2 days, always in the presence of dDAVP. Interestingly, 2DG treatment increased the TEER (Fig. 3A) and significantly reduced the lactate production (Fig. 3B). Moreover, 2DG treatment fully recovered the lithium-induced downregulation of unglycosylated AQP2, but the abundance of complex-glycosylated AQP2 remained low after co-treatment with lithium and 2DG (Figs. 3C-E). Earlier, the Golgi complex retention of AQP2-N123Q, which cannot be glycosylated anymore, in polarized cells indicated that glycosylation is important for cell surface expression of AQP2 (29) and, as such, the reduced abundance of complex-glycosylated AQP2 could indicate that AQP2 was impaired in its trafficking to the

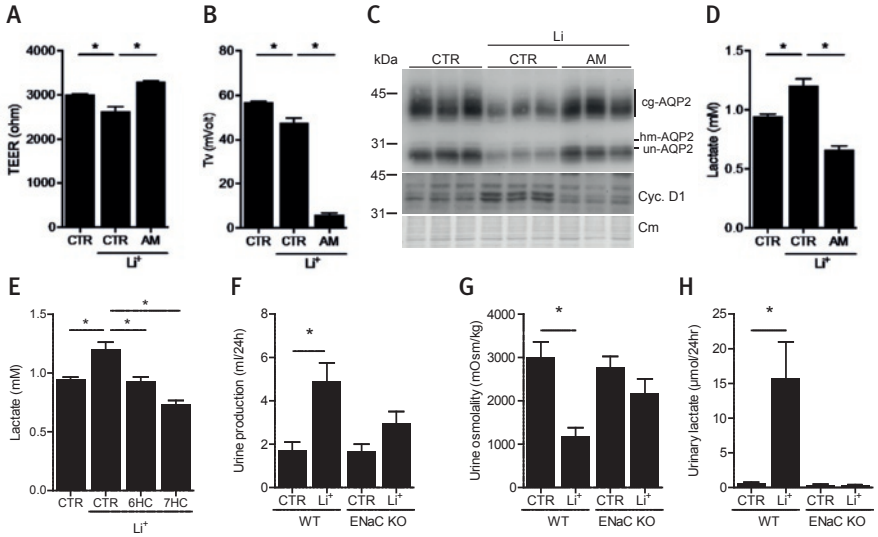

Figure 2. Lithium increases lactate production in mpkCCD cells and wildtype mice but not in ENaC KO mice. MpkCCD cells were cultured on Transwell filters for 8 days with or without lithium or lithium and amiloride in the last 2 days. Then resistance (**A**) and transcellular voltage (**B**) were determined prior to the collection of cells and apical medium, which were used to perform AQP2 and cyclin D1 immunoblot analyses (**C**) and measure lactate (**D**), respectively. Lactate release was also measured in apical medium of cells treated with 6HC and 7HC (**E**) The data presented is the mean of three independent experiments. In the animal experiment, mice received normal rodent diet (CTR), while the other mice received the same diet supplemented with 40 mmol LiCl/kg food for 10 days. They were individually housed in metabolic cages for the last 48 hours. Urine production (**F**), osmolality (**G**) and lactate (**H**) were determined for the last 24h. An asterisk denotes a significant difference ($P<0.05$) from CTR. Abbreviations: CTR, control; Li+, lithium; AM, amiloride; 6HC and 7HC, 6- and 7-hydroxycoumarin; WT, wildtype, ENaC KO, Epithelial sodium channel knockout mice; AQP2, aquaporin-2, cg; complex glycosylated, hm; high mannose glycosylated, un; unglycosylated and Cm, coomassie blue staining.

plasma membrane. To test whether 2DG impaired proper trafficking of AQP2 to the plasma membrane, a cell surface biotinylation assay and immunocytochemistry was performed. Immunoblotting of biotinylated cell surface proteins, however, revealed that the abundance of unglycosylated AQP2 in the plasma membrane of lithium-2DG co-treated cells was indifferent from control cells, but significantly higher than of lithium-treated cells (Figs. 3F-H). These data were supported by our Immunocytochemistry, as a clear apical membrane expression of AQP2 was observed in cells treated with Li and 2DG, which was similar to dDAVP-control cells, but not observed in Li-treated cells (Fig. 3I).

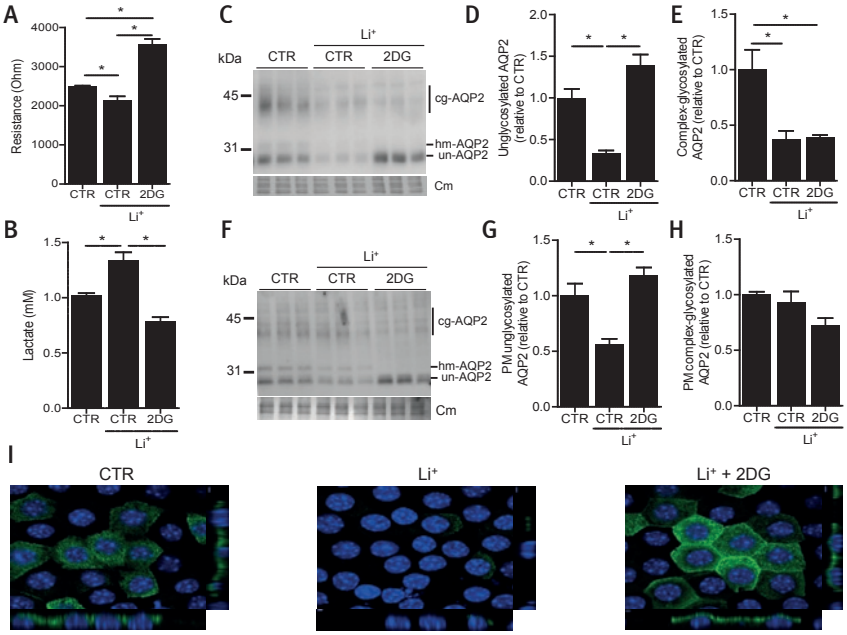

Figure 3. 2DG partly rescues lithium-induced AQP2 downregulation in mpkCCD cells MpkCCD cells were cultured on Transwell filters for 8 days with or without lithium or lithium and 2DG in the last 2 days. The resistance (**A**) was measured prior to the collection of apical medium, which was used for lactate measurements (**B**). Then, cells were either collected for immunoblot analysis to determine total AQP2 (**C-E**) and cell surface AQP2 protein abundance (**F-H**) or stained using immunocytochemical analysis for AQP2 (**I**; AQP2 green; DAPI blue). The data presented is the mean of at least three independent experiments performed in triplicate. A significant difference ($P<0.05$) from CTR is denoted by an asterisk. Abbreviation: CTR, control; Li+, lithium; 2DG, 2-deoxyglucose; AQP2, aquaporin-2, cg; complex glycosylated, hm; high mannose glycosylated, un; unglycosylated and Cm, coomassie blue staining.

2DG does not attenuate lithium-NDI in mice

Considering the positive *in vitro* effects, we subsequently investigated the effect of 2DG on Li-NDI *in vivo*. For this, mice were exposed to food without or with lithium or lithium with 2DG for 10 days. However, the lithium-induced increase in urine volume and decrease in urine osmolality were not attenuated by 2DG (Fig. 4A, B). The urinary lithium concentrations were similar in both lithium treated groups (Fig. 4C). To measure lactate and other metabolites in urine, NMR was employed (Figs. 4D-I). Importantly, the 2DG treatment reduced the lithium-induced increase in lactate production, indicating that the 2DG treatment on blocking aerobic glycolysis was effective (Fig. 4D).

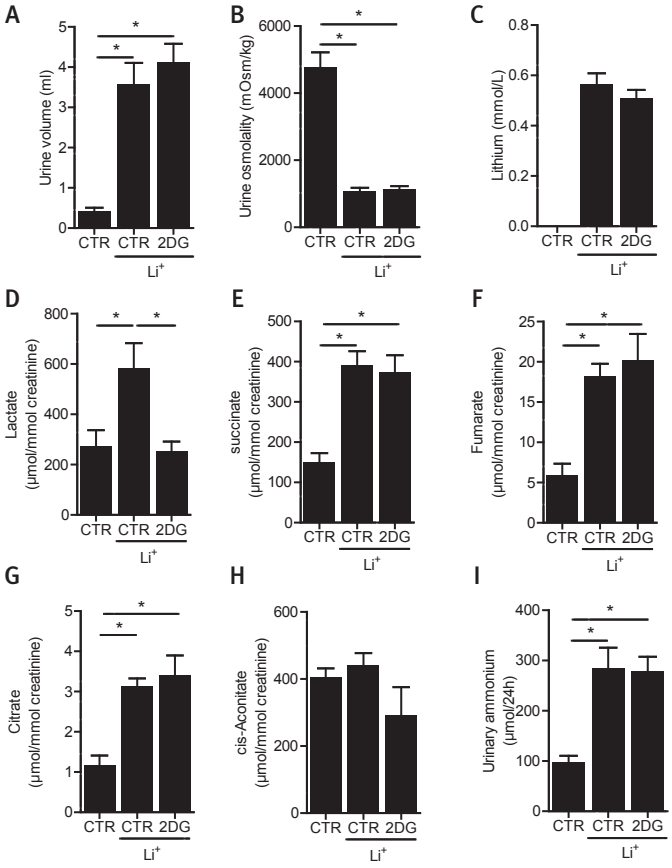

Figure 4. 2DG does not attenuate lithium-induced NDI in mice One group of the mice received normal rodent diet while the other mice received the same diet supplemented with 40 mmol LiCl/kg food or LiCl with 2-deoxyglucose (2DG; 250 mg/kg food) for 10 days and individually housed in metabolic cages for the last 48 hours. Urine production (**A**), urine osmolality (**B**) were determined for the last 24h and blood was collected to measure plasma lithium levels (**C**). 1H-NMR analysis was performed to determine urinary lactate (**D**), succinate (**E**), fumarate (**F**), citrate (**G**) and cis-aconitate (**H**) levels while urinary ammonium (**I**) was measured using ammonium assay. A significant difference ($P<0.05$) from CTR is denoted by an asterisk. Abbreviation: CTR, control; Li+, lithium and 2DG, 2-deoxyglucose.

Interestingly, however, NMR analysis revealed that the creatinine-normalized levels of metabolites such as succinate, fumarate and citrate were increased with lithium, but not attenuated by 2DG (Figs. 4E-G). The cis-aconitate levels were similar in all groups (Fig. 4H) and biochemical analysis further revealed that the increased excretion of ammonium with lithium treatment was not decreased by 2DG (Fig. 4I).

Discussion

ENaC mediated lithium influx into principal cells causes aerobic glycolysis

Earlier, we and others have shown that, by entering via ENaC, lithium initiates proliferation of principal cells *in vitro* and *in vivo (7, 8)*. Moreover, we have shown that lithium influx in principal cells also induces a G2/M cell cycle phase block *in vitro* and *in vivo*, which may at least partially explain the overall loss of principal cells observed in Li-NDI (8). Here, we provide *in vitro* and *in vivo* data which show that the lithium-induced principal cell proliferation coincides with metabolic changes, characteristic for aerobic glycolysis. In the continuous presence of oxygen, lithium treatment induced an increased (*in vitro*) release and (*in vivo*) urinary excretion of lactate, which was absent in mice lacking ENaC in collecting ducts. The observed slight increase in urine volume and decrease in urine osmolality with lithium in ENaC-KO mice may be due to remaining ENaC-mediated influx of lithium in connecting tubules, as these cells contribute weakly to urine concentration and AQP2 and ENaC are still expressed in these cells of these mice (27). Blocking lithium entry into mpkCCD cells with amiloride did not only attenuate lithium-induced AQP2 downregulation but also prevented cell proliferation and aerobic glycolysis. Our NMR analysis furthermore revealed that lithium treatment strongly increased urinary levels of succinate, fumarate and citrate, metabolites which are known to increase during glutaminolysis (30). With aerobic glycolysis, glutaminolysis is typically upregulated as well, because glutamine provides the cell of nitrogen and citrate, needed for amino acid and lipid synthesis, respectively (31). Moreover, during aerobic glycolysis, the increased intracellular acid production, such as lactate, necessitates the cell to ignite pathways to buffer acid excess, besides secretion of lactate through MCT proteins. Cellular glutamine influx and glutaminolysis serve this buffering function, as the two molecules of NH_3 released from glutamine and glutamate during glutaminolysis are effective H^+ buffers (32). In line with this, urinary ammonium (NH_4^+) was strongly increased with lithium.

Our in vitro data on the CAs involved in the ACZ-induced suppression of lithium-induced downregulation of AQP2 are in line with the above. Although we have not solidly proven that the mix of four siRNAs against the different CAs indeed downregulated the expression of each CA, a dogma concluded from an extensive study in which thousands of siRNAs were tested to block cancer cell growth (13, 14),

our siRNA (Fig. 1 C, D) and CA-specific drug treatments clearly revealed that inhibition of CA9, and possibly CA12, attenuated the lithium-induced AQP2 downregulation in mpkCCD cells. The increase in CA9 abundance was higher in the siRNA experiment compared to the experiment with CA-specific drugs. This is possibly due to the longer culturing time in drug treatment assay that allowed the polarization of the cells that will express more AQP2 even in the control condition. CA9 and -12 are normally located to the basolateral membrane of epithelial cells, but appear in both plasma membranes in proliferative cells (33-35). CA12 is abundantly expressed in the collecting duct of healthy kidneys, however the cell specificity seems to depend on the species tested: while in humans and rabbits CA12 is mainly found in principal cells, its expression seems restricted to type-A intercalated cells in rodents (33, 36, 37). CA9 is hardly expressed in healthy kidneys, but CA9 and CA12 expression is markedly increased in renal carcinomas, where they facilitate proliferation of these tumor cells by facilitating the cellular removal of acids (25, 26). CA9/12 generate HCO_3^-, which is taken up by tumor cells to neutralize their excessive production of acids, such as lactate, produced during aerobic glycolysis (10). The action of CA9/12 allows tumor cells to continue their Warburg-like proliferation and acid secretion, of which the latter helps cell proliferation by disassembling junctional proteins (38-40). Unfortunately, the CA9 antibodies used in clinics to reduce tumor growth (41) did not reveal any signal with our kidney samples, which has been attributed to human CA9 specificity (42).

Unfortunately, and in contrast to mice suffering from ADPKD (28), inhibition of aerobic glycolysis with 2DG did not attenuate Li-NDI. *In vitro*, 2DG attenuated the Li-induced downregulation of total and apical membrane abundance of AQP2. AQP2 with 2DG was mainly of the unglycosylated form, which is in line with the fact that glucose uptake is necessary for Asn-glycosylation of proteins through its utilization in the hexosamine biosynthetic pathway. The hexosamine pathway branches off from glycolysis at fructose-6-phosphate and produces UDP-N-acetylglucosamine (UDP-GlcNAc), the substrate for N-glycosylation (43). 2DG enters the cells via glucose transporters (GLUTs) (44). In mpkCCD cells, GLUT1 and GLUT8 are likely present, as their mRNAs were detected by RNAseq analysis, whereas GLUT1, GLUT4, GLU6 and GLUT8 mRNA expression was detected in rat collecting ducts (45) (46). This difference is, however, not likely to explain the difference in response of AQP2 rescue with between mpkCCD cells and the kidney, because the normalization of urinary lactate excretion with 2DG illustrated the blocking effect of aerobic glycolysis of 2DG in our mice. However, 2DG did not attenuate the lithium-induced increases in urinary succinate, fumarate, citrate and ammonium excretion, indicating that 2DG did not affect the effect of lithium on glutaminolysis. Our data indicate lithium, which can still enter principal cells through ENaC in our 2DG experiment, induces aerobic glycolysis and glutaminolysis through different pathways, and may suggest that the increased glutaminolysis is of more relevance to Li-NDI, as Li-NDI was not improved with 2DG. As

such, future studies should focus on the potential role of glutaminolysis in the pathogenesis of Li-NDI.

Principal cell aerobic glycolysis may underlie collecting duct remodeling in Li-NDI.

It is well-known that Li-NDI coincides with collecting duct cell remodeling in which the number of principal cells decrease and the number of acid-secreting (alpha) intercalated cells increase (6), but how lithium causes this remodeling is unclear. An important stimulus could be the development of metabolic acidosis, which is often, but not always, observed with lithium treatment in rodents and man (9, 47), because a state of metabolic acidosis increases the numbers of alpha-intercalated cells as an adaptive response (48, 49). How lithium causes metabolic acidosis, however, is unclear. As lithium attenuated the activity of H^+-ATPase and H^+/K^+-ATPase, earlier studies suggested lithium-induced that metabolic acidosis and collecting duct remodeling could be due to a direct inhibition of these transporters of intercalating cells (50, 51). However, if true, the effect of lithium on collecting duct remodeling should be independent from its influx in the principal cells, which does not seem to be the case: First, Kortenoeven et al. showed that amiloride, which inhibits lithium entry in principal cells only, attenuated collecting duct remodeling (4). Moreover, the abundance of H^+ATPase, a marker protein for alpha-intercalated cells, was not increased lithium-treated ENaC-KO (27). These studies thus indicate that lithium-induced remodeling is a direct effect of principal cell lithium entry. Our present data now reveal that lithium induces aerobic glycolysis in principal cells, a condition coinciding with increased lactic acid production and principal cell acid secretion. As such, the increased number of alpha-intercalated cells in Li-NDI may be induced by the increased local acidification due to principal cell acid secretion. Future studies are required to test this hypothesis.

Lithium and renal cancer

The lithium-induced increase in proliferation rate and the metabolic switches towards aerobic glycolysis and glutaminolysis as found here are hallmarks of cancer cells (30) Moreover, we also found that, at least *in vitro*, the lithium-induced downregulation of AQP2 is inhibited by CA9/12 siRNAs or blockers, which are also often upregulated in diverse cancers to counteract intracellular acidification due to extensive lactate production (1, 25). Although these data could be interpreted to fuel the thought that lithium may increase renal cancer development in bipolar patients, as has recently been suggested in a small epidemiological study (52), this hypothesis has later been convincingly refuted in several larger and more robust epidemiological studies (53-55). Moreover, several other arguments can be brought about against a connection between lithium and renal cancer. At first, one should realize that glutaminolysis

fueling cell proliferation is also a feature of a normal cell-physiological responses of cells to increased metabolic demands, which occurs daily in many tissues (56). In this respect, one should also realize that, in contrast to an oncogenic mutation, activation of these pathways by lithium is only temporarily and not complete, as drugs never block proteins fully. Secondly, we did not observe any tumor in the kidneys of 40 weeks old mice that were treated from birth onwards with a clinical dose of lithium (not shown).

In conclusion, this study demonstrates that lithium induces aerobic glycolysis and glutaminolysis in renal principal cells. While aerobic glycolysis does not seem to play a role in the development of Li-NDI, future research will have to elucidate whether blocking glutaminolysis by e.g. CA9 inhibitors may attenuate Li-NDI development.

Acknowledgments

We thank Prof. Edith Hummler, Lausanne, Switzerland for providing the ENaC-KO mice. This project received support from a grant from the Society of Experimental Laboratory Medicine to PMTD, a Marie Curie Fellowship PIOF-GA-2012-332395 to TG and a grant by the Danish Medical Research Council to MLAK.

References

1. Yatham LN, Kennedy SH, Parikh SV, Schaffer A, Beaulieu S, Alda M, et al. Canadian Network for Mood and Anxiety Treatments (CANMAT) and International Society for Bipolar Disorders (ISBD) collaborative update of CANMAT guidelines for the management of patients with bipolar disorder: update 2013. Bipolar Disord. 2013;15(1):1-44.
2. Gold AB, Herrmann N, Lanctot KL. Lithium and its neuroprotective and neurotrophic effects: potential treatment for post-ischemic stroke sequelae. Curr Drug Targets. 2011;12(2):243-55.
3. Bendz H, Aurell M. Drug-induced diabetes insipidus: incidence, prevention and management. Drug Saf. 1999;21(6):449-56.
4. Kortenoeven ML, Li Y, Shaw S, Gaeggeler HP, Rossier BC, Wetzels JF, et al. Amiloride blocks lithium entry through the sodium channel thereby attenuating the resultant nephrogenic diabetes insipidus. Kidney Int. 2009;76(1):44-53.
5. Walker RJ, Weggery S, Bedford JJ, McDonald FJ, Ellis G, Leader JP. Lithium-induced reduction in urinary concentrating ability and urinary aquaporin 2 (AQP2) excretion in healthy volunteers. Kidney Int. 2005;67(1):291-4.
6. Christensen BM, Marples D, Kim YH, Wang W, Frokiaer J, Nielsen S. Changes in cellular composition of kidney collecting duct cells in rats with lithium-induced NDI. Am J Physiol Cell Physiol. 2004;286(4):C952-64.
7. Christensen BM, Kim YH, Kwon TH, Nielsen S. Lithium treatment induces a marked proliferation of primarily principal cells in rat kidney inner medullary collecting duct. Am J Physiol Renal Physiol. 2006;291(1):F39-48.
8. de Groot T, Alsady M, Jaklofsky M, Otte-Holler I, Baumgarten R, Giles RH, et al. Lithium causes G2 arrest of renal principal cells. J Am Soc Nephrol. 2014;25(3):501-10.
9. de Groot T, Sinke AP, Kortenoeven ML, Alsady M, Baumgarten R, Devuyst O, et al. Acetazolamide Attenuates Lithium-Induced Nephrogenic Diabetes Insipidus. J Am Soc Nephrol. 2016;27(7):2082-91.
10. Vander Heiden MG, Cantley LC, Thompson CB. Understanding the Warburg effect: the metabolic requirements of cell proliferation. Science. 2009;324(5930):1029-33.
11. Hummler E, Barker P, Talbot C, Wang Q, Verdumo C, Grubb B, et al. A mouse model for the renal salt-wasting syndrome pseudohypoaldosteronism. Proc Natl Acad Sci U S A. 1997;94(21):11710-5.
12. Engelke UF, Tassini M, Hayek J, de Vries M, Bilos A, Vivi A, et al. Guanidinoacetate methyltransferase (GAMT) deficiency diagnosed by proton NMR spectroscopy of body fluids. NMR Biomed. 2009;22(5):538-44.
13. Berns K, Hijmans EM, Mullenders J, Brummelkamp TR, Velds A, Heimerikx M, et al. A large-scale RNAi screen in human cells identifies new components of the p53 pathway. Nature. 2004;428(6981):431-7.
14. Martens-de Kemp SR, Nagel R, Stigter-van Walsum M, van der Meulen IH, van Beusechem VW, Braakhuis BJ, et al. Functional genetic screens identify genes essential for tumor cell survival in head and neck and lung cancer. Clin Cancer Res. 2013;19(8):1994-2003.
15. Li Y, Shaw S, Kamsteeg EJ, Vandewalle A, Deen PM. Development of lithium-induced nephrogenic diabetes insipidus is dissociated from adenylyl cyclase activity. J Am Soc Nephrol. 2006;17(4):1063-72.
16. Rozen S, Skaletsky H. Primer3 on the WWW for general users and for biologist programmers. Methods in molecular biology. 2000;132:365-86.
17. de Groof AJ, te Lindert MM, van Dommelen MM, Wu M, Willemse M, Smift AL, et al. Increased OXPHOS activity precedes rise in glycolytic rate in H-RasV12/E1A transformed fibroblasts that develop a Warburg phenotype. Mol Cancer. 2009;8:54.
18. Lee HW, Verlander JW, Bishop JM, Igarashi P, Handlogten ME, Weiner ID. Collecting duct-specific Rh C glycoprotein deletion alters basal and acidosis-stimulated renal ammonia excretion. Am J Physiol Renal Physiol. 2009;296(6):F1364-75.
19. Baumgarten R, Van De Pol MH, Wetzels JF, Van Os CH, Deen PM. Glycosylation is not essential for vasopressin-dependent routing of aquaporin-2 in transfected Madin-Darby canine kidney cells. J Am Soc Nephrol. 1998;9(9):1553-9.
20. Kamsteeg EJ, Wormhoudt TA, Rijss JP, van Os CH, Deen PM. An impaired routing of wild-type aquaporin-2 after tetramerization with an aquaporin-2 mutant explains dominant nephrogenic diabetes insipidus. EMBO J. 1999;18(9):2394-400.

21. Deen PM, Verdijk MA, Knoers NV, Wieringa B, Monnens LA, van Os CH, et al. Requirement of human renal water channel aquaporin-2 for vasopressin-dependent concentration of urine. Science. 1994;264(5155): 92-5.
22. Deen PM, Van Balkom BW, Savelkoul PJ, Kamsteeg EJ, Van Raak M, Jennings ML, et al. Aquaporin-2: COOH terminus is necessary but not sufficient for routing to the apical membrane. Am J Physiol Renal Physiol. 2002;282(2):F330-40.
23. Purkerson JM, Schwartz GJ. The role of carbonic anhydrases in renal physiology. Kidney Int. 2007;71(2): 103-15.
24. Carta F, Maresca A, Scozzafava A, Supuran CT. Novel coumarins and 2-thioxo-coumarins as inhibitors of the tumor-associated carbonic anhydrases IX and XII. Bioorg Med Chem. 2012;20(7):2266-73.
25. Tostain J, Li G, Gentil-Perret A, Gigante M. Carbonic anhydrase 9 in clear cell renal cell carcinoma: a marker for diagnosis, prognosis and treatment. Eur J Cancer. 2010;46(18):3141-8.
26. Wykoff CC, Beasley NJ, Watson PH, Turner KJ, Pastorek J, Sibtain A, et al. Hypoxia-inducible expression of tumor-associated carbonic anhydrases. Cancer research. 2000;60(24):7075-83.
27. Christensen BM, Zuber AM, Loffing J, Stehle JC, Deen PM, Rossier BC, et al. alphaENaC-mediated lithium absorption promotes nephrogenic diabetes insipidus. J Am Soc Nephrol. 2011;22(2):253-61.
28. Rowe I, Chiaravalli M, Mannella V, Ulisse V, Quilici G, Pema M, et al. Defective glucose metabolism in polycystic kidney disease identifies a new therapeutic strategy. Nat Med. 2013;19(4):488-93.
29. Hendriks G, Koudijs M, van Balkom BW, Oorschot V, Klumperman J, Deen PM, et al. Glycosylation is important for cell surface expression of the water channel aquaporin-2 but is not essential for tetramerization in the endoplasmic reticulum. J Biol Chem. 2004;279(4):2975-83.
30. Lunt SY, Vander Heiden MG. Aerobic glycolysis: meeting the metabolic requirements of cell proliferation. Annu Rev Cell Dev Biol. 2011;27:441-64.
31. Li C, Zhang G, Zhao L, Ma Z, Chen H. Metabolic reprogramming in cancer cells: glycolysis, glutaminolysis, and Bcl-2 proteins as novel therapeutic targets for cancer. World J Surg Oncol. 2016;14(1):15.
32. Weiner ID, Verlander JW. Renal ammonia metabolism and transport. Compr Physiol. 2013;3(1):201-20.
33. Kyllonen MS, Parkkila S, Rajaniemi H, Waheed A, Grubb JH, Shah GN, et al. Localization of carbonic anhydrase XII to the basolateral membrane of H+-secreting cells of mouse and rat kidney. The journal of histochemistry and cytochemistry : official journal of the Histochemistry Society. 2003;51(9):1217-24.
34. Gut MO, Parkkila S, Vernerova Z, Rohde E, Zavada J, Hocker M, et al. Gastric hyperplasia in mice with targeted disruption of the carbonic anhydrase gene Car9. Gastroenterology. 2002;123(6):1889-903.
35. Saarnio J, Parkkila S, Parkkila AK, Waheed A, Casey MC, Zhou XY, et al. Immunohistochemistry of carbonic anhydrase isozyme IX (MN/CA IX) in human gut reveals polarized expression in the epithelial cells with the highest proliferative capacity. The journal of histochemistry and cytochemistry : official journal of the Histochemistry Society. 1998;46(4):497-504.
36. Parkkila S, Parkkila AK, Saarnio J, Kivela J, Karttunen TJ, Kaunisto K, et al. Expression of the membrane-associated carbonic anhydrase isozyme XII in the human kidney and renal tumors. JHistochemCytochem. 2000;48(12):1601-8.
37. Schwartz GJ, Kittelberger AM, Watkins RH, O'Reilly MA. Carbonic anhydrase XII mRNA encodes a hydratase that is differentially expressed along the rabbit nephron. Am J Physiol Renal Physiol. 2003; 284(2):F399-410.
38. Dorai T, Sawczuk IS, Pastorek J, Wiernik PH, Dutcher JP. The role of carbonic anhydrase IX overexpression in kidney cancer. European journal of cancer. 2005;41(18):2935-47.
39. Svastova E, Zilka N, Zat'ovicova M, Gibadulinova A, Ciampor F, Pastorek J, et al. Carbonic anhydrase IX reduces E-cadherin-mediated adhesion of MDCK cells via interaction with beta-catenin. Experimental cell research. 2003;290(2):332-45.
40. Kroemer G, Pouyssegur J. Tumor cell metabolism: cancer's Achilles' heel. Cancer cell. 2008;13(6):472-82.
41. Tafreshi NK, Lloyd MC, Bui MM, Gillies RJ, Morse DL. Carbonic anhydrase IX as an imaging and therapeutic target for tumors and metastases. Subcell Biochem. 2014;75:221-54.
42. Zatovicova M, Jelenska L, Hulikova A, Ditte P, Ditte Z, Csaderova L, et al. Monoclonal antibody G250 targeting CA : Binding specificity, internalization and therapeutic effects in a non-renal cancer model. Int J Oncol. 2014;45(6):2455-67.

43. Vasconcelos-Dos-Santos A, Oliveira IA, Lucena MC, Mantuano NR, Whelan SA, Dias WB, et al. Biosynthetic Machinery Involved in Aberrant Glycosylation: Promising Targets for Developing of Drugs Against Cancer. Front Oncol. 2015;5:138.
44. Waki A, Kato H, Yano R, Sadato N, Yokoyama A, Ishii Y, et al. The importance of glucose transport activity as the rate-limiting step of 2-deoxyglucose uptake in tumor cells in vitro. Nucl Med Biol. 1998;25(7):593-7.
45. Knepper M. mpkCCD Transcriptome Database [Available from: http://sbel.mc.ntu.edu.tw/mpkCCDTranscriptome/mpkCCDTr.htm.
46. Knepper M. RNA-seq Analysis of Microdissected Rat Kidney Tubule Segments.
47. Weiner ID, Leader JP, Bedford JJ, Verlander JW, Ellis G, Kalita P, et al. Effects of chronic lithium administration on renal acid excretion in humans and rats. Physiol Rep. 2014;2(12).
48. Bagnis C, Marshansky V, Breton S, Brown D. Remodeling the cellular profile of collecting ducts by chronic carbonic anhydrase inhibition. Am J Physiol Renal Physiol. 2001;280(3):F437-48.
49. Welsh-Bacic D, Nowik M, Kaissling B, Wagner CA. Proliferation of acid-secretory cells in the kidney during adaptive remodelling of the collecting duct. PLoS One. 2011;6(10):e25240.
50. Dafnis E, Kurtzman NA, Sabatini S. Effect of lithium and amiloride on collecting tubule transport enzymes. The Journal of pharmacology and experimental therapeutics. 1992;261(2):701-6.
51. Eiam-Ong S, Dafnis E, Spohn M, Kurtzman NA, Sabatini S. H-K-ATPase in distal renal tubular acidosis: urinary tract obstruction, lithium, and amiloride. The American journal of physiology. 1993;265(6 Pt 2):F875-80.
52. Zaidan M, Stucker F, Stengel B, Vasiliu V, Hummel A, Landais P, et al. Increased risk of solid renal tumors in lithium-treated patients. Kidney Int. 2014;86(1):184-90.
53. Licht RW, Grabenhenrich LB, Nielsen RE, Berghofer A, International Group for the Study of L. Lithium and renal tumors: a critical comment to the report by Zaidan et al. Kidney Int. 2014;86(4):857.
54. Kessing LV, Gerds TA, Feldt-Rasmussen B, Andersen PK, Licht RW. Lithium and renal and upper urinary tract tumors - results from a nationwide population-based study. Bipolar Disord. 2015;17(8):805-13.
55. Pottegard A, Hallas J, Jensen BL, Madsen K, Friis S. Long-Term Lithium Use and Risk of Renal and Upper Urinary Tract Cancers. J Am Soc Nephrol. 2016;27(1):249-55.
56. Moncada S, Higgs EA, Colombo SL. Fulfilling the metabolic requirements for cell proliferation. Biochem J. 2012;446(1):1-7.

Chapter 5

The succinate receptor 1 has no role in the development of lithium-induced nephrogenic diabetes insipidus

Alsady M [1], Godefa TM [1], Bekkenkamp-Grovenstein M [1], Carmone C [1], Baumgarten R [2],Engelke U [3], Wevers RA [3], Bedford JJ [4], Leader JP [4], Walker RJ [4] and Deen PMT [1]*

[1] Department of Physiology and [3] Translational Metabolic Laboratory, Department of Laboratory Medicine, Radboud University Medical Center, the Netherlands; [2] Society of Experimental Laboratory Medicine, Amersfoort, The Netherlands; [4] Department of Medicine, University of Otago, Dunedin, New Zealand.

Abstract

Lithium remains the drug of choice in the treatment of bipolar disorder. However, the drug treatment causes lithium-induced nephrogenic diabetes insipidus (Li-NDI) that is marked by the downregulation of aquaporin-2 (AQP2) water channel. Recently, we have shown that lithium treatment was associated with a metabolic switch towards aerobic glycolysis that goes with elevated succinate release. SUCNR1 in principal cells has been coupled to calcium pathway, which normally reduces AQP2. Therefore, in this study we investigated the involvement of the SUCNR1 receptor in Li-NDI development. Succinate was elevated in the urine of lithium treated humans and mice compared to controls. No increase in succinate level was observed in lithium treated ENaC KO mice, indicating that succinate was derived from principal cells. Finally, to determine whether the SUCNR1 had a role in the development of Li-NDI, wildtype and SUCNR1 knockout mice received either control or lithium containing diet. Based on the indifferent urine output and urine osmolality we can conclude that SUCNR1 has no role in Li-NDI development.

Introduction

Lithium is the drug of choice for the treatment of bipolar disorder and is also regularly used to treat schizoaffective disorders and depression. Lithium is a frequently prescribed drug as it is provided to 0.1% of the western population (1, 2). Unfortunately, in 20% of the patients, lithium usage leads to nephrogenic diabetes insipidus (NDI), a disorder characterized by an impaired response of the kidney to vasopressin (AVP) leading to polyuria and polydipsia (3-5). Therewith, lithium-induced NDI is the most common form of NDI. Patients with lithium-NDI are at risk for dehydration and hypernatremia. Moreover, prolonged lithium treatment might lead to cyst formation and end stage renal disease (6). However, cessation of lithium therapy is not an option for most patients with NDI, because bipolar disorder symptoms have a larger impact on the patient's quality of life.

From studies in rats, it became clear that lithium-NDI develops in two stages. At short term, lithium-NDI coincides with downregulation of aquaporin-2 (AQP2) water channels, which is due to a reduced AQP2 transcription (7-9). Despite an increased proliferation of the AQP2-expressing principal cells of the collecting duct, long-term lithium treatment also results in a severe loss of AQP2-expressing principal cells, which might be attributed to a lithium-induced G2/M phase cell cycle arrest (10, 11). This principal cell loss is 'compensated' by an increased number of intercalated cells, which are involved in acid/base homeostasis (10).

Interestingly, purinergic signaling mediated by extracellular nucleotides opposes the action of AVP on renal collecting duct by decreasing the cellular cAMP and thus AQP2 protein levels (12). Kishore et al., showed that rat inner medullary collecting ducts that were perfused with ATP reduced the AVP-induced intracellular cAMP levels and transcellular water permeability (13). The same group also showed that mice lacking the purinergic $P2Y_2$ receptor were significantly more resistant to develop Li-NDI than healthy littermates and that pharmaceutical blockage of the ADP-activated $P2Y_{12}$ receptor in the kidney ameliorated their Li-induced NDI (12). These findings indicate that activation of purinergic receptors aggravate the development of Li-NDI and that targeting the purinergic signalling pathway may attenuate Li-NDI development.

Recently, we have shown that, besides cell proliferation, lithium also induces aerobic glycolysis, which coincides with the cellular release of lactate and succinate (14). Succinate is a metabolite released from mitochondria and cells under conditions of stress (15). Succinate is specifically bound by the succinate receptor type 1 (SUCNR1), also known as GPR91, which is a plasma membrane G-protein coupled receptor. The SUCNR1 is a member of the P2Y purinergic receptor family and reported to be expressed

in different segments of the kidney, including the collecting duct (15). As Li-NDI can be considered a consequence of a toxic cell stress event of lithium on collecting duct principal cells and lithium treatment led to elevated urinary levels of succinate, we here tested whether the SUCNR1 has a role in Li-NDI development using SUCNR1 knockout (SUCNR1 KO) mice.

Material and Methods

Human urine samples

Human urine samples were from an earlier clinical study and were collected and stored as described (16). In short, urines were collecting in the morning after an overnight fluid deprivation, centrifuged at 2000xg for 5 min to remove sediment and stored at -80°C until succinate was measured. The samples were derived from bipolar patients (seven females, three males), who were on chronic lithium therapy for the management of their mood disorder. These patients were matched with six healthy volunteers (three females, three males). Participants were recruited from a cohort of individuals on long-term lithium therapy who have previously participated in our clinical studies (17). Inclusion criteria included individuals with bipolar disorder treated with lithium carbonate, who were clinically stable, with no change in their medications over the preceding 3 months, and who had no known history of renal disease. Exclusion criteria included the inability to give informed consent, a history of known renal disease, the continued use of a diuretic or angiotensin-converting enzyme inhibitor, unstable psychiatric condition, or recent changes in psychotropic medications. All participants gave written informed consent to take part in the study, which was approved by the New Zealand (Lower South Regional) Ethics Committee.

Animal experiments

Animal experiments were performed as described (11). Heterozygous SUCNR1 mice on a C57BL/6 background were a kind gift from Amgen (Thousand Oaks, CA, USA) and were generated as described (18, 19). The animals were intercrossed with wildtype (WT) C57BL/6 littermates to yield homozygous SUCNR1 KO offsprings as described (19). Collecting duct-specific epithelial sodium channel knockout (NMR16J ENaC KO) mice (20) were kindly provided by Edith Hummler, Lausanne, Switzerland and crossed with C57BL/6 mice, obtained from Harlan Laboratories (Horst, the Netherlands). 8-12 weeks old male SUCNR1 KO, ENaC KO mice and their WT littermates were used in the experiments. The mice were housed in a climate-controlled facility with a 12-hour:12-hour light-dark cycle. All mice had free access to rodent diet (7013, NIH-31 Modified, Harlan Laboratories, Inc., Madison, WI, USA), acidified water and a sodium chloride block throughout the experiment. During the experiment, one group (n=6) of mice

received normal rodent diet, while the other mice received the same diet supplemented with 40 mmol lithium chloride (LiCl)/kg food. During the last 48 hours of an experiment, mice were housed in metabolic cages in order to measure water intake and urine output of the last 24 hours. Next, mice were anesthetized with isoflurane and euthanized by cervical dislocation, after which the kidneys were removed. All animal studies were approved by the Animal Ethical Committee of the Radboud University Medical Center.

Urine analysis

Urine samples from the mice experiment were centrifuged at 2000xg for 5 minutes to remove any sediment precipitated. Subsequently, the supernatant was transferred to a new tube and urine osmolality was measured using a Micro-Osmometer Model 3320 (Advanced Instruments, Inc., Norwood, MA). After that, urine was stored in eppendorf tubes at -80°C until NMR analysis was performed.

1H NMR Spectroscopy

One-dimensional 1H NMR spectroscopy was performed as described (21). 24h Urine was centrifuged for 10 minutes at 3000xg before analysis. 20 µL of 20.2 mM trimethylsilyl-2,2,3,3-tetradeuteropropionic acid (TSP, sodium salt; Aldrich) in D2O was added to 700 µL of the urine to serve as an internal quantity reference for subsequent handlings. The pH of each sample was adjusted to 2.50 ± 0.05 with concentrated HCl. Finally, 650 µL of the sample was placed in a 5 mm NMR tube (Wilmad Royal Imperial; Wilmad LabGlass, USA). 1H NMR spectra were obtained using a Bruker 500 MHz spectrometer (pulse angle, 90°; delay time, 4 s; number of scans, 256). Water resonance was suppressed by gated irradiation centered on the water frequency. The spectral width in the F1 and F2 domains was 5500 Hz. A total of 2K data points were collected in t2, 256 t1 increments with 32 transients per increment were used. The relaxation delay was set to 2 seconds. Before the Fourier transformation, a sine-bell function was applied in both time domains. During the relaxation delay, the water resonance was pre-saturated. The free-induction decays measured for these samples were processed using Topspin software (Bruker BioSpin, Rheinstetten, Germany). Fourier transformation was applied on the free-induction decay of the samples and the resulting spectra were phase and baseline corrected. The chemical shifts in the spectra were referenced to the internal standard, TSP. Assignment of peak positions for compound identification was performed by comparing the peak positions in the spectra of the metabolites with the reference spectral database of model compounds at pH 2.5 using Amix version 3.9.14 (Bruker BioSpin, Rheinstetten, Germany). Quantification of identified compounds was performed by manual integration of chosen peak(s) for a specific metabolite.

Statistics

One-way ANOVA with Bonferroni correction was applied. A *p* value of less than 0.05 was considered significant. Data are presented as mean and standard error of the mean (SEM).

Results

Lithium increases urinary succinate in mice and humans

Recently, we have shown that lithium treatment increased urinary succinate in mice (14). To investigate whether the released succinate was coming from collecting duct principal cells, we determined whether the urinary content of succinate with lithium differed between WT and ENaC KO mice. In the kidney, ENaC is specifically expressed in the apical membrane of the principal cells of the collecting duct. It is the entry site for lithium into the principal cells, as NDI development was prevented in ENaC KO mice treated with lithium (14). NMR analysis revealed that lithium treatment increased the urinary succinate content in WT mice, but not in ENaC KO mice (Fig. 1A).To determine whether lithium also increases succinate excretion in urine of humans, urine was collected from participants that were chronically treated with lithium and healthy volunteers who have previously participated in our clinical studies (17). Subsequent NMR analysis revealed that urinary succinate levels were indeed also elevated in lithium-treated patients (Fig. 1B). These data revealed that lithium increases urinary succinate release in mice and man.

Lithium induces NDI in wildtype and SUCNR1 KO mice

To subsequently determine whether the presence of the SUCNR1 may affect Li-NDI development, WT and SUCNR1 KO mice received a normal rodent diet with or without 40 mmol lithium chloride/kg food for 10 days after which their 24-hr urine was collected. Lithium treatment led to a somewhat reduced urine output in SUCNR1 KO mice as compared to WT littermates, but the difference was not significant (Fig. 2A). Lithium also reduced the urine osmolality, which was indifferent between SUCNR1 KO and WT mice (Fig. 2B). These results reveal that the presence of the SUCNR1 does not influence Li-NDI development in mice.

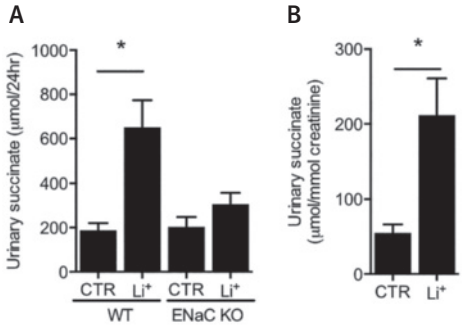

Figure 1. Lithium increases urinary succinate in mice and humans. (**A**) Mice received normal rodent diet (CTR) or the same diet supplemented with 40 mmol lithium chloride/kg food for 10 days (Li+). They were individually housed in metabolic cages for the last 48 hours. Of the urine collected during the last 24h, succinate concentration was determined using NMR. (**B**) To determine urinary succinate in humans, NMR analysis was performed on urines derived from participants, who were on chronic lithium therapy for the management of their mood disorder (Li+) and healthy volunteers (CTR). An asterisk denotes a significant difference ($P<0.05$) from CTR. Abbreviations: CTR, control; Li+, lithium; WT, wildtype, ENaC KO, Epithelial sodium channel knockout mice.

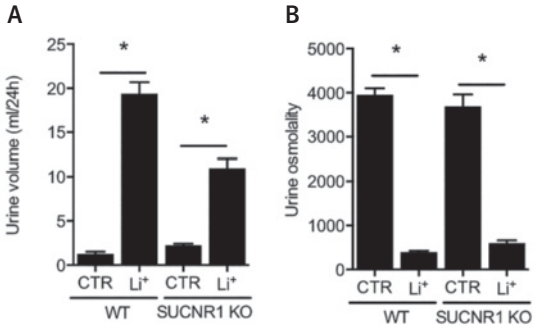

Figure 2. Lithium induces NDI in wildtype and SUCNR1 KO mice. WT and SUCNR1 KO mice received normal rodent diet (CTR), or the same diet supplemented with 40 mmol lithium chloride/kg food for 10 days. Mice were individually housed in metabolic cages for the last 48 hours, urine collected during the last 24 hrs and analysed for volume (**A**) and osmolality (**B**). An asterisk denotes a significant difference ($P<0.05$) from CTR. Abbreviations: CTR, control; Li+, lithium; WT, wildtype, SUCNR1 KO, Succinate receptor 1 knockout mice.

Discussion

The origin of succinate

Previously, we and others have shown that, by entering via ENaC, lithium initiates proliferation of principal cells *in vitro* and *in vivo (11, 22)*. Furthermore, we have shown that lithium influx in principal cells also induces a G2/M cell cycle phase block *in vitro* and *in vivo*, which may at least partially explain the overall loss of principal cells observed in Li-NDI (11). We also provided *in vitro* and *in vivo* data which show that the lithium-induced principal cell proliferation coincides with metabolic changes, characteristic for aerobic glycolysis and glutaminolysis (14). Succinate was one of the metabolites that was increased. Although we cannot exclude the possibility that ENaC KO mice do not release succinate, because they have an NMR16J instead of a C57BL6 background, it is most likely that the lack of lithium entry in principal cells in these mice prevented the observed absence of succinate excretion. Lithium induces principal cell glycolysis and glutaminolysis. With glycolysis, pyruvate is mainly converted into lactate, whereas the TCA cycle is mainly fueled by glutaminolysis with the use of glutamine, the most abundant circulating amino acid in blood, as an energy source. Moreover, when urinary succinate was measured in humans, the concentration of succinate in lithium-treated patients was significantly higher than in healthy volunteers. This suggests that the metabolic switch towards glycolysis and glutaminolysis also takes place in humans. Future studies might compare amiloride treated and non-treated lithium receiving patients to determine whether succinate is also coming from principal cells in humans.

The role of the succinate receptor in the development of Li-NDI

The SUCNR1, located in the luminal membrane of macula densa cells, or in the plasma membrane of afferent arteriole cells, induces the release of PGE2 and nitric oxide (23). This mediates the release of renin from the juxtaglomerular apparatus (JGA) in the kidney and subsequently the activation of the renal RAAS (23). With Li-NDI, RAAS is continuously activated due to the hypovolemia that is caused by the downregulation of AQP2 in the collecting duct. Therefore, the absence of SUCNR1 was expected to result in the loss of this compensatory mechanism and worsening of Li-NDI. However, in our study, the absence of SUCNR1 did not reduce nor aggravate Li-NDI development. As explained, SUCNR1 is a local sensor of stress and has been shown to expressed in collecting duct principal cells (15). Robben et al. showed that the activation of the MDCK cells by succinate caused Gq and Gi-mediated intracellular calcium mobilization, transient phosphorylation of extracellular regulated kinase (ERK)1/2 and the release of arachidonic acid along with PGE2 (24). In lithium-induced NDI, urinary PGE2 levels are increased and contribute significantly to the development of Li-NDI (25-27). PGE2 activates the EP3 receptor in principal cells, leading to a reduced cAMP signaling,

AQP2 expression, and plasma membrane targeting (28, 29). Our study reveals that development of Li-NDI is not influenced by the SUCNR1, as both WT and SUCNR1 KO mice developed LI-NDI to a similar extent. At present, it is unclear whether the SUCNR1 does not play a role at all in LI-NDI development or whether compensatory mechanisms play a role here: Missing SUCNR1, as in SUCNR1 KO mice, might be disadvantageous on the systemic level where the renin-angiotensin system (RAAS) cannot be activated properly to compensate for Li-induced hypovolemia, but advantageous for principal cells where less AQP2 is downregulated by prostaglandin E2 (PGE2).

Taken together, we have shown that lithium treatment increases urinary succinate in mice and humans, supporting our hypothesis that Li-NDI is a stress condition, and that urinary succinate is specifically coming from principal cells. Our mouse study, however, reveals that the SUCNR1 does not influence Li-NDI development.

Acknowledgments

This project received support from a grant from the Society of Experimental Laboratory Medicine to PMTD.

References

1. Timmer RT, Sands JM. Lithium intoxication. J Am Soc Nephrol. 1999;10(3):666-74.
2. Manji HK, Moore GJ, Chen G. Bipolar disorder: leads from the molecular and cellular mechanisms of action of mood stabilisers. BrJ Psychiatry. 2001;178(Suppl 41):S107-S19.
3. Stone KA. Lithium-induced nephrogenic diabetes insipidus. J Am Board FamPract. 1999;12(1):43-7.
4. Boton R, Gaviria M, Batlle DC. Prevalence, pathogenesis, and treatment of renal dysfunction associated with chronic lithium therapy. American Journal of Kidney Diseases. 1987;10:329-45.
5. Walker RJ, Weggery S, Bedford JJ, McDonald FJ, Ellis G, Leader JP. Lithium-induced reduction in urinary concentrating ability and urinary aquaporin 2 (AQP2) excretion in healthy volunteers. Kidney Int. 2005;67(1):291-4.
6. Alsady M, Baumgarten R, Deen PM, de Groot T. Lithium in the Kidney: Friend and Foe? J Am Soc Nephrol. 2016;27(6):1587-95.
7. Laursen UH, Pihakaski-Maunsbach K, Kwon TH, Ostergaard JE, Nielsen S, Maunsbach AB. Changes of rat kidney AQP2 and Na,K-ATPase mRNA expression in lithium-induced nephrogenic diabetes insipidus. Nephron ExpNephrol. 2004;97(1):e1-16.
8. Marples D, Christensen S, Christensen EI, Ottosen PD, Nielsen S. Lithium-induced downregulation of aquaporin-2 water channel expression in rat kidney medulla. J Clin Invest. 1995;95:1838-45.
9. Li Y, Shaw S, Kamsteeg EJ, Vandewalle A, Deen PM. Development of lithium-induced nephrogenic diabetes insipidus is dissociated from adenylyl cyclase activity. J Am Soc Nephrol. 2006;17(4):1063-72.
10. Christensen BM, Marples D, Kim YH, Wang W, Frokiaer J, Nielsen S. Changes in cellular composition of kidney collecting duct cells in rats with lithium-induced NDI. Am J Physiol Cell Physiol. 2004;286(4):C952-C64.
11. de Groot T, Alsady M, Jaklofsky M, Otte-Holler I, Baumgarten R, Giles RH, et al. Lithium causes G2 arrest of renal principal cells. J Am Soc Nephrol. 2014;25(3):501-10.
12. Kishore BK, Carlson NG, Ecelbarger CM, Kohan DE, Muller CE, Nelson RD, et al. Targeting renal purinergic signalling for the treatment of lithium-induced nephrogenic diabetes insipidus. Acta Physiol (Oxf). 2015;214(2):176-88.
13. Kishore BK, Chou CL, Knepper MA. Extracellular nucleotide receptor inhibits AVP-stimulated water permeability in inner medullary collecting duct. Am J Physiol. 1995;269(6 Pt 2):F863-9.
14. Alsady M, de Groot T, Kortenoeven MLA, Carmone C, Neijman K, Bekkenkamp-Grovenstein M, et al. Lithium induces aerobic glycolysis and glutaminolysis in collecting duct principal cells. Am J Physiol Renal Physiol. 2017:ajprenal 00297 2017.
15. Deen PM, Robben JH. Succinate receptors in the kidney. J Am Soc Nephrol. 2011;22(8):1416-22.
16. Weiner ID, Leader JP, Bedford JJ, Verlander JW, Ellis G, Kalita P, et al. Effects of chronic lithium administration on renal acid excretion in humans and rats. Physiol Rep. 2014;2(12).
17. Bedford JJ, Weggery S, Ellis G, McDonald FJ, Joyce PR, Leader JP, et al. Lithium-induced nephrogenic diabetes insipidus: renal effects of amiloride. Clin J Am Soc Nephrol. 2008;3(5):1324-31.
18. He W, Miao FJ, Lin DC, Schwandner RT, Wang Z, Gao J, et al. Citric acid cycle intermediates as ligands for orphan G-protein-coupled receptors. Nature. 2004;429(6988):188-93.
19. van Diepen JA, Robben JH, Hooiveld GJ, Carmone C, Alsady M, Boutens L, et al. SUCNR1-mediated chemotaxis of macrophages aggravates obesity-induced inflammation and diabetes. Diabetologia. 2017;60(7):1304-13.
20. Hummler E, Barker P, Talbot C, Wang Q, Verdumo C, Grubb B, et al. A mouse model for the renal salt-wasting syndrome pseudohypoaldosteronism. Proc Natl Acad Sci U S A. 1997;94(21):11710-5.
21. Engelke UF, Tassini M, Hayek J, de Vries M, Bilos A, Vivi A, et al. Guanidinoacetate methyltransferase (GAMT) deficiency diagnosed by proton NMR spectroscopy of body fluids. NMR Biomed. 2009;22(5):538-44.
22. Christensen BM, Kim YH, Kwon TH, Nielsen S. Lithium treatment induces a marked proliferation of primarily principal cells in rat kidney inner medullary collecting duct. Am J Physiol Renal Physiol. 2006;291(1):F39-48.
23. Toma I, Kang JJ, Sipos A, Vargas S, Bansal E, Hanner F, et al. Succinate receptor GPR91 provides a direct link between high glucose levels and renin release in murine and rabbit kidney. J Clin Invest. 2008;118(7):2526-34.

24. Robben JH, Fenton RA, Vargas SL, Schweer H, Peti-Peterdi J, Deen PM, et al. Localization of the succinate receptor in the distal nephron and its signaling in polarized MDCK cells. Kidney Int. 2009;76(12):1258-67.
25. Allen HM, Jackson RL, Winchester MD, Deck LV, Allon M. Indomethacin in the treatment of lithium-induced nephrogenic diabetes insipidus. Arch Intern Med. 1989;149(5):1123-6.
26. Jia Z, Wang H, Yang T. Mice lacking mPGES-1 are resistant to lithium-induced polyuria. Am J Physiol Renal Physiol. 2009;297(6):F1689-96.
27. Kim GH, Choi NW, Jung JY, Song JH, Lee CH, Kang CM, et al. Treating lithium-induced nephrogenic diabetes insipidus with a COX-2 inhibitor improves polyuria via upregulation of AQP2 and NKCC2. Am J Physiol Renal Physiol. 2008;294(4):F702-9.
28. Olesen ET, Fenton RA. Is there a role for PGE2 in urinary concentration? J Am Soc Nephrol. 2013;24(2):169-78.
29. Rao R, Zhang MZ, Zhao M, Cai H, Harris RC, Breyer MD, et al. Lithium treatment inhibits renal GSK-3 activity and promotes cyclooxygenase 2-dependent polyuria. Am J Physiol Renal Physiol. 2005;288(4):F642-9.

Chapter 6

Amiloride prevents lithium-induced acidification and proliferation of collecting duct cells

Alsady M [1], de Groot T [1], Christensen BM [2], Deen PMT [1]*

[1] Department of Physiology, Radboud University Medical Center, Nijmegen, The Netherlands;
[2] Department of Biomedicine, Aarhus University, Denmark.

Abstract

Lithium is the drug of choice in the treatment of bipolar disorder. However, this drug is associated with devastating side effects including lithium-induced nephrogenic diabetes insipidus (Li-NDI). The mechanism how lithium causes NDI is not clearly understood, but it is known that lithium downregulates aquaporin-2 (AQP2) water channel. Moreover, lithium also induces cell proliferation, collecting duct remodeling, and metabolic acidosis. Amiloride blocks the entry of lithium into the principal cells of the collecting duct. Previous studies demonstrated that amiloride attenuates lithium-induced AQP2 downregulation and collecting duct remodeling, but the effects of amiloride on metabolic acidosis and proliferation of collecting duct cells is not determined. Here, we treated rats with standard chow or supplemented with lithium or lithium and amiloride to investigate the development of these side effects. First, we found that amiloride attenuated Li-NDI, which coincided with the rescue of AQP2 in the inner and outer medulla but not in the cortex. Moreover, amiloride also prevented lithium-induced collecting duct remodeling and cell proliferation. Lithium did not induce hypercalcemia nor did it affect blood pH. However, analysis of urinary ammonium revealed that amiloride attenuated lithium-induced increase in urinary ammonium. Taken together, our data reveal that amiloride does not only rescue AQP2 downregulation but also prevents the development of metabolic acidosis and proliferation of collecting duct cells.

Introduction

Lithium is the main treatment of bipolar disorder and is also frequently used to treat other mental diseases such as schizoaffective disorders and depression. Lithium is prescribed to 0.1% of the western population (1, 2). However, 20% of the patients that receive lithium develop nephrogenic diabetes insipidus (NDI), which is characterized by an impaired response of the kidney to vasopressin (AVP) leading to polyuria and polydipsia (3-5). Therewith, lithium-induced NDI is the most common form of NDI. Patients with lithium-NDI are at risk for dehydration and hypernatremia. Moreover prolonged lithium treatment might lead to metabolic acidosis and collecting duct remodeling (1).

From studies in rodents, it became clear that lithium-NDI develops in two stages. At short term, lithium-NDI coincides with downregulation of aquaporin-2 (AQP2) water channels (6-8). Despite an increased proliferation of the AQP2-expressing principal cells of the collecting duct, long-term lithium treatment also results in a severe loss in the fraction of principal cells, which might be partially attributed to a lithium-induced G2/M phase cell cycle arrest (9, 10). This principal cell loss is 'compensated' by an increased number of intercalated cells, which are involved in acid/base homeostasis (9). Interestingly, lithium treatment is known to cause metabolic acidosis, which might be the trigger for intercalated cells to divide to remove excess acid (11-13).

To reduce polyuria in patients receiving lithium, a low-sodium diet together with thiazide and amiloride diuretics is prescribed (14). Amiloride acts on the principal cell epithelial sodium channel (ENaC) and others and we found that amiloride blocks principal cell lithium entry through ENaC, thereby attenuating polyuria in rodents and humans (15-17). Kortenoeven et al. showed that amiloride prevented lithium-induced AQP2 downregulation and collecting duct remodeling in the kidneys of rats (18). However, the effect of amiloride on lithium-induced metabolic acidosis and lithium-induced cell proliferation are not known. Therefore, in this study we investigated whether amiloride, besides the attenuation of Li-NDI and collecting duct remodeling, also prevents metabolic acidosis development and proliferation of principal cells.

Material and Methods

Animal experiments

The animal protocols were approved by the Animal Experiments Inspectorate, Ministry of Environment and Food of Denmark. Male Wistar rats were obtained from Janvier LABS (France). Lithium chloride and amiloride containing food was prepared as

described (18, 19). The control group (n=6) of rats received normal rodent diet during the entire experiment. Two other groups of rats received the same diet supplemented with 40 mmol LiCl/kg of dry food for the first 7 days, followed by 60 mmol LiCl/kg of dry food the next 3 weeks in the presence (group 2; n=6) or absence (group 3; n=6) of amiloride (200 mg/kg dry food). All rats had free access to water and a NaCl block. During the last 3 days of the experiments, the animals were housed in metabolic cages to measure daily urine output and water intake. Rats were anesthetized by isofluoran. One kidney was removed and divided in two parts. One part was dissected into cortex, outer medulla and inner medulla then subjected to homogenization for immunoblotting. The other part of the kidney was stored in -80°C. The other kidney was washed by retrograde perfusion via the abdominal aorta by 0.01 M PBS (pH 7.4) and then fixed by 3% paraformaldehyde for Immunohistochemistry.

Urine analysis

Urine samples were centrifuged at 2000xg for 5 minutes to remove any sediment precipitated. Then the urine was decanted and stored in eppendorf tubes. Urine osmolality was measured using a Micro-Osmometer Model 3320 (Advanced Instruments, Inc., Norwood, MA).

Immunohistochemistry

Immunohistochemistry was performed as described (20). In short, one kidney was immersion fixed in 3% paraformaldehyde before dehydration in a graded series of ethanol (2 h in 70, 96, and 99%, respectively) and xylene (overnight). This was followed by embedding in paraffin. Paraffin sections (2 µm) were cut on a Leica RM 2126 microtome and dried overnight at 37°C.

Double-labeling: Sections were incubated with anti-AQP2 antibody (7661AP, dilution, 1:2,000) followed by incubation with goat anti-rabbit peroxidase (HRP)-conjugated secondary antibody and 3'-Diaminobenzidine (DAB; brown color). The potential remaining peroxidase from the first staining was removed by incubating the sections in 3.5% H_2O_2. After blocking for endogenous biotin (Biotin Blocking System; Dako, Glostrup, Denmark), sections were incubated with biotinylated H^+-ATPase antibody (7659AP; dilution 1:10) and labeling was visualized by HRP-conjugated streptavidin (Dako) and Vector SG substrate (blue-gray color). For single labeling, sections were incubated with PCNA (1:16000 dilution) and labeling was visualized by use of a HRP-conjugated secondary antibody and 3,3-diaminobenzidine (DAB). Cell counting was performed on kidney sections labeled with antibodies against PCNA or H^+-ATPase/AQP2. Counting was performed directly under the microscope as described for 1 section per rat (n = 6) (21).

Immunoblotting

The dissected cortex, outer medulla en inner medulla were homogenized in dissecting buffer as described (19). This homogenate was centrifuged at 4000 g for 15 min at 4°C. Laemmli sample buffer was added to the supernatant and samples were stored at -20°C. Before running the gels, laemmli samples were denatured for 30 minutes at 37°C. SDS-PAGE, blotting, and blocking of the PVDF membranes was done as described (22). Membranes were incubated for 16 hours at 4°C with 1:1000 affinity–purified rabbit (Rb2) C-tail AQP2 antibody in Tris-Buffered Saline Tween-20 (TBS-T) supplemented with 1% nonfat dried milk (23). After washing in TBS-T, all blots were incubated for 1 hour in TBS-T containing 1:10000-diluted goat anti–rabbit IgGs (Sigma-Aldrich, St. Louis, USA) coupled to horseradish peroxidase. Proteins were visualized using enhanced chemiluminescence (ECL; Pierce, Rockford, USA). Densitrometric analyses were performed using Bio-Rad quantification equipment (Bio-Rad 690c Densitometer; Chemidoc XRS) and Image studio software (LI-COR, Nebraska, USA). Equal loading of the samples was confirmed by staining of the blots with coomassie brilliant blue R-250 (BioRad, Hercules, USA).

Urinary ammonium assay

Urinary ammonium was determined using a Pointe Scientific kit (A7553; Canton, USA) modified for small volumes as described (24).

Statistics

One-way ANOVA with Bonferroni correction was applied. A p value of less than 0.05 was considered significant. Data are presented as mean and standard error of the mean (SEM).

Results

Effect of amiloride on electrolyte levels and lithium-induced NDI development

To investigate whether amiloride attenuates development of Li-NDI, rats were maintained on normal rodent diet, lithium-containing diet or on a diet that containing lithium and amiloride for 4 weeks. As reported (15, 25), rodents treated with lithium developed severe polyuria and polydipsia, combined with a significantly reduced urine osmolality (**Figs. 1A-B**). Moreover, as shown before (18), amiloride treatment induced a significant antidiuresis and increased urine osmolality. Consistent with the antidiuresis, water intake was significantly reduced with amiloride treatment as compared to lithium only (**Fig. 1C**). Lithium treatment did not affect blood calcium, sodium and potassium levels nor did it change blood pH and other blood gases (**Table 1**). Urinary ammonium, however, was significantly increased with lithium and significantly attenuated again with amiloride.

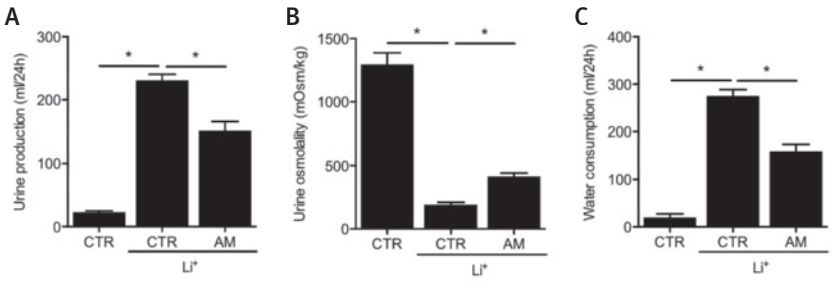

Figure 1. Amiloride attenuates lithium-induced NDI. One group of the rats received normal rodent diet while the other rats received the same diet supplemented with lithium or lithium and amiloride for 4 weeks and individually housed in metabolic cages for the last 48 hours. Urine production (**A**), urine osmolality (**B**) and water intake (**C**) were determined for the last 24h. A significant difference (P<0.05) from CTR is denoted by an asterisk. Abbreviation: CTR, control; Li+, lithium and AM, Amiloride.

Table 1. Metabolic parameters of rats treated for 4 weeks with standard chow only (CTR) or together with lithium (Li^+). Lithium + amiloride (Li^+ + Am).

	CTR	Li^+	Li^++ AM
Blood pH	7.30 ± 0.01	7.24 ± 0.03	7.27 ± 0.02
pCO2 (mmHg)	8.446 ± 0.2	9.092 ± 0.5	8.33 ±0.3
PO2 (mmHg)	1.4 ± 0.2	1.84 ± 0.5	1.8 ±0.3
HCO3 (mmol/L)	31.44 ± 0.3	29.24 ± 0.9	28.56 ±1.4
TCO2 (mmol/L)	32.5 ± 0.5	31.2 ± 1.0	30.4 ±1.5
Serum Sodium (mmol/L)	137.4 ± 0.9	138 ± 0.9	137.4 ±1.5
Serum Potassium (mmol/L)	4.82 ± 0.10	4.92 ± 0.07	5.26 ±0.14
Serum lithium (mmol/L)	/	1.045 ±0.08	1.372 ±0.09
Blood Ionized Calcium (mmol/L)	1.444 ± 0.05	1.452 ±0.01	1.476 ±0.03
Urinary ammonium (mmol/24h)	0.102±0.05	0.940 ±0.09*	0.554 ±0.09

Values are means ± s.e.m.
*P<0.05 Compared with lithium treatment.
/ Below detection limit

Segment-specific effects of amiloride therapy on AQP2 abundance

To examine segment-specific effects of amiloride therapy, immunoblotting for AQP2 was performed. Immunoblot analysis revealed that lithium reduced AQP2 abundance in the cortex, outer medulla and the inner medulla (**Figs. 2A-D**). Consistent with earlier

data (18), amiloride fully rescued AQP2 downregulation in the inner medulla, partially rescued AQP2 abundance in the outer medulla but, in contrary to earlier findings, had no effect on AQP2 levels in the cortex.

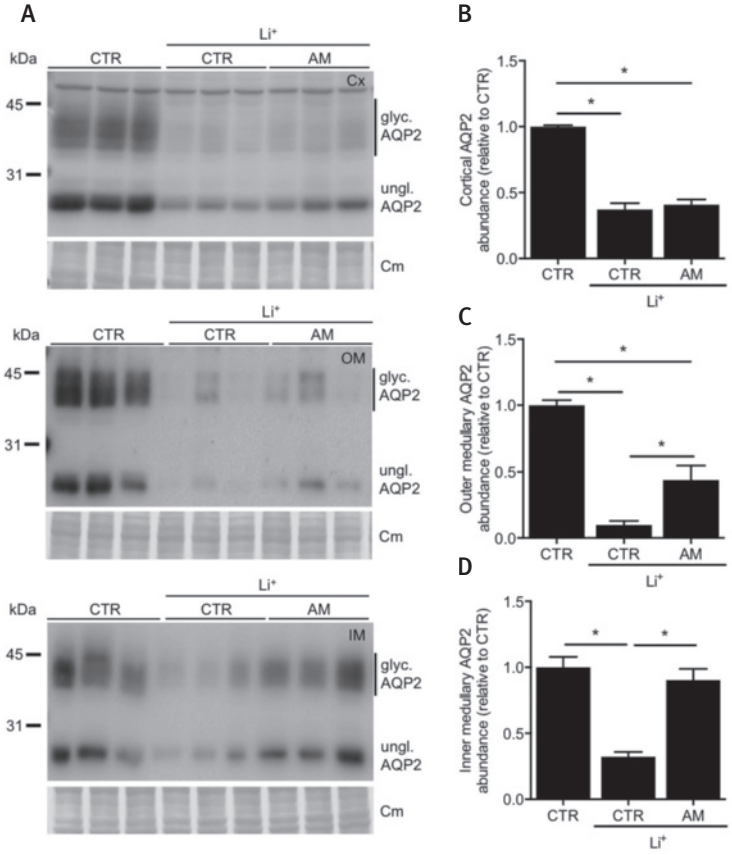

Figure 2. Amiloride attenuates AQP2 mainly in the inner medulla of the collecting duct. Rats were treated for 4 weeks with a control, lithium or lithium and amiloride containing diet. After sacrifice, kidneys were rapidly isolated, one part of the kidney was dissected into cortex, outer medulla and inner medulla then snap frozen in liquid nitrogen and stored at -20°C. Immunoblot analysis (**A**) on lysates was performed to determine protein abundance of AQP2. Unglycosylated AQP2 bands were quantified for cortex (Cx; **B**), outer medulla (OM; **C**) and inner medulla (IM; **D**). A significant difference ($P<0.05$) from CTR is denoted by an asterisk. CTR, control; Li+, lithium; AM, Amiloride and Cm, coomassie blue staining.

Effect of amiloride on lithium-induced collecting duct remodeling

Earlier, it has been shown that 4 weeks lithium treatment leads to collecting duct remodeling with a loss of principal cells and increased intercalated cells, which was rescued by the use of amiloride (18, 19). The data of figure 2 indicated that amiloride mainly attenuated Li-NDI development in the inner medulla, we investigated whether this coincided with a similar segment-specific protection against remodeling. For this, immunohistochemistry was performed. As shown before (18), lithium significantly increased the fraction of H^+-ATPase-labeled intercalated cells and decreased the fraction of AQP2-labeled principal cells in the cortex and the medulla (**Fig. 3**), underscoring collecting duct remodeling with lithium. Amiloride treatment partially

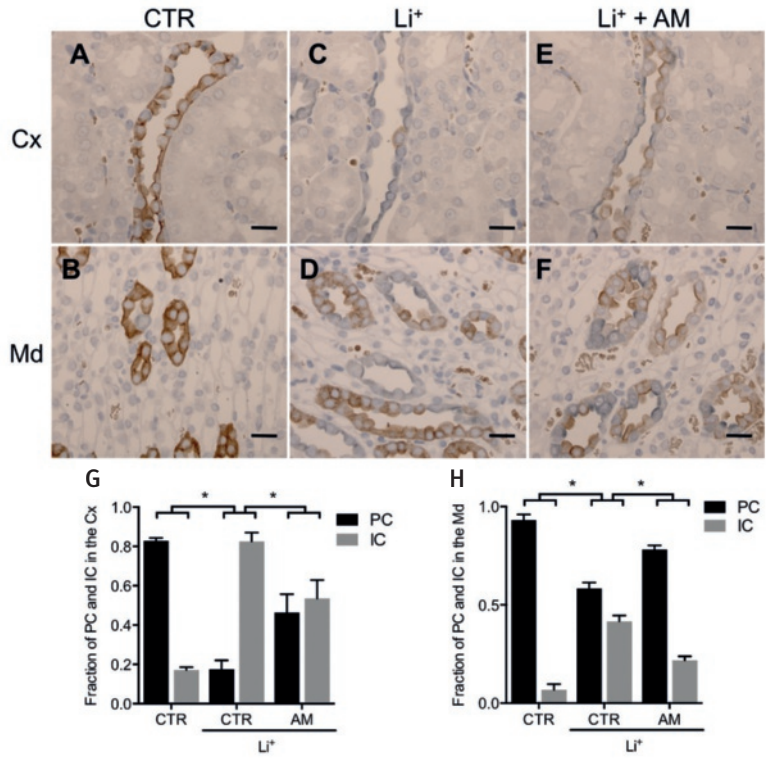

Figure 3. Amiloride attenuates lithium-induced collecting duct remodeling. Immunocytochemistry using whole kidney sections from control (***A-B***), lithium-treated (***C-D***) and lithium and amiloride (**E-F**) treated rats. Sections were incubated with anti-H^+-ATPase and anti-AQP2 antibodies. Average fraction of AQP2 positive principal cells and H^+-ATPase positive intercalated cells is shown for cortex (**G**) and the medulla (**H**). A significant difference ($P<0.05$) from CTR is denoted by an asterisk. CTR, control; Li+, lithium; AM, Amiloride; PC, Principal cells; IC, Intercalated cells; Cx, cortex and Md. Medulla.

prevented collecting duct remodeling as shown by a lower fraction of H^+-ATPase positive cells compared to lithium in the cortex and the medulla. Earlier, others and we have shown that lithium initiates proliferation of principal cells *in vitro* and *in vivo (10, 26)*. Here, we found that lithium also increased the fraction of proliferating cells, as shown by the increase in PCNA staining. Importantly, amiloride treatment reduced the increase in PCNA staining, indicating that amiloride treatment also attenuated lithium-induced cell proliferation (**Fig. 4**).

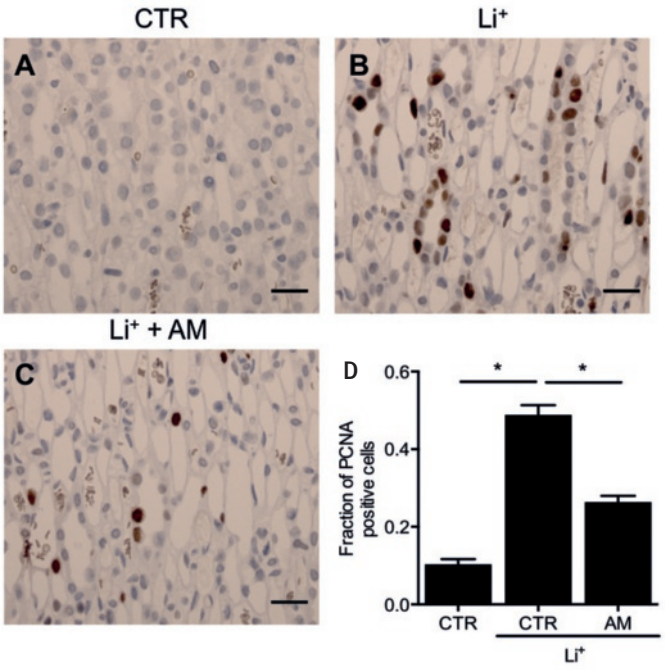

Figure 4. Amiloride treatment reduces lithium-induced proliferation. Immunohistochemistry using whole kidney sections from control (***A***), lithium-treated (***B***) and lithium and amiloride (**C**) treated rats. Sections were incubated with an anti-PCNA antibody and labeling was visualized by use of a HRP-conjugated secondary antibody and DAB. A significant difference ($P<0.05$) from CTR is denoted by an asterisk. CTR, control; Li^+, lithium; AM, Amiloride; Cx, cortex and Md, Medulla.

Discussion

Amiloride attenuates lithium-induced collecting duct AQP2 expression, cell proliferation, and remodeling.

Earlier, others and we have shown *in vitro* and *in vivo* that lithium downregulates AQP2 and initiates proliferation, but that this is for a fraction of principal cells halted in the G2/M cell cycle phase, which may at least partially explain the overall loss of principal cells observed in Li-NDI *(10,26)*. Furthermore, lithium treatment also caused metabolic reprogramming towards aerobic glycolysis in principal cells (27). Here, we show that blocking lithium entry into principal cells with amiloride did not only attenuate lithium-induced AQP2 downregulation but also prevented cell proliferation and collecting duct remodeling. This is in line with our earlier *in vitro* findings in mpkCCD cells where amiloride, in addition to the rescued AQP2 abundance, prevented proliferation and aerobic glycolysis (27).

Amiloride attenuates development of metabolic acidosis

As the G2-phase arrest of principal cells with lithium only affects a fraction of principal cells, it may well not ne the sole factor leading to collecting duct cell remodeling. Earlier studies demonstrated that lithium treatment of rats also induced an increase in collecting duct intercalated cells(28-30). An important stimulus for this could be the development of metabolic acidosis, which is often, but not always, observed with lithium treatment in rodents and man (31, 32), because a state of metabolic acidosis increases the numbers of a-intercalated cells as an adaptive response (33, 34). In our recent study, we proposed that lithium-induced aerobic glycolysis in principal cells, therewith acidifying the micro-environment, could be a cause of acidosis and lead to increased numbers of intercalated cells instead of the earlier suggested hypothesis of a direct inhibition of intercalated cell H^+-ATPase and H^+/K^+-ATPase by lithium (27, 35, 36).

Here, we provide evidence that aerobic glycolysis of principal cells may indeed be a trigger for intercalated cell proliferation. With lithium, we did not find observe a change in plasma pH, HCO_3^- or pCO_2 levels indicating that our mice did not show metabolic acidosis with lithium. However, a crucial renal mechanism to eliminate acid is the production and tubular release of NH_3, which, by acceptor H^+, becomes ammonium. Indeed, urinary ammonium was significantly elevated in our lithium-treated rats. Moreover, urinary ammonium was again strongly reduced with amiloride. As we showed here and before that amiloride also attenuated collecting duct remodeling (18), our present data support the view that lithium entry of principal cells through ENaC induces aerobic glycolysis. The aerobic glycolysis acidifies the micro-environment of the intercalated cells which stimulates them to proliferate. With blocking lithium entry through ENaC, amiloride prevents all these steps.

Interestingly, approximately 1.5% of the lithium-users develop end stage renal disease, which is the final stage of chronic kidney disease (Li-CKD). A hallmark of Li-CKD is the development of renal interstitial fibrosis and a recent study revealed that administration of amiloride to rats that had already developed NDI also limited the progressive development of cortical fibrosis resulting from the chronic lithium exposure (37).

Taken together, we have shown that amiloride does not only attenuate lithium-induced NDI, but also prevents lithium-induced cell proliferation, acidification and collecting duct remodeling. Together with the discovery that amiloride also limits fibrosis formation in rats, amiloride seems an excellent prophylactic medication for the development of the renal side effects of lithium.

Acknowledgments

We thank Helle Hoyer, for her expert technical assistance. This project received support from a grant from the Society of Experimental Laboratory Medicine to PMTD, a Niels Stensen Fellowship and a Marie Curie Fellowship PIOF-GA-2012-332395 to TdG.

References

1. Timmer RT, Sands JM. Lithium intoxication. J Am Soc Nephrol. 1999;10(3):666-74.
2. Manji HK, Moore GJ, Chen G. Bipolar disorder: leads from the molecular and cellular mechanisms of action of mood stabilisers. BrJ Psychiatry. 2001;178(Suppl 41):S107-S19.
3. Stone KA. Lithium-induced nephrogenic diabetes insipidus. J Am Board FamPract. 1999;12(1):43-7.
4. Boton R, Gaviria M, Batlle DC. Prevalence, pathogenesis, and treatment of renal dysfunction associated with chronic lithium therapy. American Journal of Kidney Diseases. 1987;10:329-45.
5. Walker RJ, Weggery S, Bedford JJ, McDonald FJ, Ellis G, Leader JP. Lithium-induced reduction in urinary concentrating ability and urinary aquaporin 2 (AQP2) excretion in healthy volunteers. Kidney Int. 2005;67(1):291-4.
6. Laursen UH, Pihakaski-Maunsbach K, Kwon TH, Ostergaard JE, Nielsen S, Maunsbach AB. Changes of rat kidney AQP2 and Na,K-ATPase mRNA expression in lithium-induced nephrogenic diabetes insipidus. Nephron ExpNephrol. 2004;97(1):e1-16.
7. Marples D, Christensen S, Christensen EI, Ottosen PD, Nielsen S. Lithium-induced downregulation of aquaporin-2 water channel expression in rat kidney medulla. J Clin Invest. 1995;95:1838-45.
8. Li Y, Shaw S, Kamsteeg EJ, Vandewalle A, Deen PM. Development of lithium-induced nephrogenic diabetes insipidus is dissociated from adenylyl cyclase activity. J Am Soc Nephrol. 2006;17(4):1063-72.
9. Christensen BM, Marples D, Kim YH, Wang W, Frokiaer J, Nielsen S. Changes in cellular composition of kidney collecting duct cells in rats with lithium-induced NDI. Am J Physiol Cell Physiol. 2004;286(4):C952-C64.
10. de Groot T, Alsady M, Jaklofsky M, Otte-Holler I, Baumgarten R, Giles RH, et al. Lithium causes g2 arrest of renal principal cells. J Am Soc Nephrol. 2014;25(3):501-10.
11. Kim YH, Kwon TH, Christensen BM, Nielsen J, Wall SM, Madsen KM, et al. Altered expression of renal acid-base transporters in rats with lithium-induced NDI. Am J Physiol Renal Physiol. 2003;285(6):F1244-57.
12. Perez GO, Oster JR, Vaamonde CA. Incomplete syndrome of renal tubular acidosis induced by lithium carbonate. J Lab Clin Med. 1975;86(3):386-94.
13. Roscoe JM, Goldstein MB, Halperin ML, Wilson DR, Stinebaugh BJ. Lithium-induced impairment of urine acidification. Kidney Int. 1976;9(4):344-50.
14. Batlle DC, von Riotte AB, Gaviria M, Grupp M. Amelioration of polyuria by amiloride in patients receiving long- term lithium therapy. N Engl J Med. 1985;312:408-14.
15. Kortenoeven ML, Li Y, Shaw S, Gaeggeler HP, Rossier BC, Wetzels JF, et al. Amiloride blocks lithium entry through the sodium channel thereby attenuating the resultant nephrogenic diabetes insipidus. Kidney Int. 2009;76(1):44-53.
16. Bedford JJ, Leader JP, Jing R, Walker LJ, Klein JD, Sands JM, et al. Amiloride restores renal medullary osmolytes in lithium-induced nephrogenic diabetes insipidus. AmJPhysiol Renal Physiol. 2008;294(4):F812-F20.
17. Bedford JJ, Weggery S, Ellis G, McDonald FJ, Joyce PR, Leader JP, et al. Lithium-induced nephrogenic diabetes insipidus: renal effects of amiloride. Clin J Am Soc Nephrol. 2008;3(5):1324-31.
18. Kortenoeven ML, Li Y, Shaw S, Gaeggeler HP, Rossier BC, Wetzels JF, et al. Amiloride blocks lithium entry through the sodium channel thereby attenuating the resultant nephrogenic diabetes insipidus. Kidney Int. 2009;76(1):44-53.
19. Christensen BM, Marples D, Kim YH, Wang W, Frokiaer J, Nielsen S. Changes in cellular composition of kidney collecting duct cells in rats with lithium-induced NDI. Am J Physiol Cell Physiol. 2004;286(4):C952-64.
20. Nielsen J, Kwon TH, Praetorius J, Kim YH, Frokiaer J, Knepper MA, et al. Segment-specific ENaC down-regulation in kidney of rats with lithium-induced NDI. Am J Physiol Renal Physiol. 2003;285(6):F1198-209.
21. Trepiccione F, Capasso G, Nielsen S, Christensen BM. Evaluation of cellular plasticity in the collecting duct during recovery from lithium-induced nephrogenic diabetes insipidus. Am J Physiol Renal Physiol. 2013;305(6):F919-29.
22. Kamsteeg EJ, Wormhoudt TA, Rijss JP, van Os CH, Deen PM. An impaired routing of wild-type aquaporin-2 after tetramerization with an aquaporin-2 mutant explains dominant nephrogenic diabetes insipidus. EMBO J. 1999;18(9):2394-400.
23. Deen PM, Verdijk MA, Knoers NV, Wieringa B, Monnens LA, van Os CH, et al. Requirement of human renal water channel aquaporin-2 for vasopressin-dependent concentration of urine. Science. 1994;264(5155):92-5.

24. Lee HW, Verlander JW, Bishop JM, Igarashi P, Handlogten ME, Weiner ID. Collecting duct-specific Rh C glycoprotein deletion alters basal and acidosis-stimulated renal ammonia excretion. Am J Physiol Renal Physiol. 2009;296(6):F1364-75.
25. Christensen BM, Kim YH, Kwon TH, Nielsen S. Lithium treatment induces a marked proliferation of primarily principal cells in rat kidney inner medullary collecting duct. Am J Physiol Renal Physiol. 2006;291(1):F39-F48.
26. Christensen BM, Kim YH, Kwon TH, Nielsen S. Lithium treatment induces a marked proliferation of primarily principal cells in rat kidney inner medullary collecting duct. Am J Physiol Renal Physiol. 2006;291(1):F39-48.
27. Alsady M, de Groot T, Kortenoeven MLA, Carmone C, Neijman K, Bekkenkamp-Grovenstein M, et al. Lithium induces aerobic glycolysis and glutaminolysis in collecting duct principal cells. Am J Physiol Renal Physiol. 2017:ajprenal 00297 2017.
28. Kling MA, Fox JG, Johnston SM, Tolkoff-Rubin NE, Rubin RH, Colvin RB. Effects of long-term lithium administration on renal structure and function in rats. A distinctive tubular lesion. Lab Invest. 1984;50(5): 526-35.
29. Ottosen PD, Nyengard JR, Jacobsen NO, Christensen S. A morphometric and ultrastructural study of lithium-induced changes in the medullary collecting ducts of the rat kidney. Cell Tissue Res. 1987;249(2):311-5.
30. Jacobsen NO, Olesen OV, Thomsen K, Ottosen PD, Olsen S. Early changes in renal distal convoluted tubules and collecting ducts of lithium-treated rats: light microscopy, enzyme histochemistry, and 3H-thymidine autoradiography. Lab Invest. 1982;46(3):298-305.
31. de Groot T, Sinke AP, Kortenoeven ML, Alsady M, Baumgarten R, Devuyst O, et al. Acetazolamide Attenuates Lithium-Induced Nephrogenic Diabetes Insipidus. J Am Soc Nephrol. 2016;27(7):2082-91.
32. Weiner ID, Leader JP, Bedford JJ, Verlander JW, Ellis G, Kalita P, et al. Effects of chronic lithium administration on renal acid excretion in humans and rats. Physiological reports. 2014;2(12).
33. Bagnis C, Marshansky V, Breton S, Brown D. Remodeling the cellular profile of collecting ducts by chronic carbonic anhydrase inhibition. Am J Physiol Renal Physiol. 2001;280(3):F437-48.
34. Welsh-Bacic D, Nowik M, Kaissling B, Wagner CA. Proliferation of acid-secretory cells in the kidney during adaptive remodelling of the collecting duct. PloS one. 2011;6(10):e25240.
35. Dafnis E, Kurtzman NA, Sabatini S. Effect of lithium and amiloride on collecting tubule transport enzymes. J Pharmacol Exp Ther. 1992;261(2):701-6.
36. Eiam-Ong S, Dafnis E, Spohn M, Kurtzman NA, Sabatini S. H-K-ATPase in distal renal tubular acidosis: urinary tract obstruction, lithium, and amiloride. Am J Physiol. 1993;265(6 Pt 2):F875-80.
37. Kalita DECP, Bedford JJ, Leader JP, Walker RJ. Amiloride modifies the progression of lithium-induced renal interstitial fibrosis. Nephrology. 2016.

Chapter 7

Long-term lithium treatment causes renal interstitial fibrosis in mice

Alsady M [1], van der Tholen L [1], Carmone C [1], Bekkenkamp-Grovenstein M [1], van Gemst J [2], van den Brand M [4], van Kuppevelt TH [3], van der Vlag J [2], de Groot T [1] and Deen PMT [1]

[1] Department of Physiology, Radboud University Medical Center, Nijmegen, The Netherlands.
[2] Department of Nephrology, Radboud University Medical Center, Nijmegen, The Netherlands.
[3] Department of Biochemistry, Radboud University Medical Center, Nijmegen, The Netherlands.
[4] Department of Pathology, Radboud University Medical Center, Nijmegen, The Netherlands.

Scientific reports, submitted.

Abstract

Lithium is the main treatment of bipolar disorder. Unfortunately, approximately 1.5% of the lithium-users develops end stage renal disease, which is the final stage of chronic kidney disease (Li-CKD). A hallmark of Li-CKD is the development of renal interstitial fibrosis. To prevent Li-CKD, it is essential to understand the etiology of lithium-induced renal fibrosis, but convenient animal models have not been described. Therefore, to establish this model, C57Bl/6 mouse mothers and subsequent pups were fed either a normal diet or a diet supplemented with 40 mmol lithium chloride/kg food for 40 weeks. Histological analysis revealed interstitial fibrosis development and increased α-SMA staining in the cortico-medullary region of lithium-treated mice. Staining with the anti-heparan sulfate (HS) antibody, which defines an inflammatory HS domain, revealed an increased expression in peritubular capillaries. In addition, mRNA expression of the cytokine TNFα and the macrophage marker F4/80 was increased in both the cortex and the medulla while mRNA expression of the fibrotic factor CTGF was only increased in the medulla. In conclusion, we show that 40 weeks lithium treatment of mice resulted in the development of renal interstitial fibrosis, which may serve as an experimental model to investigate renal interstitial fibrosis development.

Introduction

Bipolar disorder is a severe mental illness that affects about 2% of the world's population (1, 2). Patients suffer from a disturbance of mood with periods of depression or elation. This has a severe impact on the lives of most patients, demonstrated by the fact that more than 30% of bipolar patients attempt suicide during their lifetime (3, 4). Moreover, the annual direct and indirect economic burden of bipolar disorder was estimated to be 151 billion American dollars in the USA only (5). Lithium is the best-established long-term treatment for bipolar disorder and it has been shown to reduce the risk of manic relapses by 38%, depressive relapse by 28% and the risk of suicide by more than 50% (6, 7). At least 1 per 1000 people in western countries uses lithium and, as such, lithium usage saves our society huge amounts of health costs (8, 9).

Unfortunately, lithium treatment leads to various renal side effects (10). The majority of lithium users experience loss in urine concentrating ability while 20% develops lithium-induced nephrogenic diabetes insipidus (Li-NDI), in which the vasopressin-dependent concentration of urine is affected, leading to polyuria, dehydration, thirst, and compensatory polydipsia (11, 12). Besides the effect on the urinary concentrating ability, long-term lithium treatment results in the development of renal interstitial fibrosis that is a hallmark and common outcome in the development of chronic kidney disease (CKD). The final stage of CKD is end stage renal disease (ESRD), which is defined by a complete loss of kidney function. Such patients can only be treated by either dialysis or transplantation (13). The affection of renal function is highly dose-dependent and can be ameliorated by close monitoring of serum Li-concentrations in patients (14, 15). Approximately 1.5% of lithium-users develop ESRD, which is six to eight times more frequent than in the general population (10, 13, 16). Renal biopsies of patients with lithium toxicity revealed a chronic tubulointerstitial nephropathy in all patients associated with cortical and medullary tubular cysts (62.5%), tubular dilatation (33.3%) and segmental/global glomerulosclerosis (17-20).

To fully understand the development of lithium-induced renal fibrosis, the use of animal models is essential. Mice developing Li-CKD would be advantageous, considering the availability of many transgenic mice and the extensive existing knowledge of Li-NDI in mice (21-28). However, a Li-CKD mouse model has not yet been developed. Studies by Christensen *et al.* (1981) and Ottosen *et al.* (1984) demonstrated that newborn rats were more susceptible to develop interstitial fibrosis with lithium treatment than adult mice (29, 30). Therefore, we here wanted to perform a proof of principle experiment to determine whether, upon administration of diet-contained lithium to pregnant mice and to pups after weaning, would lead to renal fibrosis after 40 weeks of lithium treatment.

Materials and methods

Animal experiments

Male and female C57BL/6 mice were housed in a climate-controlled facility with a 12-hour:12-hour light-dark cycle. All mice had free access to food, water and a sodium chloride block throughout the experiment. It has been shown in humans and rodents that lithium passes into breast milk (31, 32). Therefore, four days after birth, one group of the mothers received normal rodent diet (7013, NIH-31 Modified, Harlan Laboratories, Inc., Madison, WI, USA), while other mothers received the same diet supplemented with 40, 60 or 80 mmol lithium chloride/kg food for 3 weeks. After weaning, groups of 7 pups/group received the same diet as their mothers. For controls, a group of 6 mice was taken. It has been shown that treatment of adult mice with 40 mmol lithium chloride/kg food results in lithium plasma concentration of 0.61 ± 0.16 mM, which represents the lowest value in the therapeutic range of patients with bipolar disorder (33). To increase the chance of obtaining interstitial fibrosis, other groups of 6 mice were given 60 and 80 mmol lithium chloride/kg food (i.e.1.5 and 2.0 times more). After three weeks, mice that received 40 mmol lithium chloride /kg food were weaned, while those receiving 60 and 80 mmol lithium chloride/kg food were sacrificed, as they showed paralysis of their rear legs and hardly responded to touch, indicating that these latter dosi were toxic for the mice. During the experiment, the appearance and behavior of the mice in addition to their weight was monitored. As per protocol of the animal welfare regullations, animals that showed signes of pain or that had a 10% weight reduction were euthanaised after consultation with the veternerian. The experment was continued with the group that received 40 mmol lithium / kg food for 40 weeks. Then the mice were killed by cervical dislocation, followed by rapid isolation of the kidneys. One kidney was fixed for immunohistochemistry by immersion in 4% (wt/vol) paraformaldehyde (PFA) in PBS overnight. The second kidney was divided in two, one half was snap frozen directly while the other half was dissected into cortex and medulla, snap frozen in liquid nitrogen, and stored at -20°C. The animal experiment was approved by the Animal Experiments Committee of the Radboud University Nijmegen Medical Center and all experiments were performed in accordance with relevant guidelines and regulations.

(Immuno)histochemistry

In general, Immunofluorescence staining was performed on paraffin-embedded sections as described (34). In short, kidney sections were incubated with blocking reagent (NEN Life Science Products, Zaventem, Belgium) and incubated overnight with primary antibodies diluted in Tris-BSA-Triton buffer at 4°C. Antibodies used were rabbit anti-CD31 (ab28364) antibody (1:50; Abcam, Cambridge, UK) to mark endothelial cells, mouse monoclonal (A5228) antibody against alpha smooth muscle actin (α-SMA;

1:200; Sigma-Aldrich, St Louis, USA), and guinea pig anti-aquaporin 4 (AQP4; 1:200; (35)) to mark (medullary) principal cells of the collecting ducts. Incubation with secondary antibodies labeled with Alexa488, -594 and/or -647 dyes (1:1000) was done for 60 minutes at room temperature. Sections were then incubated in DAPI (1:10000; ITK Diagnostics; Uithoorn, Netherlands) for 60 minutes for nuclear counter-staining. The sections were mounted in Fluoromount-G (Southern Biotech Associates, Birmingham, AL, USA) and stored in the dark at 4°C until microscopic analysis. Images were acquired using a Zeiss AX10 digital fluorescent microscope and ZEN lite software.

For the heparan sulphates, immunofluorescence staining was performed on 2-µm renal cryosections as described (36). Heparan sulfate (HS) domains were visualized with the VSV-tagged anti-HS scFv antibodies EW3D10 (N- and 6-O sulfation) and HS4C3 (N-, 2-O, 3-O and 6-O sulfation) (37-40). The exact sequences within HS that are recognized by these anti-HS scFv antibodies are not known. However, they recognize distinct domains. The HS domains recognized by EW3D10 are upregulated under inflammatory conditions, in contrast to the domain recognized by HS4C3 (36, 41, 42). Anti-VSV-Cy3 antibody (Sigma-Aldrich Chemie, Zwijndrecht, The Netherlands) was applied to detect VSV-tagged antibodies. Sections were post-fixed with 1% paraformaldehyde–PBS and embedded in VectaShield mounting medium H-1000 (Brunschwig Chemie, Amsterdam, The Netherlands). The fluorescence intensity in peritubular capillaries was quantified with Image-J software and normalized for staining intensity of tubular basement membranes (TBM). Pictures were loaded into the ImageJ software, and by using a fixed area, the mean fluorescence intensity of peritubular capillaries was determined at 25 areas per picture on at least 3 representative pictures per mouse. The individual results per picture were corrected for possible variations in staining efficiency by measuring the mean fluorescence intensity in tubular basement membranes, which were not affected by the treatment.

Immunohistochemistry for CD68 (clone KP1, dilution 1:100, DAKO, Glostrup, Denmark) was performed on the Ventana automated staining platform (Ventana Medical Systems, Tucson, AZ, USA) according to the manufacturer's instructions.

Chromotrope aniline blue (CAB) histochemistry was performed to detect collagen deposition in the kidney. 4-µm thick sections were de-paraffinized in xylene for 10 minutes followed by rehydration with a short rinse in 100% ethanol and two short rinses in 96% ethanol, followed by rinsing in water for 10 minutes. Sections were then incubated in Bouin's solution (Klinipath, Duiven, the Netherlands) at 60°C for 1h. After rinsing with water for 5 minutes and 10 min incubation in Weigert's hematoxylin, sections were again rinsed with water and incubated for 6 min in 1% phosphomolybdic acid (Merck, Darmstadt, Germany). After rinsing in water, chromotrope aniline blue

solution (0.5% aniline blue (BDH, Poole, UK), 15% hydrochloric acid and 2% chromotrope 2R (Sigma, Steinheim, Germany) was added for 8 minutes. After a short rinse with demineralized water, sections were dehydrated with two short rinses in 96% ethanol, followed by a short rinse in 100% ethanol, two short rinses in xylene and placement of a coverslip. Periodic acid-methenamine silver (MZ) staining was performed according to the method described (43).

RT-qPCR

Samples from control and lithium kidney cortex and medulla were transferred from -80°C to liquid nitrogen. Each sample (50-100 mg) was homogenized with a Warton Tissue homogenizer in a glass tube with 1mL TRIzol (Invitrogen, Bleiswijk, the Netherlands). Total RNA was isolated using TRIzol extraction reagent according to the manufacturer's instructions. RNA was then precipitated in ethanol, washed, and dissolved in nuclease-free water. Next, RNA was subjected to DNase treatment (Promega, Fitchburg, WI, USA) to prevent genomic DNA contamination according to the manufacturer's instructions. Subsequently, RNA was measured using NanoDrop 2000c UV-Vis spectrophotometer (Thermo Scientific, Wilmington, USA) then reverse-transcribed into cDNA using Moloney murine leukemia virus reverse transcriptase (Invitrogen, Bleiswijk, the Netherlands). During cDNA production, a negative control without reverse transcriptase was included. Subsequent RT-qPCR assays were performed using SYBR Green kit (Bio-Rad, Veenendaal, the Netherlands) and the primers used (Table 1) were designed using the Primer-BLAST tool (http://www.ncbi.nlm.nih.gov/tools/primer-blast/). 36B4, which encodes an acidic ribosomal phosphoprotein Po (RPLPo), was used as the housekeeping gene. This gene has been proven to be a reliable and consistent standard for use in gene expression analysis (44). Gene expression data were calculated by using the Livak ($2^{-\Delta\Delta Ct}$) method and they represent the mean fold difference from the calibrator/control group. For primer validation, standard curves with serially diluted cDNA were generated, and primer concentration was optimized to ensure highly efficient qPCR reactions. Construction of SYBR green dissociation curves after completion of 40 PCR cycles revealed the presence of single amplicons.

Statistical analysis

Student's unpaired *t*-test was performed using GraphPad Prism 5 (GraphPad Software INC, La Jolla, USA) to compare between two groups. A P value of <0.05 was considered significant. Data are presented as means ± SE unless indicated otherwise.

Table 1. Primers used in real-time polymerase chain reaction

Target gene	F/R	Primer sequence
36B4	F	AGCGCGTCCTGGCATTGTGTGG
	R	GGGCAGCAGTGGTGGCAGCAGC
IL-6	F	CAAGTCGGAGGCTTAATTACACATG
	R	ATTGCCATTGCACAACTCTTTTCT
TNFα	F	CATCTTCTCAAAATTCGAGTGACAA
	R	TGGGAGTAGACAACGTACAACCC
IFNγ	F	GGTGACCTTGTGACAAGCTC
	R	TGCTGTGTGGTCTGTCTGTC
IL-1Ra	F	AAATCTGCTGGGGACCCTAC
	R	TGAGCTGGTTGTTTCTCAGG
MCP1	F	CCCAATGAGTAGGCTGGAGA
	R	TCTGGACCCATTCCTTCTTG
F4/80	F	CTTTGGCTATGGGCTTCCAGTC
	R	GCAAGGAGGACAGAGTTTATCGTG
TGFβ1	F	CTGGAGTTGTACGGCAGTGG
	R	TGGGGCTGATCCCGTTGA
CTGF	F	GTCCAGACCACAGAGTGGAG
	R	CTCCAGGTCAGCTTCGCAG

F, forward; R, reverse; 36B4, housekeeping gene; IL-6, interleuking-6; TNFα, tumor necrosis factor-alpha, INFγ, interferon-gamma; IL-1Ra, interleukin-1 receptor antagonist; MCP1, Monocyte chemotactic protein 1; TGFβ1, transforming growth factor-beta 1; CTGF, connective tissue growth factor.

Results

Lithium induces renal fibrosis and tubular atrophy in mice.

We investigate whether C57BL/6 mice would develop renal interstitial fibrosis when long-term (40 weeks) treated with 40 mmol lithium/kg food starting with the pregnant mother mice. After this 40 weeks, the mice were sacrificed and the presence of fibrosis was assessed using CAB staining (Fig 1). In control mice, only the collagen-containing basement membranes of glomeruli and brush borders of proximal tubules were positively stained (Fig 1A and Fig. S1), while the outer and inner medulla did not show any positive staining (Figs 1C and E). In lithium-treated mice, however, fibrotic foci were present in the cortex as well as in the outer medulla, but not in the inner medulla (Figs 1B, D and F). Lithium treatment resulted in a increase in the the presense of fibrotic foci

(Fig 2A). Moreover, and consistent with the observed polyuria in Li-NDI, many proximal and distal tubuli, and collecting ducts were dilated (Fig 2B) and the brush border was lacking in most tubuli (Fig. S1). In the collecting duct of Li-treated mice, cells were also protruding into the lumen (Fig. S1). Besides renal fibrosis, the diameter of the glomeruli in lithium-treated animals was decreased by ca. 24% (Fig 2C). Scoring of the extent of segmental glomerular sclerosis revealed that 5% of the glomerulri in lithium treated mice were affected. In control mice, no segmental sclerosis was observed (Fig 2D and E).

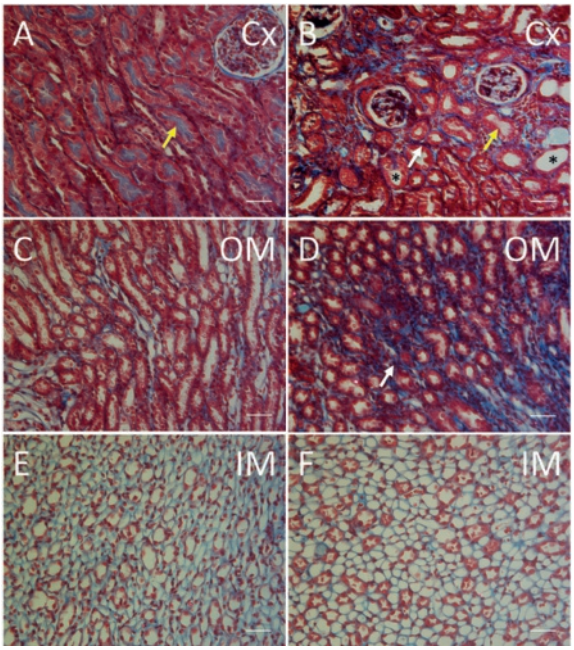

Figure 1. Lithium induces interstitial fibrosis in the renal cortex and the medulla. Newborn mice were treated with 40 mmol lithium chloride/kg food for 40 weeks or regular chow. Kidneys were harvested and stained for fibrosis using CAB staining. Shown are the cortex (A, B), outer medulla (C, D) and inner medulla (E, F) of control (A, C, E) and lithium-treated (B, D, F) mice. Scale bar represents 30 µm, white arrows indicate collagen deposition, yellow arrows indicate brush border and the asterisk symbol indicates dilatated tubules. Number of animals: CTR = 6, Li = 7.

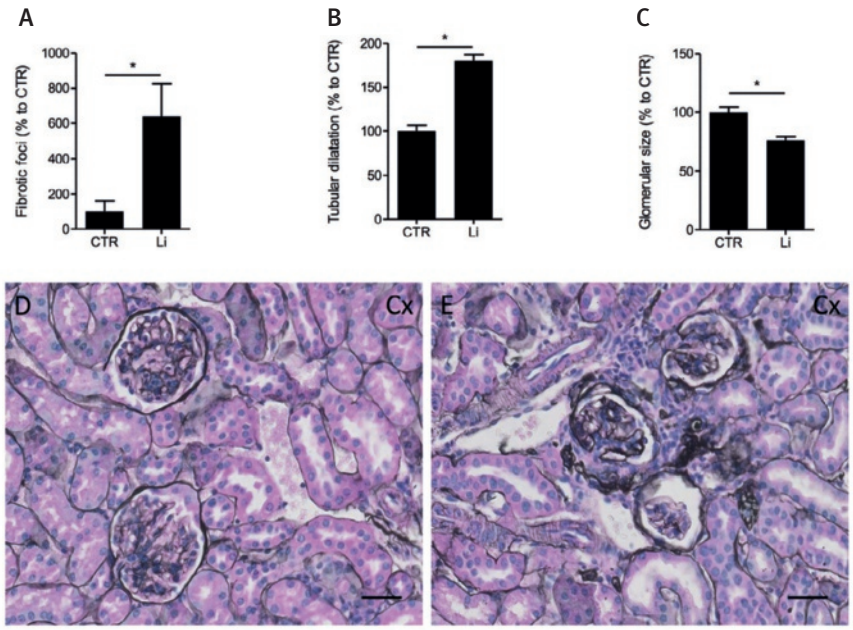

Figure 2. Lithium induces renal tubular abnormalities after 40 weeks treatment. Newborn mice were treated with 40 mmol lithium chloride/kg food for 40 weeks or regular chow. Kidneys were harvested and fibrotic foci (A), tubular dilatation (B) and glomerular size (C) were determined in the images obtained from the CAB staining. The extend of glomerular sclerosis was determined in images obtained from the methenamine silver staining (D and E). Scale bar represents 30 µm and the asterisk symbol indicates dilatated tubules. Number of animals: CTR = 6, Li = 7.

Lithium increases alpha smooth muscle actin expression in cortex and outer medulla.

The recruitment, proliferation and differentiation of extracellular matrix–producing myofibroblasts is an essential step in the development of interstitial fibrosis (45-47). To test for their presence, we stained kidney sections for α-smooth muscle actin (α-SMA), a marker for myofibroblasts, in combination with markers for blood vessels (CD31) and collecting duct cells (AQP4). In control animals, α-SMA staining was only detected around cortical blood vessels (Figs 3A, C and E). In lithium-treated mice, however, α-SMA staining was observed around tubuli in the cortex and outer medulla (Figs 3B and D), but not in the inner medulla (Fig 3F). The CD31 staining did specifically stain capillaries, but showed a non-specific green background staining, therewith visualizing the tubuli. In line with earlier stainings, the yellow staining for AQP4 was only visible in the basolateral side of principal cells in the inner medulla (48).

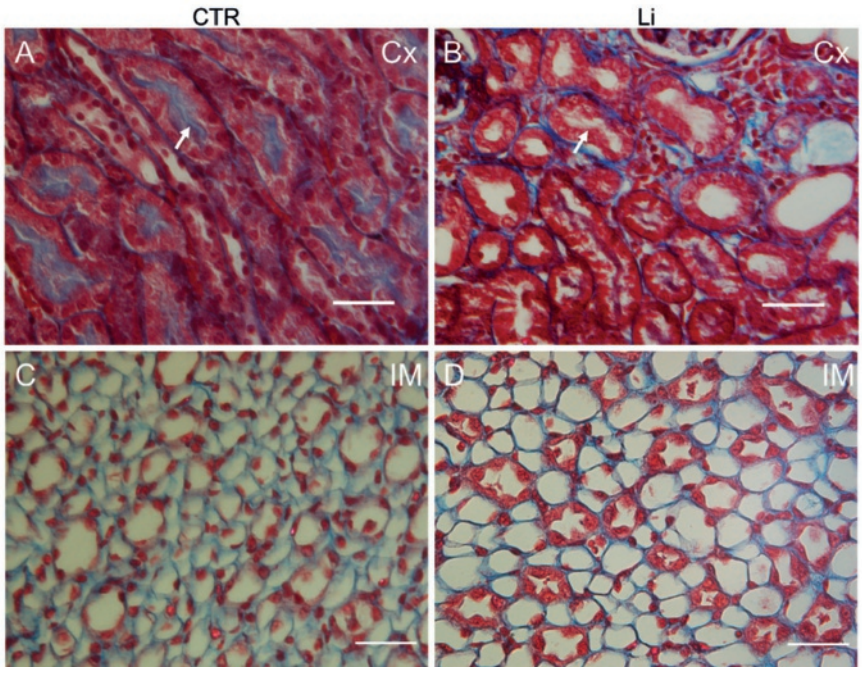

S1 Figure. Lithium treatment results in loss of brush border in the cortex and tubular atrophy of the inner medullary collecting duct. Magnification of the cortex and the inner medulla of control (A and C) and lithium treated (B and D) mice. Kidney sections were stained with CAB staining. Lithium treatment resulted in loss of brush border in the cortex and tubular atrophy of the inner medullary collecting duct cells with that showed enlarged nuclei and protruded into the lumen. Scale bar represents 30 μm.

To get an indication of factors contributing to the increase in the number of myofibroblasts, we assessed the mRNA expression of transforming growth factor beta 1 (TGFβ1) and connective tissue growth factor (CTGF), two growth factors critically involved in stimulation of conversion of fibroblasts into myofibroblasts (46). RT-qPCR analysis revealed that TGFβ1 mRNA levels were not changed by lithium-treatment, but that the CTGF mRNA expression was significantly higher in the medulla, but not the cortex, of lithium treated mice (Figs 4A-D).

Lithium treatment causes a pro-inflammatory response.

The migration of mononuclear cells into the interstitium where they mature into macrophages is a hallmark in the pathology of tubulo-interstitial fibrosis (47, 49, 50). Monocytes and macrophages contribute directly to the fibrogenic process by releasing

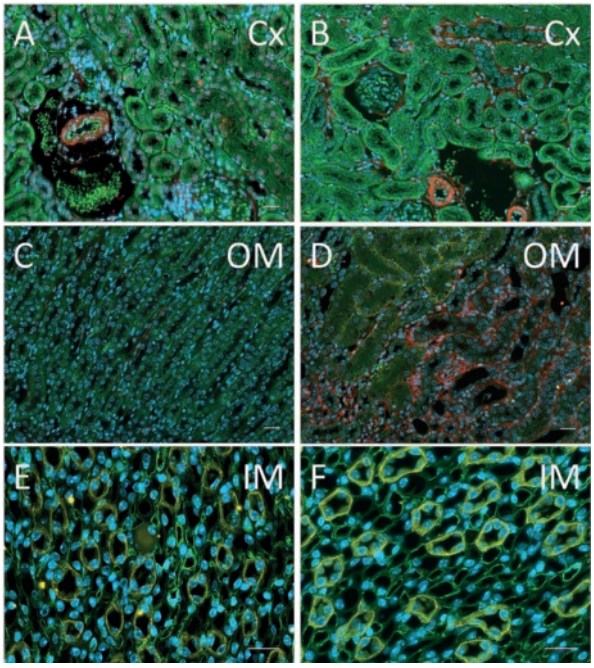

Figure 3. Lithium increases α-SMA staining in the renal cortex and the medulla. Immunofluorescence staining for α-SMA (red), CD31 (green), AQP4 (yellow) and DAPI (blue) was performed on kidneys of mice that received lithium for 40 weeks. Shown are the cortex (A, B), outer medulla (C, D) and inner medulla (E, F) of control (A, C, E) and lithium-treated (B, D, F) mice. Scale bar represents 20 µm. Number of animals: CTR = 6, Li = 7. Abbreviation: alpha smooth muscle actin (α-SMA), cluster of differentiation 31 (CD31), aquaporin-4 (AQP4) and 4',6-Diamidino-2-Phenylindole, Dihydrochloride (DAPI).

inflammatory and profibrotic molecules (50). Therefore, we determined the mRNA expression of monocyte chemotactic protein 1 (MCP1), a chemokine that recruits monocytes to the sites of inflammation, F4/80, a macrophage marker, tumor necrosis factor alpha (TNFα), interleukin-6 (IL-6), interferon gamma (IFNγ) and interleukin-1 receptor antagonist (IL-1Ra) in renal cortex and medulla (51, 52). Although the MCP1 mRNA expression was not higher in lithium groups (Figs 5A and B), F4/80 was significantly increased in both cortex and medulla of lithium-treated animals (Figs 5C and D), indicating an increased presence of macrophages. Furthermore, kidney sections of control and lithium-treated mice were stained immunohistochemically for the macrophage marker CD68. This confirmed the increase of macrophages after lithium treatment in comparison to control mice (Figs 5E and F). Furthermore, we also

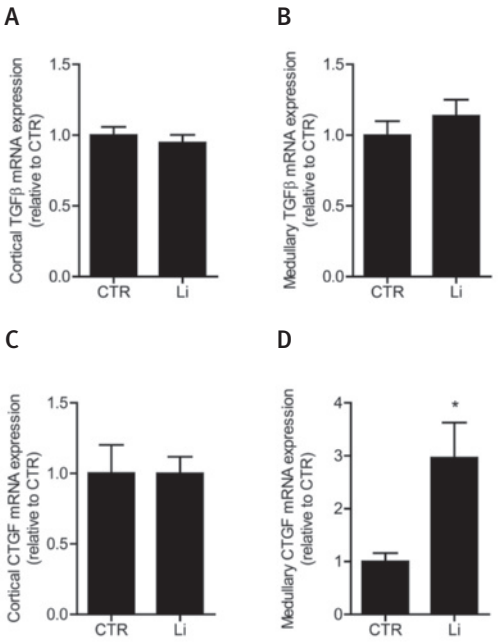

Figure 4. Lithium induces CTGF mRNA expression in the renal medulla. RT-qPCR analysis was performed on cortex and medulla samples from control and 40 weeks lithium treated mice. (A) TGFβ1 cortex, (B) TGFβ1 medulla, (C) CTGF cortex, (D) CTGF medulla. Results were normalized for 36B4 mRNA expression and a significant difference ($P<0.05$) from CTR is denoted by an asterisk. Number of animals: CTR = 6, Li = 7. Abbreviation: TGFβ1; Transforming growth factor beta 1, CTGF; connective tissue growth factor.

assessed the mRNA expression of several inflammatory markers. After lithium treatment, mRNA expression of TNFα was significantly increased in both segments (Figs 6A and B). No significant changes were observed for IL-6 (Figs 6C and D), IFNγ (Figs 6E and F), and IL-1Ra (Figs 6G and H).

For recruitment of inflammatory cells to injured tissue, immune cells in the circulation attach to the endothelium of blood vessels at the site of injury, for which the endothelial cells must have undergone several changes, such as increased expression of adhesion molecules and particular changes in heparan sulfate (HS) domains of the endothelial glycocalyx. Upon pro-inflammtory stimuli, such as the activation of the endothelium by the cytokines TNFα or IL-1β, heparan sulfate is changed to express specific highly sulfated domains. Some of these domains were identified with specific anti-HS

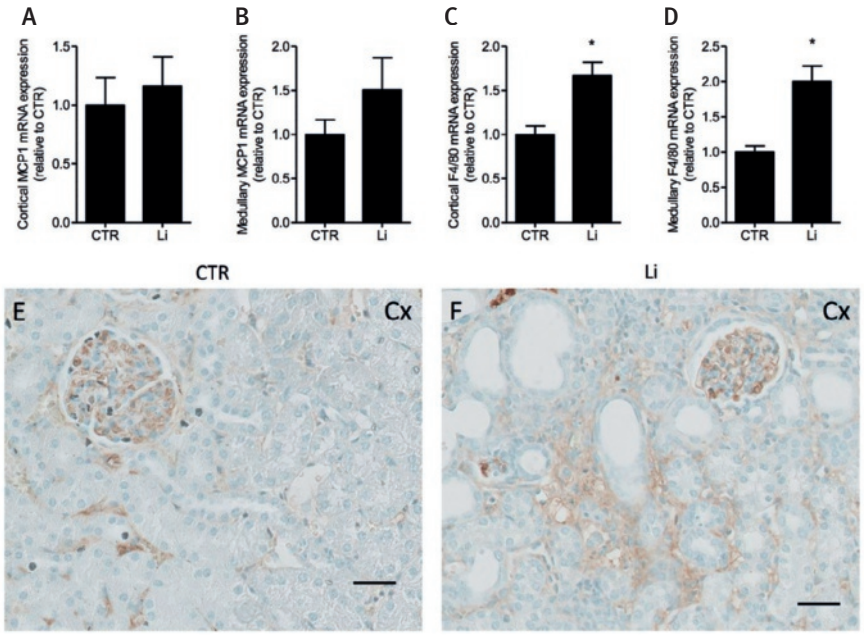

Figure 5. Lithium induces macrophage accumulation in the renal cortex and medulla. RT-qPCR analysis was performed on cortex and medulla samples from control and 40 weeks lithium treated mice. (A) MCP1 cortex, (B) MCP1 medulla, (C) F4/80 cortex, (D) F4/80 medulla. Results were normalized for 36B4 mRNA. kidney sections of control (E) and lithium-treated (F) mice were stained immunohistochemically for the macrophage marker CD68. The scale bar represents 30 µm and the asterisk denotes a significant difference ($P<0.05$) from CTR. Number of animals: CTR = 6, Li = 7. Abbreviation: MCP1; monocyte chemotactic protein 1.

antibodies on activated mouse glomerular endothelium. The expression of these domains was increased upon TNFα or IL-1β activation, and leukocyte adhesion could be inhibited by specifically blocking these domains, while targeting of other HS domains had no effect. Increased HS N-sulfation was shown to be a major determinant in this process since the inflammatory processes in a mouse model of experimental glomerulonephritis were decreased by specific knock-out of N-deacetylate/N-sulfotransferase-1 (Ndst-1), the major enzyme responsible for HS N-sulfation (41, 42, 49, 53). To test the changes in heparin sulphate domains, we performed semi-quantitative immunohistochemistry with the EW3D10 antibody, which recognizes a pro-inflammatory HS form and mediates binding of leukocytes and chemokines. The expression of the HS domain recognized by the anti-HS antibody EW3D10 was increased 2-fold on

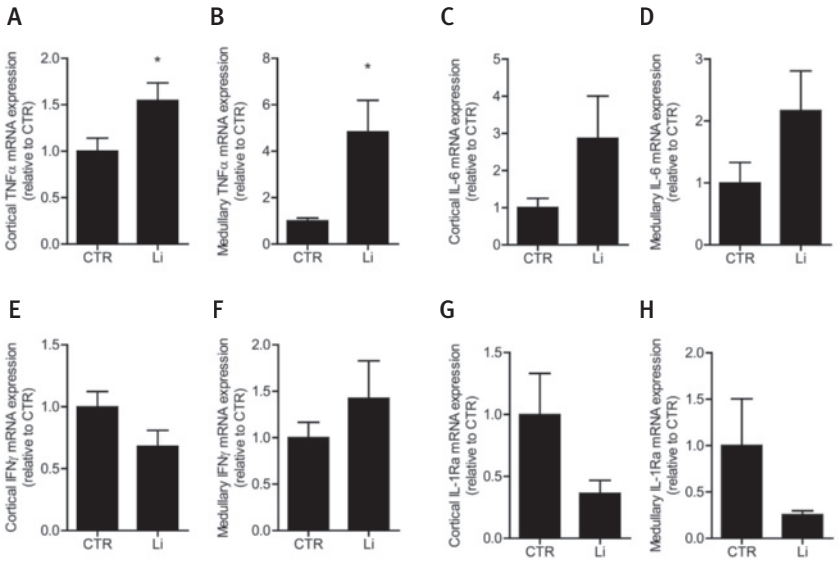

Figure 6. Minimal inflammatory reaction after long-term lithium treatment. RT-qPCR analysis was performed on cortex and medulla samples from control and 40 weeks lithium treated mice. (A) TNFα cortex, (B) TNFα medulla, (C) IL-6 cortex, (D) IL-6 medulla, (E) IFNγ cortex, (F) IFNγ medulla, (G) IL-1Ra cortex, (H) IL-1Ra medulla. Results were normalized for 36B4 mRNA expression and the asterisk denotes a significant difference ($P<0.05$) from CTR. Number of animals: CTR = 6, Li = 7 Abbreviation: IL-6; Interleuking-6, TNFα; Tumor necrosis factor alpha, IFNγ; Interferon gamma and IL-1Ra; interleukin-1 receptor antagonist.

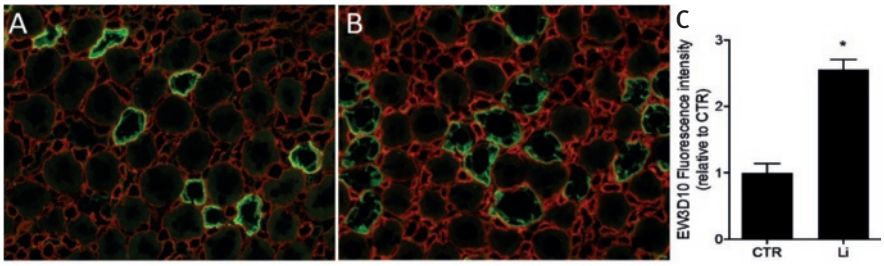

Figure 7. Inflammatory changes in the peritubular endothelial glycocalyx after lithium treatment. Pro-inflammatory changes in the glycocalyx were analyzed with anti-heparan sulphate antibody EW3D10 (red) that detects inflammatory HS domains that are involved in leukocyte trafficking and chemokine binding. The sections were also stained with AQP4 (green) to detect collecting ducts. (A) control, (B) lithium, (C) EW3D10 fluorescence intensity. The asterisk denotes a significant difference ($P<0.05$) from CTR.

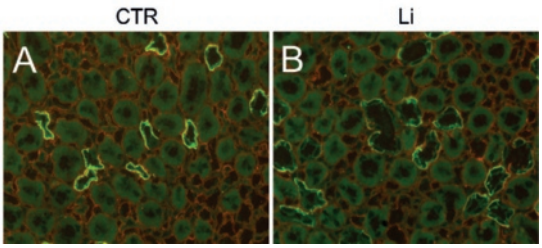

S2 Figure. No differences in expression of the HS domain defined by HS4C3. HS4C3 (red) was used as a non-inflammatory control in the detection of the endothelial glycocalyx and revealed no differences in expression in the peritubular endothelial glycocalyx between control (A) and lithium-fed groups (B). The sections were also stained with AQP4 (green) to detect collecting ducts.

peritubular capillaries of lithium chloride fed mice as compared to control mice (Fig 7). No differences in staining intensity was found with the HS4C3 antibodies, which recognize a HS domain that is not affected by inflammation (Fig. S2).

Discussion

Lithium induces renal interstitial fibrosis in mice.

Long-term lithium treatment in humans has been correlated with the development of chronic tubulointerstitial fibrosis (54-56). In this study, we investigated whether mice are a suitable model to study lithium-induced interstitial fibrosis. Based on our earlier (unpublished) data, we know that long-term lithium treatment of adult mice does not lead to interstitial fibrosis within a time frame of 8 months. In addition, studies by Christensen *et al.* (1981) and Ottosen *et al.* (1984) demonstrated that newborn rats were more susceptible to develop interstitial fibrosis after lithium treatment than adult mice (29, 30). Therefore, pregnant mice received several lithium concentrations in diet and after weaning, these diets were directly administered to the pups. Only the group that received 40 mmol lithium chloride/kg survived the study of 40 weeks lithium chloride treatment, while mice that received higher lithium concentration died at an earlier age. Lithium poisoning can affect multiple organs including the central nervous system and the cardiovascular system, in addition to the adverse effects on water homeostasis (57, 58). Although the cause of death and serum lithium levels were not determined here, their early death is likely due to lithium poisoning.

In this study, we found that treatment of newborn male and female C57Bl6 mice with 40 mmol lithium chloride/kg food for 40 weeks induced renal interstitial fibrosis

in the cortex and outer medulla (Fig 1). This coincided with a remarkable increase in collagen deposition in the cortex and the outer medulla. Walker *et al.* treated rats with lithium (60 mmol lithium chloride/kg food) for 1, 3 and 6 months and reported, in line with our findings, a progressive interstitial fibrosis that was characterized by increased numbers of myofibroblasts, interstitial collagen deposition and a minimal inflammatory cellular response (59). We, nor they, observed any microcysts, which may be partially due to our 2D way of analysis, which complicates proper identification of cysts. It is at present unclear why long-term lithium treatment yields renal cysts in humans, but not in rodents. Moreover, Ottosen et al. showed that young male rats being more affected than females by lithium (60). However, the number of included animals from each gender in this study was not enough to determine whether gender is an important aspect in the developmeant of interstitial fibrosis after lithium treatment.

Classical activation of the fibrogenic pathway by lithium

A key feature in fibrosis is the activation of extra cellular matrix (ECM)-producing myofibroblasts, which mediate the fibrogenic process (45, 47). Here, we demonstrated that lithium also induces the generation of myofibroblasts in the renal cortex and outer medulla of mice (Fig 3). Earlier findings in rats showed that α-SMA staining was present throughout the whole kidney after 6-month lithium treatment (59, 61). In our study, renal TGFβ1 mRNA expression was not increased after lithium treatment (Figs 4A and B), while it was increased in lithium-treated rats (59, 61). This difference can be explained by the fact that serum lithium levels in the rats were higher (± 1.0 mM) than the expected serum lithium concentrations in our experiment (0.6 mM) after long term lithium treatment. TGFβ is considered as the major factors driving the development of fibrosis, as it stimulates interstitial generation of myofibroblast (46, 62). However, CTGF was significantly increased in the medulla of lithium treated mice (Fig 4D) and it antagonizes bone morphogenetic protein (BMP) signaling by preventing BMP binding to BMP receptors, thereby enhancing TGFβ signaling (46, 63).

Moreover, lithium might also directly induce the conversion of resident fibroblasts into myofibroblasts as Caraci *et al.* have shown that lithium treatment of human lung fibroblasts increased total β-catenin levels, α-SMA expression and collagen production (64). However, Michalik *et al.* found contradictory results where lithium attenuated the transition of TGFβ1-stimulated bronchial fibroblasts to myofibroblasts (65). Moreover, we have shown previously that lithium caused G2 phase cell cycle arrest in principal cells (66). Under specific stress conditions, G2 arrested cells are also known to produce inflammatory cytokines and profibrotic proteins such as TGFβ1 and CTGF, mediating the fibrogenic process and increase myofibroblasts (67). Taken together, the direct effect of lithium on renal fibroblasts remains unclear and more research is required to elucidate the cellular and the molecular mechanisms responsible for the increase in myofibroblasts in the kidney.

The role of inflammation in lithium-induced renal fibrosis.

Previously we showed that specific HS domains within the endothelial glycocalyx, as defined by specific anti-HS antibodies, are upregulated under inflammatory conditions, both *in vitro* and *in vivo* (36, 41, 42). Furthermore, we have provided *in vitro* and *in vivo* evidence that these so called "inflammatory" HS domains are mediating leukocyte trafficking and chemokine binding (36, 41, 42). It appears that the expression of the inflammatory HS domain as defined by EW3D10 was upregulated in the lithium group (Fig 7). As such, this inflammatory state of the peritubular endothelial glycocalyx may have facilitated the migration of mononuclear cells into the interstitium after which they matured into macrophages, as we found an increased abundance of macrophages based on F4/80 levels (Figs 5C and D). Moreover, we observed a significant increase of TNFα in the cortex and the medulla (Figs 6A and B), suggesting that the kidneys were in a pro-inflammatory state. However, this was a minimal inflammatory response since other markers such as IL-6, IFNγ and IL-1Ra were not altered by lithium. Walker et al. also found a significant increase in the number of macrophages in the kidneys of 6-month lithium-treated rats while inflammatory changes were minimal (59). Lithium might induce renal fibrosis without inducing an acute inflammatory response, as Maarouf et al. demonstrated that activation of wnt1 caused interstitial fibrosis, while no inflammatory response was found (68). Wnt1 and lithium both target glycogen synthase kinase 3 beta (GSK3β) and a similar mechanism might underlie the observed interstitial fibrosis. But lithium might also induce fibrosis that in turn results in an inflammatory response that is inhibited by lithium, this response has been extensively reviewed by Nassar et al. (69).

In conclusion, we have shown that the most-commonly used mouse model C57BL/6, which is already extensively used to study Li-NDI, develops interstitial fibrosis when mothers and subsequent pups are treated with a lithium dose that yields clinically-relevant blood lithium levels. We furthermore showed that the histological and molecular changes with lithium-induced interstitial fibrosis formation is alike that found in lithium using patients, indicating that this approach allows the usage of C57Bl6 mice as a model to uncover the underlying mechanism, and to identify ways to prevent or treat, human Li-induced renal fibrosis and, possibly, ESRD.

Acknowledgments

This project received support from a Marie Curie Fellowship PIOF-GA-2012-332395 to T.d.G. and a grant from the Society of Experimental Laboratory Medicine to P.M.T.D.

References

1. Merikangas KR, Jin R, He JP, Kessler RC, Lee S, Sampson NA, et al. Prevalence and correlates of bipolar spectrum disorder in the world mental health survey initiative. Arch Gen Psychiatry. 2011;68(3):241-51.
2. Merikangas KR, Akiskal HS, Angst J, Greenberg PE, Hirschfeld RM, Petukhova M, et al. Lifetime and 12-month prevalence of bipolar spectrum disorder in the National Comorbidity Survey replication. Arch Gen Psychiatry. 2007;64(5):543-52.
3. Novick DM, Swartz HA, Frank E. Suicide attempts in bipolar I and bipolar II disorder: a review and meta-analysis of the evidence. Bipolar Disord. 2010;12(1):1-9.
4. Anderson IM, Haddad PM, Scott J. Bipolar disorder. BMJ. 2012;345:e8508.
5. Dilsaver SC. An estimate of the minimum economic burden of bipolar I and II disorders in the United States: 2009. J Affect Disord. 2011;129(1-3):79-83.
6. Cipriani A, Pretty H, Hawton K, Geddes JR. Lithium in the prevention of suicidal behavior and all-cause mortality in patients with mood disorders: a systematic review of randomized trials. Am J Psychiatry. 2005;162(10):1805-19.
7. Geddes JR, Miklowitz DJ. Treatment of bipolar disorder. Lancet. 2013;381(9878):1672-82.
8. Bramness JG, Weitoft GR, Hallas J. Use of lithium in the adult populations of Denmark, Norway and Sweden. J Affect Disord. 2009;118(1-3):224-8.
9. Wyatt RJ, Henter ID, Jamison JC. Lithium revisited: savings brought about by the use of lithium, 1970-1991. Psychiatr Q. 2001;72(2):149-66.
10. Alsady M, Baumgarten R, Deen PM, de Groot T. Lithium in the Kidney: Friend and Foe? J Am Soc Nephrol. 2016;27(6):1587-95.
11. Aiff H, Attman PO, Aurell M, Bendz H, Ramsauer B, Schon S, et al. Effects of 10 to 30 years of lithium treatment on kidney function. J Psychopharmacol. 2015;29(5):608-14.
12. Dols A, Sienaert P, van Gerven H, Schouws S, Stevens A, Kupka R, et al. The prevalence and management of side effects of lithium and anticonvulsants as mood stabilizers in bipolar disorder from a clinical perspective: a review. Int Clin Psychopharmacol. 2013;28(6):287-96.
13. Aiff H, Attman PO, Aurell M, Bendz H, Schon S, Svedlund J. End-stage renal disease associated with prophylactic lithium treatment. Eur Neuropsychopharmacol. 2014;24(4):540-4.
14. Gupta S, Kripalani M, Khastgir U, Reilly J. Management of the renal adverse effects of lithium. Advances in psychiatric treatment. 2013;19:457–66.
15. Grandjean EM, Aubry JM. Lithium: updated human knowledge using an evidence-based approach: part III: clinical safety. CNS Drugs. 2009;23(5):397-418.
16. Bendz H, Schon S, Attman PO, Aurell M. Renal failure occurs in chronic lithium treatment but is uncommon. Kidney Int. 2010;77(3):219-24.
17. Markowitz GS, Radhakrishnan J, Kambham N, Valeri AM, Hines WH, D'Agati VD. Lithium nephrotoxicity: a progressive combined glomerular and tubulointerstitial nephropathy. J Am Soc Nephrol. 2000;11(8):1439-48.
18. Farres MT, Ronco P, Saadoun D, Remy P, Vincent F, Khalil A, et al. Chronic lithium nephropathy: MR imaging for diagnosis. Radiology. 2003;229(2):570-4.
19. Slaughter A, Pandey T, Jambhekar K. MRI findings in chronic lithium nephropathy: a case report. J Radiol Case Rep. 2010;4(8):15-21.
20. Tuazon J, Casalino D, Syed E, Batlle D. Lithium-associated kidney microcysts. ScientificWorldJournal. 2008;8:828-9.
21. Cheung PW, Nomura N, Nair AV, Pathomthongtaweechai N, Ueberdiek L, Lu HA, et al. EGF Receptor Inhibition by Erlotinib Increases Aquaporin 2-Mediated Renal Water Reabsorption. J Am Soc Nephrol. 2016;27(10):3105-16.
22. de Groot T, Doornebal J, Christensen BM, Cockx SC, Sinke AP, Baumgarten R, et al. Lithium-induced NDI: Acetazolamide reduces polyuria, but does not improve urine concentrating ability. Am J Physiol Renal Physiol. 2017:ajprenal 00147 2017.
23. de Groot T, Sinke AP, Kortenoeven ML, Alsady M, Baumgarten R, Devuyst O, et al. Acetazolamide Attenuates Lithium-Induced Nephrogenic Diabetes Insipidus. J Am Soc Nephrol. 2016;27(7):2082-91.

24. Lin Y, Zhang T, Feng P, Qiu M, Liu Q, Li S, et al. Aliskiren Increases Aquaporin-2 Expression and Attenuates Lithium-induced Nephrogenic Diabetes Insipidus. Am J Physiol Renal Physiol. 2017:ajprenal 00553 2016.
25. Poulsen SB, Kristensen TB, Brooks HL, Kohan DE, Rieg T, Fenton RA. Role of adenylyl cyclase 6 in the development of lithium-induced nephrogenic diabetes insipidus. JCI Insight. 2017;2(7):e91042.
26. Sim JH, Himmel NJ, Redd SK, Pulous FE, Rogers RT, Black LN, et al. Absence of PKC-alpha attenuates lithium-induced nephrogenic diabetes insipidus. PLoS One. 2014;9(7):e101753.
27. Zhang Y, Peti-Peterdi J, Brandes AU, Riquier-Brison A, Carlson NG, Muller CE, et al. Prasugrel suppresses development of lithium-induced nephrogenic diabetes insipidus in mice. Purinergic Signal. 2017;13(2):239-48.
28. Zhang Y, Peti-Peterdi J, Heiney KM, Riquier-Brison A, Carlson NG, Muller CE, et al. Clopidogrel attenuates lithium-induced alterations in renal water and sodium channels/transporters in mice. Purinergic Signal. 2015;11(4):507-18.
29. Christensen S, Ottosen PD. Lithium-induced uremia in rats - a new model of chronic renal failure. Pflugers Arch. 1983;399(3):208-12.
30. Ottosen PD, Sigh B, Kristensen J, Olsen S, Christensen S. Lithium induced interstitial nephropathy associated with chronic renal failure. Reversibility and correlation between functional and structural changes. Acta Pathol Microbiol Immunol Scand A. 1984;92(6):447-54.
31. Messiha FS. Maternally-mediated developmental lithium toxicity in the mouse. Gen Pharmacol. 1993;24(1):9-15.
32. Oruch R, Elderbi MA, Khattab HA, Pryme IF, Lund A. Lithium: a review of pharmacology, clinical uses, and toxicity. Eur J Pharmacol. 2014;740:464-73.
33. Christensen BM, Zuber AM, Loffing J, Stehle JC, Deen PM, Rossier BC, et al. alphaENaC-mediated lithium absorption promotes nephrogenic diabetes insipidus. J Am Soc Nephrol. 2011;22(2):253-61.
34. van Balkom BW, Boone M, Hendriks G, Kamsteeg EJ, Robben JH, Stronks HC, et al. LIP5 interacts with aquaporin 2 and facilitates its lysosomal degradation. J Am Soc Nephrol. 2009;20(5):990-1001.
35. Deen PM, Nielsen S, Bindels RJ, van Os CH. Apical and basolateral expression of aquaporin-1 in transfected MDCK and LLC-PK cells and functional evaluation of their transcellular osmotic water permeabilities. Pflugers Arch. 1997;433(6):780-7.
36. Rops AL, Gotte M, Baselmans MH, van den Hoven MJ, Steenbergen EJ, Lensen JF, et al. Syndecan-1 deficiency aggravates anti-glomerular basement membrane nephritis. Kidney Int. 2007;72(10):1204-15.
37. Kurup S, Wijnhoven TJ, Jenniskens GJ, Kimata K, Habuchi H, Li JP, et al. Characterization of anti-heparan sulfate phage display antibodies AO4B08 and HS4E4. J Biol Chem. 2007;282(29):21032-42.
38. Smetsers TF, van de Westerlo EM, ten Dam GB, Clarijs R, Versteeg EM, van Geloof WL, et al. Localization and characterization of melanoma-associated glycosaminoglycans: differential expression of chondroitin and heparan sulfate epitopes in melanoma. Cancer Res. 2003;63(11):2965-70.
39. van de Westerlo EM, Smetsers TF, Dennissen MA, Linhardt RJ, Veerkamp JH, van Muijen GN, et al. Human single chain antibodies against heparin: selection, characterization, and effect on coagulation. Blood. 2002;99(7):2427-33.
40. van Kuppevelt TH, Dennissen MA, van Venrooij WJ, Hoet RM, Veerkamp JH. Generation and application of type-specific anti-heparan sulfate antibodies using phage display technology. Further evidence for heparan sulfate heterogeneity in the kidney. J Biol Chem. 1998;273(21):12960-6.
41. Rops AL, Loeven MA, van Gemst JJ, Eversen I, Van Wijk XM, Dijkman HB, et al. Modulation of heparan sulfate in the glomerular endothelial glycocalyx decreases leukocyte influx during experimental glomerulonephritis. Kidney Int. 2014;86(5):932-42.
42. Rops AL, van den Hoven MJ, Baselmans MM, Lensen JF, Wijnhoven TJ, van den Heuvel LP, et al. Heparan sulfate domains on cultured activated glomerular endothelial cells mediate leukocyte trafficking. Kidney Int. 2008;73(1):52-62.
43. Jones DB. Nephrotic glomerulonephritis. Am J Pathol. 1957;33(2):313-29.
44. Akamine R, Yamamoto T, Watanabe M, Yamazaki N, Kataoka M, Ishikawa M, et al. Usefulness of the 5' region of the cDNA encoding acidic ribosomal phosphoprotein Po conserved among rats, mice, and humans as a standard probe for gene expression analysis in different tissues and animal species. J Biochem Biophys Methods. 2007;70(3):481-6.

45. Hinz B, Phan SH, Thannickal VJ, Galli A, Bochaton-Piallat ML, Gabbiani G. The myofibroblast: one function, multiple origins. Am J Pathol. 2007;170(6):1807-16.
46. Kok HM, Falke LL, Goldschmeding R, Nguyen TQ. Targeting CTGF, EGF and PDGF pathways to prevent progression of kidney disease. Nat Rev Nephrol. 2014;10(12):700-11.
47. Wynn TA, Ramalingam TR. Mechanisms of fibrosis: therapeutic translation for fibrotic disease. Nat Med. 2012;18(7):1028-40.
48. Kim YH, Earm JH, Ma T, Verkman AS, Knepper MA, Madsen KM, et al. Aquaporin-4 expression in adult and developing mouse and rat kidney. J Am Soc Nephrol. 2001;12(9):1795-804.
49. Bonventre JV, Yang L. Cellular pathophysiology of ischemic acute kidney injury. J Clin Invest. 2011;121(11):4210-21.
50. Eddy AA. Molecular basis of renal fibrosis. Pediatr Nephrol. 2000;15(3-4):290-301.
51. Austyn JM, Gordon S. F4/80, a monoclonal antibody directed specifically against the mouse macrophage. Eur J Immunol. 1981;11(10):805-15.
52. Lloyd CM, Minto AW, Dorf ME, Proudfoot A, Wells TN, Salant DJ, et al. RANTES and monocyte chemoattractant protein-1 (MCP-1) play an important role in the inflammatory phase of crescentic nephritis, but only MCP-1 is involved in crescent formation and interstitial fibrosis. J Exp Med. 1997;185(7):1371-80.
53. Li L, Bonventre JV. Endothelial Glycocalyx: Not Just a Sugar Coat. American journal of respiratory and critical care medicine. 2016;194(4):390-3.
54. Aurell M, Svalander C, Wallin L, Alling C. Renal function and biopsy findings in patients on long-term lithium treatment. Kidney Int. 1981;20(5):663-70.
55. Hansen HE, Hestbech J, Sorensen JL, Norgaard K, Heilskov J, Amdisen A. Chronic interstitial nephropathy in patients on long-term lithium treatment. Q J Med. 1979;48(192):577-91.
56. Hestbech J, Hansen HE, Amdisen A, Olsen S. Chronic renal lesions following long-term treatment with lithium. Kidney Int. 1977;12(3):205-13.
57. Baird-Gunning J, Lea-Henry T, Hoegberg LC, Gosselin S, Roberts DM. Lithium Poisoning. J Intensive Care Med. 2016.
58. Asim K, Selman Y, Suleyman Y, Ozgur K, Ozlem B, Gokhan E. Heart Attack in the Course of Lithium Overdose. Iran Red Crescent Med J. 2016;18(7):e21731.
59. Walker RJ, Leader JP, Bedford JJ, Gobe G, Davis G, Vos FE, et al. Chronic interstitial fibrosis in the rat kidney induced by long-term (6-mo) exposure to lithium. Am J Physiol Renal Physiol. 2013;304(3):F300-7.
60. Ottosen PD, Nyengard JR, Olsen TS, Christensen S. Interstitial focal fibrosis and reduction in proximal tubular length in adult rats after lithium treatment. Acta Pathol Microbiol Immunol Scand A. 1986;94(6):401-3.
61. Kalita DECP, Bedford JJ, Leader JP, Walker RJ. Amiloride modifies the progression of lithium-induced renal interstitial fibrosis. Nephrology (Carlton). 2016.
62. Meng XM, Nikolic-Paterson DJ, Lan HY. TGF-beta: the master regulator of fibrosis. Nat Rev Nephrol. 2016;12(6):325-38.
63. Chuang PY, Menon MC, He JC. Molecular targets for treatment of kidney fibrosis. Journal of molecular medicine. 2013;91(5):549-59.
64. Caraci F, Gili E, Calafiore M, Failla M, La Rosa C, Crimi N, et al. TGF-beta1 targets the GSK-3beta/beta-catenin pathway via ERK activation in the transition of human lung fibroblasts into myofibroblasts. Pharmacol Res. 2008;57(4):274-82.
65. Michalik M, Wojcik KA, Jakiela B, Szpak K, Pierzchalska M, Sanak M, et al. Lithium Attenuates TGF-beta(1)-Induced Fibroblasts to Myofibroblasts Transition in Bronchial Fibroblasts Derived from Asthmatic Patients. J Allergy (Cairo). 2012;2012:206109.
66. de Groot T, Alsady M, Jaklofsky M, Otte-Holler I, Baumgarten R, Giles RH, et al. Lithium causes G2 arrest of renal principal cells. J Am Soc Nephrol. 2014;25(3):501-10.
67. Canaud G, Bonventre JV. Cell cycle arrest and the evolution of chronic kidney disease from acute kidney injury. Nephrology, dialysis, transplantation : official publication of the European Dialysis and Transplant Association - European Renal Association. 2015;30(4):575-83.

68. Maarouf OH, Aravamudhan A, Rangarajan D, Kusaba T, Zhang V, Welborn J, et al. Paracrine Wnt1 Drives Interstitial Fibrosis without Inflammation by Tubulointerstitial Cross-Talk. J Am Soc Nephrol. 2016;27(3):781-90.
69. Nassar A, Azab AN. Effects of lithium on inflammation. ACS Chem Neurosci. 2014;5(6):451-8.

Chapter 8

Single-Tubule RNA-Seq Reveals Signaling Mechanisms That Defend Against Hyponatremia in SIADH

Lee JW [1,4*], Alsady M [2*], Chou CL [1*], de Groot T [2], Deen PMT [2], Knepper MA [1†], Ecelbarger CM [1,3†]

*: equal contributions from these authors
†: equal contributions from these authors

[1] Epithelial Systems Biology Laboratory, Systems Biology Center, National Heart, Lung, and Blood Institute, National Institutes of Health, Bethesda, Maryland; [2] Department of Physiology, Radboud University Nijmegen Medical Center, Nijmegen, The Netherlands; [3] Division of Endocrinology and Metabolism, Department of Medicine, Georgetown University, Washington, DC; [4] Nephrology Clinic, National Cancer Center, Goyang, Gyeonggi-do, South Korea.

Kidney Int. 2017 Aug 23. pii: S0085-2538(17)30461-1.

Abstract

In SIADH, hyponatremia is limited by onset of vasopressin-escape, which is caused by loss of the water channel aquaporin-2 in the renal collecting duct (CD) despite high circulating vasopressin. Here, we use the methods of systems biology in a well-established rat model of SIADH to identify signaling pathways activated at the onset of vasopressin-escape. Using single-tubule RNA-Seq, full transcriptomes were determined in microdissected cortical CDs of vasopressin-treated rats at time points 1, 2, and 4 days after initiation of oral water loading (vs. time-controls without water loading). Time-dependent mRNA abundance changes were mapped to gene sets associated with curated canonical signaling pathways, revealing evidence of perturbation of TGFβ signaling (and epithelial-to-mesenchymal transition [EMT]) on Day 1, simultaneous with the initial fall in *Aqp2* gene expression. On Day 2, transcriptomic changes mapped to "notch signaling" and "transition from G0 to cell cycle". There was no evidence of cell proliferation or altered principal or intercalated cell numbers. Exposure of vasopressin-treated cultured mpkCCD cells to TGFβ resulted in a virtually complete loss of aquaporin-2. The data demonstrate a role for partial EMT in vasopressin-escape with a subsequent shift from quiescence to the cell cycle with arrest and loss of aquaporin-2.

Introduction

The syndrome of inappropriate antidiuretic hormone secretion (SIADH) is the most frequent cause of dilutional hyponatremia in hospitalized patients (1). In SIADH, high levels of circulating vasopressin persist even when serum osmolality falls to levels that normally totally suppress neurohypophyseal vasopressin secretion. Consequently, the kidney continues to reabsorb free water, leading to a progressive fall in serum osmolality (and sodium concentration). The extent of the fall is limited by the phenomenon of 'vasopressin-escape', which allows the kidneys to excrete free water despite sustained high levels of circulating vasopressin (2). Previous studies have demonstrated that vasopressin-escape is associated with a profound decrease in the expression of the *Aqp2* gene (3), which codes for the vasopressin-regulated water channel, aquaporin-2 (AQP2) (4, 5). This results in markedly reduced water permeability of the collecting duct epithelium (6), increasing water excretion.

The transcriptional regulatory mechanisms and signaling pathways responsible for vasopressin-escape are unknown. The chief limiting factor in the investigation of the vasopressin-escape phenomenon is the fact that collecting duct principal cells make up only a small fraction of the renal cortex, where the suppression of AQP2 expression in vasopressin-escape is most pronounced. Thus, standard biochemical and systems biology techniques applied at a tissue level are not effective as a way of detecting responses in collecting duct principal cells. Recently, we have introduced single-tubule RNA-Seq techniques that are capable of quantifying the entire transcriptome in samples of microdissected renal tubules from rat kidney consisting of less than 2000 cells (7). In this study, we used small sample RNA-Seq applied to microdissected renal cortical collecting ducts (CCDs) to identify transcriptomic changes during onset of vasopressin-escape in a model of SIADH. The strategy was to carry out global measurements of transcript abundances to identify the changes that occur at the earliest stages in the induction of vasopressin-escape (one, two and four days after initiation of water loading in vasopressin-treated rats). The central question that we addressed was, "What signaling pathways are activated or inactivated during development of vasopressin-escape?" Based on the RNA-Seq results, we identified elements of TGFβ signaling, epithelial-to-mesenchymal transition (EMT), Notch signaling, and cell-cycle regulatory pathways as components of the cell signaling response during initiation of the vasopressin-escape phenomenon.

Materials and Methods

The experimental design for this study (Animal Study Protocol No. H-0110R2, NHLBI) was described previously (3) (Figure 1). Male Sprague-Dawley rats (120-160 g) were subcutaneously implanted with osmotic minipumps (Alzet) releasing dDAVP (Bachem) at 5 ng/h. After 5 days of infusion, rats were divided into two groups (n=3 for each group for Day 1 and Day 4; n=4 for each group on Day 2). One group received a water load ("Escape", 50 mL/day) in the form of a daily ration of gelled food containing 72% water, 27% finely-ground rat chow, and 1% agar. The other group received only 25 mL/day of water ("Control") by feeding a gel containing 55% water, 43% chow, and 2% agar. The level of water intake in the control animals was based on a prior estimate of insensible water losses and does not result in hyponatremia (8). Each Escape rat was paired with a Control rat and both members of the pair were euthanized on the same day for tissue processing, alternating the order. Plasma sodium concentration was measured in heparinized blood samples from tail-snips, using an iSTAT hand-held analyzer with a CHEM8+ cartridge.

Microdissection of CCDs. We followed our standard protocol for microdissection of rat renal tubule segments (9). Approximately four millimeters of CCD segments were dissected per rat under a Wild M8 dissection stereomicroscope (Wild Heerbrugg) equipped with on-stage cooling.

RNA sequencing in microdissected tubules. The microdissected CCDs were processed for small sample RNA-Seq as described (6). The resulting cDNA libraries were sequenced using an Illumina HiSeq2000 (Illumina, Inc.) to generate 50-bp paired-end nucleotide sequences. The FASTQ sequences were mapped to a rat reference genome (*Ensembl* Rnor6.0) using STAR-2.4.0.1 (10). The read count data were summarized at the gene level and processed using factor analysis (11). DESeq2 (12) was used to generate Benjamini-Hochberg FDR-adjusted *p*-values for Log_2(Escape/Control) values for each transcript based on Wald tests. The FASTQ sequences and metadata generated by this work have been deposited in NCBI's *Gene Expression Omnibus* (GEO)

(http://www.ncbi.nlm.nih.gov/geo/query/acc.cgi?token=axgfmcskxzmntep&acc=GSE69779).

Quantitative real-time PCR. Quantitative real-time PCR was carried out from cDNA libraries using a 7900HT PCR system (Applied Biosystems) (13). Gene expression was compared using the ΔΔCT method (14). β-actin and glutaraldehyde-3-phosphate dehydrogenase were used as reference genes. Two-tailed Student's *t*-test was used to compare values in control versus escape animals.

Identification of gene groups over-represented. We used Chi-square analysis to ask whether genes from a particular curated gene list were over-represented among genes whose transcript abundances were changed in vasopressin-escape compared to genes whose transcript abundances did not change. Curated lists for various signaling pathways were downloaded from KEGG (Kyoto Encyclopedia of Genes and Genomes) (http://www.genome.jp/kegg/) or from the literature (see **Results**). In addition, we used DAVID (14) to identify *Gene Ontology* terms that were enriched in the set of genes whose transcripts changed relative to non-responding genes.

Quantitative immunocytochemistry in microdissected tubules. Determination of the numbers of each cell type per unit length in microdissected CCDs from escape and control rats was carried out using immunocytochemistry employing antibodies recognizing cell type specific markers, based on Purkerson et al. (15) The primary antibodies used were goat anti-pendrin (G-19, sc-23779, Santa Cruz Biotechnology, Santa Cruz, CA) and a previously characterized rabbit anti-H^+-ATPase V1-B1 subunit (L615,(16)), each at 1:50 dilution. The secondary antibodies were Alexa Fluor 488 donkey anti-goat and Alexa Fluor 555 donkey anti-rabbit IgG (A11055 and A31572, respectively, Invitrogen) each at 1:2000 dilution. Cell nuclei were also stained with DAPI. Confocal fluorescence images were recorded with a Zeiss LSM780 confocal microscope using a 20x objective lens. Cell counting was performed on three-dimensional reconstructed tubule images created by Imaris Scientific Image Processing & Analysis software (v7.7.1, Bitplane, Zurich, Switzerland). Counting was automated using Imaris "spot analysis" for nuclei and "surface analysis" to enumerate cells with apical pendrin or H^+-ATPase labeling.

Immunocytochemistry and Western blotting of rat kidney. Kidneys from vasopressin-escape rats or control rats were perfusion fixed for immunocytochemistry following previously described procedures (17). Observations were made and recorded with a Zeiss LSM780 confocal microscope. The right kidney from 2-day escape microdissection experiments was dissected into cortex, outer, and inner medulla, and prepared for Western blotting as previously described (13). Sources of primary antibodies for blotting and immunocytochemistry are found in Table 1 (18-20).

Quantitative RT-PCR. Total RNA was isolated from the samples using TRIzol extraction reagent according to the manufacturer's instructions. RNA was then precipitated in ethanol, washed, and dissolved in nuclease-free water. Subsequently, RNA was reverse-transcribed into cDNA using Moloney murine leukemia virus reverse transcriptase (Invitrogen, Bleiswijk, the Netherlands). RT-qPCR assays were performed using SYBR Green kit (Bio-Rad, Veenendaal, the Netherlands). Primers were designed using the Primer-BLAST tool (http://www.ncbi.nlm.nih.gov/tools/primer-blast/). 36B4, which

Table 1. Antibodies Used for Immunocytochemistry and Western Blotting in Native Tissue

Antibody	Species	Approach	Dilution	Source	Reference
AQP2	Rabbit	WB	1:1000	Knepper	41
AQP2	Chicken	IC	1:300	Knepper	42
AQP3	Rabbit	IC	1:100	Knepper	43
VDAC	Mouse	IC	1:500	Abcam ab14374	
H-ATPase B/B2 subunit	Mouse	IC	1:50	Santa Cruz sc55544	
PCNA	Rabbit	IC	1:100	Abcam ab18197	
WB- western blotting, IC- immunohistochemistry					

encodes an acidic ribosomal phosphoprotein Po (RPLPo), was used as the reference (housekeeping) gene. Gene expression data were calculated using the Livak method ($2^{-\Delta\Delta Ct}$) and they represent the mean fold difference from the control group.

Cell culture. Mouse mpkCCD cells were cultured as described (21).

Statistics. The statistical methods used for each data type in this study are summarized in Table 2.

Results

Using a standard animal model of SIADH (3, 6, 8, 22-24) (Figure 1A), we confirmed the marked decrease in AQP2 protein abundance in vasopressin-escape kidneys (dDAVP infusion plus water loading) relative to controls that received dDAVP and low water intake (Figure 1B and C). In a parallel set of vasopressin-escape rats, the plasma sodium decreased progressively from 137.2+0.4 on Day 1 to 124.3+1.5 on Day 2 to 114.2+1.5 mM on Day 4 (all measured in the same animals, n=5).

RNA-Seq of microdissected CCDs: General features. We focused solely on the CCD to investigate transcriptomic changes occurring in vasopressin-escape rats as a function of time following the increase in water intake (vasopressin infusion plus increase in water intake) versus control (vasopressin infusion with no increase in water intake), employing single-tubule RNA-Seq (7). Among all RNA-Seq libraries, 81.3 to 85.3% of RNA-Seq reads were uniquely mapped to the reference genome (*Rnor6.0*), which compares favorably to previous single-tubule RNA-Seq data (7) (Supplementary

Table 2. Statistical Methods

Data Type	Measure	Metrics	Purpose	Criterion
RNA-Seq	Fragments per kilobase exons for million mapped reads (FPKM)	Padj; z value	Descriptive; Strength of evidence	none
Semi-Quantitative Immunoblotting of Kidney Tissue (Figure 1)	Normalized band density	P (unpaired t-test)	Testing null hypothesis	$P<0.05$
Semi-Quantitative Immunoblotting of Cultured Cells (Figures 7 and 12)	Normalized band density	P (ANOVA; Bonferroni)	Testing null hypothesis	$P<0.05/n$
Enrichment of Genes from Cutated Lists in Vasopressin-escape Gene Lists	Number of transcripts	P (Chi-square)	Testing null hypothesis	$P<0.05$
Enrichment of Gene Ontology Terms in Vasopressin-escape Gene Lists	Number of transcripts	P (Fisher Exact; DAVID)	Testing null hypothesis	$P<0.05$
Cell Counts in Immunocytochemically Labeled, Microdissected Tubules	Number of cells	P (unpaired t-test)	Testing null hypothesis	$P<0.05$
Cell Counts of PCNA positive cells	Number of cells	P (Chi-square)	Testing null hypothesis	$P<0.05$
Cell Counts of high density DAPI-labeled nuclei	Number of cells	P (Fisher Exact)	Testing null hypothesis	$P<0.05$

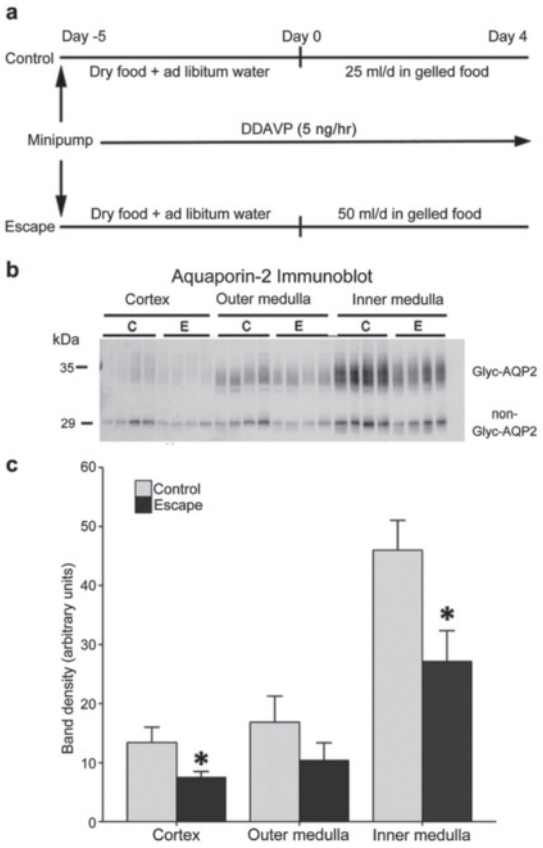

Figure 1. Experimental model. *A.* The study design was adapted from Ecelbarger et al.(3). Rats were euthanized on day 1, 2, and 4. *B.* Immunoblotting for AQP2 in the cortex, outer medulla, and inner medulla (n=4 per group) at day 2 of escape protocol. *C.* Densitometry shows a significant decrease in aquaporin-2 protein abundance in the cortex and inner medulla of the escape animals, consistent with previous reports. For each lane, 10 µg (cortex), 5 µg (outer medulla), and 2 µg (inner medulla) of total protein was loaded. *$p < 0.05$ by unpaired *t*-test. (Coomassie-stained gels, run in parallel, showed equal loading.) Glyc-AQP2, glycosylated aquaporin-2; non-Glyc-AQP2, nonglycosylated aquaporin-2.

Dataset 1 [Supplementary datasets at https://hpcwebapps.cit.nih.gov/ESBL/Database/VasopressinEscapeData]). Overall, 12,951 to 14,357 transcripts were detected in the single-tubule RNA-Seq libraries (fragments per kilobase exons for million mapped reads [FPKM] > 0, Supplementary Dataset 1). All values are reported in Supplemental Dataset 2 and a summary is presented on a permanent web page (https://hpcwebapps.

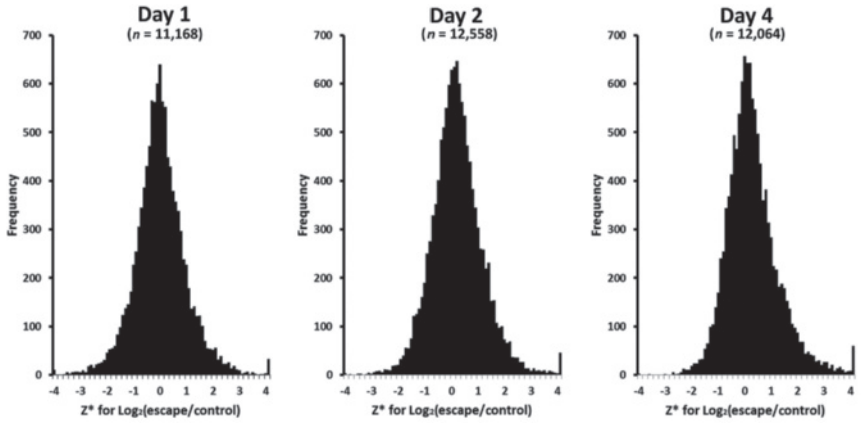

Figure 2. Distribution of Z* values for Log2(Escape/Control) across all genes. Z* is estimated as mean value for all replicates divided by the standard deviation across means for all genes.

cit.nih.gov/ESBL/Database/VasopressinEscape/). The vast majority of transcripts (Figure 2) showed little or no change (Z* near zero).

We focused first on RNA-Seq results for the water channels, AQP2 and AQP3 (Figure 3). Mapped reads (Figure 3A) coincide with the exons of the *Aqp2* and *Aqp3* genes. The reads mapped to the *Aqp2* and *Aqp3* genes were decreased in vasopressin-escape relative to the control (Figure 3A-B). The changes at Day 2 were confirmed by quantitative real-time PCR (AQP2: mean escape-to-control ratio 0.55, $p = 0.024$ by unpaired *t*-test; AQP3: mean escape-to-control ratio 0.24, $p = 0.0000052$; Supplementary Dataset 3). The decreases in AQP2 and AQP3 transcript abundances began on Day 1 and were most striking at Day 4 (Figure 3C). Among all transporters and receptors, AQP2 and AQP3 were the only ones with demonstrable changes (Table 3). Thus, the vasopressin-escape process selectively targets the two water channels.

Canonical signaling pathways. To interpret the RNA-Seq data at a systems level, we began by mapping up- and down-regulated transcripts to a set of known signaling pathways annotated in the KEGG Database. Table 4 summarizes the receptors, ligands and transcription factors (TFs) associated with each KEGG Pathway. The hypothesis is that transcripts coding for elements of one or more of these pathways will be perturbed during the development of the vasopressin-escape phenomenon.

Table 3. Transcript abundance changes in transporters and receptors expressed in principal cells of the rat renal CCD during the onset of vasopressin-escape. Values with P<0.05 in bold (Wald test).

		Log2(Escape/Control)		
Gene Symbol	Annotation	Day 1	Day 2	Day 4
Aqp2	Aquaporin-2	**-0.70**	**-0.89**	**-1.11**
Aqp3	Aquaporin-3	**-1.31**	**-1.62**	**-1.59**
Aqp4	Aquaporin-4	-0.75	0.21	0.26
Atp1a1	Na/K-ATPase subunit alpha-1	0.02	0.43	0.08
Atp1b1	Na/K-ATPase subunit beta-1	-0.41	-0.14	-0.09
Avpr2	Vasopressin receptor V2	0.22	-0.39	-0.23
Clcnka	Chloride channel ClC-Ka	-0.22	-0.69	-0.03
Clcnkb	Chloride channel ClC-Kb	0.14	0.20	0.20
Fxyd2	Na/K-ATPase subunit gamma subunit	-0.26	0.57	0.46
Kcnj1	Inward rectifier potassium channel 1 (ROMK)	0.05	0.00	0.05
Nr3c2	Mineralocorticoid receptor	0.46	-0.51	-0.03
Scnn1a	Epithelial Na channel alpha subunit	-0.09	0.17	-0.06
Scnn1b	Epithelial Na channel beta subunit	-0.07	-0.12	0.00
Scnn1g	Epithelial Na channel gamma subunit	-0.15	-0.47	0.24

Mapping RNA-Seq data to canonical signaling pathways. Figure 4 shows a summary of the RNA-Seq results with values presented as the mean Log_2(Escape/Control) for the relevant TFs for the canonical signaling pathways on Days 1, 2 and 4. Most were either unchanged or not detectable throughout the time course (yellow boxes). However, a few key TFs in some of the signaling categories were seen to change, viz. TGFβ signaling/EMT (Snail3 and Smad3 increased on Day 1; Smad2 and Tgif1 increased on Day 4), MAPK signaling (Elk1 increased on Days 2 and 4; Nr4a2 decreased on Day 1), signaling associated with transition from G0 (quiescence) into the cell cycle (E2f1 and Foxm1 increased on Days 2 and 4; E2f2 increased on Day 2; E2f4 increased on Day 1), cyclic AMP signaling (Jun decreased on Day 2; Sox17 decreased on Day1; Nfatc3, increased on Day 4), and Notch signaling (Hes1 decreased on Days 2 and 4). Thus, we hypothesize that one or more of these pathways could be responsible for vasopressin-escape. We consider them in turn.

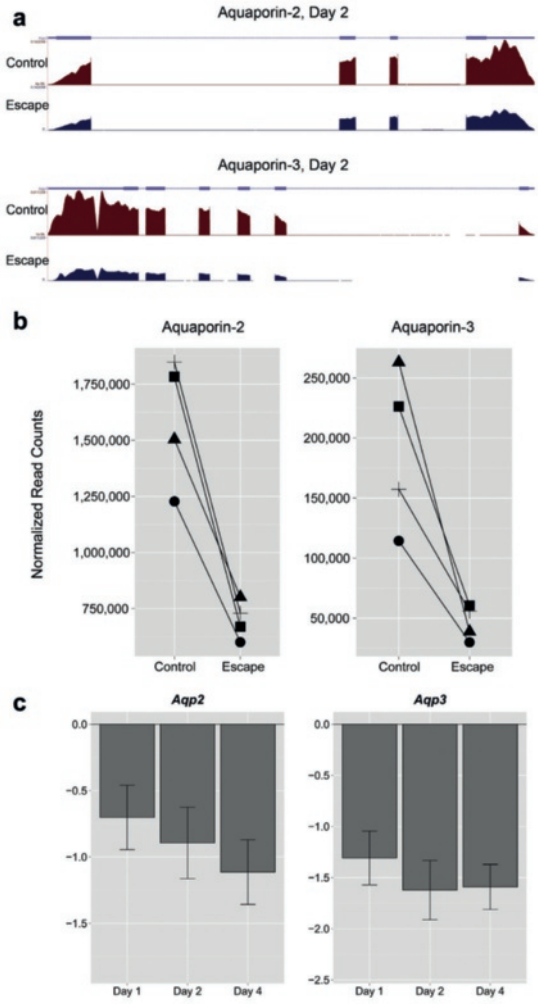

Figure 3. Abundances of aquaporin-2 (AQP2) and aquaporin-3 (AQP3) transcripts in the CCD are decreased in vasopressin-escape animals. *A.* RNA-Seq reads are mapped to the RefSeq transcript models of for rat *Aqp2* gene (top) and *Aqp3* gene (bottom). For each RefSeq transcript, exons are shown as red rectangles and introns as blue lines connecting the exons. Barbs indicate direction of transcription. The coverage was calculated as the number of reads per million nucleotides in the whole genome. *B.* Normalized RNA-Seq read counts for Aqp2 and Aqp3 in the CCD segments obtained from four pairs (control versus escape animals) at day 2. *C.* Change in AQP2 and AQP3 transcript abundances in the microdissected CCDs on different days relative to time controls (*Padj ‹ 0.05 for escape vs control at each time point, paired t-test).

Table 4. Canonical Signaling Pathways Hypothetically Involved in Vasopressin-escape

Signaling Pathway	Ligands	Receptors	TFs	Relevant KEGG Pathway*
Notch signaling	Delta, Jagged	Notch family	HES Family	Notch Signaling
Wnt signaling	Wnt family, Porcn	Frizzled receptors	TCF/LEF, MYC	Wnt Signaling
Growth signaling	Insulin/Insulin-like growth factors	Insulin receptor, Insulin-like growth factor receptor	Several Forkhead Box TFs	Insulin Signaling
Cyclic AMP signaling	Vasopressin/ PGE2	Avpr2, Avpr1a, Ptger4	AP1, CREB Family, GLI, SOX, PPARA, NFAT	cAMP Signaling
Cyclic GMP signaling	Nitric Oxide	Soluble guanylate cyclase	CREB Family	cGMP-PKG Signalng
Shift from Go to cell cycle (dedifferentiation) with arrest	EGF, FGF family, PDGF family	Growth factor receptors	E2F1, FOXM1	Cell Cycle
Epithelial to mesenchymal transition/ TGFβ signaling	TGFβ / Activin / Nodal/ BMP	TGFβ receptor / Activin receptor /BMP Receptor	SNAIL family, TWIST, SMAD family, ZEB, AP1, ATF2, TGIF, PITX	TGF-Beta Signaling
MAP kinase signaling	EGF, FGF family, PDGF family	Growth factor receptors	ELK1, AP1, p53, NR4A1	MAPK Signaling
Hedgehog signaling	Ihh, Dhh, Shh	Patched family, Smoothened	GLI family	Hedgehog Signaling
Hippo signaling	E-cadherin	E-cadherin	TEAD family	Hippo Signaling

* Pathways may be viewed at www.genome.jp or by searching “KEGG [pathway name]”.

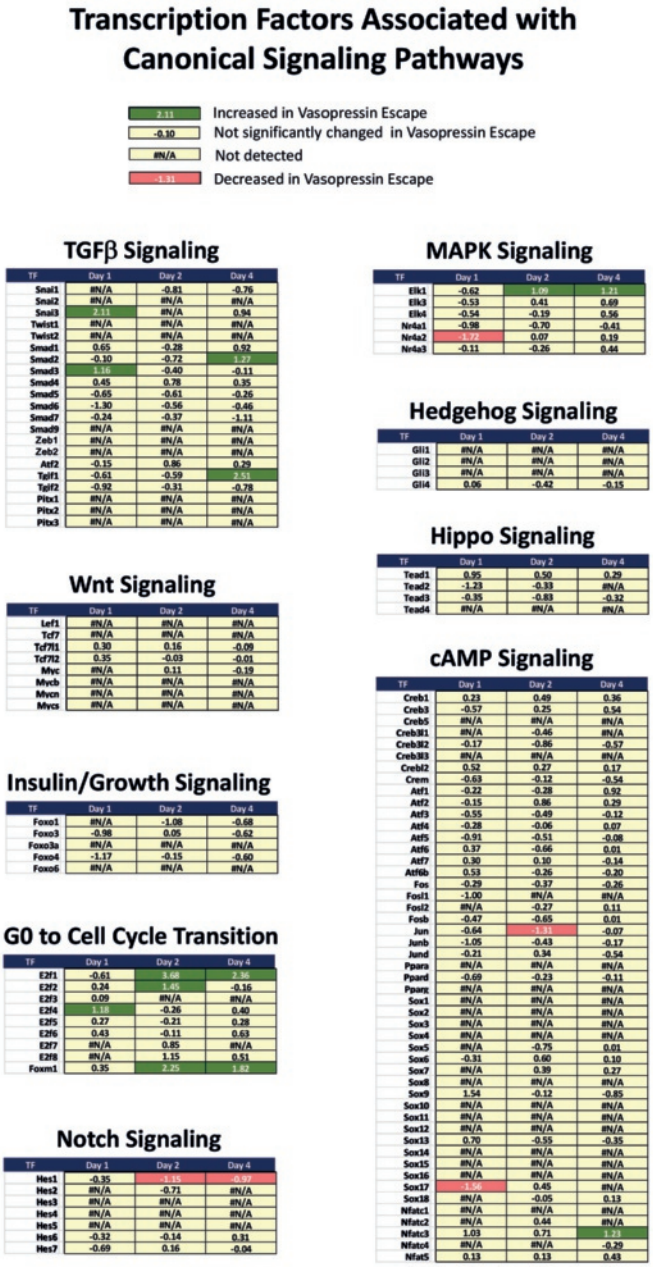

Figure 4. Changes in transcript abundances for TF genes associated with annotated KEGG pathways during the onset of vasopressin-escape.

TGFβ signaling and epithelial-to-mesenchymal transition. TGFβ signaling plays a central role in the induction of epithelial-to-mesenchymal transition (EMT) (25), so we considered the two together. The increases in transcript abundances of Smad3 (a TGFβ-signaling mediator) and Snail3 (an EMT-mediator) occur at the earliest time point studied, pointing to the possibility that a change in TGFβ signaling or induction of an EMT could be an early event in vasopressin-escape. Looking at other mediators of TGFβ signaling (Figure 5 and Table 5), there were coordinate increases in Smad3 and downstream TFs E2f4 and Snai3 on Day 1, as well as Smad2 and downstream TF Tgif1 on Day 4. Thus, the weight of the evidence is in favor of downstream activation of TGFβ-BMP-activin-dependent signaling.

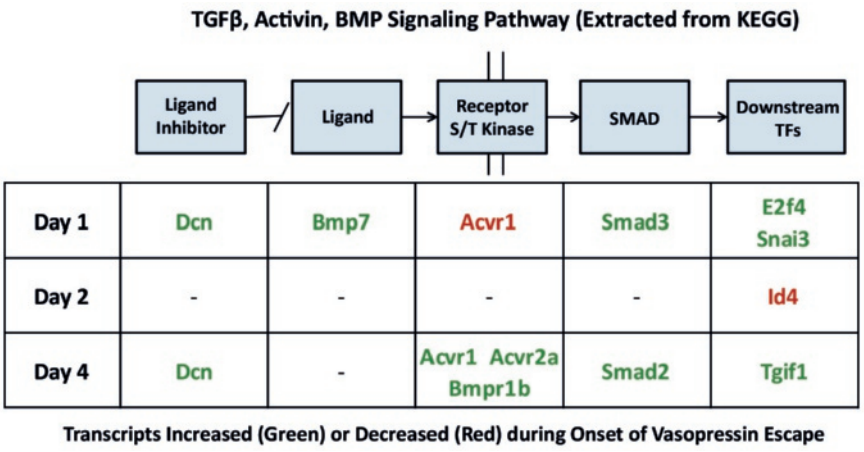

Figure 5. Official gene symbols of transcripts associated with TGFβ-activin-BMP signaling undergoing changes during onset of vasopressin-escape. Increased, green; decreased, red. See Table 4 for annotations of these genes. Specific values are available in Supplemental Dataset 2.

A recent study has presented a meta-analysis listing 130 consensus "EMT-genes" that are consistently altered in EMT (26). We use this list to ask, "Are the consensus EMT-genes statistically over-represented among genes whose transcript abundances are altered on Day 1 of vasopressin-escape versus genes whose transcripts are not altered?" The answer is that transcripts corresponding to consensus EMT genes are indeed over-represented (Table 6). Looking at the time courses of change of some of these EMT-marker genes (Figure 6A), transcripts associated with mesenchymal cells (collagen type I α-1, collagen type VI α-1, matrix metallopeptidase 2 and vimentin) show a similar trend with no change or a decrease on Day 1 of vasopressin-escape

Table 5. List of TGFβ signaling genes whose transcript abundances were seen to change significantly during onset of vasopressin-escape. See Figure 5 for day and direction of changes.

Gene Symbol	Protein Name	Function
Acvr1	activin receptor type-1 (serine/threonine-protein kinase receptor R1)	On ligand binding, forms a receptor complex consisting of two type II and two type I transmembrane serine/threonine kinases. Type II receptors phosphorylate and activate type I receptors which autophosphorylate, then bind and activate SMAD transcriptional regulators.
Acvr2a	activin receptor type-2A	On ligand binding, forms a receptor complex consisting of two type II and two type I transmembrane serine/threonine kinases. Type II receptors phosphorylate and activate type I receptors which autophosphorylate, then bind and activate SMAD transcriptional regulators. Receptor for activin A, activin B and inhibin A.
Bmp7	bone morphogenetic protein 7 precursor	Belongs to the TGF-beta family. Secreted ligand. Involved in renal development.
Bmpr1b	bone morphogenetic protein receptor type-1B (serine/threonine-protein kinase receptor R6)	On ligand binding, forms a receptor complex consisting of two type II and two type I transmembrane serine/threonine kinases. Type II receptors phosphorylate and activate type I receptors which autophosphorylate, then bind and activate SMAD transcriptional regulators. Receptor for BMP7.
Dcn	decorin	Binds to type I and type II collagen, fibronectin and TGF-beta. Belongs to the small leucine-rich proteoglycan (SLRP) family. Secreted.
E2f4	TF E2F4	Transcription activator that binds DNA cooperatively with DP proteins through the E2 recognition site. Found in the promoter region of a number of genes whose products are involved in cell cycle regulation or in DNA replication. E2F4 binds with high affinity to RBL1 and RBL2.
Id4	DNA-binding protein inhibitor ID-4	Transcriptional regulator (lacking a basic DNA binding domain) which negatively regulates the basic helix-loop-helix (bHLH) TFs by forming heterodimers and inhibiting their DNA binding and transcriptional activity.
Ppp2r1b	serine/threonine-protein phosphatase 2A 65 kDa regulatory subunit A beta isoform	Scaffolding molecule to coordinate the assembly of the catalytic subunit and a variable regulatory B subunit. PP2A consists of a common heterodimeric core enzyme, composed of a 36 kDa catalytic subunit (subunit C) and a 65 kDa constant regulatory subunit (PR65 or subunit A), that associates with a variety of regulatory subunits.

Table 5. Continued

Gene Symbol	Protein Name	Function
Smad2	mothers against decapentaplegic homolog 2	Intracellular signal transducer and transcriptional modulator activated by TGF-beta (transforming growth factor) and activin type 1 receptor kinases. Binds the TRE element in the promoter region of many genes that are regulated by TGF-beta and, on formation of the SMAD3/SMAD4 complex, activates transcription. Also, can form aSMAD3/SMAD4/JUN/FOS complex at the AP-1/SMAD site to regulate TGF-beta-mediated transcription. Dephosphorylated by phosphatase PPM1A, resulting in nuclear export.
Smad3	mothers against decapentaplegic homolog 3	Intracellular signal transducer and transcriptional modulator activated by TGF-beta (transforming growth factor) and activin type 1 receptor kinases. Binds the TRE element in the promoter region of many genes that are regulated by TGF-beta and, on formation of the SMAD3/SMAD4 complex, activates transcription. Also, can form aSMAD3/SMAD4/JUN/FOS complex at the AP-1/SMAD site to regulate TGF-beta-mediated transcription. Dephosphorylated by phosphatase PPM1A, resulting in nuclear export.
Snai3	zinc finger protein SNAI3	Transcriptional repressor of E-box-dependent transactivation of downstream basic-Helix-Loop-Helix genes.
Tgif1	homeobox protein TGIF1	Binds to RXR element and inhibits the 9-cis-retinoic acid-dependent RXR alpha transcriptional activation. Interacts with CTBP, SMAD2, SMAD3 and HDAC1.

followed by large increases on Days 2 and 4. In contrast, transcripts associated with differentiated epithelial cells (occludin and E-cadherin) show no substantial change. Thus, during the induction of vasopressin-escape, collecting duct cells show some characteristics of EMT, but do not manifest full-blown conversion to mesenchymal cells, a state that has been described by Kalluri and Weinberg as a 'partial EMT' (27).

AQP3 labeling remained on the basal and lateral aspects of the cell, while AQP2 labeling continued to be apically oriented (Figure 6B), although labeling for both was less intense. Thus, it appears that epithelial polarity is not lost in early stages of vasopressin-escape and that the reduction in water channel expression does not require loss of polarity.

Table 6. Epithelial-to-mesenchymal transition (EMT) signature genes are more frequently represented among transcripts regulated in vasopressin-escape than among non-regulated transcripts (Chi-square analysis).

	Number of Regulated Transcripts*	Number of EMT Genes among Regulated T ranscripts	Number of EMT Genes among Randomly Selected Transcripts^	Chi-square	P (Chi-square) ‡	Bayes Factor†
Day 1	412	11	2	6.135	0.013	0.047
Day 2	370	9	2	4.39	0.036	0.111
Day 4	670	9	3	2.97	0.085	0.227

* For this analysis, 'Regulated transcripts' are those with **Padj** ‹0.10 and |z*|›2.
^ Median value from 5 randomly selected sets of transcripts with the same count as the set of regulated transcripts.
‡ P(Chi-square) is presented as a measure of statistical significance.
† Bayes Factor is presented as a measure of 'weight of evidence' and is the likelihood of the null hypothesis divided by the likelihood of the hypothesis that EMT genes are more frequent among the regulated transcripts.

If activation of TGFβ signaling is critical for loss of *Aqp2* gene expression in vasopressin-escape, then it might be expected that triggering of TGFβ-signaling in another manner, namely by exposure of CCD cells directly to TGFβ, would reduce the abundance of AQP2 protein. Indeed, in AQP2-expressing mouse mpkCCD collecting duct cells (28), addition of TGFβ to vasopressin-treated cells for 48 hrs produced a profound decrease in AQP2 protein and mRNA abundance (Figure 7). The transepithelial resistance of these cells did not fall, but rather increased, indicating that the junctional barrier remained intact (Supplemental Figure 1).

Notch signaling and collecting duct remodeling. Notch signaling is an important factor in collecting duct remodeling, a process in which the relative abundances of the three major cell types in the CCD (principal cells [PCs], α-intercalated cells [α-ICs], and β-intercalated cells [β-ICs]) can undergo adaptive changes (29). The demonstrated decreases (Days 2 and 4) in the transcript abundance of the TF, Hes1, a mediator of Notch signaling, raise the possibility that Notch-related collecting duct remodeling is involved in vasopressin-escape (Figure 4). Accordingly, we used immunocytochemistry in microdissected CCDs to count the cell types using standard markers (pendrin ([β-IC marker] and Atp6v1b1 [total IC marker]; DAPI [total cell marker]) (Figure 8 and Supplemental Figure 2). (In this analysis, principal cell counts are estimated as the

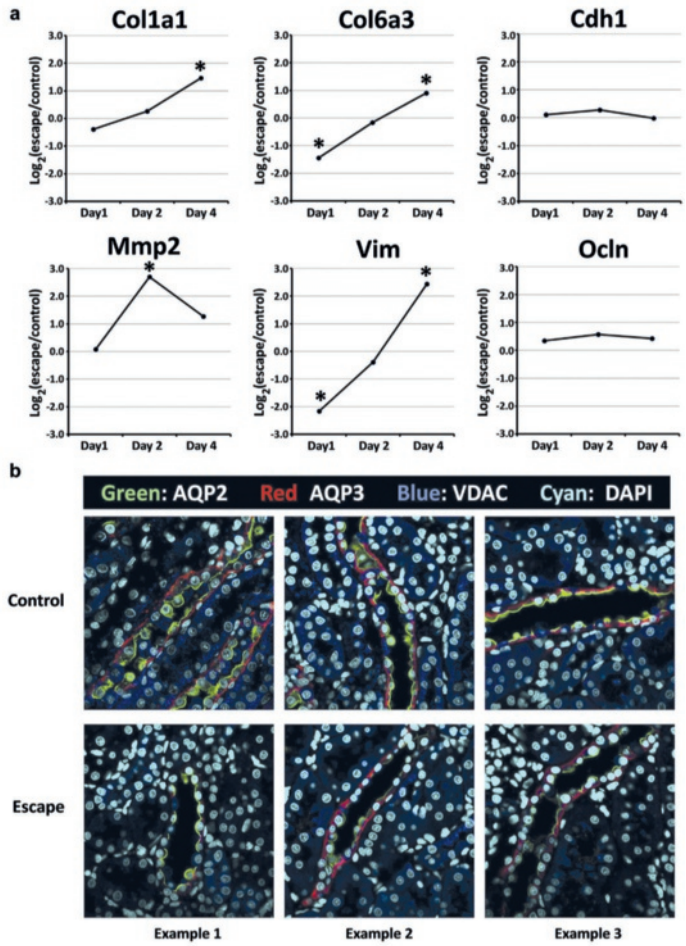

Figure 6. Onset of vasopressin-escape is associated with a partial epithelial-to-mesenchymal transition in rat CCD cells. **A.** Time course of transcript abundance changes for selected EMT marker genes during onset of vasopressin-escape in microdissected rat CCDs shows increase in mesenchyme-associated transcripts (Col1a1, Col6a3, Mmp2 and Vim) without loss of epithelium-associated transcripts (Cdh1 and Ocln). Asterisk indicates Benjamini-Hochberg FDR-adjusted P value ‹0.05. **B.** Immunocytochemical labeling for AQP2 and AQP3 in renal cortex of rats undergoing vasopressin-escape shows retention of normal epithelial polarity. VDAC labeling of mitochondria was also carried out to reveal presence of intercalated ('mitochondria-rich') cells. DAPI labeling of nuclei facilitates recognition of apical versus basal aspects of cells.

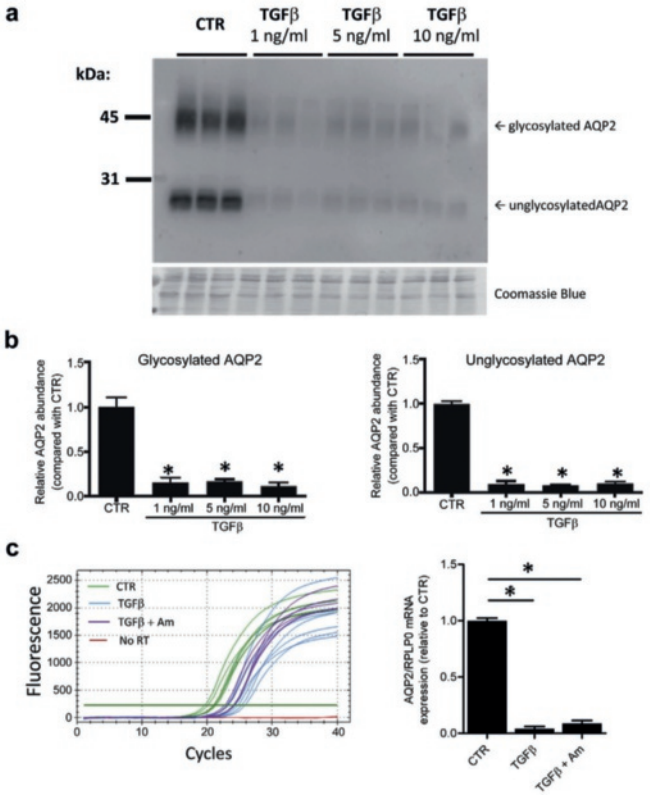

Figure 7. TGFβ exposure decreases AQP2 protein and mRNA abundance in mpkCCD cells. **A.** Representative immunoblot showing relative AQP2 abundances in control (CTR) cells and cells exposed to TGFβ (1, 5 or 10 ng/ml) for 2 days in serum-free medium. The cells were pretreated with 1 nM dDAVP on the basolateral side for 4 days to induce AQP2 expression. Bottom panel shows a Coomassie-stained gel to demonstrate equal loading. **B.** AQP2 band density was significantly decreased both for glycosylated and nonglycosylated AQP2 (n=3). **C.** SYBR Green™ fluorescence curves for RT-qPCR experiments quantifying AQP2 mRNA under the control (CTR) condition, after 1 ng/ml TGFβ (2 days) and after 1 ng/ml TGFβ plus amiloride at 10 μM (2 days). Cells were pre-treated with dDAVP at 1 nM for 4 days. Horizontal green line is the threshold used to calculate C_t. The relative AQP2 abundances (normalized to the housekeeping gene RPLP0) are shown as a bar graph.

total cell count minus the intercalated cell count.) Table 7 shows that there were no significant differences in any cell type. We conclude that the decreases in AQP2 and AQP3 abundances were not likely to be due to a loss of PCs. Thus, there was little or no remodeling of the CCD in the vasopressin-escape rats.

Table 7. Comparisons of cell populations in microdissected CCDs from rats undergoing vasopressin-escape compared with control rats.

	# Nuclei per mm length	% Pendrin-positive ICs	% Pendrin-negative ICs	% Total ICs	Ratio PCs:ICs	Ratio α-ICs: β-ICs
Control 1	547	21	15	37	1.69	0.75
Control 2	575	27	16	44	1.30	0.57
Control 3	479	22	19	41	1.45	0.84
Control 4	453	17	29	46	1.16	1.80
Mean ± SE	**514 ± 29**	**22 ± 2**	**20 ± 3**	**42 ± 2**	**1.40 ± 0.11**	**0.99 ± 0.27**
Escape 1	449	20	21	41	1.40	1.16
Escape 2	583	19	16	36	1.99	0.86
Escape 3	555	21	16	39	1.55	0.77
Escape 4	451	14	22	42	1.45	2.06
Mean ± SE	**509 ± 35**	**19 ± 1**	**19 ± 2**	**40 ± 1**	**1.60 ± 0.13**	**1.21 ± 0.29**
p-Value	**0.93**	**0.26**	**0.82**	**0.33**	**0.30**	**0.60**

A total of 35 microdissected CCDs were analyzed, 13 from Control rats and 22 from Escape rats. There were no statistically differences between two groups of animals (unpaired Student's t-test, n=4). Percent of principal cells (PCs) may be estimated as 100 minus the percent of total ICs. IC, intercalated cell.

Signaling associated with transition from Go to cell cycle. The increases in transcript abundances of E2f1 and Foxm1 (Figure 4) on Day 2 and Day 4 of vasopressin-escape point to a possible role for the signaling process that shifts cells from the quiescent state (G0) into the cell cycle. The E2f family of winged-helix TFs are classical regulators of this transition (30) and Foxm1 also plays key roles in transcriptional regulation of cell-cycle genes (31). Thus, we hypothesized that vasopressin-escape is associated with a shift from Go to cell cycle progression in CCD cells. To test this, we identified *Gene Ontology Biological Process* terms enriched among transcripts altered in abundance on Day 2 of vasopressin-escape relative to unregulated genes (Table 8). The four *Biological Process* terms with the lowest false discovery rates were all associated with the cell cycle and cell division. The 49 regulated transcripts with the term 'cell cycle' are listed in Table 9. Remarkably, 46 of the 49 cell-cycle genes showed increases in transcript abundance (Log_2[Escape/Control] › 0). The striking changes are further illustrated in Figure 9 and Supplemental Figure 3. Thus, the analysis showed a dramatic increase in most mRNA species coding for cell cycle proteins at Day 2 of vasopressin-escape. A similar analysis for Day 1 revealed a lack of a significant over-rep-

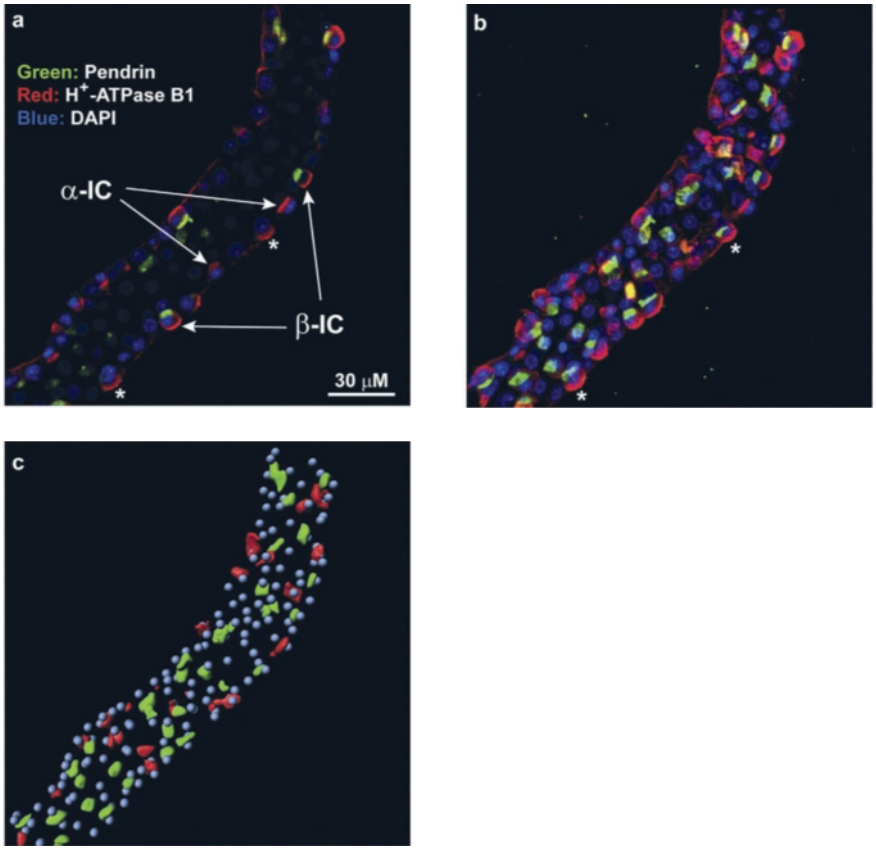

Figure 8. Cell counting in immunofluorescently labeled CCDs microdissected from rats. After micro- dissection, tubules were fixed with paraformaldehyde followed by immunofluorescence staining for intercalated cells (using pendrin and H^+-ATPase antibodies) and nuclei (DAPI). **A.** Standard confocal fluorescence image of a microdissected CCD from a control vasopressin-treated rat. Pendrin, green; B1 H^+-ATPase, red; DAPI labeling of nuclei, blue. Examples of identified α-intercalated cells (α-IC) and β-intercalated cells (β -IC) are pointed out. Asterisks indicate cells that appear to lack pendrin labeling in confocal image but are revealed to be β-intercalated cells in the 3D reconstruction. **B.** Maximum intensity projection of 3-D reconstructed tubule image generated by IMARIS image analysis software. Colors are the same as in Panel A. Asterisks mark the same cells indicated in Panel A. **C.** IMARIS-generated analytical image. The pendrin-positive IC cells and non-pendrin IC cells were labeled in green and red, respectively, based on IMARIS surface and spot analysis tools. Nuclei are shown in cyan. For details, see Supplemental Figure 2.

resentation of the transcripts with the *Gene Ontology Biological Process* term 'cell cycle'. However, on Day 4 (like Day 2), there was a marked over-representation of 'cell cycle' (Supplemental Datasets 4-6). Thus, the widespread induction of cell-cycle gene expression is not seen until Day 2, i.e. after the initial fall in AQP2 transcript abundance. The pattern of response is illustrated by Figure 10, which shows the time course for three key protein kinases involved in cell-cycle regulation (Cyclin-dependent kinase 1 [Cdk1], Polo-like kinase 1 [Plk1], and Aurora B kinase [Aurkb]) and for three transcriptional regulators involved in cell-cycle control (E2f1, Timeless, and Foxm1). These transcripts showed similar time courses of change with no change or a decrease on Day 1 and increases on Days 2 and 4, contrasting with transcripts not involved in cell-cycle regulation (Protein kinase A Catalytic α [Prkaca] and Homeobox B7 [Hoxb7]) shown in red).

Table 8. Statistically over-represented *Gene Ontology Biological Process* terms among transcripts with altered abundance on Day 2 of vasopressin-escape.^

GO Biological Process Term*	Number of Genes	Fold Enrichment†	False Discovery Rate (%)	P (Fisher Exact)
cell cycle process	44	6.6	4.10E-20	4.60E-24
cell cycle	49	5.7	5.40E-20	7.10E-24
cell division	22	8	4.30E-10	3.80E-14
chromosome segregation	15	15.1	6.40E-10	2.60E-14
organelle organization	47	2.6	2.40E-06	7.50E-10
microtubule-based process	19	5.2	2.90E-05	4.30E-09
nitrogen compound metabolic process	62	1.6	1.40E-01	7.00E-05
negative regulation of biological process	50	1.7	3.00E-01	1.50E-04
DNA packaging	9	5.2	4.10E-01	6.00E-05
cellular response to stimulus	27	2.1	5.30E-01	2.00E-04
positive regulation of biological process	55	1.6	6.30E-01	3.30E-04

^ "Altered transcripts" were those with Benjamini-Hochberg FDR-adjusted P value < 0.1.
* Analysis used DAVID Functional Annotation tools (see (Methods) to identify all terms with False Discovery Rate (FDR) < 1%.
† "Fold Enrichment" is the fraction of genes with the given GO term in the "regulated" list divided by the fraction of genes in full list ("regulated" + "unregulated") with that term.

We asked whether the frequency of cells in S phase is increased in vasopressin-escape using immunocytochemical labeling of renal cortical sections with anti-proliferating cell nuclear antigen (PCNA) antibodies (Figure 11A). PCNA-positive cell nuclei were scarce in CCDs in under both conditions. Only 1 PCNA-positive cell nucleus was

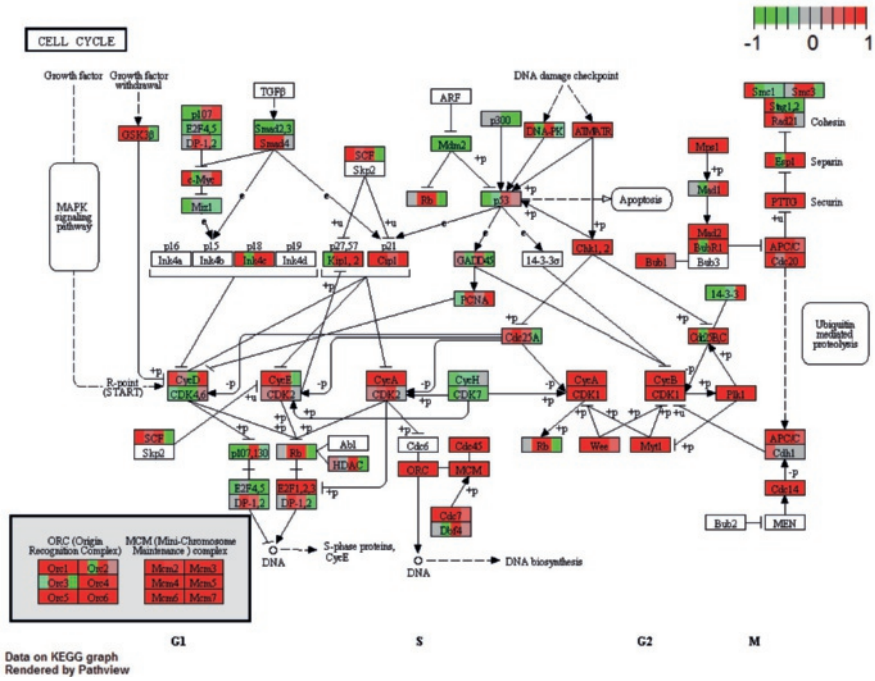

Figure 9. Transcripts corresponding to most genes present in the KEGG Cell Cycle Pathway were increased in abundance in CCDs from rats on Day 2 of development of vasopressin-escape. Values for all four Day-2 replicates are shown as individual blocks colored to show magnitude of change (red, increased; green, decreased) as generated by *Bioconductor Pathview* software (https://www.bioconductor.org/packages/devel/bioc/html/pathview.html) run on R. The specific values are available in Supplementary Dataset 1.

identified in 45 CCD profiles in dDAVP-only control animals, and only 4 PCNA-positive nuclei were detected in 89 CCD profiles observed in escape animals (p=0.67, Fisher Exact Test). To identify G2 phase and early M phase, we quantified the intensity of DAPI labeling in CCDs (Figure 11B). The median per-nucleus DAPI fluorescence is similar in the two groups (Table 10). Nuclei with total DAPI fluorescence greater than the indicated threshold (1.8 times median) were scarce in both escape (1.67% of total) and control (0.48% of total) CCDs. However, these proportions were statistically significantly different (P=0.005, Fisher Exact Test). This finding is compatible with a modest increase in the frequency of cells in G2/M. However, the previous observation that the total number of each cell type per total tubule length in microdissected CCDs does not change (Table 7) argues against a major increase in cell proliferation, and the

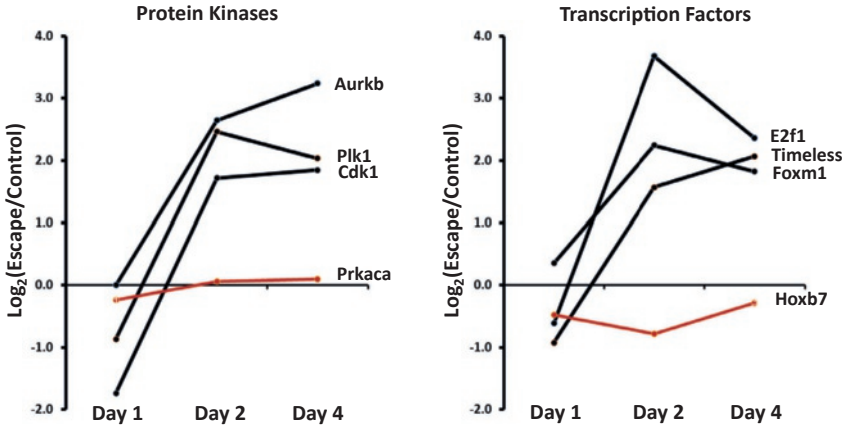

Figure 10. Time courses of abundance change for mRNAs coding for protein kinases (left) and TFs (right) involved in regulation of cell-cycle. All six cell-cycle related transcripts (black) showed significant increases only on Days 2 and 4. Only Foxm1 was significantly changed on Day 1, a decrease. Abundant non-cell-cycle transcripts (Prkaca and Hoxb7), shown in red, are included as controls. Cdk1, Cyclin-dependent kinase 1; Plk1, Polo-like kinase 1; Aurkb, Aurora B kinase, Prkaca, Protein kinase A catalytic α; E2f1, E2F TF 1; Timeless, timeless circadian clock; Foxm1, Forkhead Box M1 ; Hoxb7, Homeobox B7.

entirety of the data could be viewed as consistent with arrest at G2/M. If a shift from quiescence to the cell cycle is in part responsible for the loss of AQP2 expression in vasopressin-escape, it may be predicted that inducing such a shift in cultured CCD (mpkCCD) cells by serum addition, with or without addition of agents that inhibit cell cycle progression at specific points, would reduce the abundance of AQP2 despite the continued presence of vasopressin. Indeed, in such experiments, AQP2 protein appears to be maximally expressed only in cells grown in the absence of fetal calf serum, i.e. in G0 (Figure 12). However, we cannot rule out the possibility that the decrease in AQP2 could also be caused by addition of factors that inhibit Aqp2 gene transcription independent of changes in the cell cycle.

Table 9. Altered transcripts in CCD on Day 2 of vasopressin-escape with *Gene Ontology Biological Process* term 'Cell Cycle'*

Gene Symbol	Annotation	Log2 (Escape/ Control)	Padj (Benjamini-Hochberg)
Mlf1	myeloid leukemia factor 1	4.17	2.52E-13
Tacc3	transforming, acidic coiled-coil containing protein 3	3.57	2.39E-12
Tubb5	tubulin, beta 5	1.90	3.33E-12
Cenpf	centromere protein F	3.75	4.17E-12
E2f1	E2F TF 1	3.68	2.80E-11
Uhrf1	ubiquitin-like with PHD and ring finger domains 1	3.43	1.80E-08
Ube2c	ubiquitin-conjugating enzyme E2C	2.82	2.58E-08
Aurkb	aurora kinase B	2.64	2.34E-07
Kifc1	kinesin family member C1	2.02	2.54E-07
Pole	polymerase (DNA directed), epsilon	2.79	3.28E-07
Fancd2	Fanconi anemia, complementation group D2	2.96	1.92E-06
Dscc1	defective in sister chromatid cohesion 1	2.16	4.72E-06
Spc25	SPC25, NDC80 kinetochore complex component	2.43	7.80E-06
Cdca8	cell division cycle associated 8	2.61	2.02E-05
Plk1	polo-like kinase 1 (Drosophila)	2.46	4.09E-05
Mcm6	minichromosome maintenance complex component 6	1.83	6.77E-05
Id4	inhibitor of DNA binding 4	-2.15	7.41E-05
Brca1	breast cancer 1	2.52	1.93E-04
Ncaph	non-SMC condensin I complex, subunit H	1.66	3.33E-04
Aurka	aurora kinase A	1.61	1.33E-03
Racgap1	Rac GTPase-activating protein 1	1.87	1.45E-03
Mad2l1	MAD2 (mitotic arrest deficient, homolog)-like 1	1.98	2.44E-03
Stmn1	stathmin 1	1.56	3.30E-03
Cdc25b	cell division cycle 25 homolog B (S. pombe)	1.57	3.61E-03
Birc5	baculoviral IAP repeat-containing 5	1.78	3.82E-03
Cdc5l	CDC5 cell division cycle 5-like (S. pombe)	1.38	4.31E-03
Pttg1	pituitary tumor-transforming 1	2.09	4.89E-03
Cdc20	cell division cycle 20 homolog (S. cerevisiae)	1.64	4.97E-03
Kif2c	kinesin family member 2C	2.07	5.96E-03
Katna1	katanin p60 (ATPase-containing) subunit A1	1.49	7.35E-03
Wee1	wee 1 homolog (S. pombe)	1.29	7.35E-03
Kif18a	kinesin family member 18A	1.98	7.83E-03
Haus4	HAUS augmin-like complex, subunit 4	1.19	7.84E-03

Table 9. Altered transcripts in CCD on Day 2 of vasopressin-escape with *Gene Ontology Biological Process* term 'Cell Cycle'*

Gene Symbol	Annotation	Log2 (Escape/ Control)	Padj (Benjamini-Hochberg)
Pola1	polymerase (DNA directed), alpha 1	1.86	9.08E-03
Cenpa	centromere protein A	1.82	9.69E-03
Nusap1	nucleolar and spindle associated protein 1	1.65	9.69E-03
Trip13	thyroid hormone receptor interactor 13	1.68	9.69E-03
Msh5	mutS homolog 5	1.57	1.17E-02
Ccna2	cyclin A2	1.82	1.49E-02
Cdca3	cell division cycle associated 3	1.57	3.32E-02
Rad51c	Rad51 homolog c	1.55	3.62E-02
Calm2	calmodulin 2	1.21	3.95E-02
Cdkn1b	cyclin-dependent kinase inhibitor 1B	-1.16	4.57E-02
Txnl4b	thioredoxin-like 4B	1.42	4.72E-02
Mdm2	Mdm2 p53 binding protein	-1.16	4.73E-02
Timeless	timeless homolog	1.57	5.35E-02
Dlgap5	discs, large homolog-associated protein 5	1.47	5.36E-02
Nuf2	NDC80 kinetochore complex component	1.54	7.70E-02
Ska2	family with sequence similarity 33, member A	1.49	9.01E-02

* Includes all transcripts for "cell cycle" Gene Ontology term in Table 8.

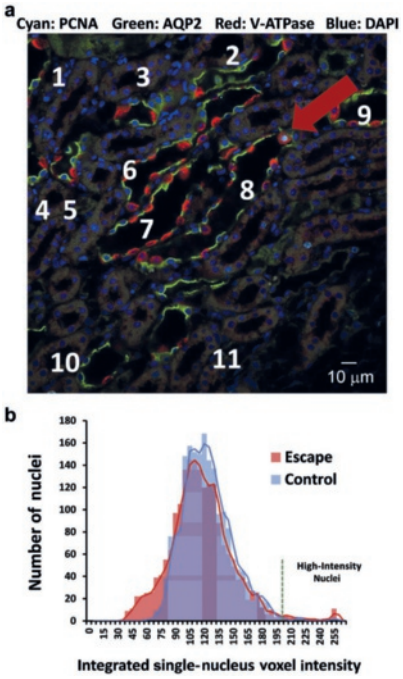

Figure 11. Cell cycle indices in renal CCDs from vasopressin-escape versus control rats. **A.** Nuclei labeled with antibody to PCNA (S-phase marker) are scarce. Image shows section of renal cortex from rat undergoing vasopressin-escape (Day 2). Labeling for AQP2 (green) and the B1 subunit of the vacuolar proton-ATPase (red) identify collecting ducts (numbered). A single collecting duct cell with PCNA labeling (cyan) is seen (red arrow). DAPI, blue. **B.** Distribution of integrated DAPI fluorescence signal in nuclei of microdissected CCDs from rats undergoing vasopressin-escape (Day 4 of escape protocol) versus control rats. See Table 10 for quantitation.

Table 10. DAPI-Fluorescence per Nucleus in 4-Day Escape Versus Control Rats†

	Median Intensity	Standard Deviation	Total Nuclei Counted	Number of High Intensity Nuclei*	Percent High Intensity Nucleus	P (Fisher Exact)‡
Control	116	26	1038	5	0.48	
Escape	111	33	1921	32	1.67	0.005

† Values (arbitrary units) represent summation of fluorescence levels in all voxels mapping to a given nucleus using Imaris software (See Methods).

* Number of nuclei above threshold of 200 arbitrary units (green vertical line in Figure 11B).

‡ Probability of the null hypothesis that the proportion of high intensity nuclei is the same in CCDs from escape and control rats.

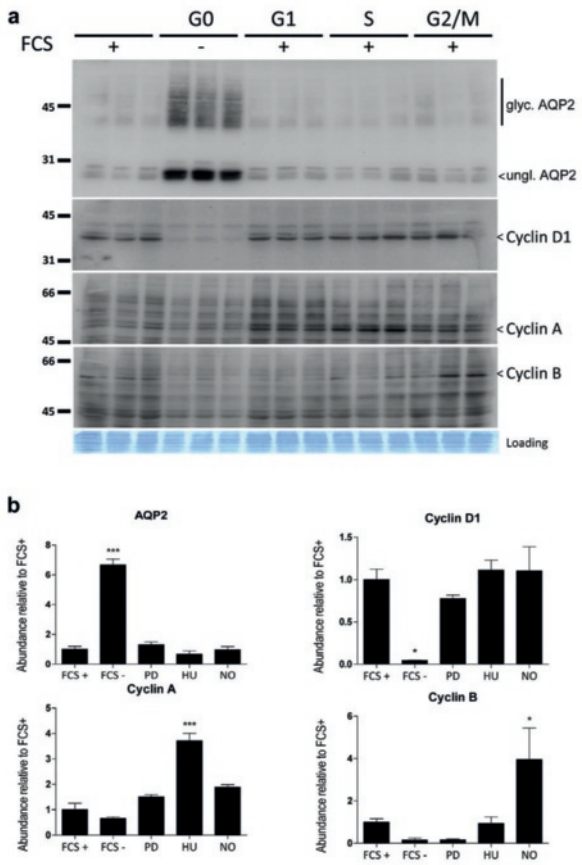

Figure 12. AQP2 protein is strongly expressed in cultured CCD cells in Go, but not when in the cell cycle. dDAVP-treated (1 nM) mpkCCD cells were grown on a semi-permeable filter and synchronized in the different phases of the cell cycle (FCS withdrawal for Go phase, PD0332991 for G1, Hydroxyurea for S and Nocodazole for G2/M phase), then immunoblotted for AQP2 and Cyclins D1, A, and B.

Discussion

Vasopressin-escape is a safety-valve mechanism that limits dilutional hyponatremia in SIADH and possibly other hyponatremic disorders (2). It attenuates water retention through the loss of expression of the *Aqp2* gene, which codes for the aquaporin-2 water channel (3). Here, we have adopted a systems-biology-based approach (32, 33) to address the mechanism of vasopressin-escape. "Systems biology" uses large-scale

data acquisition techniques (here, "single-tubule RNA-Seq") to study a biological process (here, "vasopressin-escape") by investigating all genes or gene products together to understand biological mechanisms, rather than focusing on one or a few selected genes (32). The data are interpreted, not on a gene-by-gene basis, but rather through detection of coordinate changes in curated groups of genes (here, genes whose products are elements of the canonical signaling pathways listed in Table 4). In the present study, we found statistically significant overlaps between the set of genes whose transcripts changed in abundance in vasopressin-escape and the sets of genes associated with two biological processes, namely "epithelial-to-mesenchymal transition (EMT)/TGFβ signaling" and "the cell cycle". The earliest detectable changes in the former process were seen on Day 1 of vasopressin-escape, coincident with the first detectable decreases in AQP2 and AQP3 proteins. The earliest statistically significant response for the cell-cycle pathway was seen on Day 2. We discuss these responses in turn. It is important to point out however, that the changes we observe in microdissected CCD include changes occurring in both intercalated and principal cells, thus it is premature to suggest they are unequivocally related to the fall in AQP2 or AQP3.

TGFβ signaling/EMT. The decrease of *Aqp2* gene expression in the CCD during the onset of vasopressin-escape is temporally associated with gene expression changes resembling a partial EMT (27, 34). A recent study by Li et al. (35) has demonstrated a high degree of plasticity in collecting duct principal cells owing to a reversible EMT. The authors isolated AQP2-expressing principal cells from mouse kidney and the cells underwent an EMT (associated with loss of AQP2 expression) under culture conditions, but when they were re-injected into the renal medulla, they integrated selectively into the collecting duct and again expressed AQP2. This suggests that principal cells can lose AQP2 expression by EMT and then gain it back by mesenchymal-to-epithelial transition (MET). That is, according to this model, principal cells can reversibly switch between AQP2-expressing and AQP2-nonexpressing phenotypes. We speculate that the sort of partial EMT seen in the present study may represent a physiological mechanism, independent of vasopressin signaling, that may control AQP2 expression in response to decreases in serum sodium concentration or osmolality. Ureteral obstruction, another pathophysiological state accompanied by loss of AQP2 expression (36), has also been shown to be associated with induced EMT of collecting duct cells (37). Thus, the general picture of the CCD principal cell during the onset of vasopressin-escape appears to be consistent with a reversible state of 'partial EMT' (27). The fact that the cells maintained their normal polarity also suggests a limited form of EMT, since full blown EMT is normally associated with loss of apical/basolateral polarity (38). A further question is whether EMT-like transcriptional changes or TGFβ signaling can account for the loss of AQP2 mRNA and protein in vasopressin-escape. To address this, we exposed vasopressin-treated mouse mpkCCD collecting duct cells to TGFβ, observing a profound decrease in AQP2 protein abundance in the cells. It is

unclear, however, whether TGFβ or a similar extracellular mediator like BMP7, a key mediator in renal development (39) whose mRNA was markedly increased on Day 1 (Figure 5), could play a role in vasopressin-escape.

Induction of expression of cell-cycle genes. The loss of AQP2 expression during vasopressin-escape was associated with a widespread increase in the expression of genes associated with the cell-cycle, seen on Days 2 and 4. Most of the genes annotated in the *KEGG Cell Cycle Pathway* exhibited increases in transcript abundance on Day 2 of the development of vasopressin-escape. Included were two TFs, E2f1 and Foxm1, which play critical roles in the regulation of the transition between quiescence and the cell cycle and were markedly increased on Days 2 and 4 of vasopressin-escape. E2f1 is the classical regulator of the transition from Go to the cell cycle (30). In addition to E2f1, a second member of the E2F TF family, namely E2f4 also shows increased expression during vasopressin-escape (Figure 5). E2f4 mediates some of the transcriptional effects of TGFβ through binding interactions with Smad3 (40). Thus, it is possible that the increase in expression of cell-cycle genes in vasopressin-escape is a downstream consequence of activation of TGFβ related signaling via E2f4, and that the EMT-like response and the induction of cell-cycle gene expression are parts of the same pathophysiological program. The Foxm1 TF, which like E2f1 regulates expression of cell-cycle genes critical for progression into S-phase (31), was also markedly increased in expression on Days 2 and 4 during vasopressin-escape (Figure 10). Despite the broad increase in expression of cell-cycle genes, there is little evidence for a proliferative response in CCD cells in the early stages of vasopressin-escape. A similar picture with cell cycle arrest at all stages is seen when mammalian cells are challenged with hypertonicity (41).

Relationship to vasopressin signaling. Because of the strong, selective, down-regulation of *Aqp2* and *Aqp3* in vasopressin-escape and the known action of vasopressin to increase expression of these genes (3), an important question to ask is, "Is vasopressin-escape just a simple reversal of normal vasopressin-mediated signaling in the collecting duct?" There is considerable evidence in opposition to this idea. First, the β- and γ-subunits of ENaC (*Scnn1b* and *Scnn1g*) are also transcriptionally upregulated by vasopressin (42), but were not found to be decreased in the current study. Second, transcriptional and proteomic profiling of mpkCCD cells (13) showed a response profile that has little similarity to the list of transcripts downregulated in vasopressin-escape in the present study. Thus, we conclude that the transcriptional response in vasopressin-escape is not simply the mirror image of the response to vasopressin, but represents a vasopressin-independent regulatory mechanism.

Acknowledgments

The work was primarily funded by the Division of Intramural Research, National Heart, Lung, and Blood Institute (project ZIA-HL001285 and ZIA-HL006129, M.A.K.) with

additional salary support to C.M.E. Georgetown University, Department of Medicine. Work by C.M.E. was done with the support of an Intergovernmental Personnel Agreement (IPA) for a sabbatical in the Epithelial Systems Biology Laboratory, NHLBI, NIH. Next-generation sequencing was done in the NHLBI DNA Sequencing and Genomics Core Facility (Jun Zhu, Director). The confocal immunofluorescence imaging was done in the NHLBI Light Microscopy Core Facility (Christopher Combs, Director) under the kind tutelage of Dr. Daniela Malide. Subcutaneous osmotic minipump implantation was performed by the NHLBI Animal Surgery and Resources Core staff. Some of the results were presented at the American Society of Nephrology Annual Meeting 2013 (Atlanta, GA), 2014 (Philadelphia, PA), and 2015 (San Diego, CA), as well as the Experimental Biology 2016 Meeting (San Diego, CA).

References

1. Hannon MJ, Thompson CJ. The syndrome of inappropriate antidiuretic hormone: prevalence, causes and consequences. Eur J Endocrinol. 2010;162 Suppl 1:S5-12.
2. Levinsky NG, Davidson DG, Berliner RW. Changes in urine concentration during prolonged administration of vasopressin and water. Am J Physiol. 1959;196(2):451-6.
3. Ecelbarger CA, Nielsen S, Olson BR, Murase T, Baker EA, Knepper MA, et al. Role of renal aquaporins in escape from vasopressin-induced antidiuresis in rat. J Clin Invest. 1997;99(8):1852-63.
4. Deen PM, Verdijk MA, Knoers NV, Wieringa B, Monnens LA, van Os CH, et al. Requirement of human renal water channel aquaporin-2 for vasopressin-dependent concentration of urine. Science. 1994;264(5155): 92-5.
5. Sasaki S, Fushimi K, Saito H, Saito F, Uchida S, Ishibashi K, et al. Cloning, characterization, and chromosomal mapping of human aquaporin of collecting duct. J Clin Invest. 1994;93(3):1250-6.
6. Ecelbarger CA, Chou CL, Lee AJ, DiGiovanni SR, Verbalis JG, Knepper MA. Escape from vasopressin-induced antidiuresis: role of vasopressin resistance of the collecting duct. Am J Physiol. 1998;274(6 Pt 2):F1161-6.
7. Lee JW, Chou CL, Knepper MA. Deep Sequencing in Microdissected Renal Tubules Identifies Nephron Segment-Specific Transcriptomes. J Am Soc Nephrol. 2015;26(11):2669-77.
8. Hoorn EJ, Hoffert JD, Knepper MA. Combined proteomics and pathways analysis of collecting duct reveals a protein regulatory network activated in vasopressin escape. J Am Soc Nephrol. 2005;16(10):2852-63.
9. Wright PA, Burg MB, Knepper MA. Microdissection of kidney tubule segments. Methods Enzymol. 1990;191:226-31.
10. Dobin A, Davis CA, Schlesinger F, Drenkow J, Zaleski C, Jha S, et al. STAR: ultrafast universal RNA-seq aligner. Bioinformatics. 2013;29(1):15-21.
11. Risso D, Ngai J, Speed TP, Dudoit S. Normalization of RNA-seq data using factor analysis of control genes or samples. Nat Biotechnol. 2014;32(9):896-902.
12. Love MI, Huber W, Anders S. Moderated estimation of fold change and dispersion for RNA-seq data with DESeq2. Genome Biol. 2014;15(12):550.
13. Khositseth S, Pisitkun T, Slentz DH, Wang G, Hoffert JD, Knepper MA, et al. Quantitative protein and mRNA profiling shows selective post-transcriptional control of protein expression by vasopressin in kidney cells. Mol Cell Proteomics. 2011;10(1):M110 004036.
14. Livak KJ, Schmittgen TD. Analysis of relative gene expression data using real-time quantitative PCR and the 2(-Delta Delta C(T)) Method. Methods. 2001;25(4):402-8.
15. Purkerson JM, Heintz EV, Nakamori A, Schwartz GJ. Insights into acidosis-induced regulation of SLC26A4 (pendrin) and SLC4A9 (AE4) transporters using three-dimensional morphometric analysis of beta-intercalated cells. Am J Physiol Renal Physiol. 2014;307(5):F601-11.
16. Na KY, Kim GH, Joo KW, Lee JW, Jang HR, Oh YK, et al. Chronic furosemide or hydrochlorothiazide administration increases H+-ATPase B1 subunit abundance in rat kidney. Am J Physiol Renal Physiol. 2007;292(6):F1701-9.
17. Fenton RA, Chou CL, Ageloff S, Brandt W, Stokes JB, Knepper MA. Increased collecting duct urea transporter expression in Dahl salt-sensitive rats. Am J Physiol Renal Physiol. 2003;285(1):F143-51.
18. Barile M, Pisitkun T, Yu MJ, Chou CL, Verbalis MJ, Shen RF, et al. Large scale protein identification in intracellular aquaporin-2 vesicles from renal inner medullary collecting duct. Mol Cell Proteomics. 2005;4(8):1095-106.
19. Ecelbarger CA, Terris J, Frindt G, Echevarria M, Marples D, Nielsen S, et al. Aquaporin-3 water channel localization and regulation in rat kidney. Am J Physiol. 1995;269(5 Pt 2):F663-72.
20. Hoffert JD, Fenton RA, Moeller HB, Simons B, Tchapyjnikov D, McDill BW, et al. Vasopressin-stimulated increase in phosphorylation at Ser269 potentiates plasma membrane retention of aquaporin-2. J Biol Chem. 2008;283(36):24617-27.
21. Kortenoeven ML, Li Y, Shaw S, Gaeggeler HP, Rossier BC, Wetzels JF, et al. Amiloride blocks lithium entry through the sodium channel thereby attenuating the resultant nephrogenic diabetes insipidus. Kidney Int. 2009;76(1):44-53.

22. Ecelbarger CA, Knepper MA, Verbalis JG. Increased abundance of distal sodium transporters in rat kidney during vasopressin escape. J Am Soc Nephrol. 2001;12(2):207-17.
23. Murase T, Ecelbarger CA, Baker EA, Tian Y, Knepper MA, Verbalis JG. Kidney aquaporin-2 expression during escape from antidiuresis is not related to plasma or tissue osmolality. J Am Soc Nephrol. 1999;10(10):2067-75.
24. Tiwari S, Packer RK, Hu X, Sugimura Y, Verbalis JG, Ecelbarger CA. Increased renal alpha-ENaC and NCC abundance and elevated blood pressure are independent of hyperaldosteronism in vasopressin escape. Am J Physiol Renal Physiol. 2006;291(1):F49-57.
25. Moustakas A, Heldin CH. Mechanisms of TGFbeta-Induced Epithelial-Mesenchymal Transition. J Clin Med. 2016;5(7).
26. Groger CJ, Grubinger M, Waldhor T, Vierlinger K, Mikulits W. Meta-analysis of gene expression signatures defining the epithelial to mesenchymal transition during cancer progression. PLoS One. 2012;7(12):e51136.
27. Kalluri R, Weinberg RA. The basics of epithelial-mesenchymal transition. J Clin Invest. 2009;119(6):1420-8.
28. Yu MJ, Miller RL, Uawithya P, Rinschen MM, Khositseth S, Braucht DW, et al. Systems-level analysis of cell-specific AQP2 gene expression in renal collecting duct. Proc Natl Acad Sci U S A. 2009;106(7):2441-6.
29. Grimm PR, Lazo-Fernandez Y, Delpire E, Wall SM, Dorsey SG, Weinman EJ, et al. Integrated compensatory network is activated in the absence of NCC phosphorylation. J Clin Invest. 2015;125(5):2136-50.
30. Alberts B, Johnson A, Lewis J, Raff M, Roberts K, Walter P. Molecular Biology of the Cell. 4th Edition ed: Garland Science; 2002.
31. Wang IC, Chen YJ, Hughes D, Petrovic V, Major ML, Park HJ, et al. Forkhead box M1 regulates the transcriptional network of genes essential for mitotic progression and genes encoding the SCF (Skp2-Cks1) ubiquitin ligase. Mol Cell Biol. 2005;25(24):10875-94.
32. Knepper MA. Systems biology in physiology: the vasopressin signaling network in kidney. Am J Physiol Cell Physiol. 2012;303(11):C1115-24.
33. Knepper MA. Systems biology of diuretic resistance. J Clin Invest. 2015;125(5):1793-5.
34. Lovisa S, LeBleu VS, Tampe B, Sugimoto H, Vadnagara K, Carstens JL, et al. Epithelial-to-mesenchymal transition induces cell cycle arrest and parenchymal damage in renal fibrosis. Nat Med. 2015;21(9):998-1009.
35. Li J, Ariunbold U, Suhaimi N, Sunn N, Guo J, McMahon JA, et al. Collecting duct-derived cells display mesenchymal stem cell properties and retain selective in vitro and in vivo epithelial capacity. J Am Soc Nephrol. 2015;26(1):81-94.
36. Frokiaer J, Marples D, Knepper MA, Nielsen S. Bilateral ureteral obstruction downregulates expression of vasopressin-sensitive AQP-2 water channel in rat kidney. Am J Physiol. 1996;270(4 Pt 2):F657-68.
37. Butt MJ, Tarantal AF, Jimenez DF, Matsell DG. Collecting duct epithelial-mesenchymal transition in fetal urinary tract obstruction. Kidney Int. 2007;72(8):936-44.
38. Rodriguez-Boulan E, Macara IG. Organization and execution of the epithelial polarity programme. Nat Rev Mol Cell Biol. 2014;15(4):225-42.
39. Vukicevic S, Kopp JB, Luyten FP, Sampath TK. Induction of nephrogenic mesenchyme by osteogenic protein 1 (bone morphogenetic protein 7). Proc Natl Acad Sci U S A. 1996;93(17):9021-6.
40. Chen CR, Kang Y, Siegel PM, Massague J. E2F4/5 and p107 as Smad cofactors linking the TGFbeta receptor to c-myc repression. Cell. 2002;110(1):19-32.
41. Burg MB, Ferraris JD, Dmitrieva NI. Cellular response to hyperosmotic stresses. Physiol Rev. 2007;87(4):1441-74.
42. Nicco C, Wittner M, DiStefano A, Jounier S, Bankir L, Bouby N. Chronic exposure to vasopressin upregulates ENaC and sodium transport in the rat renal collecting duct and lung. Hypertension. 2001;38(5):1143-9.

Chapter 9

Flow, cell proliferation and microcyst formation in relation to Aquaporin-2

Alsady M [1], Trimpert C [1], Cockx S [1], Kortenoeven MLA [1]*, Dekker H [2], Cornelissen M [3], Nijenhuis T [4] and Deen PMT [1]

[1] Department of Physiology, [2] Radiology, [3] Pediatric Nephrology and [4] Nephrology, Radboud University Medical Center, Nijmegen, The Netherlands;
*: Present address: department of Biomedicine, Aarhus University, Aarhus, Denmark.

Abstract

Aquaporin-2 (AQP2) water channels are expressed in principal cells of the renal connecting tubules and collecting ducts (CD). These proteins play key role in the fine tuning of water in the body. The absence or reduced expression of AQP2 underlies congenital and acquired Nephrogenic Diabetes Insipidus (NDI), a disorder characterised by polyuria and polydipsia. Recently a hypothesis was proposed that AQP2 itself was involved in principal cell proliferation, and formation of renal microcysts. In this study, using mpkCCD cells, endogenously expressing AQP2, and MRI analysis of a kidney of an NDI patient lacking AQP2, we investigated whether AQP2 has a direct role in principal cell proliferation and renal cyst formation. We observed reduced AQP2 expression in proliferating FCS/growth factor treated mpkCCD cells and no AQP2 expression in proliferating dDAVP stimulated mpkCCD cells. Additionally, flow-released adenosine decreased AQP2 abundance in mpkCCD cells. Moreover, no microcysts were formed in the kidney of patient lacking AQP2. Our data thus reveal that proliferation affects AQP2 abundance, but that AQP2 itself does not affect the proliferative status of principal cells nor lead to renal microcysts development. In contrary, we propose that a high collecting duct pro-urine flow not only results in renal microcyst development as seen in Li-NDI patients, but also reduces AQP2 abundance in the collecting duct.

Introduction

Water is the main component of the human body and is essential to facilitate many enzymatic processes, but also to maintain blood volume and osmolality homeostasis. Aquaporin-2 (AQP2) water channels expressed in principal cells of renal connecting tubules and collecting ducts (CD) are key in fine tuning of water in the body, because the absence or reduced expression of AQP2 underlies congenital and acquired Nephrogenic Diabetes Insipidus (NDI), a disorder characterised by polyuria and polydipsia (1-3). With hypernatremia or hypovolemia, centrally-released vasopressin (AVP) binds its V2R receptor, which is expressed in the basolateral membrane of principal cells. This binding leads to an increase in intracellular cAMP levels and redistribution of AQP2 from intracellular vesicles to the plasma membrane thereby allowing water reabsorption from pro-urine (4).

Based on findings in several mouse models with increased diuresis, it is generally thought that tubular abnormalities such as dilated tubules and cyst formation as found in AQP2 KO mice are secondary to polyuria and increased flow (5-7). Recently, however, Chen et al. provided evidence and proposed that AQP2 itself was involved in principal cell proliferation and formation of renal microcysts (6). Chen et al., based their hypothesis on the observation that AQP1, AQP3 and AQP4 KO mice manifest with similar concentrating defects as AQP2 KO mice, but do not have renal microcysts or renal failure. For cell migration and proliferation, the binding of AQP2 with its second external loop to integrin, present in the extracellular matrix, was of importance.

However, several arguments against those of Chen et al. can be brought forward. At first, there is a large difference in the extent of aquaresis between AQP2 on the one side and AQP1/AQP3/AQP4 on the other side in mice and man (8). Whereas AQP2 KO mice die shortly after birth because of dehydration (9), AQP1/AQP3 and AQP4 KO mice urinate much smaller volumes and survive (10-12). Similarly, in humans lacking the diverse aquaporins, those lacking AQP2 are born with NDI, while those born without AQP1, AQP3 or AQP4, show subclinical 'polyuria' or no increased aquaresis at all (3, 13-16).

Furthermore, a role for AQP2 in principal cell migration and binding of beta-integrin, which is part of the extracellular matrix, requires expression of AQP2 in the plasma membrane and during proliferation. This is the case for the cells used by Chen et al., but these cells are stably-transfected with a construct driving constitutive expression of AQP2 (6). It is unclear, however, whether endogenous AQP2 is expressed in proliferating CD cells. A hint that this may not be the case comes from our recent discovery that polarized mpkCCD cells, which endogenously express AQP2 in response to vasopressin, reduce their AQP2 abundance following stimulation with growth factor containing fetal calf serum (17). Moreover, we also showed that in proliferating epithelial MDCK cells exogenously expressed AQP2 as well as V2R are mainly intracellularly localized (18).

A consensus on whether AQP2 has a direct role in principal cell migration, proliferation and whether it contributes to cyst formation is thus lacking. Employing mpkCCD cells and with the help of an NDI patient lacking AQP2, we here tested the potential link between flow, cell proliferation and microcyst formation in relation to Aquaporin-2.

Materials and methods

Patient

Our 20-year-old male patient was diagnosed with congenital NDI in early infancy, which was confirmed at age 1, by demonstrating a homozygous mutation in the *AQP2* gene (559C->T; R187C) (3). Repeated renal ultrasound studies did not show any abnormalities, apart from a mild dilatation of the renal pelvis and proximal ureters. The Committee on Research Involving Human Participants (CMO) of the region Arnhem and Nijmegen, the Netherlands, approved the study. Participant provided informed consent.

Cell culture assays

Unless specified otherwise, mpkCCD cells were cultured as described (19). In short, cells were cultured in a modified defined medium containing DMEM:Ham's F12 1:1 vol/vol; 60 nM sodium selenate, 5 µg/ml transferrin, 2 mM glutamine, 50 nM dexamethasone, 1 nM triiodothyronine, 10 ng/ml epidermal growth factor (EGF), 5 µg/ml insulin, 28 mM D-glucose, 2% fetal calf serum (FCS), and 20 mM HEPES (pH 7.4). Cells were seeded at a density of $1.5x10^5$ cells/cm^2 on semi permeable filters (Transwell, 0.4 µm pore size, Corning Costar, Cambridge, MA). After 96 hours, cells were treated with 1 nM 1-deamino-8-D-arginine vasopressin (dDAVP) at the basolateral side to induce AQP2 expression. For the last 48 hours, cells were cultured in a FCS/EGF-free medium, unless mentioned otherwise. Cells could be treated with 10 µM 8cyclopentyl1,3dipropylxanthine (DPCPX; RBI, Poole, UK) at the basolateral and apical side under static or shaking conditions. The shaking condition was provided by an UltraCruz 2-dimensional rocker (Santa Cruz Biotechnology, Heidelberg, Germany) with a tilt angle of 30° and an oscillation frequency of 20 cycles/min. On day 8, cells were harvested and prepared for immunoblotting as described (19). To determine the effect of cell polarity on AQP2 abundance, cells were seeded as described above, but collected after 1, 2 or 4 days. The cells were cultured in presence of 1nM dDAVP or 10 µM forskolin during the last 24 hours. Cells were used for immunoblotting or immunocytochemistry.

Immunoblotting

Laemmli samples were denatured for 30 minutes at 37°C. SDS-PAGE, blotting, and blocking of the PVDF membranes was done as described (20). Membranes were incubated for 16 hours at 4°C with 1:1000 affinity–purified rabbit (Rb2) C tail AQP2 antibody in Tris-Buffered Saline Tween-20 (TBS-T) supplemented with 1% nonfat dried milk (3). In an identical way, other blots were incubated with 1:1000 Cyclin D1 antibody (Rabbit; cell signaling, Massachusetts, USA). After washing in TBS-T, all blots were incubated for 1 hour in TBS-T containing 1:10000-diluted goat anti–rabbit IgGs (Sigma-Aldrich, St. Louis, USA) coupled to horseradish peroxidase. Proteins were visualized using enhanced chemiluminescence (ECL; Pierce, Rockford, USA). Densitrometric analyses were performed using Bio-Rad quantification equipment (Bio-Rad 690c Densitometer; Chemidoc XRS) and Image studio software (LI-COR, Nebraska, USA). Equal loading of the samples was confirmed by staining of the blots with coomassie brilliant blue R-250 (BioRad, Hercules, USA).

Immunocytochemistry

Immunocytochemistry was done as described (21). In short, after removal of culture medium, mpkCCD cells were washed 3 times with ice-cold PBS-CM and fixed for 30 min at room temperature with 4% w/v paraformaldehyde in PBS. After washing twice with PBS, cells were treated with a permeabilization buffer (0.5% v/v Triton X-100 and in PBS with 0.7% w/v gelatin) for 30 min. Then, cells were incubated at 4°C overnight with AQP2 (Rb2 1:50; (3)), E-cadherin (rat; Sigma-Aldrich, St. Louis, USA) or acetylated alpha tubulin (rabbit; cell signaling, Massachusetts, USA) primary antibody in permeabilization buffer. After 3 washing steps, cells were incubated with anti-rabbit or anti-rat secondary antibody conjugated to an Alexa dye (Invitrogen, 1:500) for 2-3 hours at 37°C. Finally, cells were mounted in Vectashield containing DAPI (Vector Laboratories, Burlingame, USA) and imaged by confocal microscopy (Olympus FV1000, Center Valley, PA, USA).

Magnetic resonance imaging

Magnetic resonance imaging (MRI) was performed on a 3.0 T MR scanner (Skyra, Siemens Healthcare, Erlangen, Germany) with a pelvic phased-array coil. The following sequences were performed: coronal and axial T2-weighted half-Fourier single-shot turbo spin-echo (HASTE) with fat saturation, axial T1 volumetric interpolated breath-hold examination (VIBE) in-phase and out-of-phase, coronal T1 volumetric interpolated breath-hold examination (VIBE) with fat saturation. Diffusion weighted imaging was performed with *b*-factors of 50, 400 and 800 s/mm^2. Contrast enhanced dynamic imaging was performed with coronal gradient-echo T1-weighted MR sequence at 5 measurements, after administration of 15 ml Dotarem and contrast enhanced axial T1 VIBE was performed.

Statistical analysis

Analysis of the difference between groups was performed with student t-test or one-way ANOVA corrected by the Bonferroni multiple-comparisons procedure. A p-value < 0.05 was considered statistically significant.

Results

In mpkCCD cells, flow-released adenosine decreases AQP2 abundance

Epithelial cells in the kidney have non-motile cilia, which allows them to sense flow (22). This mechanic stimulus is the trigger for purinergic signaling cascades and gene transcription mediated by ATP and its degradation products, including adenosine, binding to their respective receptors (7). To determine whether we could test the effect of flow on the regulation of the abundance of endogenously-expressed AQP2 in mpkCCD cells, these cells were grown to confluence on transwell filter in the presence of dDAVP and stained for acetylated alpha tubulin, a marker for primary cilia. Confocal analysis revealed that mpkCCD cells indeed express primary cilia on their apical side (Fig. 1A).

To subsequently test whether endogenous AQP2 abundance is influenced by flow, mpkCCD cells were grown to confluence, treated with dDAVP, and placed on a rocking shaker for the last two days. Anticipating an effect of shaking on AQP2 abundance, we additionally treated the cells with or without the adenosine purinergic receptor antagonist DPCPX during the last two days. Subsequent immunoblotting revealed that the abundance of AQP2 was significantly reduced with shaking, which was precluded with DPCPX (Fig. 1B, C). This indicates that the adenosine receptor is involved in flow-mediated reduction of AQP2 in mpkCCD cells.

Proliferation suppresses AQP2 expression in mpkCCD cells

To determine whether endogenous AQP2 abundance is affected by the proliferative status of cells, mpkCCD cells were cultured to confluence in the presence of dDAVP with or without fetal calf serum (FCS) for the last 48 hours. FCS contains growth factors that stimulate cells to enter the proliferative cycle (23). Immunoblotting revealed that the AQP2 abundance was lower in the cells cultured in the presence of FCS (Fig. 2). Immunoblotting furthermore showed that cyclin D1 abundance was increased with FCS, which underscored that FCS stimulated proliferation. While these mpkCCD cells had already formed a monolayer and did not have extra 2D space to expand due to the plastic borders of the transwells, we wanted to test the effect of unrestricted proliferation on AQP2 abundance. For this, mpkCCD cells were seeded on transwell filters and cultured for 1, 2 or 4 days in the presence of dDAVP during the final 24 hours after which they were subjected to immunoblotting and immunocytochemistry.

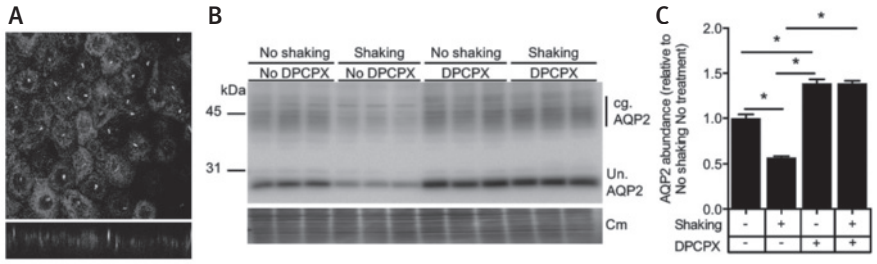

Figure 1. AQP2 abundance in mpkCCD cells is reduced by flow-mediated purinergic signaling. **(A)** To determine the presence of cilia on mpkCCD cells, cells were grown to confluence, treated with dDAVP, and immunostained for acteylated alpha tubulin. **(B)** To test whether endogenous AQP2 abundance is influenced by flow, mpkCCD cells were grown and treated as described under (A) and placed on a rocking shaker for the last two days in the presence or absence of a adenosine receptor selective antagonist (DPCPX) and immunoblotted for AQP2**.** **(C)** The unglycosylated AQP2 band were quantified. Coomassie blue staining of the blots (Cm) revealed loading of protein equivalents. Data presented are mean ± SEM of three independent experiments. A significant difference ($P<0.05$) from the condition with no shaking and no treatment is denoted by an asterisk.

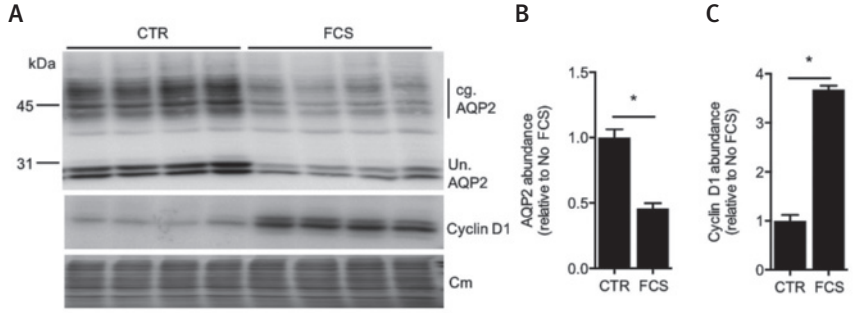

Figure 2. AQP2 abundance is reduced the the presence of fetal calf serum. **(A)** MpkCCD cells were cultured on filters for 8 days in the presence of dDAVP. During the final 48 hours cells were cultured in absence (CTR) or presence (FCS) of fetal calf serum **and** collected and immunoblotted for AQP2 and cyclin D1, Loading of protein equivalents is shown by Coomassie blue staining of the blots (Cm). Quantification of unglycosylated bands revealed a decreased **(B)** and increased **(C)** abundance of AQP2 and cyclin D1 with FCS, respectively. Data presented are mean ± SEM of three independent experiments. An asterisk denotes a significant difference ($P<0.05$) from control condition.

Immunoblotting of protein equivalents showed that AQP2 was not detected on day 1, increased at 2 days of culturing and was most pronounced, after 4 days of culture (Fig. 3A-B). In line with these data, immunocytochemistry showed no AQP2 staining after one day of culturing, some apical AQP2 staining at day 2, and extensive apical membrane AQP2 staining at day 4 (Fig. 3C). Despite the fact that the cells at day 1 and 2 could still expand, the clear basolateral expression of E-cadherin revealed that most cells were already polarized.

Our data above reveal that the abundance and apical membrane expression of AQP2 is strongly attenuated in proliferating cells. Considering that in proliferating Madin Darby Canine kidney (MDCK) cells stably expressing AQP2 the V2R is localized intracellularly (24), the absence of AQP2 protein expression on day 1 could be due to a lack of plasma membrane expression of the V2R. To test whether the lack of AQP2 expression was due to an intracellular expression of the V2R in mpkCCD cells, we

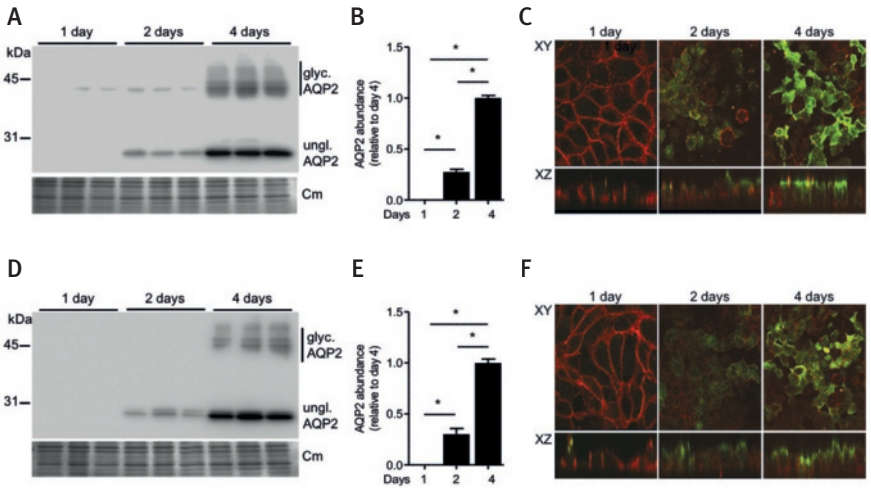

Figure 3: polarization is essential for AQP2 expression. MpkCCD cells were grown for 1,2 or 4 days on filters, of which the last day in the presence of dDAVP (**A-C**) or forskolin (**D-F**). Next, the cells were lysed and immunoblotted for AQP2 (**A, D**). Coomassie blue (Cm) staining of the blots revealed loading of protein equivalents . **(B, E)** The AQP2 bands of A/D were quantified and presented relative to the AQP2 abundance at day 4. **(C, F)** To determine the localisation of AQP2, cells were fixed, subjected to immunocytochemistry for AQP2 (green) and the basolateral membrane protein E-cadherin (red), and analyzed by confocal microscopy. Data presented are mean ± SEM of three independent experiments. A significant difference ($P<0.05$) from day 4 is denoted by an asterisk.

repeated the experiment above with the adenylate cyclase activator forskolin instead of dDAVP, thereby bypassing V2R. Immunoblot and immunocytochemical analysis, however, showed similar results as found for cells treated with dDAVP (Fig. 3D-F), indicating that the influence of proliferation on the AQP2 abundance was independent of V2R activation.

No renal microcysts in a patient lacking AQP2

Our data above revealed that in a cell model with endogenous expression of AQP2, flow as well as proliferation attenuated its abundance. To get the ultimate proof of whether the lack of AQP2 would lead to principal cell proliferation and microcyst formation in humans during kidney development or later, we contacted congenital NDI patients to ask their participation in an MRI analysis of their kidneys. The patient that responded positively was a 20-year-old male patient who was homozygous for the 559C->T AQP2 gene mutation, encoding AQP2-R187C (3). Importantly, R187 is a highly

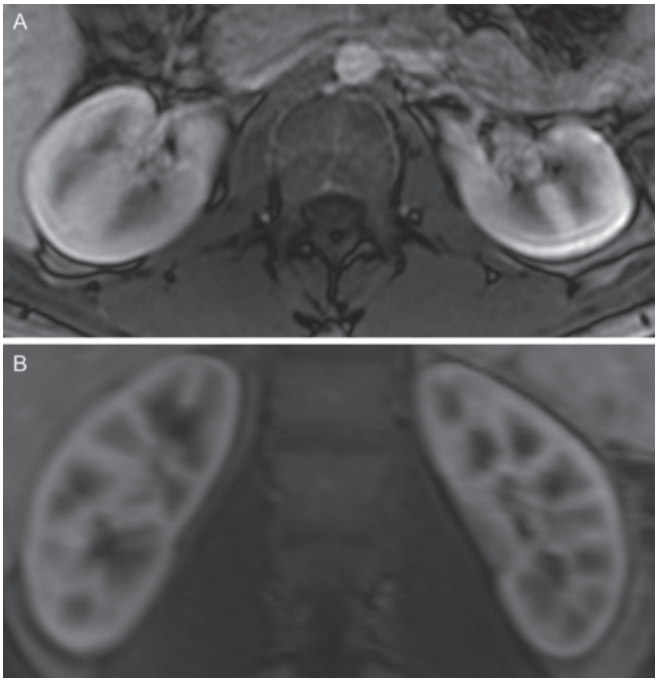

Figure 4. MRI analysis on kidneys of a patient lacking AQP2. Magnetic resonance imaging (MRI) was performed on a 3.0 T MR scanner (Skyra, Siemens Healthcare, Erlangen, Germany) with a pelvic phased-array coil to investigate whether the lack of AQP2 leads to the development of renal microcysts. No microcysts were detected (**A**; coronal plane, **B**; transversal plane).

conserved amino acid of AQP2 and cell biological analyses showed that AQP2-R187C is a misfolded non-functional AQP2 protein that is retained in the endoplasmic reticulum (20, 25). The MRI images revealed that the length of the patient's kidneys was approximately 12.5 cm and were normally located. The left pyelum appeared wider than the right pyelum. Critical scanning of both kidneys, however, revealed no lesions, nor any microcyst (Fig. 4).

Discussion

Proliferation reduces AQP2 abundance, but AQP2 does not influence proliferation.

Our data reveal that endogenous AQP2 abundance is strongly attenuated by the proliferative state of the cells. We observed reduced AQP2 abundance in polarized mpkCCD cells of which proliferation was stimulated (Fig. 2), and absent or reduced AQP2 expression in mpkCCD cells proliferating for one or 2 days, respectively, in the presence of dDAVP for the last day, (Fig. 3).). Moreover, when expressed in proliferating cells, AQP2 mainly localized in the apical membrane of our dDAVP-stimulated mpkCCD cells. In line with this, we have shown earlier *in vitro* and *in vivo* that the cell cycle status of principal cells determines the abundance of AQP2 water channel (26). The AQP2 abundance was found to be highest in the G0 cell cycle phase and reduced in all other phases. Moreover, although we have not investigated whether AQP2 affects proliferation *in vitro*, renal microcysts were not developed in our patient lacking AQP2, indicating that AQP2 does not induce principal cell proliferation *in vivo*.

Our data are in contrast to the data of Chen et al (6). Although we cannot exclude that (a low level of) expression of AQP2 may influence proliferation of principal cells during kidney development, as our proliferating cells will likely express some AQP2, their data are likely due to the constitutive expression of AQP2 in their cell model and the fact that in their used transfected LLCPK cells, AQP2 is targeted to the basolateral membrane.

Flow reduces AQP2 abundance

Besides the status of proliferation, our data provide further support that flow and the connected purinergic signalling affects AQP2 abundance. Changes in tubular flow are sensed by the primary cilia that have a crucial role in a number of cellular processes that include mechano and chemo-sensation as well as the transduction of signaling cascades critical for the development and maintenance of different tissues and organs (27). Accordingly, cilia are cellular antennas that coordinate the balance between cells and their environment. While our mpkCCD cells express primary cilia, we showed that flow reduced AQP2 abundance and that this effect was conferred by the adenosine receptor. Considering that our medium is not refreshed during 2 days, and that

degradation of flow-released ATP is mostly degraded fast to ADP, AMP and adenosine, it may well be that receptors for ATP, ADP and AMP may reduce AQP2 abundance with flow as well. This data is line with earlier *ex-vivo* findings in AVP-stimulated rat inner medullary collecting ducts that were (flow-)perfused with ATP and resulted in reduced intracellular cAMP levels and subsequent reduced water permeability (28). In addition, increased urine production in lithium-induced nephrogenic diabetes insipidus, and therewith collecting duct pro-urine flow, is also stimulated by ATP, because blockade of the ATP/UTP-activated $P2Y_2$ receptor ameliorated Li-induced NDI in rodents (29). Besides ATP, TGFβ may have an important role in flow-mediated attenuation of AQP2, because fluid shear stress activated the TGFβ pathway in renal epithelial cells and we showed that TGFβ downregulate AQP2 (26, 30).

In this respect, flow might also be an advantageous factor in diseases such as the syndrome of inappropriate antidiuretic hormone secretion (SIADH). SIADH is marked by increased water retention due to high AQP2 abundance that is induced by high circulating AVP. Ecelbarger et al. showed that, due to an unknown mechanism, AQP2 water channels were reduced in rats that received high water load, despite the high circulating AVP levels that were induced by the mini-pumps (31). The reduced AQP2 abundance in this so-called vasopressin escape may be due to the increased a flow. These and earlier data thus indicate that flow is an important modulating factor for AQP2 abundance and that it may be an aggravating factor in diseases such as Li-NDI.

Differences in the extent of collecting duct flow might also explain why renal microcysts do develop in cNDI in mice but not in patients. At first, the extent of flow increase in mice in cNDI is higher than in humans. Whereas the urine volume increases about 30-fold (urine osmolality from 3000 to 100 mOsm) with mice, it 'only' increases about 12-fold (1200 to 100 mOsm) with humans (32, 33). Moreover, whereas most patients have a reduced flow, because they are treated for their polyuria with diuretics, cNDI mice are not treated. In this respect, it is worth to mention that in the far past, when cNDI patients did not receive medication to reduce their voiding volume, the patients developed tubular dilations. Recent patients, who receive thiazide/amiloride treatment and therefore have reduced polyuria, develop less renal deformation as e.g. seen in our patient (34, 35). As such it would be interesting to see whether kidney deformation and cyst formation in AQP2 knockout mice would be attenuated in conditions of reduced polyuria, as observed with diuretic treatment.

Taken together, we showed that the proliferation attenuates AQP2 abundance and that the absence of AQP2 cannot be the cause for renal microcyst development in man. In addition, we propose that a high renal flow not only results in renal microcyst development as seen in cNDI mice and Li-NDI patients, but also as an important factor modulating AQP2 abundance in the collecting duct.

References

1. Moeller HB, Rittig S, Fenton RA. Nephrogenic diabetes insipidus: essential insights into the molecular background and potential therapies for treatment. Endocr Rev. 2013;34(2):278-301.
2. Fushimi K, Uchida S, Hara Y, Hirata Y, Marumo F, Sasaki S. Cloning and expression of apical membrane water channel of rat kidney collecting tubule. Nature. 1993;361(6412):549-52.
3. Deen PM, Verdijk MA, Knoers NV, Wieringa B, Monnens LA, van Os CH, et al. Requirement of human renal water channel aquaporin-2 for vasopressin-dependent concentration of urine. Science. 1994;264(5155):92-5.
4. Pearce D, Soundararajan R, Trimpert C, Kashlan OB, Deen PM, Kohan DE. Collecting duct principal cell transport processes and their regulation. Clin J Am Soc Nephrol. 2015;10(1):135-46.
5. Boone M, Deen PM. Congenital nephrogenic diabetes insipidus: what can we learn from mouse models? Exp Physiol. 2009;94(2):186-90.
6. Chen Y, Rice W, Gu Z, Li J, Huang J, Brenner MB, et al. Aquaporin 2 promotes cell migration and epithelial morphogenesis. J Am Soc Nephrol. 2012;23(9):1506-17.
7. Praetorius HA, Leipziger J. Primary cilium-dependent sensing of urinary flow and paracrine purinergic signaling. Semin Cell Dev Biol. 2013;24(1):3-10.
8. Boone M, Deen PM. Congenital nephrogenic diabetes insipidus: what can we learn from mouse models? ExpPhysiol. 2009;94(2):186-90.
9. Rojek A, Fuchtbauer EM, Kwon TH, Frokiaer J, Nielsen S. Severe urinary concentrating defect in renal collecting duct-selective AQP2 conditional-knockout mice. Proc Natl Acad Sci U S A. 2006;103(15):6037-42.
10. Ma T, Song Y, Yang B, Gillespie A, Carlson EJ, Epstein CJ, et al. Nephrogenic diabetes insipidus in mice lacking aquaporin-3 water channels. Proc Natl Acad Sci U S A. 2000;97(8):4386-91.
11. Ma T, Yang B, Gillespie A, Carlson EJ, Epstein CJ, Verkman AS. Generation and phenotype of a transgenic knockout mouse lacking the mercurial-insensitive water channel aquaporin-4. J Clin Invest. 1997;100(5):957-62.
12. Ma T, Yang B, Gillespie A, Carlson EJ, Epstein CJ, Verkman AS. Severely impaired urinary concentrating ability in transgenic mice lacking aquaporin-1 water channels. J Biol Chem. 1998;273(8):4296-9.
13. van Lieburg AF, Verdijk MA, Knoers VV, van Essen AJ, Proesmans W, Mallmann R, et al. Patients with autosomal nephrogenic diabetes insipidus homozygous for mutations in the aquaporin 2 water-channel gene. Am J Hum Genet. 1994;55(4):648-52.
14. King LS, Choi M, Fernandez PC, Cartron JP, Agre P. Defective urinary concentrating ability due to a complete deficiency of aquaporin-1. N Engl J Med. 2001;345(3):175-9.
15. Roudier N, Ripoche P, Gane P, Le Pennec PY, Daniels G, Cartron JP, et al. AQP3 deficiency in humans and the molecular basis of a novel blood group system, GIL. J Biol Chem. 2002;277(48):45854-9.
16. Sorani MD, Zador Z, Hurowitz E, Yan D, Giacomini KM, Manley GT. Novel variants in human Aquaporin-4 reduce cellular water permeability. Hum Mol Genet. 2008;17(15):2379-89.
17. Lee JW, Alsady M, Chou C-L, Groot Td, Deen PMT, Knepper MA, et al. Single-Tubule RNA-Seq Reveals Signaling Mechanisms That Defend Against Hyponatremia in SIADH. Kidney International. 2017.
18. van Beest M, Robben JH, Savelkoul PJ, Hendriks G, Devonald MA, Konings IB, et al. Polarisation, key to good localisation. Biochim Biophys Acta. 2006;1758(8):1126-33.
19. Kortenoeven ML, Li Y, Shaw S, Gaeggeler HP, Rossier BC, Wetzels JF, et al. Amiloride blocks lithium entry through the sodium channel thereby attenuating the resultant nephrogenic diabetes insipidus. Kidney Int. 2009;76(1):44-53.
20. Kamsteeg EJ, Wormhoudt TA, Rijss JP, van Os CH, Deen PM. An impaired routing of wild-type aquaporin-2 after tetramerization with an aquaporin-2 mutant explains dominant nephrogenic diabetes insipidus. EMBO J. 1999;18(9):2394-400.
21. Deen PM, Van Balkom BW, Savelkoul PJ, Kamsteeg EJ, Van Raak M, Jennings ML, et al. Aquaporin-2: COOH terminus is necessary but not sufficient for routing to the apical membrane. Am J Physiol Renal Physiol. 2002;282(2):F330-40.
22. Madsen KM, Clapp WL, Verlander JW. Structure and function of the inner medullary collecting duct. Kidney Int. 1988;34(4):441-54.

23. Rosner M, Schipany K, Hengstschlager M. Merging high-quality biochemical fractionation with a refined flow cytometry approach to monitor nucleocytoplasmic protein expression throughout the unperturbed mammalian cell cycle. Nat Protoc. 2013;8(3):602-26.
24. van Beest M, Robben JH, Savelkoul PJ, Hendriks G, Devonald MA, Konings IB, et al. Polarisation, key to good localisation. Biochim Biophys Acta. 2006;1758(8):1126-33.
25. Mulders SM, Bichet DG, Rijss JP, Kamsteeg EJ, Arthus MF, Lonergan M, et al. An aquaporin-2 water channel mutant which causes autosomal dominant nephrogenic diabetes insipidus is retained in the Golgi complex. J Clin Invest. 1998;102(1):57-66.
26. Lee JW, Alsady M, Chou CL, de Groot T, Deen PMT, Knepper MA, et al. Single-tubule RNA-Seq uncovers signaling mechanisms that defend against hyponatremia in SIADH. Kidney Int. 2017.
27. Irigoin F, Badano JL. Keeping the balance between proliferation and differentiation: the primary cilium. Curr Genomics. 2011;12(4):285-97.
28. Kishore BK, Chou CL, Knepper MA. Extracellular nucleotide receptor inhibits AVP-stimulated water permeability in inner medullary collecting duct. Am J Physiol. 1995;269(6 Pt 2):F863-9.
29. Kishore BK, Carlson NG, Ecelbarger CM, Kohan DE, Muller CE, Nelson RD, et al. Targeting renal purinergic signalling for the treatment of lithium-induced nephrogenic diabetes insipidus. Acta physiologica. 2015;214(2):176-88.
30. Kunnen SJ, Leonhard WN, Semeins C, Hawinkels L, Poelma C, Ten Dijke P, et al. Fluid shear stress-induced TGF-beta/ALK5 signaling in renal epithelial cells is modulated by MEK1/2. Cell Mol Life Sci. 2017;74(12): 2283-98.
31. Ecelbarger CA, Chou CL, Lee AJ, DiGiovanni SR, Verbalis JG, Knepper MA. Escape from vasopressin-induced antidiuresis: role of vasopressin resistance of the collecting duct. Am J Physiol. 1998;274 (6 Pt 2):F1161-6.
32. Boron WF, Boulpaep EL. Medical Physiology. second ed: ELSEVIER; 2009.
33. Sands JM, Layton HE. The physiology of urinary concentration: an update. Semin Nephrol. 2009;29(3):178-95.
34. Robertson GL. Diabetes insipidus: Differential diagnosis and management. Best Pract Res Clin Endocrinol Metab. 2016;30(2):205-18.
35. Sands JM, Bichet DG, American College of P, American Physiological S. Nephrogenic diabetes insipidus. Ann Intern Med. 2006;144(3):186-94.

Chapter 10

Summary and general discussion

Introduction

Each day, the kidneys filtrate about 170–180 L of blood. If these large volumes of ultra-filtrate were excreted unchanged as urine, it would be necessary to ingest huge amounts of water and electrolytes to stay in balance. This is avoided by the selective reabsorption of water, essential electrolytes and other blood constituents from the filtrate along the nephron. The fine-tuning of water homeostasis takes place in the collecting duct principal cells that express AQP2 water channel. Considering the importance of AQP2 in water homeostasis, increase or decrease in the abundance of AQP2 on the cell surface directly affects the urine concentrating ability thus also the amount of water in the body resulting in diseases such as syndrome of inappropriate antidiuretic hormone secretion (SIADH) or nephrogenic diabetes insipidus (NDI). The most common form of NDI is acquired and is a side effect of lithium treatment that is given to bipolar patients. This thesis aimed to gain insight into pathophysiological mechanisms involved in the development of renal side effects of lithium and explored the possibility to introduce novel treatments for Li-NDI.

The impact of aerobic glycolysis in lithium-induced renal pathology

Lithium-induced metabolic reprogramming of principal cells

Earlier, others and we have shown that, by entering via ENaC, lithium initiated proliferation of principal cells *in vitro* and *in vivo (1, 2)*. In **chapter 4** of this thesis, we provided *in vitro* and *in vivo* data, which showed that lithium-induced principal cell proliferation coincided with metabolic changes toward aerobic glycolysis and glutaminolysis. In the continuous presence of oxygen, lithium treatment induced an increased (*in vitro*) release and (*in vivo*) urinary excretion of lactate, which was absent in mice lacking ENaC in collecting ducts. Our NMR analysis furthermore revealed that lithium treatment strongly increased urinary levels of succinate, fumarate and citrate, which are known to increase during glutaminolysis (3). With aerobic glycolysis, glutaminolysis is typically upregulated as well, because glutamine provides the cell of nitrogen and citrate, needed for amino acid and lipid synthesis, respectively (4). Moreover, during aerobic glycolysis, the increased intracellular acid production, such as lactate, necessitates the cell to ignite pathways to buffer acid excess, besides secretion of lactate through MCT proteins. Cellular glutamine influx and glutaminolysis serve this buffering function, as the two molecules of NH_3 released from glutamine and glutamate during glutaminolysis are effective H^+ buffers (5). In line with this, urinary ammonium (NH_4^+) was strongly increased with lithium (Figure 1).

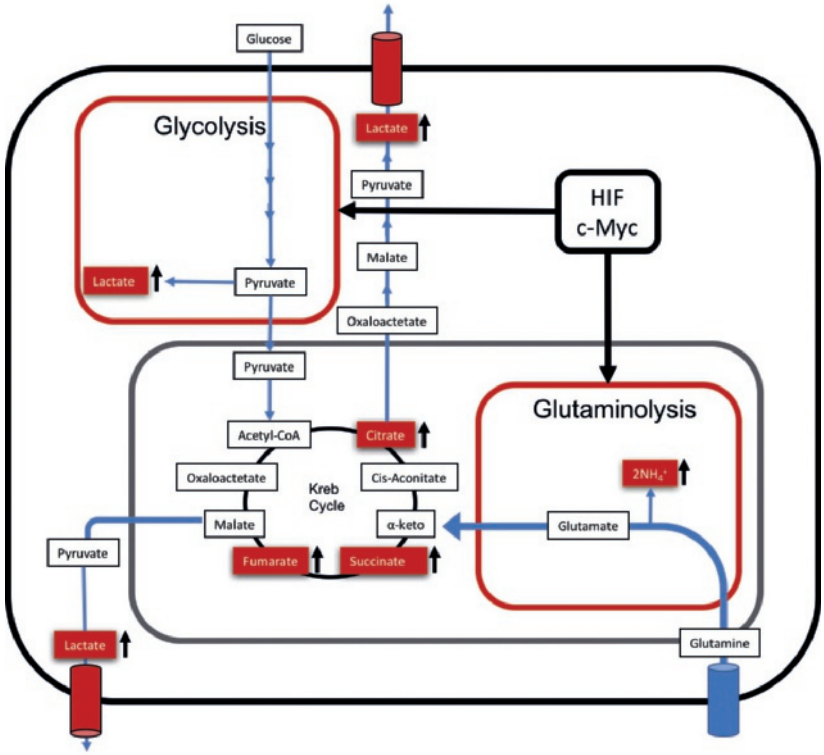

Figure 1. Lithium induces aerobic glycolysis and glutaminolysis. Lithium treatment increases the excretion of lactate, succinate, fumarate, citrate and ammonium. The increase in these metabolites indicate that lithium switched the cellular metabolism from oxidative phosphorylation into aerobic glycolysis that often goes together with use of glutamine as energy source in glutaminolysis for the generation of energy and H^+ acceptors. The mechanism by which lithium induces these changes is still not known but likely involves the HIF and/or the c-Myc pathways that are known to regulate these metabolic processes.

Our *in vitro* data on the carbonic anhydrases (CAs) involved in the acetazolamide-induced suppression of lithium-induced downregulation of AQP2 are in line with the above. Although we have not solidly proven that the mix of four siRNAs against the different CAs indeed downregulated the expression of each CA, a dogma concluded from an extensive study in which thousands of siRNAs were tested to block cancer cell growth (6, 7), our siRNA and CA-specific drug treatments clearly revealed that inhibition of CA9, and possibly CA12, attenuated the lithium-induced AQP2 downregulation in mpkCCD cells. CA9 and -12 are normally located to the basolateral membrane of epithelial cells, but appear in the plasma membranes of proliferating cells (8-10). CA12

is abundantly expressed in the collecting duct of healthy kidneys, however the cell specificity seems to depend on the species tested: while in humans and rabbits, CA12 is mainly found in principal cells, its expression seems restricted to type-A intercalated cells in rodents (8, 11, 12). CA9 is hardly expressed in healthy kidneys, but CA9 and CA12 expression is markedly increased in renal carcinomas, where they facilitate proliferation of these tumor cells by facilitating the cellular removal of acids (13, 14). HCO_3^-, extracellularly generated by CA9/12, is taken up by tumor cells to neutralize their excessive production of acids, such as lactate, produced during aerobic glycolysis (15, 16). The action of CA9/12 allows tumor cells to continue their Warburg-like proliferation and acid secretion, of which the latter helps cell proliferation by disassembling junctional proteins (17-19).

Unfortunately, inhibition of aerobic glycolysis with 2DG did not attenuate Li-NDI. *In vitro*, 2DG attenuated the Li-induced downregulation of total and apical membrane abundance of AQP2. *In vivo*, the urinary lactate excretion normalized, illustrating the blocking effect of aerobic glycolysis of 2DG in our experiments, but not those of succinate, fumarate, citrate and ammonium, indicating that 2DG did not block the effect of lithium on glutaminolysis. Our data indicate that lithium, which can still enter principal cells through ENaC in our 2DG experiment, induces aerobic glycolysis and glutaminolysis through different pathways, and may suggest that the increased glutaminolysis is of more relevance to Li-NDI, as Li-NDI was not improved with 2DG. As such, future studies should focus on the potential role of glutaminolysis in the pathogenesis of Li-NDI. Furthermore, although we did not determine pathways involved in this metabolic switch, glycolysis and glutaminolysis are possibly induced by HIF and/or c-Myc (20). We found that HIF1α was significantly increased in medulla of mice that were treated with lithium for 10 days (Figure 2). Additionally, increased cyclin D1 abundance indicate that c-Myc is probably increased as the transcription factor for both c-Myc and cyclin D1 is β-catenin (21). Future research will have to determine whether these or other pathways are responsible for this switch.

Li-NDI and ADPKD

Although blocking aerobic glycolysis with 2DG did not attenuate Li-NDI, the resemblance between Li-NDI and ADPKD is striking, as both involve cell proliferation and aerobic glycolysis (**chapter 4** and (22). Interestingly, 62.5% of bipolar patients on long-term lithium therapy also develop microcysts (23), but it is at present unclear whether that has any relationship with cysts being formed in ADPKD. Of interest in this respect is that, to stimulate cyst formation in conditional ADPKD knockout mice, a stress factor (1,2-dichlorovinyl-cysteine; DCVC) is given (24). It would be interesting to test whether lithium could also serve as such a stress factor, as this could be an indication that patients developing microcysts with lithium therapy may be carriers of subclinical mutations in the ADPKD genes.

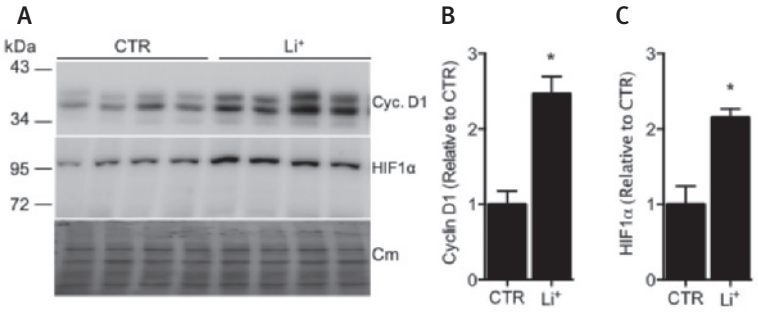

Figure 2. Lithium increases cyclin D1 and HIF1α abundance in the renal medulla. Mice were treated for 10 days with a control or lithium containing diet. After sacrifice, kidneys were rapidly isolated, one kidney was dissected into cortex and medulla, snap frozen in liquid nitrogen, and stored at -20°C. Immunoblot analysis (A) of medulla lysates was performed to determine protein abundance of cyclin D1 and HIF1α, which were subsequently semi-quantified (B/C) The abundance of both proteins was increased with lithium. A significant difference (P= *‹0.05) from CTR is denoted by an asterisk. CTR, control; Li+, lithium; HIF1α, hypoxia-inducible factor 1 alpha and Cm, coomassie blue staining.

Moreover, due to the increased diuresis in both disorders, both are characterized by elevated plasma vasopressin levels (25, 26), which, in ADPKD, has been found to contribute to cyst growth and ADPKD development (27). Indeed, vasopressin type-2 receptor (AVPR2) antagonists, such as tolvaptan, have shown to be beneficial in attenuating ADPKD development and have recently been approved as a therapy for ADPKD (28). It is highly unlikely, however, that AVPR2 antagonists will be of use in Li-NDI, for several reasons. At first, the loss of AQP2 expression and principal cell numbers is central to Li-NDI and blocking the AVPR2 will only worsen NDI, increase RAAS and therewith increase lithium entry in remaining proper principal cells. Moreover, the developing microcysts with lithium are (thus) small and, although typical for kidneys of lithium-using patients, they have never been associated with a worsened kidney function. Furthermore, while microcysts have been suggested to be derived from principal cells, vasopressin levels are already elevated in the early phase of Li-NDI, whereas microcysts have only been found in kidneys of patients treated with lithium for ›10 year. As such, the elevated vasopressin levels in Li-NDI is unlikely to induce development nor growth of microcysts in kidneys of lithium-treated patients but more likely by the increased renal flow as proposed in **chapter 9** of this thesis.

Lithium, aerobic glycolysis, and the brain

Administration of lithium to rats was found to affect brain glucose metabolism where the concentrations of brain glucose, brain lactate and brain glycogen were increased,

and the concentration of brain glutamate was decreased (29). The incorporation of (14)C from U-(14)C D-glucose, administered intraperitoneally to the rats, was increased in brain glucose and brain lactate, and decreased in brain glutamate (29). Therefore, we think that increased glucose uptake and lactate release in the brain is also due to a metabolic switch towards aerobic glycolysis. Decrease in glutamate concentration might be due to increased glutamate consumption because of glutaminolysis. However, other metabolites were not measured in this study to support this. Interestingly, however, in the last decades, a beneficial side of lactate as an alternative 'glucose sparing' fuel of the brain has been demonstrated and extensively reviewed by Taher et al. (30). Aerobic glycolysis induced lactate release might be beneficial for bipolar disorder patients as released lactate might also serve as fuel in the brain. It is worth to mention, however, that a number of studies have indicated that lactate is increased and pH is decreased in the brain of patients with bipolar disorder (31-33). It is important to determine whether these changes are part of the pathophysiology of bipolar disorder or they are treatment artifacts as most of the patients with this disorder receive chronic lithium treatment throughout their lives. New studies should determine glucose uptake and lactate release in the brain of medication-free patients with bipolar disorder to elucidate the importance of these changes in the unset of bipolar disorder.

Impact of the cell cycle on AQP2 abundance

In **chapter 4**, we showed that lithium induced proliferation and a metabolic switch towards aerobic glycolysis in principal cells. Aerobic glycolysis did not seem to affect AQP2 abundance but the impact of proliferation on AQP2 abundance was still not determined. While we were investigating the pathophysiology of SIADH in **chapter 8**, we found that AQP2 abundance was the highest in the G0 phase and strongly reduced in all other phases of the cell cycle (34). These results are also important in understanding the role of the cell cycle in the downregulation of AQP2 in Li-NDI and whether it is worth to target proteins in this pathway to rescue AQP2 and propose this as a new treatment for Li-NDI. Most proliferation inhibitors stop the cell cycle at the restriction point in G1 phase or in later phases (35). For example, this was shown in mice where rapamycin, which inhibits the cell cycle at the G1 phase (36), prevented lithium induced proliferation but did not attenuate lithium induced NDI and did not restore the expression of collecting duct AQP2 (37). This means that principal cells have to remain in the G0 phase to maintain high AQP2 abundance. However, there are currently no drugs available that can do this. Nevertheless, the finding that AQP2 abundance is highly dependent on the state of the cell in the cell cycle is interesting and also raises the question whether the body also regulates AQP2 abundance by modulating the cell cycle status under physiological conditions. In **chapter 8**, we used the methods of systems biology in a well-established rat model of SIADH to identify

signaling pathways activated at the onset of vasopressin-escape. On Day 2 of water loading, transcriptomic changes mapped to the transition from G0 into the cell cycle but arrest at the G2/M stage. There was no evidence of actual cell division. This highlights the impact of the cell cycle on AQP2 in diseases other than Li-NDI.

Finally, although the mechanism of lithium induced proliferation is still poorly understood, we can, based on current knowledge, propose a mechanism that involves GSK3β. It has been shown that lithium inhibits GSK3β *in vitro* and *in vivo* (38-40). GSK3β is a core component of the β-catenin destruction complex that prevents β-catenin translocation into the nucleus (41). In the nucleus, β-catenin serves as a transcription factor for several genes including cyclin D1 which, together with cyclin E, phosphorylates the Retinoblastoma (Rb) protein. This results in the release of E2F, which induces the transcription of several proliferation genes (Figure 3) (42). Additionally, GSK3β also directly regulates cyclin D1 proteolysis (43). Thus, the inhibition of GSK3β by lithium results in increased expression and activity of cyclin D1 that stimulates the cells to enter the cell cycle.

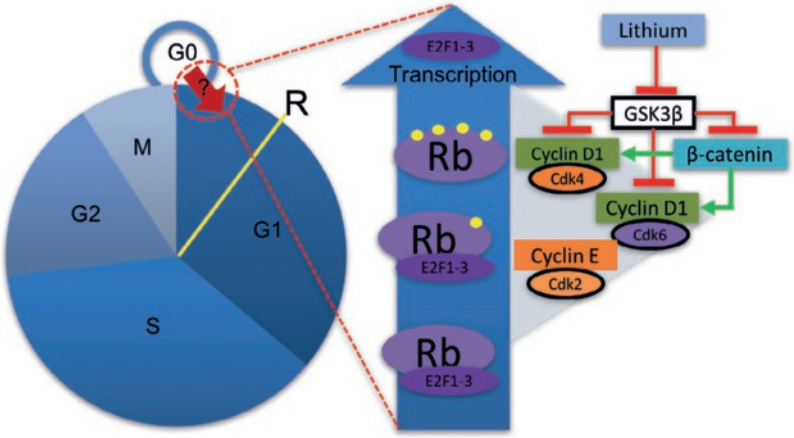

Figure 3. A likely mechanism by which lithium induces cell proliferation. GSK3β is a core component of the β-catenin destruction complex and normally this complex prevents β-catenin translocation into the nucleus. In the nucleus, β-catenin acts as a transcription factor for cyclin D1. Increased cyclin D1 together with the cyclin E, phosphorylate Retinoblastoma (Rb) protein. Phosphorylation of the Rb protein result in detachment of E2F from Rb, which induces transcription of several proliferation genes. GSK3β furthermore also regulates cyclin D1 proteolysis. Lithium is known to inhibit GSK3β. Thus, the inhibition of GSK3β by lithium results in increased expression and activity of cyclin D1 that passes the cell from the G0 phase into the G1 phase of the cell cycle, which eventually result in downregulated AQP2 water channels.

Lithium induced collecting duct remodeling

Besides the loss of AQP2 expression, lithium treatment induces collecting duct remodeling, in which the ratio of principal-to-intercalated cells decreases (44, 45). The paradoxical finding that lithium induces cell proliferation of principal cells, but nevertheless ends up in a reduced principal/intercalated cell ratio is not understood. Christensen et al. checked different options, but only sparsely observed apoptosis of principal cells or conversion into intercalated cells during lithium treatment and therefore excluded these as potential causes for the reduced percentage of principal cells (1). In **chapter 2** of this thesis, we provided an explanation for this paradox as a large proportion of PCNA-positive principal cells is arrested in the late G2 phase, indicating that they do not divide further.

We, however, believe that the G2-phase arrest of principal cells is not the sole factor leading to collecting duct cell remodeling. Different earlier studies demonstrated that lithium treatment of rats induced an increased number of cells in the collecting duct (46-48). The increased number of cells likely constitutes mostly intercalated cells. The question remains why intercalated cells proliferate. An important stimulus could be the development of metabolic acidosis, which is often, but not always, observed with lithium treatment in rodents and man (49, 50), because a state of metabolic acidosis increases the numbers of α-intercalated cells as an adaptive response (51, 52). Earlier studies suggested that lithium-induced metabolic acidosis and collecting duct remodeling could be due to a direct inhibition of H^+-ATPase and H^+/K^+-ATPase these transporters of intercalated cells (53, 54). However, if true, the effect of lithium on collecting duct remodeling should be independent from its influx in the principal cells, which does not seem to be the case for the following reasons: Kortenoeven et al. showed that amiloride, which inhibits lithium entry in principal cells only, attenuated collecting duct remodeling (55). Moreover, the abundance of H^+-ATPase, a marker protein for α-intercalated cells, was not increased in lithium-treated ENaC-KO mice (56). These studies, thus, indicate that lithium-induced remodeling is a direct effect of principal cell lithium entry. In **chapter 4** of this thesis we showed that lithium induced aerobic glycolysis in principal cells, a condition coinciding with increased lactic acid production and principal cell acid secretion. As such, the increased number of α-intercalated cells in Li-NDI might be induced by lactic acid release during aerobic glycolysis (Figure 4). Thus, the lithium-induced collecting duct remodeling could be explained by a rather stable population of principal cells, which are partly in a cell cycle arrest, and a proliferating population of intercalated cells due to lithium-induced aerobic glycolysis.

Fluid shear stress-mediated aggravation of Li-NDI

Lithium-induced NDI is caused by the direct downregulation of AQP2 in principal cells. However, reduced AQP2 abundance in the collecting duct results in increased water

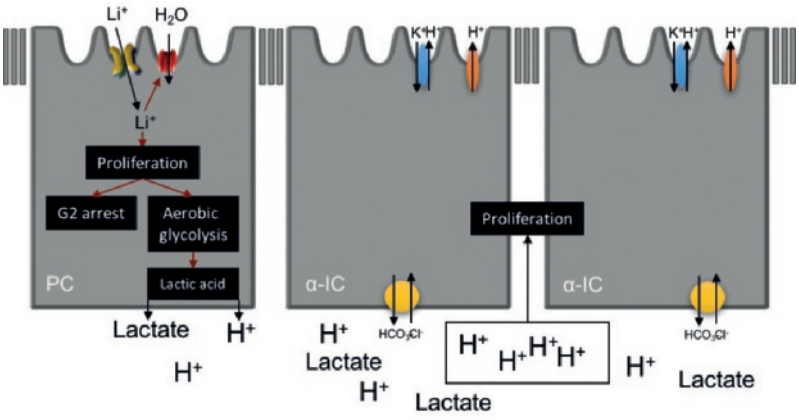

Figure 4. Lithium treatment causes collecting duct remodeling. Besides the downregulation of AQP2 water channel, lithium also causes renal collecting remodeling that is marked by a decrease in the percentage of principal cells and increase in the percentage of intercalated cells. This is surprising, as lithium treatment also induces proliferation mainly in the principal cells. In this thesis, we provided an explanation for this paradox. Besides proliferation, lithium also induces aerobic glycolysis that is marked by lactic acid release that stimulates acid secreting intercalated cells to proliferate and secrete this acid in the urine. So, while principal cells get arrested at G2 phase, intercalated cells continue to increase and eventually represent the majority of the collecting duct.

flow that might aggravate NDI development. Kunnen et al. showed, in an *in vitro* study, that fluid shear stress induces TGFβ signaling in renal epithelial cells (57) and in **chapter 8** we showed that TGFβ downregulates AQP2 (34). Therefore, fluid shear stress induced activation of the TGFβ pathway might contribute to the inability of the principal cells to concentrate urine. However, the release of TGFβ as a consequence of increased renal flow and shear stress has not been determined. Therefore, measurement of urinary TGFβ in Li-NDI patients or rodents is highly desirable to determine the importance of TGFβ in the aggravation of Li-NDI.

In **chapter 9**, we showed that flow-mediated purinergic signaling also reduced AQP2 abundance. MpkCCD cell were grown under shaking and non-shaking conditions and in the presence or absence of a selective adenosine receptor antagonist. Flow mediated AQP2 downregulation was only seen in the untreated samples. Purinergic signaling mediated by extracellular nucleotides opposes the action of AVP on renal collecting duct by decreasing the cellular cAMP and thus AQP2 protein levels. This was also shown in *ex-vivo* studies of AVP stimulated rat inner medullary collecting ducts that were perfused with ATP and resulted in reduced intracellular cAMP levels and

subsequent reduced water permeability (58). In addition, Kishore et al. studied the potential involvement of ATP/UTP-activated $P2Y_2$ receptor in lithium-induced NDI in rats, and showed that $P2Y_2$ receptor knockout mice are significantly more resistant to develop Li-NDI (59). They also showed that ADP-activated $P2Y_{12}$ receptor is expressed in the kidney, and its blockade by the administration of clopidogrel bisulfate ameliorates Li-induced NDI in rodents. These findings indicate that by targeting the purinergic signalling pathway, we might enhance the sensitivity of the kidney to AVP action to reduces the severity of Li-NDI.

Lithium-induced renal interstitial fibrosis

Besides the effect of lithium on the urinary concentrating ability, long-term lithium treatment results in the development of renal interstitial fibrosis that is a hallmark and common outcome in the development of chronic kidney disease (CKD). The final stage of CKD is end stage renal disease (ESRD), which is defined by a complete loss of kidney function. Such patients can only be treated by either dialysis or transplantation (60). The decay in renal function is highly dose-dependent and can be ameliorated by close monitoring of serum Li-concentrations in patients (61, 62). Approximately 1.5% of lithium-users develop ESRD, which is six to eight times more frequent than in the general population (60, 63, 64). To fully understand the development of lithium-induced renal fibrosis, the use of animal models is essential. Therefore, we performed a proof of principle experiment in **chapter 7** to determine whether, upon administration of diet-contained lithium to pregnant mice and to pups after weaning, would lead to renal fibrosis after 40 weeks of lithium treatment. We have shown that the most-commonly used mouse model C57BL/6, which is already extensively used to study Li-NDI, develops interstitial fibrosis when mothers and subsequent pups are treated with a lithium dose that yields clinically-relevant blood lithium levels. We furthermore showed that the histological and molecular changes with lithium-induced interstitial fibrosis formation is alike that found in lithium using patients, indicating that this approach allows the usage of C57Bl6 mice as a model to uncover the underlying mechanism, and to identify ways to prevent or treat, human Li-induced renal fibrosis and, possibly, ESRD. Furthermore, based on our data shown in **chapter 7** and the extensive literature data on fibrosis development (65-67), the following order of lithium-induced fibrosis formation is anticipated. Lithium-induced interstitial fibrosis is likely initiated in the principal cells that release chemotactic factors that affects the glycocalyx layer on the surface of endothelial cells. Then, adhesion molecules that are expressed on the cell surface of endothelial cells bind and facilitate the entrance of monocytes into the interstitium, where they differentiate into macrophages. Epithelial cells, macrophages and endothelial cells then produce TGFβ, which stimulates the proliferation and conversion of fibroblasts into myofibroblasts. Myofibroblasts are extracellular matrix-producing cells that deposit collagen in the interstitium (Figure 5).

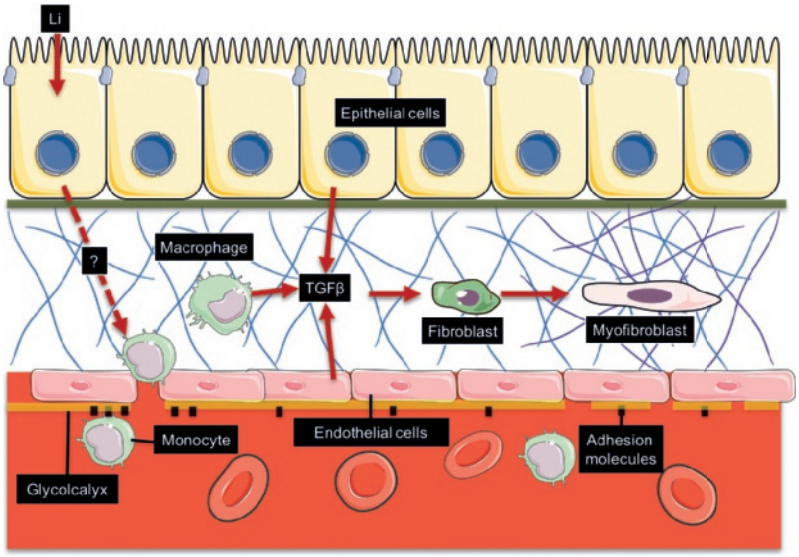

Figure 5. Proposed mechanism by which lithium may induce renal interstitial fibrosis. The mechanism by which lithium induces interstitial fibrosis is poorly understood. However, we can postulate the following model: after entry of lithium in the principal cells, an (inflammatory)process is initiated that results in the release of chemotactic substances, which affect the glycocalyx layer on the surface of endothelial cells. Subsequently, adhesion molecules that are also expressed on the cell surface of endothelial cells bind monocytes that enter the interstitial space and differentiate to macrophages. Epithelial cells, macrophages and endothelial cells produce TGFβ, which stimulates the proliferation and conversion into fibroblasts into myofibroblasts that produces extracellular matrix proteins such as collagen and lead to the observed fibrosis.

Concluding remarks

In this thesis, I studied the molecular mechanisms involved in the pathophysiology of lithium-induced nephrogenic diabetes insipidus. We found that besides proliferation, lithium also alters the metabolism of principal cells by inducing aerobic glycolysis and glutaminolysis. Targeting glycolysis did not rescue lithium induced AQP2 down-regulation in mice but targeting glutaminolysis might still be an interesting target that might eventually lead to novel treatment for Li-NDI. We also explored the use acetazolamide as an alternative treatment for Li-NDI and found that this drug has similar effects as hydrochlorothiazide and amiloride in the inhibition of Li-NDI but with fewer side effects. We also found that AQP2 abundance was the highest in the G0 phase of the cell cycle and was strongly reduced even in the G1 phase. Thus, targeting the cell cycle is not recommended as cell cycle inhibitors usually have major side

effects and probably inhibit the cell cycle in later phases and therefore, will not rescue AQP2. Finally, we were also able to set up for the first time an experimental condition that resulted in the development of interstitial fibrosis in mice. The application of this model will allow mechanistic research into the cause of lithium induced interstitial fibrosis.

References

1. Christensen BM, Kim YH, Kwon TH, Nielsen S. Lithium treatment induces a marked proliferation of primarily principal cells in rat kidney inner medullary collecting duct. Am J Physiol Renal Physiol. 2006;291(1):F39-48.
2. de Groot T, Alsady M, Jaklofsky M, Otte-Holler I, Baumgarten R, Giles RH, et al. Lithium causes G2 arrest of renal principal cells. J Am Soc Nephrol. 2014;25(3):501-10.
3. Lunt SY, Vander Heiden MG. Aerobic glycolysis: meeting the metabolic requirements of cell proliferation. Annu Rev Cell Dev Biol. 2011;27:441-64.
4. Li C, Zhang G, Zhao L, Ma Z, Chen H. Metabolic reprogramming in cancer cells: glycolysis, glutaminolysis, and Bcl-2 proteins as novel therapeutic targets for cancer. World J Surg Oncol. 2016;14(1):15.
5. Weiner ID, Verlander JW. Renal ammonia metabolism and transport. Compr Physiol. 2013;3(1):201-20.
6. Berns K, Hijmans EM, Mullenders J, Brummelkamp TR, Velds A, Heimerikx M, et al. A large-scale RNAi screen in human cells identifies new components of the p53 pathway. Nature. 2004;428(6981):431-7.
7. Martens-de Kemp SR, Nagel R, Stigter-van Walsum M, van der Meulen IH, van Beusechem VW, Braakhuis BJ, et al. Functional genetic screens identify genes essential for tumor cell survival in head and neck and lung cancer. Clin Cancer Res. 2013;19(8):1994-2003.
8. Kyllonen MS, Parkkila S, Rajaniemi H, Waheed A, Grubb JH, Shah GN, et al. Localization of carbonic anhydrase XII to the basolateral membrane of H+-secreting cells of mouse and rat kidney. The journal of histochemistry and cytochemistry : official journal of the Histochemistry Society. 2003;51(9):1217-24.
9. Gut MO, Parkkila S, Vernerova Z, Rohde E, Zavada J, Hocker M, et al. Gastric hyperplasia in mice with targeted disruption of the carbonic anhydrase gene Car9. Gastroenterology. 2002;123(6):1889-903.
10. Saarnio J, Parkkila S, Parkkila AK, Waheed A, Casey MC, Zhou XY, et al. Immunohistochemistry of carbonic anhydrase isozyme IX (MN/CA IX) in human gut reveals polarized expression in the epithelial cells with the highest proliferative capacity. The journal of histochemistry and cytochemistry : official journal of the Histochemistry Society. 1998;46(4):497-504.
11. Parkkila S, Parkkila AK, Saarnio J, Kivela J, Karttunen TJ, Kaunisto K, et al. Expression of the membrane-associated carbonic anhydrase isozyme XII in the human kidney and renal tumors. JHistochemCytochem. 2000;48(12):1601-8.
12. Schwartz GJ, Kittelberger AM, Watkins RH, O'Reilly MA. Carbonic anhydrase XII mRNA encodes a hydratase that is differentially expressed along the rabbit nephron. Am J Physiol Renal Physiol. 2003;284(2):F399-410.
13. Tostain J, Li G, Gentil-Perret A, Gigante M. Carbonic anhydrase 9 in clear cell renal cell carcinoma: a marker for diagnosis, prognosis and treatment. Eur J Cancer. 2010;46(18):3141-8.
14. Wykoff CC, Beasley NJ, Watson PH, Turner KJ, Pastorek J, Sibtain A, et al. Hypoxia-inducible expression of tumor-associated carbonic anhydrases. Cancer research. 2000;60(24):7075-83.
15. Vander Heiden MG, Cantley LC, Thompson CB. Understanding the Warburg effect: the metabolic requirements of cell proliferation. Science. 2009;324(5930):1029-33.
16. Supuran CT. Carbonic anhydrases: novel therapeutic applications for inhibitors and activators. Nat Rev Drug Discov. 2008;7(2):168-81.
17. Dorai T, Sawczuk IS, Pastorek J, Wiernik PH, Dutcher JP. The role of carbonic anhydrase IX overexpression in kidney cancer. European journal of cancer. 2005;41(18):2935-47.
18. Svastova E, Zilka N, Zat'ovicova M, Gibadulinova A, Ciampor F, Pastorek J, et al. Carbonic anhydrase IX reduces E-cadherin-mediated adhesion of MDCK cells via interaction with beta-catenin. Experimental cell research. 2003;290(2):332-45.
19. Kroemer G, Pouyssegur J. Tumor cell metabolism: cancer's Achilles' heel. Cancer cell. 2008;13(6):472-82.
20. Gordan JD, Thompson CB, Simon MC. HIF and c-Myc: sibling rivals for control of cancer cell metabolism and proliferation. Cancer Cell. 2007;12(2):108-13.
21. Kaldis P, Pagano M. Wnt signaling in mitosis. Dev Cell. 2009;17(6):749-50.
22. Magistroni R, Boletta A. Defective glycolysis and the use of 2-deoxy-D-glucose in polycystic kidney disease: from animal models to humans. J Nephrol. 2017;30(4):511-9.
23. Markowitz GS, Radhakrishnan J, Kambham N, Valeri AM, Hines WH, D'Agati VD. Lithium nephrotoxicity: a progressive combined glomerular and tubulointerstitial nephropathy. J Am Soc Nephrol. 2000;11(8):1439-48.

24. Happe H, Leonhard WN, van der Wal A, van de Water B, Lantinga-van Leeuwen IS, Breuning MH, et al. Toxic tubular injury in kidneys from Pkd1-deletion mice accelerates cystogenesis accompanied by dysregulated planar cell polarity and canonical Wnt signaling pathways. Hum Mol Genet. 2009;18(14):2532-42.
25. Padfield PL, Park SJ, Morton JJ, Braidwood AE. Plasma levels of antidiuretic hormone in patients receiving prolonged lithium therapy. Br J Psychiatry. 1977;130:144-7.
26. Zittema D, Boertien WE, van Beek AP, Dullaart RP, Franssen CF, de Jong PE, et al. Vasopressin, copeptin, and renal concentrating capacity in patients with autosomal dominant polycystic kidney disease without renal impairment. Clin J Am Soc Nephrol. 2012;7(6):906-13.
27. van Gastel MDA, Torres VE. Polycystic Kidney Disease and the Vasopressin Pathway. Ann Nutr Metab. 2017;70 Suppl 1:43-50.
28. Torres VE, Chapman AB, Devuyst O, Gansevoort RT, Grantham JJ, Higashihara E, et al. Tolvaptan in patients with autosomal dominant polycystic kidney disease. N Engl J Med. 2012;367(25):2407-18.
29. Plenge P. Acute lithium effects on rat brain glucose metabolism - in vivo. Int Pharmacopsychiatry. 1976;11(2):84-92.
30. Taher M, Leen WG, Wevers RA, Willemsen MA. Lactate and its many faces. Eur J Paediatr Neurol. 2016;20(1):3-10.
31. Machado-Vieira R, Zanetti MV, Otaduy MC, De Sousa RT, Soeiro-de-Souza MG, Costa AC, et al. Increased Brain Lactate During Depressive Episodes and Reversal Effects by Lithium Monotherapy in Drug-Naive Bipolar Disorder: A 3-T 1H-MRS Study. J Clin Psychopharmacol. 2017;37(1):40-5.
32. Chu WJ, Delbello MP, Jarvis KB, Norris MM, Kim MJ, Weber W, et al. Magnetic resonance spectroscopy imaging of lactate in patients with bipolar disorder. Psychiatry Res. 2013;213(3):230-4.
33. Callaly E, Walder K, Morris G, Maes M, Debnath M, Berk M. Mitochondrial dysfunction in the pathophysiology of bipolar disorder: effects of pharmacotherapy. Mini Rev Med Chem. 2015;15(5):355-65.
34. Lee JW, Alsady M, Chou CL, de Groot T, Deen PMT, Knepper MA, et al. Single-tubule RNA-Seq uncovers signaling mechanisms that defend against hyponatremia in SIADH. Kidney Int. 2017.
35. Dickson MA, Schwartz GK. Development of cell-cycle inhibitors for cancer therapy. Curr Oncol. 2009;16(2):36-43.
36. Faivre S, Kroemer G, Raymond E. Current development of mTOR inhibitors as anticancer agents. Nat Rev Drug Discov. 2006;5(8):671-88.
37. Gao Y, Romero-Aleshire MJ, Cai Q, Price TJ, Brooks HL. Rapamycin inhibition of mTORC1 reverses lithium-induced proliferation of renal collecting duct cells. Am J Physiol Renal Physiol. 2013;305(8):F1201-8.
38. Kortenoeven ML, Schweer H, Cox R, Wetzels JF, Deen PM. Lithium reduces aquaporin-2 transcription independent of prostaglandins. Am J Physiol Cell Physiol. 2012;302(1):C131-40.
39. Rao R, Zhang MZ, Zhao M, Cai H, Harris RC, Breyer MD, et al. Lithium treatment inhibits renal GSK-3 activity and promotes cyclooxygenase 2-dependent polyuria. Am J Physiol Renal Physiol. 2005;288(4):F642-9.
40. Norregaard R, Tao S, Nilsson L, Woodgett JR, Kakade V, Yu AS, et al. Glycogen synthase kinase 3alpha regulates urine concentrating mechanism in mice. Am J Physiol Renal Physiol. 2015;308(6):F650-60.
41. Stamos JL, Weis WI. The beta-catenin destruction complex. Cold Spring Harb Perspect Biol. 2013;5(1):a007898.
42. Takahashi-Yanaga F, Sasaguri T. GSK-3beta regulates cyclin D1 expression: a new target for chemotherapy. Cell Signal. 2008;20(4):581-9.
43. Diehl JA, Cheng M, Roussel MF, Sherr CJ. Glycogen synthase kinase-3beta regulates cyclin D1 proteolysis and subcellular localization. Genes Dev. 1998;12(22):3499-511.
44. Christensen BM, Marples D, Kim YH, Wang W, Frokiaer J, Nielsen S. Changes in cellular composition of kidney collecting duct cells in rats with lithium-induced NDI. Am J Physiol Cell Physiol. 2004;286(4):C952-64.
45. Ecelbarger CA. Lithium treatment and remodeling of the collecting duct. Am J Physiol Renal Physiol. 2006;291(1):F37-8.
46. Kling MA, Fox JG, Johnston SM, Tolkoff-Rubin NE, Rubin RH, Colvin RB. Effects of long-term lithium administration on renal structure and function in rats. A distinctive tubular lesion. Lab Invest. 1984;50(5):526-35.

47. Ottosen PD, Nyengard JR, Jacobsen NO, Christensen S. A morphometric and ultrastructural study of lithium-induced changes in the medullary collecting ducts of the rat kidney. Cell Tissue Res. 1987;249(2):311-5.
48. Jacobsen NO, Olesen OV, Thomsen K, Ottosen PD, Olsen S. Early changes in renal distal convoluted tubules and collecting ducts of lithium-treated rats: light microscopy, enzyme histochemistry, and 3H-thymidine autoradiography. Lab Invest. 1982;46(3):298-305.
49. de Groot T, Sinke AP, Kortenoeven ML, Alsady M, Baumgarten R, Devuyst O, et al. Acetazolamide Attenuates Lithium-Induced Nephrogenic Diabetes Insipidus. J Am Soc Nephrol. 2016;27(7):2082-91.
50. Weiner ID, Leader JP, Bedford JJ, Verlander JW, Ellis G, Kalita P, et al. Effects of chronic lithium administration on renal acid excretion in humans and rats. Physiol Rep. 2014;2(12).
51. Bagnis C, Marshansky V, Breton S, Brown D. Remodeling the cellular profile of collecting ducts by chronic carbonic anhydrase inhibition. Am J Physiol Renal Physiol. 2001;280(3):F437-48.
52. Welsh-Bacic D, Nowik M, Kaissling B, Wagner CA. Proliferation of acid-secretory cells in the kidney during adaptive remodelling of the collecting duct. PLoS One. 2011;6(10):e25240.
53. Dafnis E, Kurtzman NA, Sabatini S. Effect of lithium and amiloride on collecting tubule transport enzymes. The Journal of pharmacology and experimental therapeutics. 1992;261(2):701-6.
54. Eiam-Ong S, Dafnis E, Spohn M, Kurtzman NA, Sabatini S. H-K-ATPase in distal renal tubular acidosis: urinary tract obstruction, lithium, and amiloride. The American journal of physiology. 1993;265(6 Pt 2): F875-80.
55. Kortenoeven ML, Li Y, Shaw S, Gaeggeler HP, Rossier BC, Wetzels JF, et al. Amiloride blocks lithium entry through the sodium channel thereby attenuating the resultant nephrogenic diabetes insipidus. Kidney Int. 2009;76(1):44-53.
56. Christensen BM, Zuber AM, Loffing J, Stehle JC, Deen PM, Rossier BC, et al. alphaENaC-mediated lithium absorption promotes nephrogenic diabetes insipidus. J Am Soc Nephrol. 2011;22(2):253-61.
57. Kunnen SJ, Leonhard WN, Semeins C, Hawinkels L, Poelma C, Ten Dijke P, et al. Fluid shear stress-induced TGF-beta/ALK5 signaling in renal epithelial cells is modulated by MEK1/2. Cell Mol Life Sci. 2017; 74(12):2283-98.
58. Kishore BK, Chou CL, Knepper MA. Extracellular nucleotide receptor inhibits AVP-stimulated water permeability in inner medullary collecting duct. Am J Physiol. 1995;269(6 Pt 2):F863-9.
59. Kishore BK, Carlson NG, Ecelbarger CM, Kohan DE, Muller CE, Nelson RD, et al. Targeting renal purinergic signalling for the treatment of lithium-induced nephrogenic diabetes insipidus. Acta Physiol (Oxf). 2015;214(2):176-88.
60. Aiff H, Attman PO, Aurell M, Bendz H, Schon S, Svedlund J. End-stage renal disease associated with prophylactic lithium treatment. Eur Neuropsychopharmacol. 2014;24(4):540-4.
61. Gupta S, Kripalani M, Khastgir U, Reilly J. Management of the renal adverse effects of lithium. Advances in psychiatric treatment. 2013;19:457–66.
62. Grandjean EM, Aubry JM. Lithium: updated human knowledge using an evidence-based approach: part III: clinical safety. CNS Drugs. 2009;23(5):397-418.
63. Bendz H, Schon S, Attman PO, Aurell M. Renal failure occurs in chronic lithium treatment but is uncommon. Kidney Int. 2010;77(3):219-24.
64. Alsady M, Baumgarten R, Deen PM, de Groot T. Lithium in the Kidney: Friend and Foe? J Am Soc Nephrol. 2016;27(6):1587-95.
65. Bonventre JV, Yang L. Cellular pathophysiology of ischemic acute kidney injury. J Clin Invest. 2011;121(11): 4210-21.
66. Eddy AA. Molecular basis of renal fibrosis. Pediatr Nephrol. 2000;15(3-4):290-301.
67. Wynn TA, Ramalingam TR. Mechanisms of fibrosis: therapeutic translation for fibrotic disease. Nat Med. 2012;18(7):1028-40.

Chapter 11

Nederlandse samenvatting

Inleiding

Elke dag filtreren onze nieren ongeveer 170-180 liter bloed. Als deze grote volumes ultrafiltraat onveranderd als urine zouden worden uitgescheiden zou het nodig zijn om grote hoeveelheden water en zouten in te nemen om in balans te blijven. Dit wordt voorkomen door de selectieve reabsorptie van water, zouten en andere bloedbestanddelen uit het filtraat dat langs het nefron stroomt. Het reguleren van waterhomeostase vindt plaats in de hoofdcellen van de verzamelbuis die het AQP2-waterkanaal bezitten. Toename of afname van de hoeveelheid AQP2 op het celoppervlak heeft directe invloed op urine concentrerend vermogen en daarmee ook de hoeveelheid water in het lichaam. Dus afwijkingen van de hoeveelheid AQP2 kunnen leiden tot ziekten zoals het syndroom van inadequate secretie van antidiuretisch hormoon (SIADH) of nefrogene diabetes insipidus (NDI). De meest voorkomende vorm van NDI is verkregen en is een bijwerking van lithium, dat als behandeling aan bipolaire patiënten wordt gegeven. Het doel van dit proefschrift was meer inzicht krijgen in de pathofysiologische mechanismen die betrokken zijn bij de ontwikkeling van renale bijwerkingen van lithium. Daarnaast zijn nieuwe mogelijkheid onderzocht om Li-NDI te behandelen.

Lithium verlaagt de verhouding hoofdcellen tot intercalaire cellen in de verzamelbuis

Zoals hierboven gemeld, is de regulatie van AQP2 waterkanalen in de luminale membraan van de renale hoofdcellen essentieel voor de urine concentrerend vermogen. Ongeveer 20% van de patiënten die lithium behandeling krijgt, ontwikkelt NDI waarbij de urine concentrerend vermogen van de patiënten verstoord raakt. Lithium-geïnduceerde NDI wordt veroorzaakt door een verlaging in de hoeveelheid van het AQP2 eiwit. Daarnaast wordt de ziekte erger door een verlaagde percentage hoofdcellen in de verzamelbuis. Het is echter verrassend dat lithium proliferatie van voornamelijk de hoofdcellen induceert. In **hoofdstuk 2** hebben we onderzoek gedaan naar hoe lithium-geïnduceerde proliferatie gepaard kan gaan met een verlaagd percentage aan hoofdcellen. Dit hebben we bestudeerd in 2D en 3D gekweekte nier cellen die afkomstig zijn van verzamelbuizen (mpkCCD-cellen) van muizen en dieren experimenten in muizen. Dit zijn muizen die behandeld werden met klinisch relevante lithiumconcentraties. We hebben het effect van lithium op de celcyclus bestudeerd met behulp van DNA-beeldcytometrie en door te immunoblotten voor eiwitten van verschillende celcyclusstadia. In deze studie laten we zien dat lithium inderdaad proliferatie van mpkCCD-cellen induceert. Maar dit leidt ook tot een verhoogde G2/S-fase verhouding, wat een G2/M-fase stop aangeeft. De muizen werden gedurende 4, 7, 10 of 13 dagen behandeld met lithium. Deze muizen ontwikkelden NDI (polyurie, verminderde osmolaliteit van de urine en AQP2 verlaging) en lieten veel PCNA-positieve hoofdcellen in de papilla zien. Opmerkelijk was dat 30-40% van de PCNA-positieve

hoofdcellen ook kleurden voor pHistone-H3, een late G2/M-fase-marker. Onze resultaten tonen dus aan dat lithiumbehandeling de proliferatie van renale hoofdcellen initieert, maar dat een significant percentage wordt geremd in de late G2-cyclusfase, wat een verklaring biedt voor de verminderde hoofdcel percentage.

Wij zijn echter van mening dat de remming van de hoofdcellen in de G2-fase niet de enige factor is die leidt tot de remodeling van de verzamelbuis. Verschillende eerdere onderzoeken hebben aangetoond dat de lithiumbehandeling van ratten het aantal cellen, voornamelijk intercalaire cellen, in de verzamelbuis verhoogd. Waarom intercalaire cellen prolifereren is nog niet bekend. Een belangrijke stimulus zou de ontwikkeling van metabole acidose zijn, die vaak, maar niet altijd, waargenomen wordt bij lithiumbehandeling van knaagdieren. Een toestand van metabole acidose verhoogt het aantal α-intercalaire cellen als een adaptieve respons. Eerdere studies suggereren dat lithium geïnduceerde metabole acidose en verzamelbuis remodeling veroorzaakt worden door een directe remming van H^+-ATPase en H^+/K^+-ATPase die in de intercalaire cellen tot expressie worden gebracht. Recentere data laten echter zien dat dit niet waar kan zijn om de volgende redenen: in het experiment van Kortenoeven en anderen (2009), is amiloride, die de toegang van lithium tot de hoofdcellen remt, niet alleen Li-NDI tegen gegaan maar ook verzamelbuis remodeling. Bovendien was de hoeveelheid H^+-ATPase, een markereiwit voor α-intercalaire cellen, niet verhoogd bij lithium behandelde ENaC-KO muizen. Deze studies suggereren dus dat lithium geïnduceerde remodeling van de verzamelbuis een direct effect is van lithium in de hoofdcellen. In **hoofdstuk 4** van dit proefschrift tonen we aan dat lithium aerobe glycolyse induceert in hoofdcellen, een proces dat gepaard gaat met een verhoogde productie van lactaat en waterstof. Zodanig kan de toename aan het aantal α-intercalaire cellen dus ook een gevolg zijn van de zuurafgifte tijdens aerobe glycolyse. In het kort, de remodeling van de verzamelbuis door lithium kan verklaard worden door een stabiele populatie van hoofdcellen, die gedeeltelijk geremd zijn in de G2-fase van de celcyclus en delende populatie intercalaire cellen als gevolg van lithium geïnduceerde aerobe glycolyse.

De impact van aerobe glycolyse op lithium-geïnduceerde nierpathologie

Lithium-geïnduceerde metabole herprogrammering van hoofdcellen

Eerder hebben anderen en wij aangetoond dat lithium de hoofdcellen binnenkomt door het epitheliale natrium-kanaal (ENaC). Eenmaal binnen de hoofdcel induceert lithium proliferatie van de hoofdcellen. In **hoofdstuk 4** van dit proefschrift laten we *in vitro* en *in vivo* data zien die aangeeft dat lithium-geïnduceerde proliferatie gepaard gaat met metabole veranderingen richting aerobe glycolyse en glutaminolyse. Lithium behandeling induceerde een toename *(in vitro)* en afgifte *(in vivo)* van lactaat die afwezig zijn in muizen die ENaC eiwit niet bezitten. De NMR-analyse toont verder aan

dat lithiumbehandeling sterk de urine niveaus van succinaat, fumaraat en citraat verhoogde. Het is bekend dat deze metabolieten verhoogd zijn tijdens een proces genaamd glutaminolyse. Tijdens aerobe glycolyse wordt glutaminolyse verhoogd omdat glutamine afbraak de cel voorziet van stikstof en citraat, die nodig zijn voor aminozuren en lipiden synthese, respectievelijk. Bovendien vindt tijdens aerobe glycolyse verhoogde intracellulaire zuurproductie plaats. Tijdens glutaminolyse komen twee moleculen NH_3 vrij die de vrijgekomen H^+ bufferen.

Onze *in vitro* experimenten met siRNA- en behandeling met carboanhydrasen (CA) remmers van mpkCCD-cellen laten zien dat van de acht CA-en die aanwezig zijn in mpkCCD-cellen CA9 en tot op zekere hoogte CA12 voornamelijk betrokken zijn bij de effecten van lithium. CA9 en -12 bevinden zich normaal gesproken op de basolaterale membraan van epitheelcellen, maar lijken sterk verhoogd te zijn in de plasmamembranen van delende cellen. CA9 wordt nauwelijks tot expressie gebracht in gezonde nieren. Maar CA9 en CA12 expressie zijn aanmerkelijk verhoogd in renale carcinomen. Deze eiwitten vergemakkelijken de groei van tumorcellen door de vrijgekomen zuren te neutraliseren die tijdens aerobe glycolyse vrijkomen. Helaas remde de remming van aerobe glycolyse met 2DG Li-NDI niet. *In vitro* ging 2DG de Li-geïnduceerde down-regulatie van AQP2 tegen. *In vivo,* werd de excretie van lactaat in de urine genormaliseerd, wat aanduidt dat aerobe glycolyse geremd werd door 2DG in onze experimenten. Echter werden succinaat, fumaraat, citraat en ammonium niet verlaagd door 2DG, wat aangeeft dat 2DG glutaminolyse niet remde. Toekomstige studies zouden zich op de mogelijke rol van glutaminolyse moeten richten waarbij de remming hiervan mogelijk de pathogenese van Li-NDI tegen kan gaan.

Impact van de celcyclus op de expressie van AQP2

Zoals eerder aangegeven, veroorzaakt lithiumbehandeling verlaging in hoeveelheid AQP2 in de hoofdcellen van de verzamelbuis. Deze verlaging gaat gepaard met proliferatie en metabole switch richting aerobe glycolyse. Hoewel de impact van aerobic glycolyse op AQP2 verlaging nu onwaarschijnlijk lijkt, was de invloed van cel proliferatie op de expressie van AQP2 nog niet bepaald. Terwijl we de pathofysiologie van SIADH onderzochten in **hoofdstuk 8,** vonden we dat AQP2 eiwit expressie het hoogste was in de G0-fase en sterk gereduceerd was in alle andere fasen van de celcyclus. Deze resultaten zijn niet alleen van belang om de rol van de celcyclus bij SIADH te begrijpen maar ook belangrijk om de pathogenese van Li-NDI te snappen aangezien lithium ook proliferatie induceert in de hoofdcellen. In **hoofdstuk 8** gebruiken we methoden van de systeembiologie om bij een rattenmodel van SIADH cascades te identificeren die betrokken zijn bij de ontwikkeling van de ziekte. Door het inplanteren van minipompen die constant vasopressine afgeven en verhoogde water opname in voedsel ontstaat een fenomeen dat vasopressine-escape wordt genoemd

waarbij AQP2 verlaagd wordt ook al is vasopressine niveau hoog. Veranderingen op transcriptie niveau werden in deze model in kaart gebracht en bleek dat cascades die belangrijk zijn bij de overgang van Go naar de celcyclus sterk verhoogd waren. Hierdoor lijk het remmen van eiwitten die betrokken zijn bij celdeling een logische en aantrekkelijke keuze lijkt om Li-NDI tegen te gaan. Maar onze data laten zien dat het geen zin heeft om te investeren in blokkers voor dit proces. Dit komt doordat proliferatie remmers de celcyclus stoppen in de G1 of latere fasen. Maar voor het behouden van een hoge AQP2 eiwit expressie moeten de cellen in de Go fase blijven, wat niet mogelijk is met huidige celcyclus blokkers.

Verergering van Li-NDI door shear-stress

Verminderde AQP2 in de verzamelbuis resulteert in een verhoogde waterstroom die NDI-ontwikkeling zou kunnen verergeren. Kunnen en anderen (2017) lieten zien dat shear-stress, geïnduceerd door verhoogde flow, leidt tot de activatie van de TGFβ signalering cascade in renale epitheelcellen. In **hoofdstuk 8** tonen we aan dat TGFβ AQP2 eiwit expressie verlaagd. Aldus kan de verhoogde flow de activering van TGFβ cascade initiëren, wat leidt tot de verlaging van AQP2 en daarmee bijdraagt aan het onvermogen van hoofdcellen om urine te concentreren. Maar de afgifte van TGFβ in de urine als gevolg van verhoogde renale flow en shear-stress is nog niet vastgesteld. Daarom is de bepaling van TGFβ in de urine van Li-NDI-patiënten of knaagdieren van belang om het belang van TGFβ in de verergering van Li -NDI te bepalen.

In **hoofdstuk 9** hebben we verder laten zien dat de flow-gemedieerde purinerge signalering ook invloed heeft op AQP2 eiwit expressie. MpkCCD-cellen worden gekweekt onder statische en schuddende omstandigheden in aanwezigheid of afwezigheid van een selectieve adenosine receptor antagonist. Flow gemedieerde AQP2 downregulatie wordt alleen waargenomen in de onbehandelde condities. Purinerge signalering gemedieerd door extracellulaire nucleotiden gaan de werking van AVP op de hoofdcellen tegen door verlaging van de cellulaire cAMP en dus AQP2 eiwitniveaus. Dit wordt ook aangetoond in een *ex-vivo* studie van AVP gestimuleerde rat verzamelbuizen die waren geperfundeerd met ATP. De onderzoekers zagen een afname in intracellulaire cAMP-niveaus en de daaropvolgende lagere waterpermeabiliteit. Bovendien, bestudeerde Kishore en collega's de mogelijke betrokkenheid van de ATP/UTP geactiveerd $P2Y_2$ receptor in lithium-geïnduceerde NDI bij ratten. Ze toonden aan dat $P2Y_2$ receptor knockout muizen significant resistenter waren tegen de ontwikkeling van Li-NDI. Ze toonden ook aan dat ADP-geactiveerde $P2Y_{12}$ receptor tot expressie wordt gebracht in de nier en de blokkade hiervan door de toediening van clopidogrel bisulfaat Li-geïnduceerde NDI tegen gaat bij knaagdieren. Deze bevindingen geven allemaal het belang purinerge signaleringsroute in de ontwikkeling van Li-NDI.

Lithium-geïnduceerde renale interstitiële fibrose

Naast het effect van lithium op het urine concentratievermogen leidt langdurige lithium behandeling tot het ontwikkelen van renale interstitiële fibrose die een kenmerk is van chronische nierfalen (CKD). De laatste fase van CKD is terminale nierziekte (ESRD), die wordt gedefinieerd door een volledig verlies van nierfunctie. Dergelijke patiënten kunnen alleen behandeld worden met dialyse of transplantatie. Het verval in nierfunctie is sterk dosisafhankelijk en kan worden verbeterd door zorgvuldige controle van serum Li-concentraties bij patiënten. Ongeveer 1,5% lithium-gebruikers ontwikkelen ESRD dat zes tot acht keer hoger is dan bij de algemene populatie. Om de ontwikkeling van lithium-geïnduceerde nier fibrose volledig te begrijpen, is het gebruik van diermodellen essentieel. In **hoofdstuk 7** tonen we aan dat het meest gebruikte muismodel, C57BL/6, gebruikt kan worden om Li-CKD te bestuderen. Lithium-geïnduceerde interstitiële fibrose wordt waarschijnlijk geïnitieerd in de hoofdcellen die chemotactische factoren uitscheiden die de glycocalyx laag op het oppervlak van endotheelcellen aantasten. Vervolgens zou de expressie van adhesiemoleculen op het oppervlak van endotheelcellen verhoogd worden waardoor monocyten makkelijker aan de endotheelcellen binden en het interstitium binnentreden en differentiëren tot macrofagen. Epitheelcellen, macrofagen en endotheelcellen scheiden dan TGFβ af die de proliferatie en de transformatie van fibroblasten tot myofibroblasten stimuleren. Myofibroblasten produceren colageen in het interstitium wat uiteindelijk tot functieverlies in de niet leidt.

De behandeling van Li-NDI?

Om Li-NDI te verminderen, worden bipolaire patiënten behandeld met thiazide/amiloride, waarvan wordt gedacht dat ze antidiurese induceren door een compensatoire verhoogde pro-urine opname in proximale tubuli. Maar thiazide induceerde ook een antidiurese bij lithium-NDI-muizen zonder de natriumchloride-co-transporter (NCC) en maakte hun urine basaal. Dit suggereert dat de remming van carboanhydrasen door thiazide de mogelijk oorzaak kan zijn van de gunstige effect van thiazide. Daarom besloten we in **hoofdstuk 3** het effect van de CA-specifieke blokker, acetazolamide, in lithium-NDI te bestuderen.

Acetazolamide ging, in mpkCCD-cellen het effect van lithium op AQP2 verlaging tegen. Behandeling van lithium-NDI-muizen met acetazolamide of thiazide/amiloride onthulde een vergelijkbare antidiurese, verhoogde urine osmolaliteit en verhoogde hoeveelheid AQP2. Onze data wijzen erop dat de waargenomen antidiurese en verminderde GFR met acetazolamide het gevolg is van een tubulaire glomerulaire feedbackrespons veroorzaakt door de remming van carboanhydrasen in de proximale tubulus. Met thiazide/amiloride behandelde muizen hadden ook hyponatriëmie, hyperkaliëmie, hypercalciëmie, metabole acidose en verhoogde serumlithiumconcentraties. Deze bijwerkingen worden ook waargenomen bij patiënten, maar werden niet

gezien bij met acetazolamide behandelde muizen. Samengevat hebben we aangetoond dat CA-activiteit bijdraagt aan de ontwikkeling van lithium-NDI. Acetazolamide vermindert lithium-geïnduceerde NDI door het induceren van een TGF-reactie en door een direct effect op de cellen van de verzamelbuis. Verder verlaagt acetazolamide lithium-NDI-ontwikkeling vergelijkbaar met thiazide/amiloride, maar met minder bijwerkingen. Of acetazolamide uiteindelijk in de kliniek toegepast zal worden is de vraag. Er zijn ondertussen meerdere humane studies die het effect van acetazolamide hebben bestudeerd waarbij zowel positieve als negatieve uitkomsten waargenomen zijn. Ondertussen blijft amiloride tot heden de beste manier om de effecten van lithium tegen te gaan waarbij, zoals eerder beschreven, de toegang van lithium in de cellen geremd wordt. Hoewel, het effect van amiloride op AQP2 goed is bestudeerd, is het effect van amiloride op andere bijwerkingen van lithium nog niet onderzocht. Daarom kijken we in **hoofdstuk 6** of amiloride, naast het verlagen van Li-NDI, ook metabole acidose en het verlagen in het percentage van hoofdcellen voorkomt. In deze studie zagen we dat amiloride ook hier Li-NDI tegen ging waarbij AQP2 nog wel in de cortex verlaagd werd maar niet de medulla. Bovendien verlaagde amiloride ook de door lithium geïnduceerde proliferatie van hoofdcellen en ging het verzamelbuis remodeling tegen. Lithium induceerde in deze studie geen hypercalciëmie noch had het invloed op de pH van het bloed. Analyse van ammonium in de urine toont aan dat amiloride lithium-geïnduceerde toename in ammonium in de urine verlaagt. Samengevat liet onze studie zien dat amiloride niet alleen de verlaging van AQP2 tegen gaat, maar ook de ontwikkeling van verschillende andere neveneffecten in de nier voorkomt.

Slotopmerkingen

In dit proefschrift, worden de moleculaire mechanismen bestudeerd die betrokken zijn bij de pathofysiologie van lithium geïnduceerde nefrogene diabetes insipidus. We vinden dat naast proliferatie, lithium ook het metabolisme verandert van de hoofdcellen door het induceren van aerobe glycolyse en glutaminolyse. Remmen van glycolyse gaat het lithium geïnduceerde AQP2 downregulatie bij muizen niet tegen. Mogelijk is het remmen glutaminolyse interessant en zou uiteindelijk kunnen leiden tot ontwikkelen van nieuwe middelen om Li-NDI tegen te gaan. Verder hebben we het gebruik van acetazolamide als een alternatieve behandeling voor Li-NDI onderzocht en vonden dat deze middel eenzelfde effect heeft als hydrochloorthiazide en amiloride in de remming van Li-NDI, maar met minder bijwerkingen. We vonden ook dat AQP2 eiwit expressie het hoogste was in de G0 fase van de celcyclus en sterk werd gereduceerd in alle andere fasen. Ten slotte konden we ook voor het eerst een experimentele conditie opstellen die resulteerde in de ontwikkeling van interstitiële fibrose bij muizen. De toepassing van dit model zal mechanistisch onderzoek mogelijk maken naar de oorzaak van lithium-geïnduceerde interstitiële fibrose.

Chapter 12

List of abbreviations

List of publications

Curriculum vitae

Research data management

RIMLS portfolio

List of abbreviations

A

AQP2	Aquaporin-2
ADP	Adenosine diphosphate
AMP	Adenosine monophosphate
ANOVA	Analysis of variance
ATP	Adenosine triphosphate
AVP	Arginine vasopressin

C

°C	Degree Celsius
Ca^{2+}	Calcium ion
cAMP	Cyclic AMP
cDNA	Complementary DNA
CD	Collecting Duct
CKD	Chronic kidney disease
Cl^-	Chloride
CREB	cAMP responsive element binding protein

D

DI	Diabetes insipidus
DMEM	Dulbecco's modified eagle's medium
DNA	Deoxyribonucleic acid
DTT	Dithiothreitol

E

ECL	Enhanced Chemiluminescence
EDTA	Ethylene diamine tetraacetic acid
eGFR	Estimated glomerular filtration rate
ENaC	Epithelial Na+ channel
ER	Endoplasmic reticulum
ESRD	End stage renal disease

G

GFR	Glomerular filtration rate
GSK	Glycogen synthase kinase

H

HCTZ	Hydrochlorothiazide

I

IB	Immunoblotting
IHC	Immunohistochemistry

K

K^+	Potassium
KDa	Kilo Dalton
KO	Knockout

L

Li^+	Lithium

M

Mg^{2+}	Magnesium
MQ	Milli-Q water
mRNA	Messenger ribonucleic acid

N

Na/K-ATPase	Na^+/K^+ pump
Na^+	Sodium
NCC	NaCl cotransporter
NDI	Nephrogenic diabetes insipidus
NHE3	Na^+/H^+ exchanger type 3

P

PCR	Polymerase chain reaction
PKA	Protein kinase A
PKC	Protein kinase C
RNA	Ribonucleic acid
PNGase F	N-glycosidase F
PT	Proximal tubule
PVDF	Polyvinylidene difluoride

R

RAAS	Renin-angiotensin-aldosterone system
RT-qPCR	Reverse transcriptase quantitative PCR

S

SEM	Standard error of the mean
SIADH	Syndrome of inappropriate antidiuretic hormone secretion
SDS-PAGE	Sodium dodecyl sulfate polyacrylamide gel electrophoresis

W

WT	Wildtype

List of publications

1. de Groot T, **Alsady M**, Jaklofsky M, Otte-Höller I, Baumgarten R, Giles RH and Deen PMT. Lithium causes a G2 cell cycle arrest of renal principal cells. *J Am Soc Nephrol*. 25(3):501-10, 2014.

2. de Groot T, Sinke AP, Kortenoeven ML, **Alsady M**, Baumgarten R, Devuyst O, Loffing J, Wetzels JF, Deen PMT. Acetazolamide Attenuates Lithium-Induced Nephrogenic Diabetes Insipidus. *J Am Soc Nephrol*. 27(7):2082-91, 2015.

3. **Alsady M**, Baumgarten R, Deen PMT, de Groot T. Lithium in the Kidney: Friend and Foe? *J Am Soc Nephrol*. 27(6):1587-95, 2016.

4. Janas S, Seghers F, Schakman O, **Alsady M**, Deen PMT, Vriens J, Tissir F, Nilius B, Loffing J, Gailly P, Devuyst O. TRPV4 is associated with central rather than nephrogenic osmoregulation. *Pflugers Arch*. 468(9):1595-607, 2016

5. **Alsady M**, de Groot T, Kortenoeven MLA, Carmone C, Neijman K, Bekkenkamp-Grovenstein M, Engelke U, Wevers RA, Baumgarten R, Korstanje R, Deen PMT. Lithium induces aerobic glycolysis and glutaminolysis in collecting duct principal cells. *Am J Physiol Renal Physiol*. 2017.

6. Lee JW*, **Alsady M***, Chou CL*, de Groot T, Deen PMT, Knepper MA, Ecelbarger CM, Single-tubule RNA-Seq uncovers signaling mechanisms that defend against hyponatremia in SIADH, *Kidney Int*. 2017.

7. **Alsady M**, van der Tholen L, Carmone C, Bekkenkamp-Grovenstein M, van Gemst J, van den Brand M, van Kuppevelt TH, van der Vlag J, de Groot T and Deen PMT, Long-term lithium treatment causes renal interstitial fibrosis in mice, *submitted*. 2017

8. **Alsady M**, Godefa TM, Bekkenkamp-Grovenstein M, Carmone C, Baumgarten R, Engelke U, Wevers RA, Bedford JJ, Leader JP, Walker RJ and Deen PMT, The succinate receptor 1 has no role in the development of lithium-induced nephrogenic diabetes insipidus, *in prep*. 2017

9. **Alsady M**, de Groot T, Christensen BM, Deen PMT. Amiloride prevents lithium-induced metabolic acidosis and proliferation of collecting duct cells. *in prep*. 2017

10. **Alsady M**, Cockx S, Trimpert C, Kortenoeven MLA, Cornelissen M, Dekker H, Nijenhuis T and Deen PMT, Flow, cell proliferation and microcyst formation in relation to Aquaporin-2, *in prep*. 2017

11. van Diepen JA, Robben JH, Hooiveld GJ, Carmone C, Bekkenkamp-Grovenstein M, **Alsady M**, Hijmans A, Netea MG, Tack CJ, Stienstra R, Deen PMT, SUCNR1-mediated chemotaxis of macrophages aggravates obesity-induced inflammation and diabetes, *Diabetologia*, 60(7):1304-1313, 2017

12. de Groot T, Damen L, Kosse L, **Alsady** M, Doty R, Baumgarten R, Sheehan S, van der Vlag J, Korstanje R, Deen PMT. Lithium reduces blood glucose levels, but aggravates albuminuria in BTBR-ob/ob mice. *PLoS One*, 2017

13. Bongers CCWG, **Alsady M**, Hartman YAG, Eijsvogels TMH, Deen PMT and Hopman MTE. Impact of Acute versus Repetitive Moderate Intensity Endurance Exercise on Kidney Injury Markers. *Physiological reports*, 2017

14. Bongers CCWG, **Alsady M**, Nijenhuis T, Tulp ADM, Eijsvogels TMH, Deen PMT and Hopman MTE. Impact of Acute versus Prolonged Exercise and Dehydration on Kidney Function and Injury. *submitted*, 2017

*Authors contributed equally to this work

Curriculum vitae

Mohammad Alsady was born on 7 April 1987 in Arbil, Iraq. He graduated from high school at the Merletcollege in Grave in 2006. In 2010, he obtained his bachelor in Applied Life Sciences from the HAN University in Nijmegen with a major in medical microbiology and a minor in biochemistry. During his bachelor, he performed three internships, of which two at the department of medical microbiology at the Radboudumc and one internship at the department of zoonosis and environmental microbiology at the dutch national institute for public health and the environment (RIVM) where he investigated the persistence and inactivation of human Norovirus on fresh produce. He then started his master in Biomedical Sciences with two majors at the Radboud University in Nijmegen. For his major in toxicology, Mohammad performed his internship at the department of physiology where he investigated, under the supervision of dr. Theun de Groot and prof. Peter Deen, the cause of reduction of principal cells in lithium-induced nephrogenic diabetes insipidus. For his second major in human pathobiology, Mohammad performed an internship at the chromosome biogenesis research unit, institute for research in immunology and cancer (IRIC) at the université de Montréal in Canada. He investigated nicotinamide metabolism in the human pathogen Candida Albicans that affects cancer patients who receive chemo- or radiotherapy. After obtaining his master in 2013, he joined the department of physiology where he investigated, under the supervision of prof. Peter Deen, the renal side effects of lithium therapy. His work resulted in publications in the highest-ranking journals in the renal field and several presentation awards in national and international congresses.

Research data management

Research data presented in this thesis and obtained during this PhD at the department of Physiology, Radboud university medical center (Radboudumc) were archived according to the Findable, Accessible, Interoperable and Reusable (FAIR) principles. Initially, the data was stored digitally at local server of the department of Physiology and on paper in the form of labjournals. Later, Labguru, a digital lab book, was introduced at our department that replaced the regular labjournals. Both the local server of our department and Labguru are supported by the Information and Communications Technology (ICT) of Radboudumc. Moreover, labguru is daily backed up on the local server of Radboudumc, while data stored on the local servers were weekly backed-up on the servers of the university. The data files on Labguru and the local server are accessible by the associated scientific staff members. Human studies in **Chapters 5** and **9** were conducted according to the principles accepted in the declaration of Helsinki. All participants gave written informed consent to participate in the study. The study protocols, including the data management plan were approved by the associated Medical Ethics Committee of the Radboudumc (**Chapter 9**) and New Zealand (Lower South Regional) Ethics Committee (**Chapter 5**). Animal studies performed in **Chapters 2, 3, 4, 5, 6, 7 and 8** were approved by the Animal Ethical Committees of the associated Universities. All data generated or analyzed in this thesis are included in published articles and its additional files are available from the associated corresponding authors on request. To ensure general accessibility of the data, all files were documented according to the protocol of the department of Physiology.

RIMLS Portfolio

Institute for Molecular Life Sciences
Radboudumc

Name PhD student:	*Mohammad Alsady*	PhD period:	*12-08-2013 – 12-08-2017*
Department:	*Physiology*	Promotors:	*Prof. dr. P.M.T. Deen*
Research School:	*Radboud Institute for Molecular Life Sciences*	Copromotor:	*Dr. T. De Groot*

TRAINING ACTIVITIES	Year(s)	ECTS
a) Courses & Workshops		
- Introduction day Radboudumc	2013	0.50
- RIMLS Graduate Course	2014	2.00
- Winterschool Nierstichting	2015	1.00
- Academic Writing	2015	2.80
- Scientific Integrity course	2015	1.00
b) Seminars & lectures		
- RIMLS Radboud Research Rounds / Lecture Series	2013-2016	0.90
- RIMLS Seminars	2014-2017	1.00
- RIMLS Spotlights / Kidney Theme Meetings *	2015-2017	1.00
- RIMLS Technical Forums	2016	0.20
c) (Inter)national Symposia & Congresses		
- RIMLS Radboud New Frontiers #	2013-2016	1.25
- RIMLS PhD retreat *#	2013-2017	3.75
- NfN Najaarssymposium *	2013	0.50
- ASN Review Utrecht *	2014	0.50
- Dutch Nephrology Days *	2013-2017	2.50
- Radboud Science Day *	2015	0.50
- Benelux Kidney meeting *#	2016	0.75
- ASN Kidney Week *#	2016	1.50
d) Other		
- Organization RIMLS Technical Forum	2016	0.50

TEACHING ACTIVITIES		
e) Lecturing		
- Teaching dentistry course: supervision during computer assignment	2014-2017	0.80
- Teaching dentistry course: supervision during workgroup assignments	2014-2017	1.20
- Teaching medical course: practicum water en zouthuishouding	2014-2017	1.60
- Teaching MMD course: lectures master class	2014, 2016	0.40

f) Students		
- Supervision Master student: Steef Kurtjens	2014	2.00
- Supervision Honours programme: Dewi Blom	2014	1.00
- Supervision Bachelor student: Kim Neijman	2015	2.00
- Supervision Master student: Leunie van der Tholen	2015	2.00
- Supervision Master student: Eva-Leonne Göttgens	2015	2.00
- Supervision Master student: Tesfay Godefa	2015	2.00
- Supervision Master student: Daniela Pinheiro	2016	2.00
- Supervision Master student: Kim Neijman	2016	2.00
- Supervision Honours programme: Sam janssen	2016	1.00
- Supervision Master student Mathijs van Bladel	2017	2.00
TOTAL		**44.15**

Oral and poster presentation are indicated with a * and # after the name of the activity, respectively

Chapter 13

Dankwoord | Acknowledgements

Finally, after finishing all the scientific chapters in this thesis, I can say “Alhamdulilah” (Arabic: Thanks to God). My quest for knowledge started when I was a kid in Baghdad reading the inspiring verses from the holy Quran and sayings of the prophet Muhammed (PBUH) that praised those who seek knowledge. That is when I decided to spend the rest of my life gaining knowledge to help others. However, this thesis never came without the help of many. Therefore, I want to thank everyone who has contributed to this in any way. I would like to mention a number of people, starting with the people that had the biggest impact on my education and PhD.

Father and **mother**, despite the challenging life we had, you always managed to provide me with whatever necessary to succeed in my study. I cannot thank you enough for all the support and love you have given me. You always showed me what is important and what is right in life. I would not be where I am today without your help and support. Thank you for everything! **Father**, your discipline and determination have always been inspirational for achieving all my objectives. **Mother**, thank you for everything especially the attention and patience that you tirelessly showed me during all these years, listening to all my scientific adventures and thoughts. You have sacrificed so much for me and the family and I can never thank you enough for that. Today, it’s not me getting a PhD, but you!

Claudia, meeting you at the department of physiology was the best thing happened to me during my PhD. Although we did not work on the same project, your scientific input was always very valuable to me. Thanks to your advice and help, I was able to finish and publish most of the projects. And then…magic happened…and you turned my life into a magical story. With you, a whole new world opened up for me. We are living from one great event to another. I’m truly blessed to have you in my life and that I’m spending the rest of my life with you. With the birth of our baby girl **Maryam**, we started the nicest and most wonderful chapter in our lives. Thank you so much for being part of my life.

Maryam, my baby girl, before you even entered our world, we waited for you with an enormous amount of love. Now that I can hold you in my arms, no words can explain the happiness and love I have for you in my heart. I look at you with complete wonder and I melt with each sound and move you make. You are the most precious gift from God to us.

Dear **Peter**, thank you for making my PhD research at the Department of Physiology possible. I always admired your great enthusiasm and endless energy. Even after hours of work discussion, you were still unstoppable. As a promoter, you have taught me a lot. Thank you for your trust, your commitment and your guidance.

Theun, my internship supervisor, my co-promotor, and my friend, it was an honor working with you during my master internship and PhD. I learned many things from you. Our efforts resulted in many nice papers and presentation awards. I wish you, **Karolina** and the always smiling **Celina**, a joyful and happy life

Prof. dr, Frans Russel, **prof. dr. Luuk Hilbrands** and **prof. dr. Ewout Hoorn**, thank you for being part of the manuscript committee and reading through my thesis. Also many thanks to **prof. dr. Dorien Peters**, **dr. Rachel Giles** and **dr. Bart Smeets**, for joining the Doctoral Examination Board.

My sincere gratitude also to all collaborators that made the work in this thesis possible. Special thanks to **prof. dr. Mark knepper** from the USA, **prof. dr. Rob Walker**, **dr. Jennifer Bedford** and **dr. John Leader** from New Zealand and **Birgitte Christensen** from Denmark.

Having a caring family is one of the greatest gifts in life. **Mustafa**, my brother, due to the small age difference, you are the only one that can remember many events in our childhood. We have been through good and bad times, and we always managed to go on with a big smile on our faces ☺. Thanks for being always present in all the important steps of my life. Your marriage with **Sara** brought a lot of happiness and joy to our family. **Sara**, thank you for your support during these years, especially with the Dutch summary. **Mutez**, my little brother! You grew up to be much bigger and more muscular than me, but I will keep calling you "little brother". We also have a lot of nice and funny memories that are unforgettable, especially when you put, as a child, an entire field on fire in Iraq to solve the "garbage" problem ☺. I would like to thank you for your sincere interest in my research and for the (sometimes too long ☺) scientific discussions we had in the last years. **Mina**, my little sister, the princess of our house, I still remember how happy we (the three brothers) were the day you were born. Seeing you growing-up in the Netherlands, without any problem is one of the biggest blessings in my life. Thank you for always showing me how proud you were. I wish you a lot of success at the University of Wageningen.

Despite my short stay in Iraq, my grandparents always provided me with great love that I highly appreciated. I also would like to thank my uncles **Kawa**, **Ali**, **Kamaran** and my aunts **Awaz** and **Dilkhwaz** from Arbil and my uncles **Hamid**, **Sami**, **Khalid**, **Riadth** and aunts **Ginan**, **Niran** and **Aswan** from Baghdad for their continuous support.

Also, many thanks to my family in Italy, especially my mother in law **Patrizia**, for her support in the past years. Thank you for taking care of Claudia during the pregnancy. Thanks to you I was able to continue writing and finalizing my thesis.

I would like to thank all my colleagues of the Department of Physiology for their support, both professionally and socially. This thesis was possible in part because of the enthusiastic, international and encouraging environment that exists in the lab. I enjoyed the coffee breaks, the lunches at the canteen, but I certainly also enjoyed working with all of you. Special thanks to **Joost** and **René** for their efforts in realizing this highly organized department.

Omar, my life's companion and my afghan brother, our journey started shortly after our arrival in the Netherlands. Two refugee kids that were determined to make something of their lives. Years later and despite all challenges, we made it brother. Your great optimism was always inspiring. I wish you, **Nargis**, **Asiya** and **Aisha** a happy life and a lot of success in your career.

Sami, Cilia-Man, my Eritrean brother, you, Omar and me, received our master degrees on the same day. Now we will receive our PhD degrees in the same year. Your realistic perspective on things has been very valuable to me. It was incredible how similar our views were on so many things. Good luck in Maastricht and I wish you a lot of success in your career brother.

Selma, although we worked on different projects, I appreciated very much all your useful and critical comments during our osmomeetings. I wish you and Bas a happy and wonderful life and a lot of success in becoming our next clinical chemist at the Radboudumc.

My special thanks go also to all current and former colleagues from the department of physiology, especially **Kim**, **Elja**, **Marjolein**, **Erik**, **Melissa** and **Seng** from the osmoregulation group and **Marco**, **Sabina**, **Hacene**, **Paco**, **Femke**, **Sjoerd**, **Ellen**, **Lauriane**, **Maxime**, **Wilco**, **Jitske**, **Jenny**, **Lisanne**, **Jeroen**, **Steef**, **Andreas**, **Chao, Caro**, **Anique**, and **Eric** from the Ion transport group.

During my PhD, I supervised several students during their bachelor or master internships. Thanks a lot for your help, especially members of the "Dream Team" (**Kim**, **Leunie**, **Eva** and **Tesfay**). Your input was very valuable to my PhD.

I also would like to thank all my friends that supported me during all these years, especially **Yasser, Hemen**, **Yasien, Zain**, **Yahya**, **Pieter, Sarmen**, **Edo**, **Anoush** and **Hassan**.

Finally, I would like to thank "the Netherlands" and its Dutch people for giving me the possibility to make something out of my life.

تأثير دورة الخلية على قنوات المياه (AQP2)

كما ذكر سابقا ، فإن الليثيوم يؤدي إلى انخفاض كمية AQP2 في خلايا ال principal cells لأنبوب التجميع في الكلى. هذا التخفيض يرافقه زيادة في الحث على تكاثر الخلايا و تغيير كبير في طريقة صنع الطاقة الخلوية. على الرغم من هذا فان تأثير ال aerobic glycolysis على كمية قنوات المياه يبدو غير محتمل بما ان العلاج بمادة ال 2DG لم تعيد نسبة قنوات المياه الى النسبة اللتي تعتبر صحية. في **الفصل الثامن**، وجدنا أن نسبة قنوات مياه ال AQP2 كانت الأعلى في مرحلة G0 من دورة التكاثرية للخلايا و لاكن تقلصت إلى حد كبير في جميع المراحل الأخرى من مراحل دورة الخلية. هذه النتائج مهمة ليس فقط لفهم دور دورة الخلية في مرض ال SIADH ولكن أيضا لفهم سبب نقصان ال AQP2 بعد العلاج بالليثيوم. للحفاظ على بروتين ال AQP2 عاليا، يجب أن نبقى الخلايا في مرحلة ال G0، وهو أمر غير ممكن حاليا.

التليف الليفي الكلوي الناجم عن الليثيوم

بالإضافة إلى تأثير الليثيوم على قدرة تركيز البول، فإن العلاج بالليثيوم يؤدي الى التليف الخلالي الكلوي الذي هو سمة من سمات المرض الكلوي المزمن (CKD). المرحلة النهائية من ال CKD هي ال ESRD والتي يخسر خلالها المريض كل وظائف الكلى. والعلاج الوحيد لهؤلاء المرضى هو الغسيل الكلوي أو زرع كلية جديدة. لا يوجد حاليا اى علاج لهذا المرض لاننا ما زلنا لا نفهم كيف يسبب الليثيوم التليف في الكلى، ومن اهم الاسباب التي تصعب البحث في هذا المجال هو غياب نموذج حيواني او خلوي لبحث هذا الموضوع. في **الفصل السابع**، تبين لنا أن الفئران قد تكون النموذج المثالي لدراسة هذا الموضوع. تدل نتائجنا الى ان التليف الكلوي يبدأ من خلايا ال principal cells التي تفرز مواد كيميائية بعد دخول الليثيوم فيها.

هذه المواد الكيميائية تؤثر على طبقة السكرية التي موجودة على سطح الخلايا البطانية للأوعية الدموية. هذا التغيير يسهل دخول الخلايا البلعمية الى النسيج خارج الخلية اللتي تلعب دورا مهما بتحويل الخلية اليفية اليافعة الى خلايا مختلفة تنسج النسيج خارج الخلية والكولاجين. وهذا ما يسبب فقدان الكلية لوضائفها.

علاج ال NDI؟

للحد من ال NDI يتم علاج المرضى الثنائي القطب مع Thiazide او/مع Amiloride، ولكن العلاج بهذه الادوية وخصوصا Thiazide ليس هو الحل المثالي لان نسبة الليثيوم ترتفع الى نسب عالية جدا غير مقبولة طبيا. لهذا يتم مراقبة نسبة الليثيوم في الدم ويتم خفض جرعة الليثيوم لإبقائه في النسبة المقبولة. لهذا درسنا في **الفصل الثالث** امكانية استعمال ال Acetazolamide وقارناها بالأدوية التي تستعمل حاليا. كشفت ابحاثنا بان Acetazolamide يكافح ال NDI مثل الادوية الحالية ولكن دون اي اثار جانبية. هذه النتائج مهمة جدا ولكن لا بد ان تجرى تجارب سريرية قبل قبول هذا العلاج لكل المرضى. الى ذلك الوقت تبقى الادوية الحالية وخاصة Amiloride هي افضل الادوية لعلاج ال NDI خصوصا بعد اكتشافنا في **الفصل السادس**، ان Amiloride يخفض اعراض ال NDI بل وانه أيضا يخفض تحمض البول و إنخفاض نسبة خلايا ال principal cells. بالإختصار، أظهرت دراستنا أن Amiloride ليس فقط يقلل من تخفيض AQP2، ولكن أيضا يمنع تطور مختلف الآثار الجانبية الأخرى في الكلى.

ملاحظات ختامية

في هذا الكتاب، درسنا الآليات الجزيئية والفيزيولوجية التي تشارك في نشئة مرض السكري الكاذب الذي هو من الاعراض الجانبية لليثيوم. تمكنا من الكشف عن اليات جديدة تلعب دورا هاما في تطور هذا المرض وطرحنا انضمة وطرق جديدة لدراسة مرض ال NDI وكيفية معالجته.

مقدمة

تصفي الكلى حوالي ١٨٠ لتر من الدم يوميا. لو أفرزت هذه الكميات الكبيرة في البول دون تغيير لأحتجنا الى كميات كبيرة من الماء والأملاح لإبقاء الجسم في توازن. ولكن الكليون، الذي هو الوحدة الفاعلة الاساسية في الكلية، يمنع خسارة المياه والأملاح وغيرها من مكونات الدم التي تتدفق خلالها. تنظيم توازن الماء يحدث في خلايا ال principal cells التي تحتوي على قنوات مياه تسمى aquaporin-2. زيادة أو نقصان في كمية هذه البروتينات على سطح الخلية لديها تأثير مباشر على قدرة تركيز البول وبذلك كمية الماء في الجسم. لذلك، خلل في هذا النظام يؤدي الى أمراض مثل SIADH أو الى المرض السكري الكاذب (NDI). أكبر مسبب لمرض السكري الكاذب هو استخدام الليثيوم الذي يستخدم من اجل علاج الاضطراب ثنائي القطب. وكان الهدف من هذا البحث العلمي هو الحصول على المزيد من المعلومات عن تأثير مادة الليثيوم على كمية قنوات المياه الموجودة على سطح الخلايا والبحث عن طرق جديدة لعلاج مرض السكري الكاذب.

الليثيوم يخفض نسبة خلايا ال Principal cells مقارنتا إلى خلايا ال Intercalated cells.

حوالي ٢٠٪ من المرضى الذين يتلقون علاج الليثيوم، يعانون من الاثار الجانبية التي تؤدي الى تطور مرض ال NDI. مرضى ال NDI يكون عندهم ضعف في قدرة تركيز البول. وهذا الضعف سببه انخفاض في كمية بروتين ال AQP2. وبالإضافة إلى ذلك، فإن المرض يزداد سوءا بسبب انخفاض نسبة خلايا ال principal cells في نظام القنوات الجامعة الذي يعرف بال collecting duct. ولكن هذا غريب وغير متوقع لأن الليثيوم يحث تكاثر خلايا ال principal cells. في **الفصل الثاني** من هذا الكتاب درسنا هذه الضاهرة من خلال زرع خلايا الكلية في انضمة ثنائية و ثلاثية الأبعاد و ايضا من خلال تجارب على الفئران. تبين لنا في هذه الدراسة بأن الليثيوم يحث الخلايا على التكاثر و لكن يبقيها عالقا في مرحلة ال G2/M دون ان تكمل الخلايا دورتها التكاثرية وهذا ما يشرح سبب انخفاض نسبة الخلايا ال principal cells في نظام القنوات الجامعة في الكليون. ومع ذلك، فإننا نعتقد أن هذا ليس هو المسبب الوحيد لإعادة هيكلة القنات الجامعة في الكليون. قد أظهرت العديد من الدراسات السابقة أن زيادة حموضة القنات ايضا تحفز الخلايا على التكاثر و خاصتا خلايا ال Intercalated cells. في **الفصل الرابع** من هذا الكتاب اثبتنا بان الليثيون يغير طريقة توليد الطاقة في الخلايا و اللذي يؤدي الى زيادة في إنتاج اللاكتات والهيدروجين. وهذه المواد تزيد من حموضة القناة والتي بدورها ستحفز خلايا ال intercalated cell بان تتكاثر للتخلص من الحموضة في البول.

تأثير التحلل السكري على أمراض الكلى التي يسببها الليثيوم

لقد اثبتنا سابقا أن الليثيوم يدخل خلايا ال principal cells من خلال قناة الصوديوم (ENaC). في **الفصل الرابع** من هذا الكتاب، تبين لنا في التجارب المختبرية على الحيوانات ان الليثيوم, لجانب تأثيره على تكاثر الخلايا, فإنه يعيد برمجة طريقة توليد الطاقة من ما يؤدي الى إرتفاع نسبة ال glycolysis (التي تعرف ايضا ب aerobic glycolysis) و ال glutaminolysis. هذا التغيير يؤدي الى زيادة في انتاج اللاكتات، وبالإضافة إلى ذلك زيادة إنتاج الحمض داخل الخلايا أثناء هذه العملية.

تدل تجاربنا بال siRNA على خلايا ال mpkCCD في المختبر بان العلاج بمادة كيمائية التي تمنع عمل ال كاربوهيدريسيس (CA)، خاصتا CA9 و CA12، لها دور في التأثير السلبي لليثيوم على قنوات المياه الموجودة على سطح الخلايا. اللافت للإنتباه هو ان ال CA9 و CA12 تكون موجودة بكثرة في سرطان الكلى مما تسهل نمو الخلايا السرطانية من خلال تحييد الأحماض التي تتم إصدارها خلال عملية ال aerobic glycolysis. فقد اكتشفنا ان هذه العملية تحصل في خلايا ال principal cells بعد تعرضها لليثيوم.

Chapter 14

Arabic summary | ملخص عربي

Institute for Molecular Life Sciences
Radboudumc